THIOPHENE-BASED PHOTORESPONSIVE MESOGENS

D M CHAMBERS-ASMAN

A thesis submitted in partial fulfilment of the requirements of Nottingham Trent University for

the degree of Doctor of Philosophy

July 2007

THIOPHENE-BASED PHOTORESPONSIVE MESOGENS

Summary of a thesis submitted for the degree of Doctor of Philosophy

D M Chambers-Asman

Abstract

This thesis reports the synthesis, transition temperatures and structure-property relationships of a variety of thiophene-containing azobenzene esters derived from either 3-(2-thienyl)acrylic acid (**Series I**, **IV**, **VI**, **VIII**, **X** and **XII**) or 3-(3-thienyl)acrylic acid (**Series II**, **V**, **VII**, **IX**, **XI** and **XIII**) and appropriate fluoro- and non-fluoro-substituted 'azophenols', for potential use in photoresponsive applications. For comparative purposes, the non-heterocyclic cinnamate counterparts (**Series III**) were also prepared and are reported. All one hundred and thirty final esters are mesomorphic, exhibiting the nematic phase alone.

The mesomorphic properties are dependent upon the disposition of the terminal thiophene moiety. In general 3-thienyl-substitution gives thermally more stable compounds than 2-thienyl-substitution.

Influence of mono- (**Series IV**, **V**, **VI** and **VII**) and di- (**Series VIII**, **IX**, **X**, **XI**, **XII** and **XIII**) lateral fluoro-substitution on mesomorphic properties is investigated in detail. Lateral fluorination lowers mesophase thermal stability and its extent is dependent upon the number and disposition of the lateral fluoro-substituents. Di-lateral fluorination across the long molecular axis is more detrimental to mesophase thermal stability than along the long molecular axis.

UV-Vis steady state photoresponsive studies on **Series I** show that *trans-cis* photoisomerisation may be induced at 367 nm, with the reverse *cis-trans* isomerisation process occurring 434 nm. Similar behaviour is also seen for **Series IV**, **VII**, **VIII**, **X** and **XII**.

The influence of modifying or changing terminal groups on mesomorphic and photoresponsive properties is established. Replacing the acrylic ester of **Series I** with more flexible homologous alkyl esters of varying chain length (**Series XIV**), in general, lowers mesophase thermal stability, mesophase range and alters the photoresponsitivity. Replacement of the terminal alkoxy-group of **Series I** and **II** with either a cyclohexyl (**Series XV**) or a non-linear 2-thienyl moiety (**Series XVI**) increases the mesophase thermal stability, with the non-linear 2-thienyl compounds (**Series XVI**) having the greatest thermal stability of all compounds.

The diversity of the azobenzene core and thiophene moiety for future materials is reported in brief, with some showing interesting potential photoresponsive phases other than the nematic phase.

Acknowledgements

I would like express my sincerest thanks to Dr A. S. Matharu for his friendship, guidance and constant encouragement throughout the course of this work, to Nottingham Trent University for supporting me and for always encouraging me to further myself and to all the people and institutions I have visited. I wish to thank them for being so friendly and allowing me access to their facilities, particularly The University of York.

Finally, but never lastly, I would like to thank my family who have been a shining light throughout. I wish to express my deepest thanks to them for bearing with all the late nights I have worked. The knowledge that at the end of the day I would be going home to them, kept me going to the end.

CONTENTS

HOW TO USE THIS THESIS

This thesis is deigned for use by both undergraduates and experienced researchers in the areas of liquid crystals and materials chemistry. To this effect, it has been divided into relevant sections for ease of use.

1.   INTRODUCTION

This section gives an overview of the area of thermotropic low molecular mass liquid crystals, particularly for those to whom this subject is new. It covers a brief history, a short explanation of types with guidance of key references for further research and development of liquid crystals. The aims show the step-wise research plan used in order to gain an in-depth structure relationship between the molecular architecture and mesogenic properties of novel thiophene-based liquid crystals containing an azo moiety.

2.   EXPERIMENTAL

A synthetic overview is provided to explain the rationale behind techniques used, followed by complete experimental details and compound data. All experimental procedures are written in full to ensure repeatability. Compounds are numbered sequentially excluding those available commercially.

3.   RESULTS AND DISCUSSION

This section is designed for those with experience in liquid crystals, though it does lend itself to those who are gaining knowledge in this topic. It includes details such as transition temperature plots, structure-property relationships, X-Ray analysis data, Photoresponsive studies, and photographic evidence of phase types.

4.   FUTURE WORK

This section attempts to show the versatility of the original architecture. Preliminary comments and spectroscopic data from compounds that have been synthesised, but not fully investigated,

is shown in an attempt to gain further information from modification of the original core molecule.

REAGENTS AND SOLVENTS

Diethyl ether was dried over sodium wire. Acetone and dichloromethane were dried over granular anhydrous calcium chloride. Ethanol, toluene and hexane were dried over 4 Å molecular sieves. Tetrahydrofuran was dried by reflux with sodium metal and benzophenone (until dryness was indicated by a royal blue colour). Commercial starting materials were obtained from either Fisher Scientific (Acros Chemicals) or Aldrich Chemical Company Limited.

Structural information of intermediate compounds and products was obtained by infra-red spectroscopy (Perkin-Elmer FT 1605 and Spectrum 100 [fitted with a UATR] spectrophotometers) and nuclear magnetic resonance spectroscopy (JEOL FX60Q 270 MHz and ECX400 400 MHz spectrometer). Ultra-violet spectroscopy for cis-trans isomerisation was measured using an Agilent 8345 photodiode array UV-Vis spectrophotometer. Transition temperatures were measured using both Olympus BH2 and Vickers microscopes, fitted with a Linkam THMS 600 hot stage and control system and were confirmed by thermal analysis initially using a Perkin Elmer DSC 7 differential scanning calorimeter (DSC), followed by a Perkin Elmer Diamond DSC for the majority of the compounds at a rate of 10 $^{\circ}$C min^{-1}. The DSC internal accuracy was checked using both indium and magnesium standards. Images of textures were captured using a Pixelink PC 700 camera and Capture software. Mass Spectra were performed by the Chemistry Department at the University of York, York, England. Elemental analysis was performed by the microanalysis departments of both the University of Nottingham and London Metropolitan University. X-Ray analysis was performed by the University of York and The Risø National Laboratory, Roskilde, Denmark. Progress of reactions was monitored by thin layer chromatography (TLC) using silica coated glass plates (silica 60 Å, 250 μm layer thickness). Where appropriate, column chromatography was performed using silica gel (silica 60 Å, 220-240 mesh).

ABBREVIATIONS

DCC	1,3-*N,N*- Dicyclohexylcarbodiimide
DCM	Dichloromethane
DMAP	4-*N*-Dimethylaminopyridine
THF	Tetrahydrofuran
s	Singlet
d	Doublet
t	Triplet
quint	Quintet
m	Multiplet
m.p.	Melting point
cl.p	Clearing point
C	Crystal
Sm	Smectic
N	Nematic
N*	Chiral nematic/Cholesteric
I	Isotropic
▪	Mesophase to isotropic liquid transition temperature
●	Crystal to mesophase transition temperature
▲	Mesophase to crystal transition temperature

INTRODUCTION

1 <u>INTRODUCTION</u>

It is commonly known that there are three states of matter: solid; liquid and; gas. Crystalline solids possess 3-D order and at their melting point lose order converting in to a 0-ordered liquid state. Conversely, on cooling a 0-ordered liquid state, 3-D order is regained and the crystalline solid reforms.

However, there is a class of compounds which directly neither convert to an isotropic liquid upon heating nor revert to a crystalline solid on cooling. Instead they exist in a state of matter that is intermediate between solid and liquid, possessing characteristics of both and some quite unique. Compounds exhibiting this phenomenon are termed *liquid crystals*, *mesogens*, *mesogenic* or *mesomorphic* and the intermediate state of matter is termed either the *liquid crystalline phase* or *mesophase*.

1.1 HISTORICAL BACKGROUND

The first recorded observation of a liquid crystalline state was by F. Reinitzer[1] in 1888, who noticed unusual melting behaviour on heating crystals of cholesteryl benzoate (**1**). At 145.5 °C, cholesteryl benzoate melted not in to a clear liquid as expected but gave a blue, opaque, turbid liquid, which persisted over a 33 °C temperature range, before clarifying at 178.5 °C. In 1889, Reinitzer informed O. Lehmann[2] of his observations, who subsequently viewed a sample of cholesteryl benzoate through a specially constructed polarising light microscope.
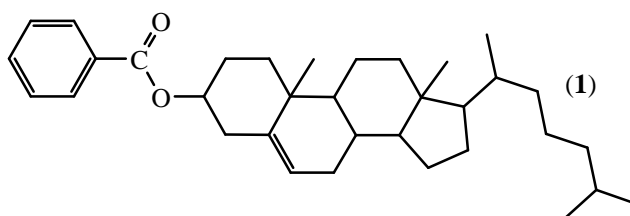
Lehmann reported that the cloudy blue fluid was in fact a new state of matter occurring between the liquid and solid states of matter, and introduced the new terms *fliessende krystalle* and

flüssige krystalle meaning 'flowing crystals'. The birth of liquid crystals had started and soon after, Gattermann and Ritschke[3] found more compounds exhibiting similar behaviour.

Synthetic activity dominated the early part of the Twentieth Century and through extensive structure-property investigations Vorländer[4, 5] set out criteria defining molecular structure with the occurrence of a liquid crystallinity, *i.e.*, the basic structure of a compound exhibiting liquid crystallinity must be linear and rod-like. In addition, during this period many theoretical investigations were also undertaken. In 1908, Bose postulated the ***Swarm theory***[6] (the nematic phase was caused by a swarm of molecules) and as an alternative, the ***Continuum theory*** proposed by Zocher[7] (the nematic phase being thought to be a continuum causing the molecules to constantly change direction in the mesophase). Both theories were later refined (the Swarm theory by Ornstein and Kast[8] and the Continuum theory by Oseen[9]).

By 1922 Friedel[10] defined three different types of liquid crystalline state and introduced the generic term ***mesophase*** (derived from the Greek words ***meso***, meaning intermediate and ***phasis***, meaning phase) to describe them. These mesophases were named nematic, smectic and cholesteric (a description of these phases is given later, section 1.4.2, p. 9-16). It is important to note Friedel did not realise the existence of sub-categories of the smectic phase, however he did foresee their layered structures. Also, that the first reported discovery of the smectic phase should be attributed to Meyer and Dahlem[11] (1902) whilst investigating the melting behaviour of ethyl *p*-azoxybenzoate. Friedel's work also disproved the much regarded notion postulated earlier by Tammann[12] and Nernst[13] that the liquid crystalline state was nothing but a colloidal suspension and not a new state that was distinct from the crystalline state and the isotropic liquid.

During the 1930's to the end of the Second World War, liquid crystal research became understandably stagnant. Thereafter, liquid crystal research emerged slowly and regained impetus in 1957 when Brown and Shaw[14] published a major review on liquid crystals. This is

now accepted as a major contributor to the creation and launch of the renowned International Liquid Crystal Conferences (ILCCs), which are now held biannually. During this time, Maier and Saupe[15] published theoretical papers referring the structure and properties of the nematic state with respect to temperature. Later Gray[16] investigated relationships between molecular structure and mesomorphism, culminating in the publication of the very notable and invaluable book titled, *"Molecular Structure and the Properties of Liquid Crystals"*. The early 1970s saw the emergence of the Twisted Nematic (TN) Display by Schadt and Helfrich[17] and coupled with the synthesis of stable 4'-alkyl- and 4-alkoxy-4-cyanobiphenyls by Gray *et al.*[18] for use in such displays, led to huge academic and commercial interest in the field of liquid crystals. Liquid Crystal Displays (LCDs) had emerged and their versatility was evident for all to see: lightweight; portable; flat panel and; low power consumption. The need for faster displays soon led to the development of the Ferroelectric Liquid Crystal (FLC) display device by Clark and Lagerwall[19], which is based on the chiral smectic C phase. Today, LCDs are everywhere and are fast replacing Cathode Ray Tube (CRT) devices. Technology has progressed rapidly and large area flat-panel LCDs, which were once a mere reality, are now common in many households.

It is always important to remember that the success of liquid crystals is due its multi-disciplinary nature where collaborations between chemists, physicists, mathematicians and biologists are an absolute necessity. This means that the future of liquid crystals is now quite diverse, stemming from potential applications in gene therapy to artificial muscles to nanoparticles as highlighted in December 2005 at the Royal Society meeting entitled '*New Directions in Liquid Crystals*'[20].

1.2 CLASSIFICATION AND MOLECULAR STRUCTURE OF LIQUID CRYSTALS

1.2.1 CLASSIFICATION

Liquid crystalline compounds may be classified according to how they are produced. If, a compound exhibits an intermediate state of matter (mesophase) due to the action of heat, then it is termed a ***thermotropic*** liquid crystal. Mesophases that are observed both on heating and on cooling above the melting point are termed ***enantiotropic***, whereas those observed on supercooling below the melting point are termed ***monotropic***. Alternatively, if, a mesophase is formed due to action of solvent, usually water and concentration dependant, then the compound is termed a ***lyotropic*** liquid crystal.

Unfortunately, the term lyotropic and thermotropic are ambiguous because lyotropic liquid crystals are affected by temperature and thermotropic liquid crystals are affected by the action of solvents. To this end, a more definitive classification based on molecular structure is used classifying liquid crystals as either ***amphiphilic*** or ***non-amphiphilic***. Amphiphilic liquid crystals are those containing both lipophilic ('lipid liking') and hydrophilic ('water-liking') groups at different places within the same molecule. Their presence allows solubility in both water and hydrocarbon-based solvents. Non-amphiphilic liquid crystals are compounds that are either non-polar or only slightly polar in character and are essentially hydrophobic. The mesophases formed during heating and/or cooling are dependent on the arrangement of individual molecules and not multi-molecular aggregates as found in amphiphilic systems. The work reported herein strictly deals with temperature induced, non-amphiphilic liquid crystals and thus amphiphilic liquid crystals and/or lyotropism will not be discussed further.

1.2.2   MOLECULAR STRUCTURE

Stemming from the earlier work of Vorländer[4,5] and Gray[16], the vast majority of low molar mass, non-amphiphilic, thermotropic liquid crystals comprise an elongated, lath-like, geometrically anisotropic structure termed *calamitic* (**Figure 1**).
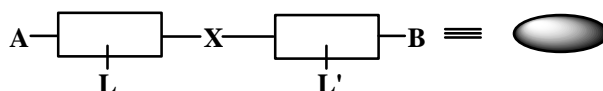
Figure 1   Representation of the component structure of a classical calamitic liquid crystal

A and **B** are terminal groups (usually alkoxy or alkyl) and these may be used to extend the linearity of the molecule along the long axis. The rectangles represent rigid, highly polarisable groups, which are normally aromatic (or more specifically benzenoid) in character. **X** is the central linking group, which provides the rigidity in the system and allows conjugation between the polarisable groups, if so desired. **L** and **L'** represent lateral groups, which may or may not be present as they tend to increase the molecular breadth of the molecule but are beneficial for lowering the melting point and enhancing certain mesophase types. The influence of each of the four components on liquid crystallinity will be discussed in section 1.6., p.21.

Many other structures have now been realised[21-24] as shown in **Figure 2**. The most notable of which are probably the *discotics*, first reported by Chandrasekhar[25], possessing a disc-like geometry. Bent core structures are currently gaining a lot of interest because they exhibit B phases and may show a biaxial nematic phase[26]. However, in the scope of this thesis discotic liquid crystals and bent core structures exhibiting B phases will not be covered in any detail.
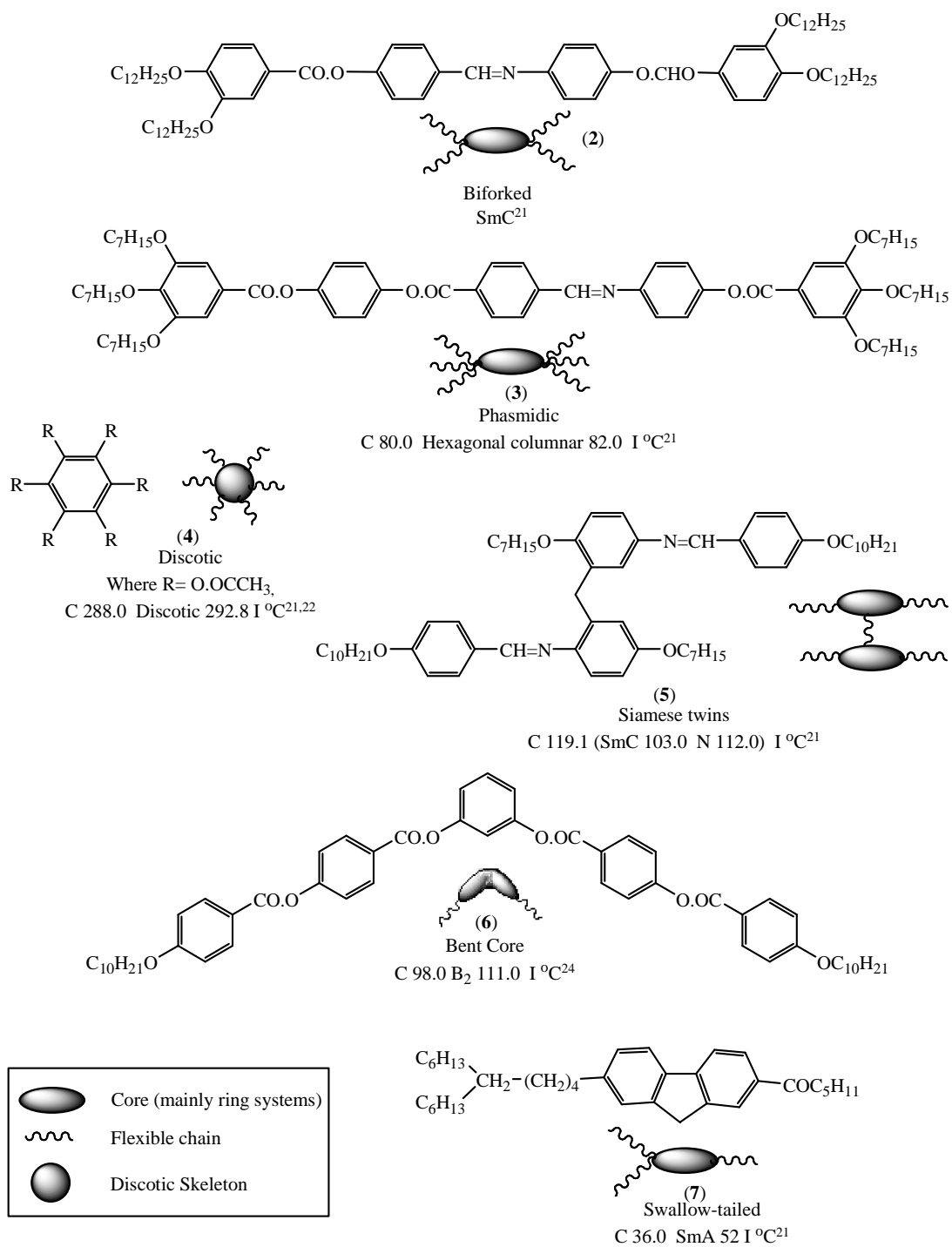
Figure 2 Structural variety of liquid crystal molecules[21-24].

1.3 MESOPHASE FORMATION

In 1933 Bernal and Crowfoot[27] examined several liquid crystalline compounds using X-ray crystallography and concluded the existence of two types of crystal lattice: *layer lattice* and; *non-layer lattice* (**Figure 3**). Due to the geometrical anisotropy of the individual calamitic molecules, anisotropy of intermolecular cohesive forces is also feasible. In fact, mesophase formation (as depicted in **Figure 3**) is due to the gradual breakdown of anisotropic intermolecular forces holding together calamitic molecules in either a layer crystal lattice or non-layer crystal lattice. There are two types of intermolecular cohesive forces: i) lateral (forces holding molecules side-on) and; ii) terminal (forces holding the molecule end-on). Lateral forces are stronger than terminal forces giving rise to anisotropy of intermolecular forces.
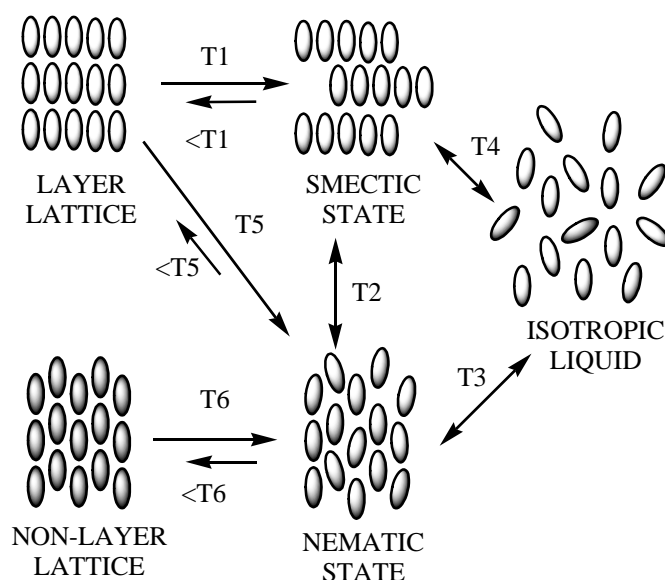
Figure 3   Diagrammatic representation of molecular re-arrangements occurring from heating a crystalline solid composed of either layer- or non-layer- lattice

On heating a calamitic liquid crystal possessing a layer crystal lattice to a temperature, T1, the terminal forces weaken whilst the lateral forces remain intact. The resultant structure resembles the smectic state in which the molecules are confined in weak layer planes. On heating to a higher temperature, T2, two possibilities may occur, either i) the lateral forces may weaken to

such an extent that the molecules slide out of the layer to give rise to the nematic state. Thereafter, heating to a higher temperature, T3, the residual lateral and terminal forces break completely, giving rise to the isotropic liquid (zero-order), or; ii) the smectic phase may pass directly to the isotropic liquid on heating to a higher temperature, T4. The calamitic liquid crystal on heating may also convert to the nematic state at a temperature, T5, which then clarifies in to the isotropic liquid at T3.

A non-layer crystal lattice initially was thought capable of giving rise to a nematic phase only on heating to a temperature, T6, and then clearing to the isotropic liquid at a higher temperature, T3. However, it has been shown that certain 4-n-alkyl- and 4-n-alkoxy-4'-cyanobiphenyls[18] (K and M series) possess a non-layer crystal lattice that give rise to a smectic phase (e.g. SmA^d), in which the d-spacing is approximately 1.4 times larger than the molecular length. An inter-digitated molecular arrangement forms.

1.4 OPTICAL CHARACTERISATION AND MESOPHASE TYPES

1.4.1 OPTICAL CHARACTERISATION

As stated earlier, in 1922 Friedel[10] identified three types of mesophase; nematic, smectic and cholesteric. To date many more phase types have been discovered which are variants of the three generic types. The identification of these phase types has been elucidated using a variety of techniques ranging from X-ray diffraction, calorimetry to neutron scattering. However, polarising optical light microscopy is probably the simplest and most widely used method for the initial identification and study of mesophases. Liquid crystals give characteristic *optical textures* (or patterns) when a small sample of mesomorphic compound sandwiched between two glass slides is viewed through a polarising optical light microscope at varying temperatures. A knowledge of the pre-alignment of the molecules on the glass substrate aids textural determination. The two most common alignments are ***homeotropic*** and ***homogeneous*** (**Figure 4**). When viewed between crossed polarisers, the homeotropic alignment appears optically

extinct, *i.e.*, dark, because the molecules have their long axes arranged approximately perpendicular to the support surface and parallel to the optic axis. In the homogeneous alignment the molecules have their long axis parallel to the glass surface and when viewed between crossed polarisers, a bright field is observed.

Homeotropic   Homogeneous
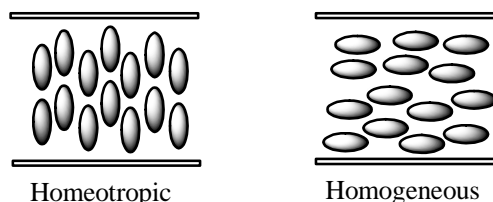
Figure 4   Homeotropic and homeogenous molecular alignments.

1.4.2   <u>MESOPHASE TYPES</u>

1.4.2.1 NEMATIC PHASE (N)

The term nematic arises from the Greek word ***nematos*** thread-like, due to its characteristic thread-like optical texture. **Figure 5** shows the generalised molecular organisation within the nematic phase, in which the rod-like molecules align approximately parallel with respect to each other along a direction defined by the director, n̂. The molecules are free to rotate in any direction, possess long range orientational order but zero positional order. The nematic phase bears similarities to the isotropic liquid and is said to be *fluid-like*.

$$S = \frac{1}{2}\{3\cos^2\theta - 1\}$$
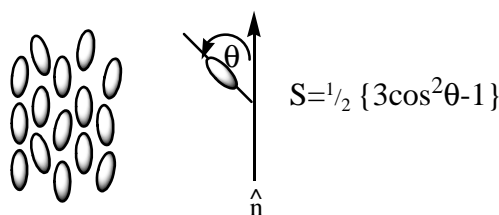
Figure 5   Idealised structure of the nematic phase

The degree of alignment of molecules with respect to the director, n̂, is termed the order parameter, S, where θ is the angle between the long axis of each of the individual molecules and

9

the director. The typical value for the order parameter, S, is in the region of 0.4-0.7 (temperature dependant).

The nematic phase can be identified easily on cooling from the isotropic liquid as it forms highly coloured droplets (nematic droplets) which coalesce into a predominantly thread- or marble-like texture.

1.4.2.2 CHIRAL NEMATIC PHASE (N*)

The introduction of a chiral centre in a nematic molecule introduces optical activity and gives rise to cholesteric behaviour (the term cholesteric is used because this phase was first detected in derivatives of cholesterol). The chiral nematic phase (N*) can be regarded as a "layered" nematic state in which the director in a given "layer" of molecules is slightly skewed either clockwise or anticlockwise with respect to the director in adjacent "layers" (**Figure 6**). The distance for one complete revolution (0-360°) is termed the **pitch** and is temperature dependent.
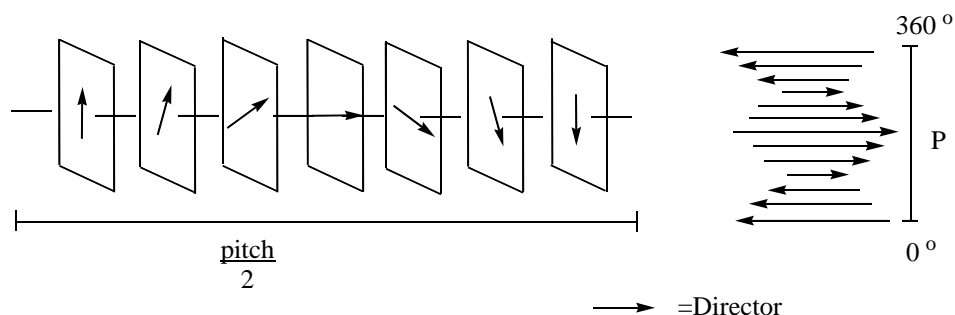
Figure 6   Diagrammatic representation of the chiral nematic phase.

The chiral nematic and nematic phases are similar except: they rarely exist together except in the unusual case of helical twist inversion[28], addition of a chiral component to a nematic phase converts the nematic phase into a chiral nematic phase; mixing two chiral nematic materials of opposite sense gives rise to a nematic phase and the X-ray diffraction patterns for both phases are similar.

The chiral nematic phase exhibits two different textures, which are dependant on the alignment of the helices on the supporting surface with respect to the optical axis (**Figure 7**):

i.   the pseudo focal-conic or undisturbed texture- formed upon cooling from the isotropic liquid. This is a birefringent, optically inactive texture. The helices lie perpendicular to the incident light;

ii. the Grandjean (planar or disturbed) texture in which the helices are aligned parallel to the light path, this texture has a brightly coloured background with 'flowing streams' and arises from shearing the focal-conic texture.

Optical axis

Grandjean   Pseudo focal-conic
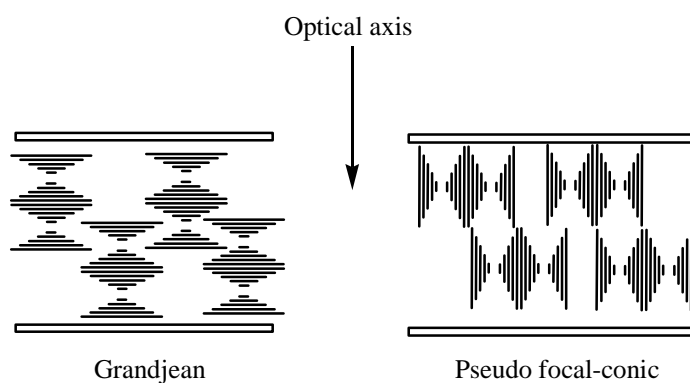
Figure 7   Helical orientation for the Grandjean and pseudo focal-conic textures

1.4.2.3 SMECTIC PHASE (S) AND SMECTIC POLYMORPHISM

The term smectic phase was derived from the Greek word ***smectos*** for 'soap-like', because it was first observed in alkaline soaps. The smectic phase differs from both the nematic and chiral nematic phases because the molecules occur in layers and possess positional and orientational order. The molecules may align either perpendicular (*e.g*., **Figure 8**) or inclined (*e.g*., **Figure 9**) with respect to the layers.

Although Friedel[10] recognised the existence of a smectic phase, he did not realise the existence of polymorphs (different smectic phase types).   In the scope of this thesis smectic

polymorphism will be described in brief detail only. The reader is directed to the book 'Smectic Liquid Crystals', by Gray and Goodby for a fuller account of smectic phases[29]. The different polymorphs arise from the amount and type of order within (and between) the layers. Sackman and Demus[30] initially classified several smectic polymorphs and designated them using coded lettering SmA, SmB, etc. So far twelve different smectic phases are known and may be placed in order of appearance on cooling from the isotropic liquid (thermodynamic sequence of phases).

Iso liquid – N, SmA, D, SmC, SmB, SmI, CrB, SmF, CrJ, CrG, CrE, CrK, CrH - Crystal
$$\longrightarrow$$
Decrease in temperature

The smectic liquid crystal phases (SmA, SmB, SmC, SmI and SmF) possess short range order whereas the smectic crystal phases (CrB, CrJ, CrG, CrE, CrK, CrH) possess long range order through several layers thus tending towards 3-D order and crystallinity.

1.4.2.3.1   *The Smectic A Phase (SmA)*

This is the least ordered of all the smectic polymorphs and X-ray diffraction patterns[31] show that the molecules are arranged with their molecular long axis perpendicular with respect to *diffuse layer planes*[32] (**Figure 8**). There is zero positional order within a *layer* and the molecules are free to rotate about their long axis. The layer spacing (d) within this polymorph is equal to the molecular length (l).

Diffuse layer plane ⟶

Calamitic molecule ⟶

Layer spacing, d=

Molecular length, l
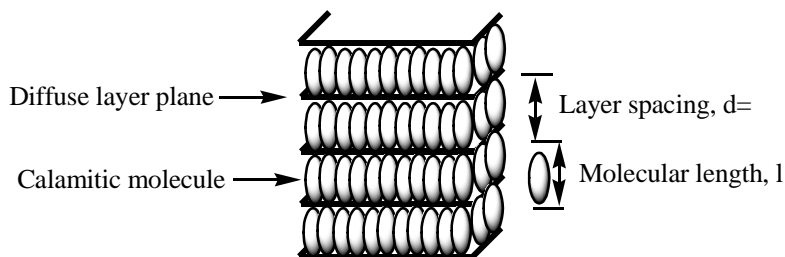
Figure 8   Idealised structure of a smectic A, SmA, phase (n.b. layers are much softer, *not shown*).

1.4.2.3.2   *The Smectic C Phase (SmC)*

The smectic C phase consists of a layered structure in which the molecules are tilted with respect to the layer planes (**Figure 9**). X-Ray studies[31] reveal the layer spacing (d) is less than the molecular length (l). The tilt angle, θ, of the molecules with respect to the diffuse layer normal, is temperature dependent.

Diffuse Layer Plane

Calamitic molecule

Layer spacing, d=

Molecular length, l
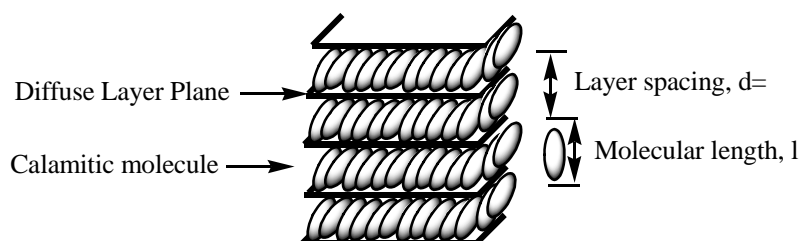
Figure 9   Idealised structure of the smectic C phase (n.b. layers are much *softer* than shown)

1.4.2.4 THE CHIRAL SMECTIC C PHASE (SmC*)

As well as the chiral nematic phase there are many different types of chiral smectic liquid crystal phases (SmC*, SmI* and SmF*) and the corresponding crystal smectic phases (J*, G*, K* and H*). The most commonly encountered chiral smectic phases are the tilted phases, with the most commonly exhibited (and most important) being the chiral smectic C phase. This is partly because it is the least ordered and least viscous within this category and can be employed in the ferroelectric display device[19], but the helix must be unwound (see later). There are other chiral mesophases that are of smectic type (e.g., TGBA*) but these are not discussed in the scope of this thesis and the reader is directed to references 33 and 34.

The chiral smectic C (SmC*) phase is the chiral analogue of the SmC phase (above). As with the SmC phase, the structure is lamellar and the molecules within the diffuse layers are tilted at a temperature dependant angle, θ, from the layer normal (ideally around 25 $^{\circ}$).

The SmC* phase is essentially the same as its achiral counterpart, except that chirality causes a slight and gradual change in the direction of the molecular tilt (with zero change in the tilt angle with respect to the layer normal). The tilt direction changes from layer to layer to describe a helix (**Figure 10**).
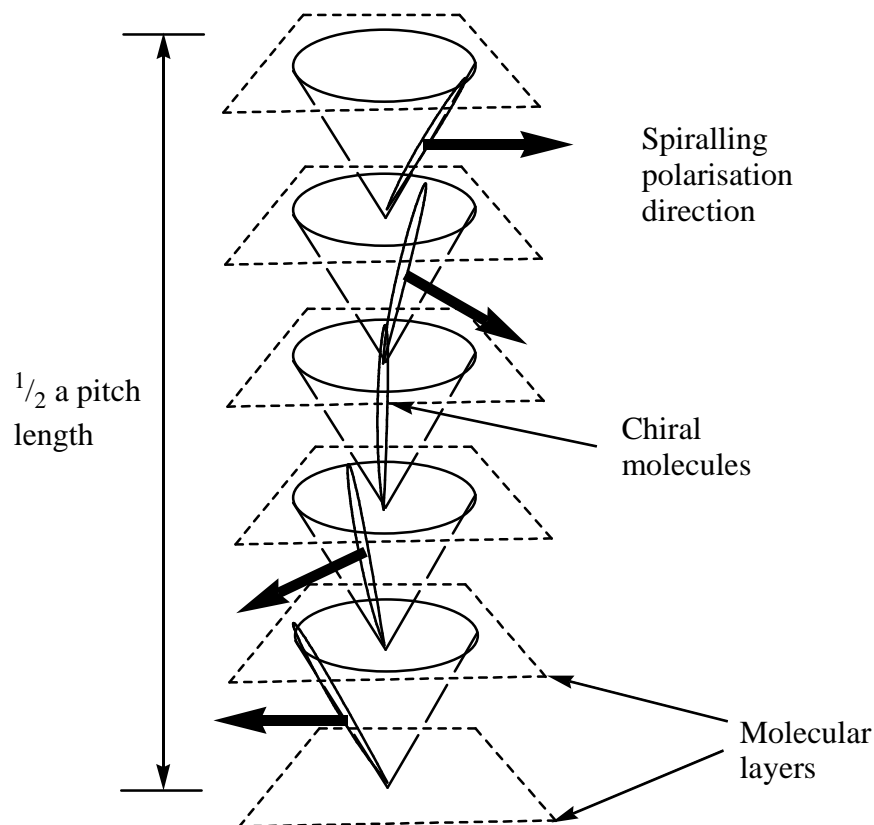
Figure 10   Helielectric structure of the SmC* phase.

The helix in the SmC* phase is temperature dependant, with high temperatures creating a small tilt angle and long pitch length, whereas temperature creates a larger tilt angle and thus a shorter pitch (this being the opposite effect to the chiral nematic phase).

The space symmetry of the achiral SmC phase can be seen to consist of a centre of inversion, a mirror plane and a two-fold axis of symmetry parallel to the layer planes. However, when the phase is chiral, the symmetry is reduced to solely a two-fold axis of rotation. With the molecules still undergoing rapid re-orientation (as in the achiral homologue) the result of the

reduction of symmetry creates non-equivalence in the dipole moment along the C2 axis. This non-equivalence creates a spontaneous polarisation along the C2 axis (the direction of which changes with the changing tilt direction within the helix). However, due to the helix the spontaneous polarisation is reduced to zero throughout the medium and is said to be 'heli-electric' (**Figure 10**).

1.4.2.5 FERRIELECTRIC AND ANTIFERROELECTRIC CHIRAL SMECTIC C PHASE TYPES

In 1989 Chandani *et al.*[35,36] reported two new sub-classes of the SmC* ferroelectric phase. These were namely the antiferroelectric chiral smectic C phase (SmC*$_{anti}$) and the ferrielectric (SmC*$_{ferri}$) phases. As with the ferroelectric SmC* phase, the molecules of the antiferroelectric phase have a tilted lamellar structure, except that the tilt direction alternates from successive layers to give a zigzag structure, resulting in a spontaneous polarisation of zero (**Figure 11**). The ferrielectric chiral smectic C phase also has an alternating tilted structure, however, the alternation is not symmetrical and more layers are tilted in one direction than the other. The spontaneous polarisation of the ferroelectric phase is dependant on the degree of alternation of tilt directions (**Figure 11**).

SmC*
ferroelectric

SmC*
ferrielectric

SmC*
antiferroelectric
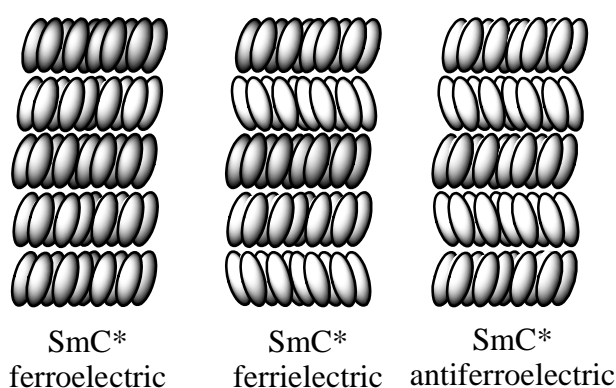
Figure 11 Structures of the ferro-, ferri- and antiferro-electric phase types in their simplified unwound helical states.

The antiferroelectric phase is the subject of much research interest because upon application of an electric field, it can convert to a ferroelectric state, which can then be switched to a second ferro-electric state. Removal of the field completely results in reversion to antiferro-electric molecular phase ordering (**Figure 12**). This phenomenon is known as 'tri-state' switching[35] and occurs at a defined electric field with a sharp threshold which differs from the ferroelectric switching.

| Ferroelectric I
Polarised | Antiferroelectric
Zero Polarisation | Ferroelectric II
Polarised |
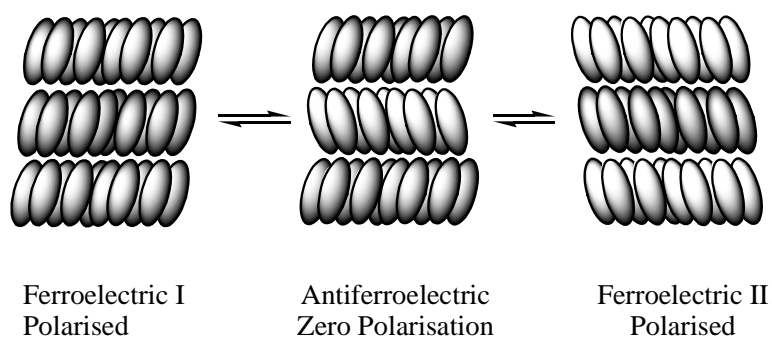
Figure 12   Antiferroelectric tristate switching

1.5   ELECTRO-OPTIC APPLICATIONS OF LIQUID CRYSTALS: TN AND SSFLC DISPLAYS

1.5.1   <u>THE TWISTED NEMATIC DEVICE</u>[17]

Based on re-orientation of nematic molecules in the presence of an applied field, the twisted nematic device (**Figure 13**) consists of a nematic material (of positive dielectric anisotropy), laminated between two glass slides.   The nematic material is homogeneously aligned and twisted through 90° by the action of alignment layers coated on the inner surfaces of the glass substrates which are rubbed at 90° with respect to each other.   Rubbing is problematical because it creates dust, debris and surface charge, which leads to defects.
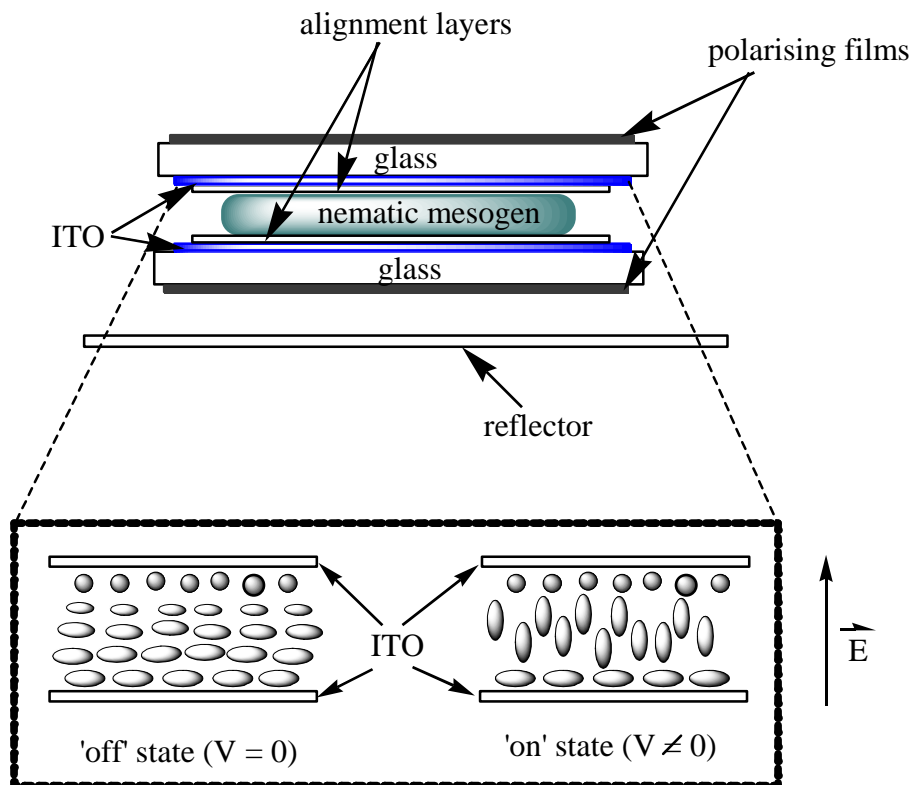
Figure 13   A typical liquid crystal display cell and the 'off' and 'on' states of the twisted nematic liquid crystal display.

The 'nematic glass sandwich' is bound by a set of crossed polarisers. In the 'off' state (*i.e.,* no electric field passing through the device), light entering the first polariser is wave guided by the

nematic material through 90 $^{\circ}$ and passes through the second polariser ('crossed' with respect to the first polariser). In this situation a bright field of view is observed. In the 'on' state the molecules align perpendicular with respect to the glass substrates (homeotropic) and parallel with respect to the field and therefore light passing through the first polariser is unable to pass through the second polariser. In this situation a dark field of view is observed. Due to the *elastic* properties of the materials, the molecules relax back to the homogenous alignment on removal of the electric field.

1.5.2 FERROELECTRICITY AND THE SURFACE STABILISED FERROELECTRIC LIQUID CRYSTAL (SSFLC) DISPLAY

The term ferroelectric refers to any system which possesses either a permanent or spontaneous polarised state. Meyer *et al.*[37] postulated prerequisites for the existence of ferroelectricity in liquid crystals which matched those ascribed to the chiral SmC phase, *i.e.*:

    i.   there must be a laminar or layer-like structure;

    ii.   the molecules should be chiral;

    iii.   the molecules should be tilted arrangement with respect to the layers;

    iv.   the molecules should contain a strong transverse dipole.

A single layer of a chiral smectic C phase is 'ferroelectric'. Clark and Lagerwall[19] discovered in the 1980 that the helix of the SmC* phase could be unwound or suppressed by using a cell gap that was less than the helical pitch and in by doing so, the dipole moments would align in the same direction, giving rise to a spontaneous or permanently polarised state (*i.e.,* ferroelectric). This discovery allowed the development of the SSFLC display (**Figure 14**)

In the SSFLC display, the molecules align parallel to the surfaces in what is termed the 'bookshelf geometry' within the confines of a thin glass cell (1-2 μm), which causes the helix to unwind (or be suppressed) due to strong boundary forces (surface stabilisation). The direction of polarisation with the molecules in this geometry is perpendicular to the glass plates and upon

the application of a small DC potential across the plates, a change in polarisation direction can be induced. When the voltage is removed the direction of polarisation remains the same and thus the ferroelectric device can be termed 'bistable'.

The optimum tilt angle for the ferroelectric device is 22.5 $^{\circ}$, so as the angle of the molecular switching as they undergo directional change from one orientation to another is ideally 45 $^{\circ}$. The SSFLC is an important commercial display as compared to the TND[17] because it confers the following advantages.

i.   a faster switching speed (in the order of microseconds compared to milliseconds);

ii.   a bistable state that is capable of being retained on a long term basis;

iii.   a high brightness: contrast ratio, enabling use at low ambient light levels.

top polariser

dipoles υ

υ

υ

layers

⊕

v   applied DC
    voltage

⊖

θ, tilt angle

Layer Normal

molecules parallel
to top polariser

bottom polariser at
right angles to top
polariser

reversal of polarity of
the applied DC field, inverts
the spontaneous polarisation

molecules no longer
parallel to top polariser

layers

⊖

v   applied DC
    voltage

⊕

Layer Normal
θ, tilt angle

υ   υ   υ

dipoles

Figure 14   Optical transmission in the SSFLC display. The top cell demonstrating light
transmission and the bottom cell light extinction.

1.6 THE RELATIONSHIP BETWEEN MOLECULAR STRUCTURE AND LIQUID CRYSTALLINE BEHAVIOUR

In the design of new liquid crystalline compounds, it is imperative to have an understanding of the relationship between molecular structure and mesophase properties. As mentioned previously (section 1.3, p.7), anisotropy of molecular shape and anisotropy of internal forces are the two main components governing the formation of thermotropic mesophases.

Calamitic liquid crystals are, in general, composed of rigid, polarisable aromatic units, connected to each other by a central linking group. Introduction of terminal groups can provide necessary elongation, with the possibility of introducing lateral groups (which are mainly present on the rigid polarisable aromatic groups). By careful manipulation of these groups the mesophase thermal stability (temperature of transition) of nematic to isotropic (T_{N-I}), smectic to nematic (T_{S-N}) or smectic to isotropic (T_{S-I}), may be increased, reduced or eliminated all together.

The anisotropy of molecular polarisability ($\Delta\alpha$), defined as the difference in polarisability of molecular long axis with respect to that of the short axis, has been identified as an important parameter in determining the stability of the mesophase. In general, an increase in $\Delta\alpha$ stabilises a particular mesophase and a decrease in $\Delta\alpha$ lowers the mesophase thermal stability. The reader is directed to the work of Gray[38], Collings and Hird[39] and Toyne[40] for a comprehensive assessment and evaluation of molecular structure and mesophase behaviour.

1.6.1   INFLUENCE OF TERMINAL GROUPS

Terminal groups generally serve to extend molecular length and linearity of the molecule. Alkyl- and alkoxy-groups are usually employed and are thought to stabilise the molecular orientation necessary for liquid crystal phase generation. The influence of varying the type of

terminal group with respect to the mesophase thermal stability, was investigated by Gray *et al.*[41,42], who proposed the following group efficiency order for T_{N-I}.

$$Ph > NHCOCH_3 > CN > OCH_3 > NO_2 > Cl > Br > N(CH_3)_2 > CH_3 > F > H$$
Group Efficiency Order
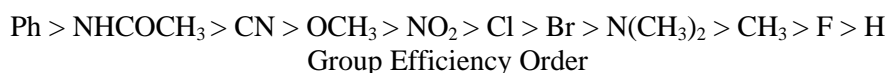
Replacement of a terminal hydrogen by one of the above groups is seen to be more beneficial to the overall mesophase thermal stability.

1.6.1.1 HOMOLOGATION

The effect of molecular structure on mesophase properties is usually best investigated by successively increasing the length of the terminal alkyl- or alkoxy-chain *i.e.*, homologation. Transition temperatures show regular trends as the length of either the terminal alkyl- or alkoxy-groups is extended in a homologous series. These trends are clearly observed by plotting transition temperatures against the number of carbon atoms in the terminal alkyl- or alkoxy-chain (**Figure 15**).
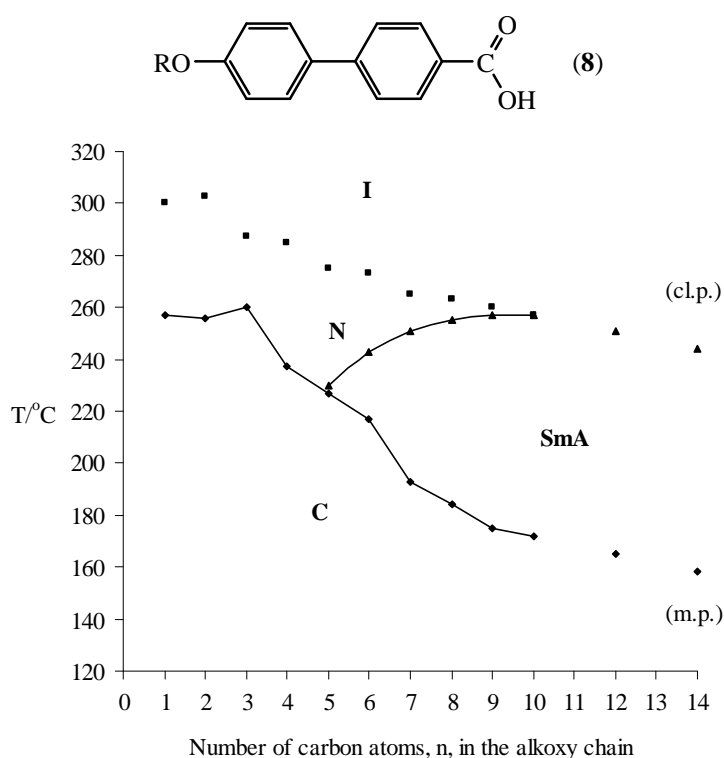
Figure 15   Plot of transition temperatures for an homologous series of 4'-*n*-alkoxybiphenyl-4-carboxylic acids (**8**)[42].

From such a plot, several conclusions can be inferred:

i.   there is no correlation between melting point and length of alkoxy chain;

ii.   nematic to isotropic liquid (N-I) transition temperatures generally fall with increasing chain length;

iii.   when both smectic and nematic properties occur, the early homologues show the nematic phase alone. The smectic phase usually occurs for the higher homologues. For homologues > 10 nematic properties completely diminish and are superseded by smectic properties;

iv.   the points for the N-I transitions for the odd numbered homologues are represented by a smooth curve (the same applies for the even numbered homologues), but the odd members lie below that of the even as the even members are more thermally stable. This is termed the ***odd-even*** effect.
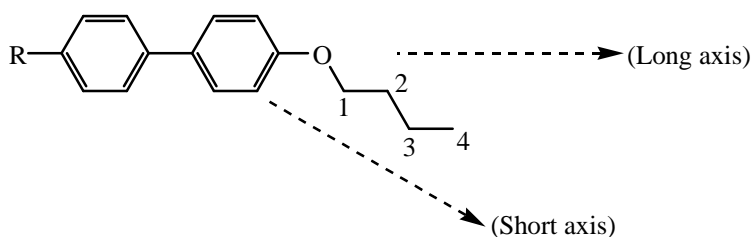
This effect may be explained by considering the number of C-C bonds directed along the long molecular axis with respect to the proportion directed along the short axis. For compounds with a terminal alkoxy-chain, the points for the N-I transition temperatures for even-n homologues lie on a smooth curve above that of the odd odd-n homologues. This can be seen to be the effect of having more C-C bonds directed along the long molecular axis as than across it. Thus the anisotropy of molecular polarisability, $\Delta\alpha$, is greater and the mesophase thermal stability is enhanced. The case is reversed for alkyl terminal chains, *i.e.*, the points for the odd-n homologues are higher than those for the even-n homologues.

1.6.2 INFLUENCE OF CENTRAL LINKING GROUPS

The central linking group is very important because it gives the entire structure rigidity, linearity and provides a means of extending the conjugation between the aromatic fragments. There are a variety of small groups that may be employed, for example: ester ($-CO_2-$ or $-O_2C-$); dimethylene ($-CH_2CH_2-$); azo ($-N=N-$) etc. The most commonly used are sp^2-hybridised groups due to their flat, planar geometry, allowing close packing of the molecule and permitting conjugation between the aromatic moieties. When sp^3-hybridised groups are used, conjugation between the rings is prevented and thus mesophase stability is reduced. However, Gray and McDonnell[43] have reported materials with low melting points and high clearing points comprising sp^3-hybridised dimethylene central linking groups.

1.6.3 INFLUENCE OF LATERAL SUBSTITUENTS

Tending to be small groups (*e.g.*, F, Cl, CN, NO_2, CH_3 or CF_3) lateral substituents are units that are attached off the linear axis of a molecule (usually on the side of an aromatic core, though they have also been incorporated in alicyclic moieties and terminal alkyl chains), broadening the molecule and as a result, lowering mesophase stability.

Laterally substituted liquid crystalline materials clearly deviate from the rod-like non-amphiphilic structure, disrupting molecular packing and decreasing liquid crystal phase stability. Though this is nearly always the case, the disrupting effect can be used to attain far more subtle effects, with the possibility of the disruption to molecular packing being advantageous to the mesomorphic and physical properties[44,45] required for some very useful materials utilised in applications[46-51].

Lateral substitution can have an important effect on both nematic and smectic systems, usually disruption to lamellar packing (required for smectic phases) results in a reduction of smectic

phase stability, whilst allowing retention of the nematic phase. Smectic phase stability can, however, be stabilised by increasing the ability to pack in a lamellar arrangement through polarity (packing being reduced by increasing size but encouraged by polarity). Any depression of nematic phase stability (T_{N-I}) by lateral substitution can be seen to be directly proportional to the size of the substituent irrespective of substituent polarity.

It is possible for the molecule itself to shield the lateral substituent either partially or, in some cases, completely. For example, in 6-n-alkoxy-5-halogeno-2-naphthoic acids (**9**)[44] the halogen substituent (X) is shielded by the molecular structure. Introduction of either a chloro- or bromo-substituent can be accommodated, and actually increases thermal stability compared to the non-halogenated parent analogue. However, introduction of the very much larger iodo-substituent decreases thermal stability.

molecular breadth

shielded

shielded

RO — O‖‖H—O — X — OR   (**9**)

O—H‖‖O
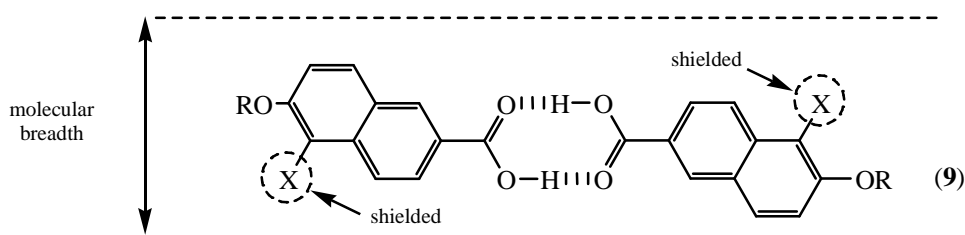
The fluoro-substituent is the most commonly used lateral substituent due to its relatively small size (1.42 Å compared to hydrogen, 1.2 Å). In general only the fluoro substituent is small enough to preserve reasonable liquid crystallinity. As such, it has been the focus of much research in establishing structure property relationships, to attain subtle changes in melting point, transition temperatures, mesophase morphology and physical properties of systems.

1.6.3.1 LATERAL FLUORINATION

Fluorine is the most electronegative element in the Periodic Table and gives rise to a moderately polar lateral C-F bond when directed across the long molecular axis. This polarity allows the design of mesogenic materials with a positive[48] or negative[52] dielectric anisotropy. The chloro-substituent has a greater dipole, however, its larger size results in low liquid crystal mesophase stability and materials with high viscosities (therefore of little use in applications, which require low viscosities).

Early examples of lateral fluorinated liquid crystals were reported in 1954 by Gray *et al.*[45] using fluoro-substituted 4-n-alkoxybenzoic acids (**11**). The acids dimerise to give mesogenic materials displaying the SmC and N phases. Compared to the parent non-fluorinated counterpart (**10**), broadening the molecule by lateral fluoro substitution resulted in the depression of the nematic phase stability (by approximately 25 ^{o}C) and the removal of the smectic phase. The increase in melting point was rather unusual and it has since been established that, commonly, a reduction in melting point with lateral substitution is observed.

$C_8H_{17}O$ —⬡— ... —OC_8H_{17} C 101.0 SmC 108.0 N 147.0 I ^{o}C
(**10**)

$C_8H_{17}O$ —⬡— ... —OC_8H_{17} C 117.0 N 120.5 I ^{o}C
(**11**)
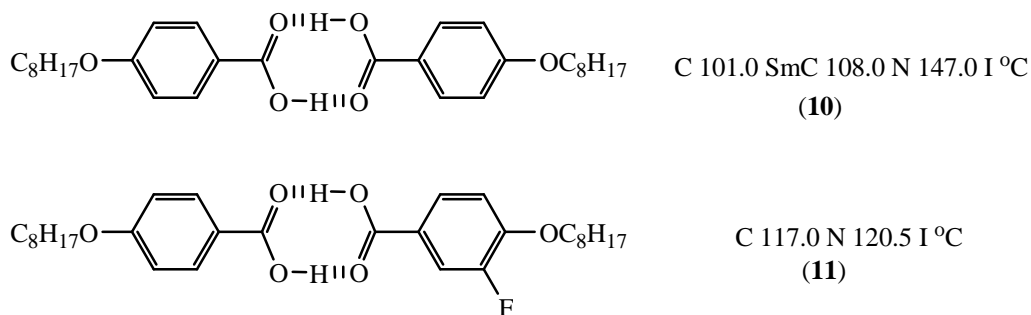
The additional increase in molecular breadth gained from lateral fluorination also gives low K_{33}/K_{11} (splay and bend elastic constants) and the polarity of the fluoro substituent, enhances the dielectric anisotropy ($\Delta\varepsilon$), both are important properties of liquid crystal materials used in displays.

The influence of a lateral fluoro substituent on physical properties of various systems (such as melting point, mesophase morphology and transition temperatures) can be greatly dependant on the number of and location of lateral fluoro substituents within the core. The reader is directed to a recent review by Hird[53] on this topic.

Esters (*e.g.*, **12-15**) are commonly used as linking groups in liquid crystal compounds, as they extend the molecular length whilst enhancing the polarisability anisotropy and are relatively easy to synthesise.   Therefore, lateral fluorination has been extensively studied in liquid crystalline esters and good examples of the effect on location and number of lateral fluorination are available. The examples below (*e.g.*, **12-15**) show compounds which display a SmC phase inferred by the alkoxy group (due to the lateral polarisability aiding molecular tilting).

C 63.0 SmC 74.0 N 91.0 I °C
(**12**)

C 48.0 (SmC 19.0) N 65.0 I °C
(**13**)

C 63.5 SmC 70.0 N 75.5 I °C
(**14**)

C 56.5 (SmC 55.0) SmA 78.0 I °C
(**15**)
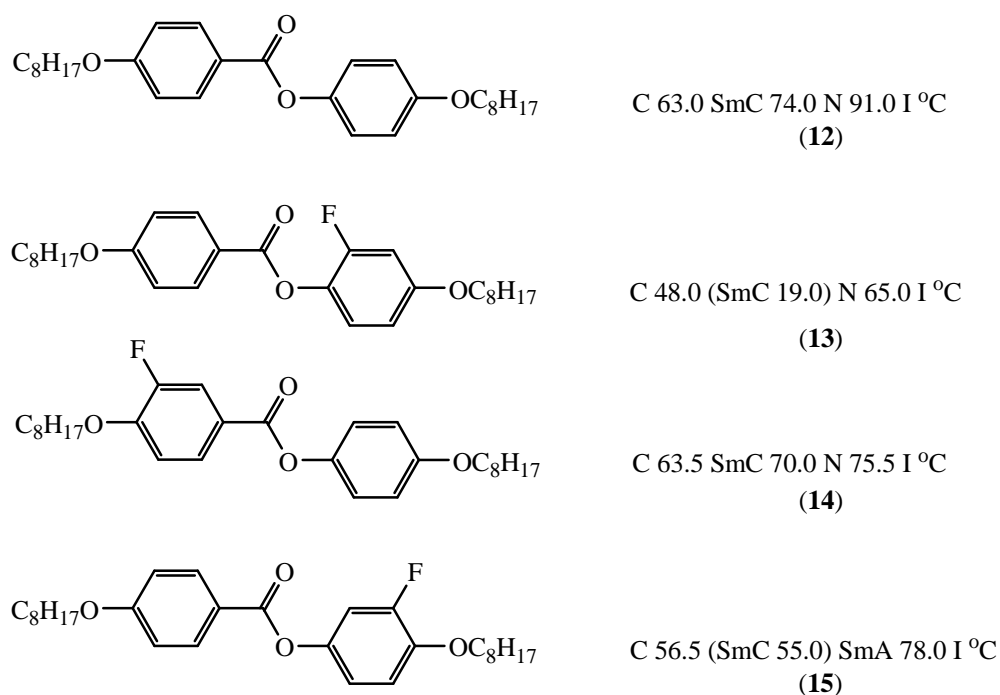
Lateral fluorination can take place on either an 'outer edge' (*meta-* to the ester group and *ortho-* to the ether linkage (**14** and **15**), or an 'inner edge' ((**13**), *ortho-* to the ester group and *meta-* to the ether linkage). Compared with the non-fluorinated homologue (**12**), lateral fluorination on an 'inner edge' (**13**), reduces the SmC phase by 55 °C, the nematic phase stability (T$_{N-I}$) by 26

^{o}C and melting point by 12 ^{o}C. 'Outer edge' lateral fluorination is seen to exhibit a '*space fill*' effect, resulting in an increase in lateral molecular forces of attraction, therefore upholding the transition temperatures. 'Outer edge' substitution (**14** and **15**) tends to be effective for smectic phases generation and compound (**14**) has a similar melting point to the parent compound (**12**) with the smectic phase being reduced only by 4 ^{o}C, but the T_{N-I} is 15.5 ^{o}C lower. 'Outer edge' fluorination can also change the morphology of the smectic phase. For compound (**15**) the smectic phase has a greater thermal stability than its non fluorinated parent (**12**) and a SmA dominates over a SmC phase.

Increasing the number of lateral fluoro-substituents within a system yields compounds (*e.g.*, **16**) with higher polarity, higher melting points and lower liquid crystal phase thermal stabilities, than for those of the mono-fluorinated homologues (*e.g.*, **14**).

C 37.0 SmC 49.0 N 57.5 I ^{o}C

(**16**)
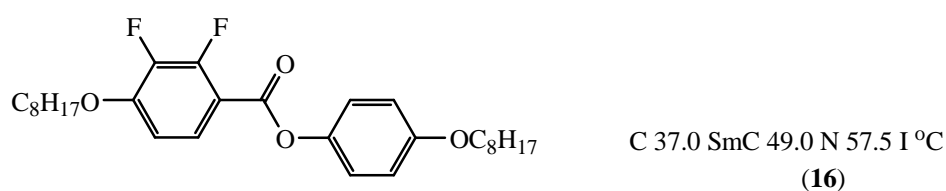
The least detrimental difluoro-substitution with respect to mesomorphic properties is with the fluorine atoms next to each other on the same side of the aromatic core (*ortho*-difluorination). This positioning has the effect of minimising the molecular breadth, whilst upholding transition temperatures and aids in keeping viscosities low. The combined lateral dipoles also confer strong negative dielectric anisotropy, useful in the ferroelectric display.

Biphenyl and terphenyl cores offer a further insight into the effect of location and number of lateral fluorination as the terphenyl system, in particular, offers a great prospect for liquid crystal phase generation (due to its increased length to breadth ratio and anisotropy of polarisability).

C 194.5 B 211.0 SmA 221.5 I °C
(**17**)

C 47.0 (J 40.0) SmI 53.5 SmC 116.5 SmA 130.0 N 155.0 I °C
(**18**)

C 69.0 G 83.0 B 100.5 SmC 124.5 SmA 158.0 N 161.0 I °C
(**19**)

C 102.0 (SmI 99.5) SmC 137.5 N 160.0 I °C
(**20**)

C 69.0 (K 25.0 J 43.5) SmC 119.5 N 158.0 I °C
(**21**)
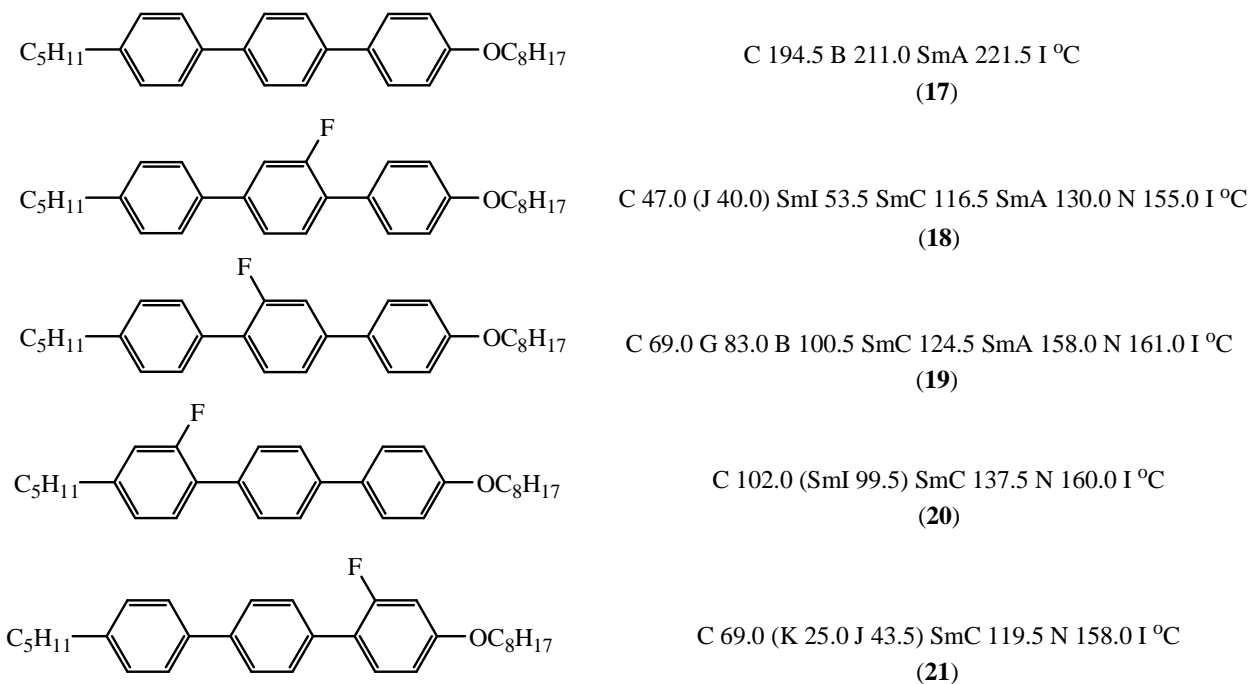
Terphenyls have 12 possible positions that can accommodate fluorination, therefore allowing the generation of 6 possible mono-fluorinated compounds, each capable of displaying different mesomorphic and physical behaviour. Similar to the fluorinated esters (**13**-**15**) there are two types of fluorination within this type of system, inner-core (**18**-**21**) and outer-core (**22** and **23**). In general inner-core lateral fluorination disrupts side to side packing, severely depresses smectic phase stability and promotes the generation of the nematic phase. Inner-core fluorination also causes interannular twisting greater than that of hydrogen at the appropriate inter-ring junction, reducing the molecular polarisability, lowering smectic mesophase phase stability and enhancing generation of the nematic phase.

G156.5 SmA 185.5 I °C
(**22**)

C 146.0 B 158.0 SmA 195.0 I °C
(**23**)
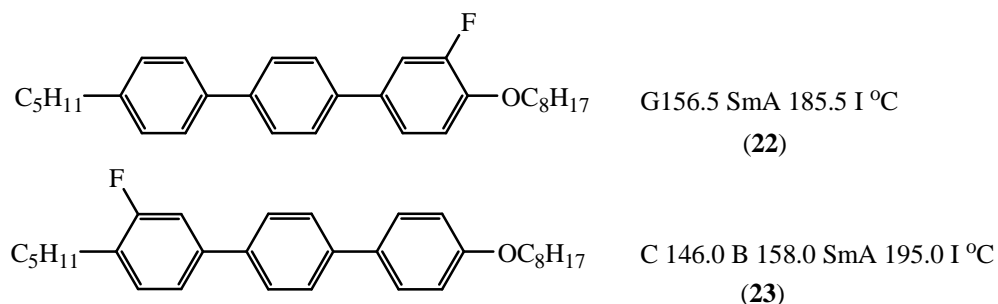
Outer-core substitution (**22** and **23**) in general, gives different mesomorphism and transition temperatures to inner-core substitution. This is due to the polar fluoro-substituent filling vacant

space on the edge of the core and strengthening lateral intermolecular forces of attraction, hence leading to smectic phase generation. Unlike inner-core substitution (**20** and **21**) there is no interannular twisting, and the polarisability anisotropy will be high, supporting high transition temperatures.

Increasing the number of lateral fluoro-substituents within a terphenyl system, as with the ester systems yields compounds with higher polarity, higher melting points and lower liquid crystal phase thermal stabilities than those of the mono fluorinated homologues. As with the mono-fluorinated homologues, the mesomorphic and physical properties are dependant the location of fluorination. Again *ortho*-difluoro-substitution is least detrimental to mesomorphic properties.

C_5H_{11}—〈ring〉—〈ring(F,F)〉—〈ring〉—OC_8H_{17} C 48.5 SmC 95.0 N 141.5 I °C

(**24**)

C_5H_{11}—〈ring〉—〈ring〉—〈ring(F,F)〉—OC_8H_{17} C 39.5 SmC 144.0 SmA 148.0 N 159.0 I °C

(**25**)

C_5H_{11}—〈ring(F,F)〉—〈ring〉—〈ring〉—OC_8H_{17} C 89.0 SmC 155.5 SmA 165.0 N 166.0 I °C

(**26**)
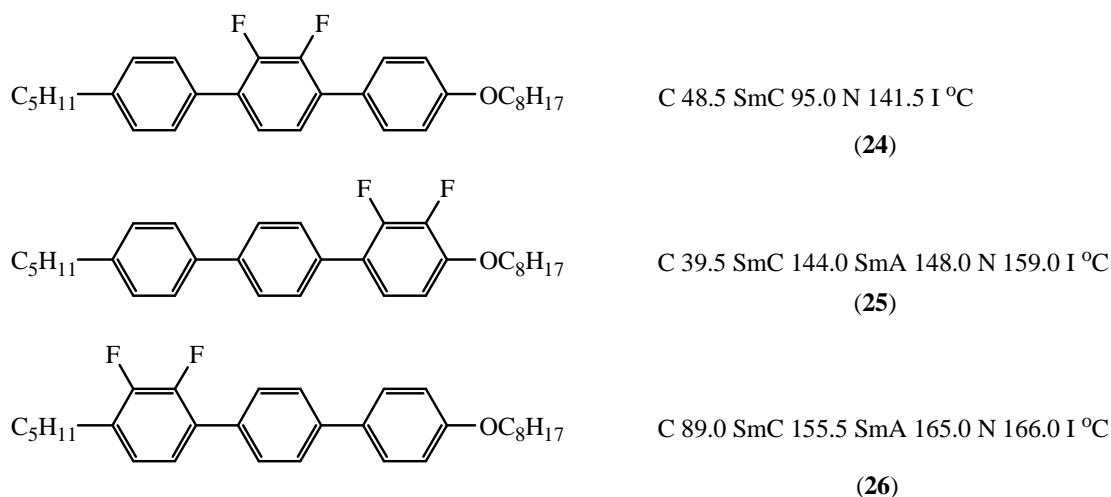
There are two types of *ortho*-difluorination.

    i.   *ortho*-difluorination of the inner core (inner ring) (**24**);

    ii.   *ortho*-difluorination of the outer core (**25** and **26**).

Inner core *ortho*-difluorination (**24**) is most detrimental to mesophase stability due to the additive effect of interannular twisting. Outer core *ortho*-difluorination (**25** and **26**) is least detrimental when it is at a position furthest from the alkoxy group (**26**), as this retains the greatest anisotropy of polarisability.
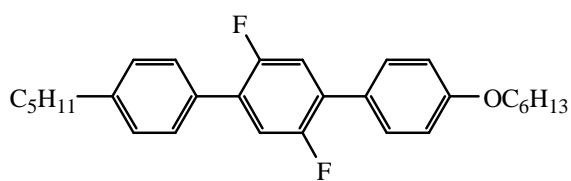
C 51.0 N 117.0 I °C
(**27**)
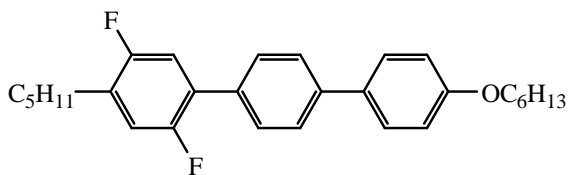
C 77.0 SmC 87.5 SmA 136.0 N 142.0 I °C
(**28**)

Across axis difluorination (**27** and **28**), as expected, decreases the thermal stability of systems (more so than mono-fluorination or *ortho*-difluoro-substitution), as it confers a significant increase in molecular breadth. The Inner core across axis difluorination (**27**) is the most detrimental to mesophase stability (particularly for the smectic phase).

1.7 PHOTORESPONSIVE LIQUID CRYSTALS

Although liquid crystal devices, such as those mentioned earlier (Section 1.5, p. 17) are used in 'cutting-edge' technology, an essential part of the design is reliant on processes developed nearly half a century ago.

An important aspect of all liquid crystal devices is the alignment layer, which dictates the alignment of the liquid crystalline molecules at the surface. Rubbed polymer (*e.g.*, polyimide) film covered substrate surfaces are the most widely used aligning layers for obtaining a planar or tilted alignment[54], however, this technique has certain disadvantages. Mechanical defects and surface charges are generated during the rubbing process and, in the case of ferroelectric liquid crystal device this can have a detrimental effect on the quality of the device.

A well studied aligning method and an alternative to 'rubbing' is the photoalignment or photoregulation method, which can provide photocontrol of the liquid crystal alignment involving alteration of the orientational direction of low-mass liquid crystals under the control of photochromic units using polarised light[54-60]. Non-contact methods can eliminate most of the problems associated with rubbing and invariably contain double bonds, such as azobenzenes, which can be isomerised by light.

Azobenzene was discovered by P. Griess[61] in 1858 and subsequently its ability to undergo *cis-trans*-photoisomerisation was reported by G. Hartley[62] in 1937. Azobenzenes (*e.g.*, **29**) interconvert between *trans-* (*E*) and *cis-* (*Z*) states upon irradiation at specific wavelengths (**Figure 16**).
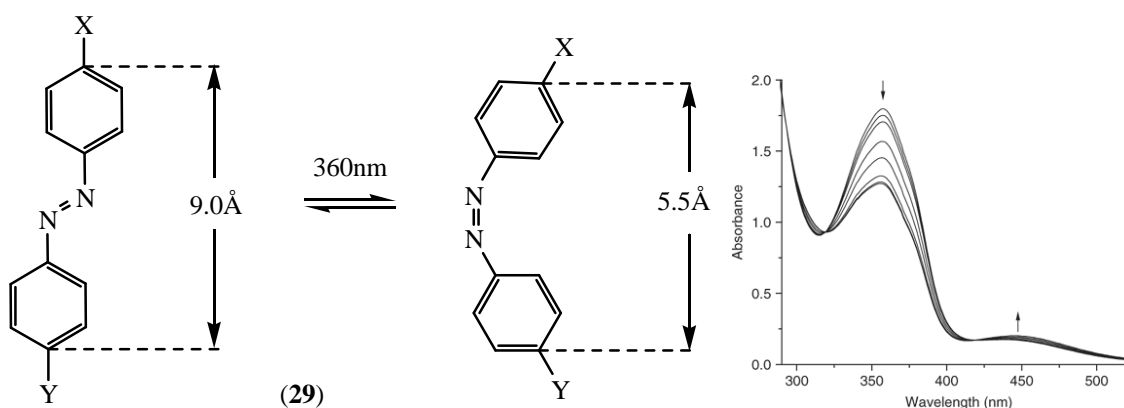
Figure 16   A diagrammatic representation of *cis-trans* (**29**) isomerisation of azobenzenes and the corresponding UV spectra showing a decrease of absorbance at 360 nm and an increase at 452 nm as isomerisation occurs.

For example photoresponsive azobenzenes (*e.g.*, **29**) and derivatives thereof, have gained considerable interest in the last two decades because of the potential use in other applications, such as photoinduced surface alignment[63], data storage[64-66] and liquid crystal elastomers[67].

Early work on photoregulation[68,69] focused on the disruption of an already present mesophase by a chromophore (already dissolved in the mesophase) undergoing a shape change during irradiation with correct wavelength of polarised light. This photoisomerisation causes a phase transition of the liquid crystal medium, enabling switching from one orientational state to another and resembling the operating principal of the twisted nematic display.

Upon irradiation at an appropriate wavelength, azobenzene undergoes *trans-cis* isomerisation followed by rapid thermal relaxation, until the dipole moment of the double bond is perpendicular to the direction of polarised incident light, resulting in co-operative alignment of the chromophore and mesogen. Longer irradiation times results in a process termed '*optical pumping*' to occur, whereby, the concentration of the less stable *cis*-form increased. The *cis*-form possesses a small cavity and has a greater affinity for the surface of a cell than the *trans*-form (**Figure 17**). The combination of these two effects causes the alignment of the mesogens

to become parallel to the cell wall and was used by Gibbons *et al.*[70] to construct the first photoaligned cell.
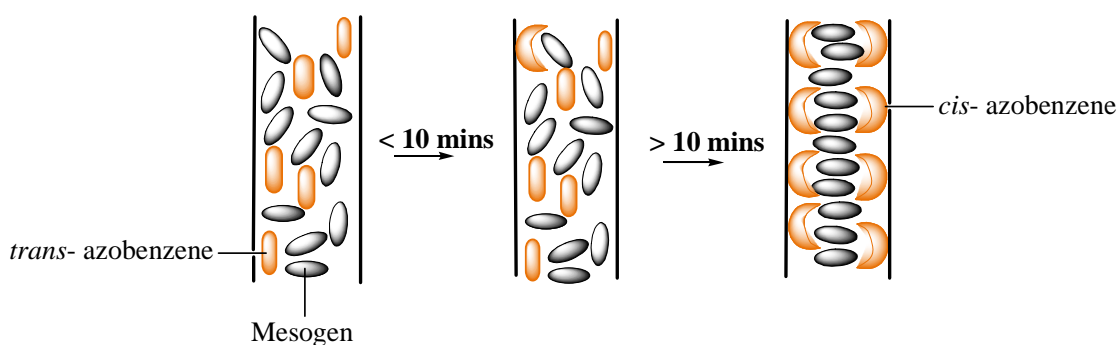
Figure 17   A diagrammatic representation of the operating principal of the first photoaligned display

Another example of photoalignment based on azobenzenes was researched by Ichimura *et al.*[58] Rather than using the photochromic molecule as a dopant, it was chemi- or physi-sorbed on to a surface. The 'tethered' azobenzene could be switched by the correct wavelength of polarised light and induce a change in the ordering of mesogens. Two examples of this induced change of alignment are shown in **Figure 18**.
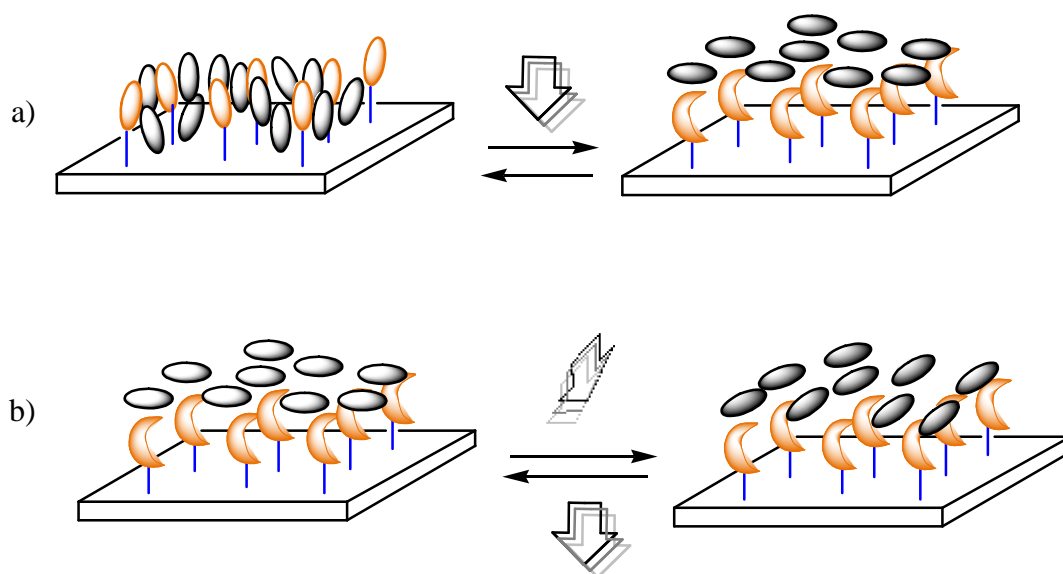
Figure 18   The effect of irradiating a chromophore-coated surface with a) linearly polarised light (out-of-plane reorientation) and b) changing the polarisation direction of the incident light (in-plane reorientation) [54, 55, 59].

Firstly, the induced ordering change was shown to go from homeotropic to planar alignment, this being termed 'out of plane reorientation with switching times and surface interaction being dependant on the type of azobenzene. Secondly, the surface was capable of inducing an in-plane reorientation of the mesogen. The double bond of the azobenzene only stopping isomerising when it is perpendicular to the polarisation of the incident light, implying that by rotating the polarisation of the incident light, reorientation of the azobenzenes at the surface will take place and thus the mesogenic molecule will follow the new order, creating a controllable in-plane movement.

The ability to switch the orientation of the mesogens resulted in these types of surfaces being termed 'command surfaces' and as has been demonstrated the 'command surface effect', provides an effective way to control alignment reversibly. Photoregulation of alignment for liquid crystal commercial applications is still in its infancy, but nevertheless is very important and rapidly expanding, as the need for highly responsive (fast) and stable materials will always be paramount.

1.8   AIMS AND OBJECTIVES

The primary aim of this research concentrates on the design, synthesis and evaluation of the mesomorphic properties of novel thiophene-based liquid crystals containing an azo -N=N- moiety, in order to develop an in-depth understanding between molecular architecture and mesogenic behaviour (**Figure 19**). Such materials may be potentially useful in applications such as photo-induced surface alignment or data storage. However, it must be stressed that the main aim is synthesis and mesomorphic characterisation and not applications.
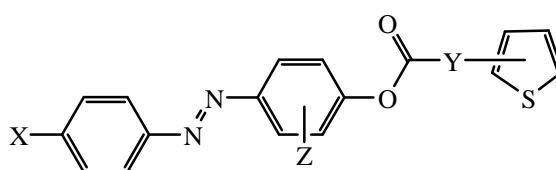
Figure 19   Diagram of the core structure whose architecture will be varied (X, Y and Z) in an attempt to understand structure-property relationships.

Nottingham Trent has a long history in the synthesis of non-linear or bent-shaped liquid crystals based on thiophene, a 5-membered heterocycle containing sulfur[71-76]. Thiophene is said to be π-excessive because it contains 6 electrons delocalised over 5 nuclei (**Figure 20**).

Lone pair of electrons delocalised within the π system

Lone pair of electrons in sp^2 hybrid orbital contained in the plane of the ring
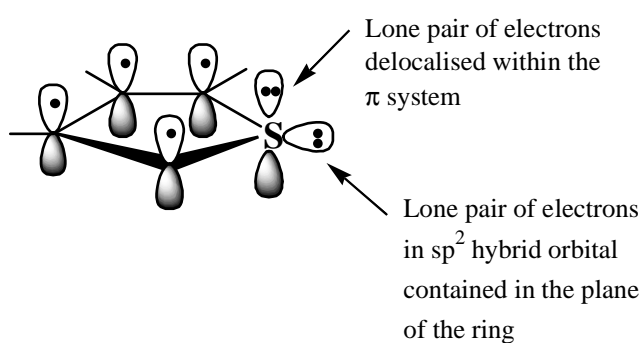
Figure 20:   Diagrammatical representation of the orbital occupancy for thiophene

Thiophene readily undergoes electrophilic substitution at the α-positions (C-2 and C-5) in preference to the β-positions (C-3 and C-4). The α-disubstitution pattern gives an exocyclic bond angle of 148°, which is intermediate to the substitution angles for 1,4-phenylene (180°) and 1,3-phenylene (120°) (**Figure 21**). Utilisation of thiophene is unusual because despite being non-linear, 2,5-thiophene containing compounds still retain liquid crystallinity[71-77]. An excellent review on thiophene based liquid crystals has just appeared in the literature. The reader's attention is drawn to reference 78.

1,4-phenylene,   2,5-thienyl,   1,3-phenylene,
180°   148°   120°
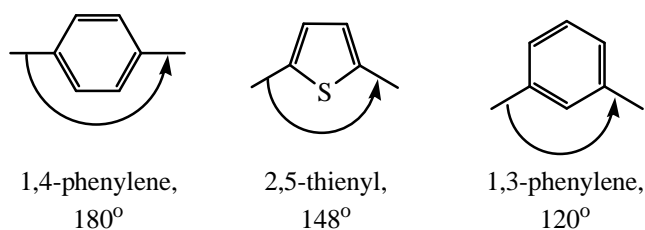
Figure 21:   Bond angles associated with substitution of benzene and thiophene

At the onset of this work, Nabeshima *et al.*[79] reported photoresponsive behaviour in a thiophene-based azobenzene, which validated our 'proof of concept'. However, to the best our knowledge, there have been no further reports on photoresponsive thiophene-based low molar liquid crystals, thus maintaining the uniqueness and novelty of this project.

In order to achieve our major aim of developing an in-depth structure-property relationship within liquid crystals comprising suitably substituted thiophene and a photoresponsive azo linkage, the following investigations were envisaged:

    i.   the influence of altering the right-hand terminally-disposed aromatic ring, which may be either 2- (**Series I**) or 3-thienyl (**Series II**) or 4-phenylene (Series III) (**Figure 22**) with respect to mesomorphic properties;

where Ar = ... ; ... ; ...

(Series I)　　(Series II)　　(Series III)
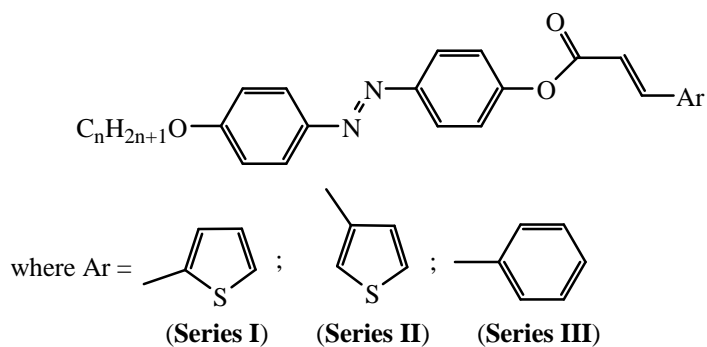
Figure 22:　　Types of right-hand terminally disposed aromatic groups used to investigate their effect on mesomorphic properties.

ii.　　the influence of introducing either one or two lateral fluoro-substituents to the *centrally-disposed* aromatic ring on mesophase thermal stability (**Figure 23**). It is envisaged that lateral fluorination will lower m.p., suppress smectic phase formation and enhance nematic phase formation[53]. This is very valuable because it may lead to commercially important low-temperature photoresponsive nematogens. Thus the synthesis of members of **Series IV - XIII** was envisaged;
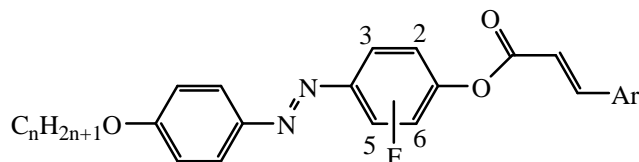
Series	fluoro-substituent	Ar=
VI	2-	2-thienyl
IV	3-	2-thienyl
VIII	2,3-	2-thienyl
XII	3,5-	2-thienyl
X	2,6-	2-thienyl
VII	2-	3-thienyl
V	3-	3-thienyl
IX	2,3-	3-thienyl
XIII	3,5-	3-thienyl
XI	2,6-	3-thienyl

Figure 23:　　Diagram of the core structure and proposed positions of lateral fluorination on the *centrally disposed* aromatic ring to investigate the effect on mesophase type and thermal stability.

iii   the influence of replacing the acrylic linkage (-O$_2$CCH=CH-) with its saturated counterparts (-O$_2$C(CH$_2$)$_n$-) on mesophase stability (**Figure 24**, **Series XIV**). It is envisaged that introducing a flexible linker will lower m.p.

Series XIV:
where n = 1-4
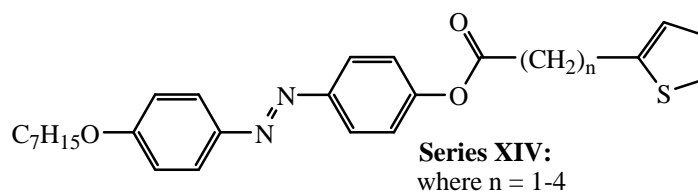
Figure 24:   Proposed structure to investigate the effect of replacing the acrylic ester with a series of aliphatic esters on mesophase and photoresponsive properties.

iv.   the influence of replacing the left-hand terminally-disposed alkoxy-chain with a second non-linear aromatic moiety (2-thienyl, **Series XVI**) or a saturated ring system (cyclohexyl, **Series XV**) on mesomorphic properties (**Figure 25**).

Series XVI

Ar = 2-thienyl, or
3-thienyl

Series XV
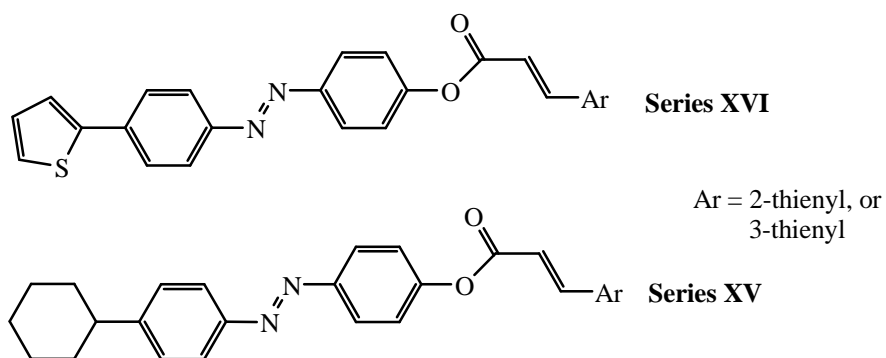
Figure 25:   Diagram of the structures whose architecture is altered from the core structure by substituting the left hand terminally disposed alkoxy-group with either a thiophene ring or a cycloalkyl- in an attempt to investigate their the effect on mesophase properties.

EXPERIMENTAL

2   EXPERIMENTAL[†]

2.1   SYNTHETIC OVERVIEW

2.1.1   SERIES I, II, IV-XIII, SCHEME 1

The synthesis of members (n=1 to 10) of a variety of thiophene-containing azobenzene esters [**Series I**, **II**, **IV-XIII**] and their non-heterocyclic counterparts [**Series III**] is generalised in **Scheme 1** (p. 60).

Commercial 4-nitrophenol was alkylated with appropriate 1-bromoalkanes to yield a series of 4-n-alkoxy-nitrobenzenes[80,81] (**30 a-j**). This is an example of the Williamson ether synthesis, where the phenolic proton of 4-nitrophenol is sufficiently acidic to be removed by the relatively weak base potassium carbonate. The resultant phenoxide anion then participates in a nucleophilic substitution reaction with the 1-bromoalkane to yield the desired 4-n-alkoxynitrobenzenes (**30 a-j**) in moderate yields (55%).

Room temperature catalytic hydrogenation (10% Pd/C) at either atmospheric or reduced pressure of an ethanolic solution of compounds (**30 a-j**) gave the desired 4-n-alkoxyanilines (**31 a-j**) in good yields (75-82%). The higher homologues were isolated as their hydrochloride salt, whereas the lower homologues were purified by vacuum distillation.

Diazotisation (conc. HCl/NaNO$_2$) of the corresponding 4-n-alkoxyanilines (**31 a-j**) followed by treatment with a solution of phenol in 4M sodium hydroxide furnished the appropriate 4-(4-n-alkoxyphenylazo)-phenols (**32-37 a-j**). The *para*-isomer (45%) was predominantly formed and since purity is essential, the compounds were rigorously purified by flash column chromatography followed by repeated recrystallisation, usually from hexane.

[†] A detailed experimental is not provided for each individual homologue of compounds **30-40 a-j**. Only salient features are reported which provide evidence of the work undertaken.

The final esters, *i.e.*, members of **Series I**, **II**, **IV-XIII**, were prepared using the DCC esterification[82] procedure because it is a room temperature, high yielding, 'one-pot' reaction. As shown in the mechanism in **Figure 26**, the DCC acts as a dehydrating agent and converts two carboxylic acid molecules into the corresponding anhydride. Dicyclohexylurea is formed as a by-product, which precipitates as a white solid from the reaction and can be isolated by filtration. The purpose of adding a catalytic amount of DMAP is to further activate the anhydride towards nucleophilic attack. The DMAP combines with the anhydride to form a highly reactive acylpyridinium intermediate, which is then attacked by the nucleophilic oxygen atom of the 'azophenol'. The desired ester is formed and the DMAP is released as a good leaving group and also functions as a catalyst.
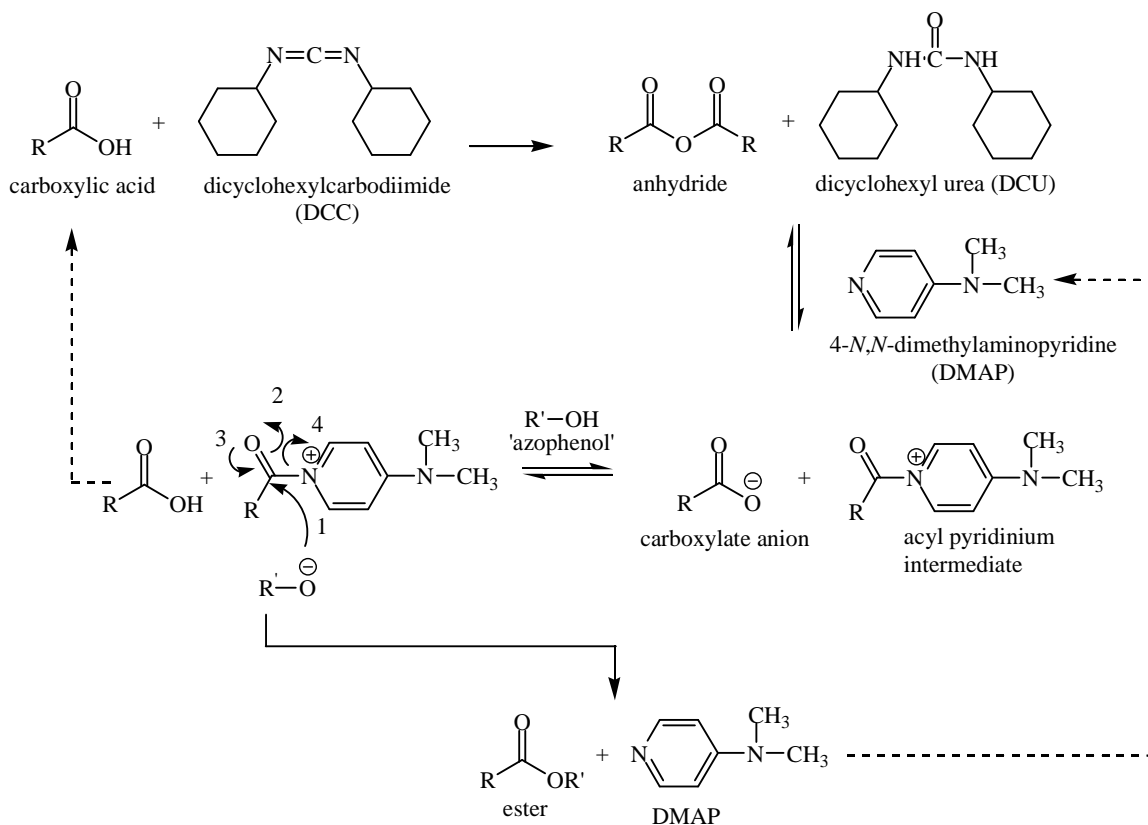
Figure 26   The mechanism of ester formation with DCC activation and DMAP catalysis.

2.1.2 SERIES XIV, SCHEME 2

Series XIV, *i.e.*, compounds **51-55**, were synthesised according to Scheme 2, p. 64. The purpose of these compounds was to investigate the effect of replacing the acrylic linkage (-O$_2$C-CH=CH-) with its corresponding saturated counterparts, *i.e.*, (-O$_2$C-(CH$_2$)$_n$-) where n= 1-4, on mesophase properties. It was envisaged that the increased flexibility would lower m.p. whilst maintaining liquid crystallinity.

4-(4-n-Heptyloxyphenylazo)phenol (0.25g) was esterified with the appropriate commercially available 3-(2-thienyl)alkane carboxylic acid to afford members of **Series XIV**.

2.1.3 SERIES XV, SCHEME 3

Following on from this, an investigation into the effect of replacing the left hand terminal alkoxy-chain with a cycloalkyl-group (**Series XV**) was undertaken to investigate the effect on mesophase properties.

Compounds **58** and **59** were realised as shown in **Scheme 3** (p. 68). Commercial 4-cyclohexylacetophenone was converted into an oxime[83] (**55**) using hydroxylamine hydrochloride. This oxime was then rearranged to an amine[83] (**56**) with pyridine and HCl and subsequently purified by Claisen distillation. This amine was diazotised and treated with phenol in 4M sodium hydroxide producing the corresponding azo-phenol (**57**) followed by DCC esterification with 3,2- and 3,3- thienyl acrylic acids to yield desired esters (**Series XV**, **58** and **59**).

2.1.4 SERIES XVI, SCHEME 4 and 5

Initial attempts to prepare compound **66** (**Series XVI**) to investigate the effect of replacing the left-hand terminally-disposed alkoxy-chain with a second non-linear aromatic moiety on

42

mesophase properties, utilised the Gomberg-Bachmann homolytic-aryl coupling [84-86] strategy as shown in **Scheme 4**. However, purification problems were encountered very early into the synthetic pathway and this strategy was soon abandoned in favour of the Suzuki-Yanagi-coupling methodology[87] (**Scheme 5**, p. 78). The Gomberg-Bachmann reaction was troublesome due to the formation of many side-products and / or isomers. The mechanism (**Figure 27**) involves free-radical coupling, which is difficult to control.
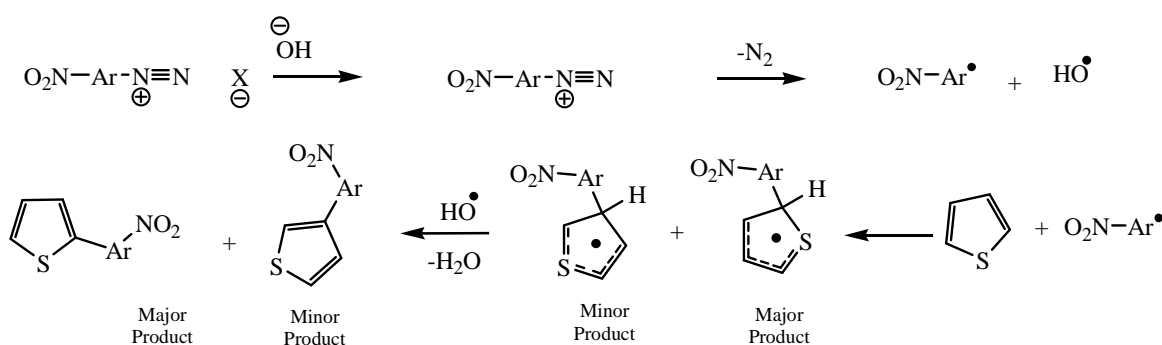
Figure 27   Schematic representation of the Gomberg-Bachmann reaction[84]

Consequently, Suzuki coupling[87] of commercial 4-bromonitrobenzene with thiophene-2-boronic acid was envisaged (**Scheme 5**), which yielded isomerically pure 3-(2-thienyl)nitrobenzene (**60**). Atmospheric hydrogenation of an ethanolic solution of compound **60** yielded the corresponding aniline (**61**) which was diazotised and converted to its phenol (**62**). Finally, DCC esterification of (**62**) with 3,2- and 3-(3-thienyl) acrylic acid gave the desired esters (**63** and **64**), *i.e.*, **Series XVI**.

The mechanism of the Suzuki coupling is yet to be completely rationalised, however there are two notable suggestions of how the coupling proceeds. Firstly Thompson e*t al.*[88] suggested that a reactive intermediate arylboronate dianion (a) attacks the arylpalladium bromide complex (b) to form a complex diarylpalladium complex (c) during reaction (**Figure 28**).

Ar—B$\overset{\ominus}{\underset{O}{\overset{O}{<}}}$ + $Br-\overset{\overset{PPh_3}{|}}{\underset{\underset{PPh_3}{|}}{Pd}}-Ar'$ $\longrightarrow$ $Ar-\overset{\overset{PPh_3}{|}}{\underset{\underset{PPh_3}{|}}{Pd}}-Ar'$ $\longrightarrow$ $Ar-Ar'$

(a)   (b)   (c)
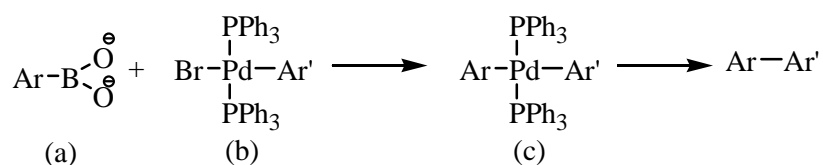
Figure 28   Suggested mechanism for the Suzuki coupling[88].

Martin and Yang[89] proposed the catalytic cycle shown in **Figure 29**.
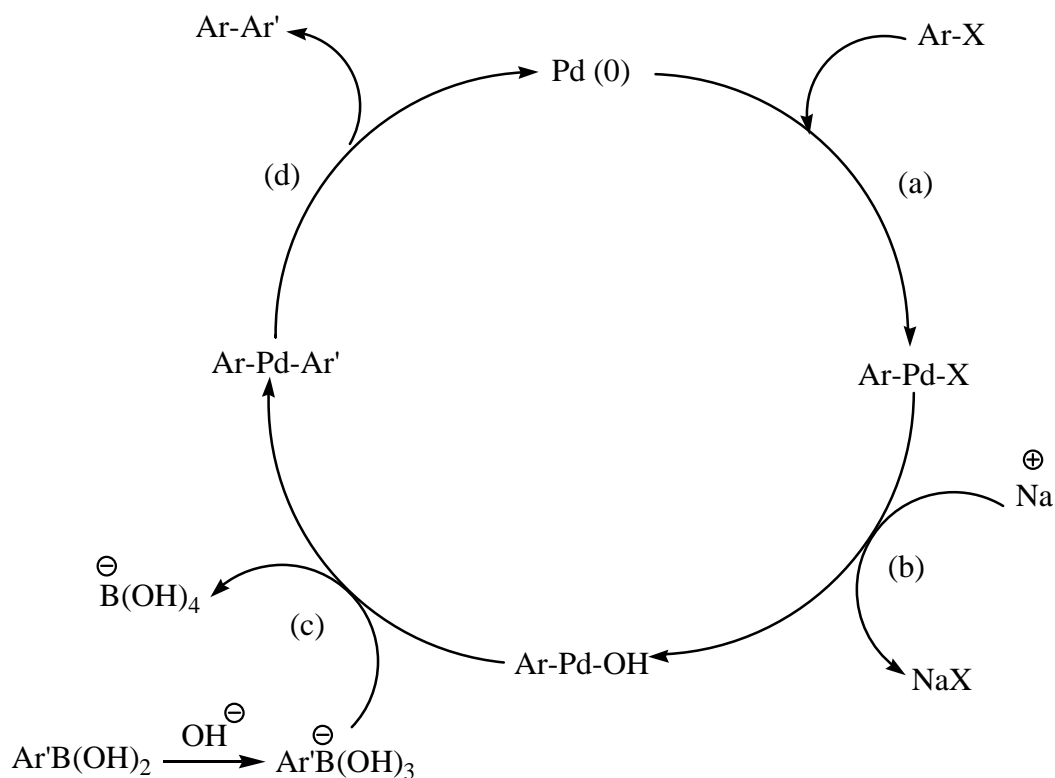
Figure 29   Martin and Yang proposed catalytic cycle of the Suzuki reaction [89].

The catalytic route represents the oxidative addition of palladium(0) complex (step a), followed by displacement of the halide ion from Ar-Pd-X by base (step b) to give the organopalladium hydroxide Ar-Pd-OH complex. This complex then reacts with the alkylboronic acid to give the biaryl palladium complex (step c). Reductive elimination of Ar-Pd-Ar' (step d) yields the desired biaryl and the regenerated Pd(0) catalyst.

2.2   SYNTHETIC PROCEDURES

2.2.1   <u>4-n-ALKOXYNITROBENZENES (**30 a-j**) – GENERAL METHOD</u>[80,81]

A vigorously stirred mixture of 4-nitrophenol (0.42 mol), the appropriate n-alkyl bromide (0.84 mol), dry acetone (30 ml) and anhydrous potassium carbonate (116 g, 0.84 mol) was heated under reflux for 24 h. Thereafter, the reaction was cooled, potassium salts filtered, washed with acetone and the filtrate was evaporated to dryness. The resultant crude residue was purified by either vacuum distillation or by recrystallisation from ethanol: n=1 (**30 a**) and n=2 (**30 b**) were supplied commercially; n=3 (**30 c**), 92-94 ^{o}C @ 0.45 mm Hg, (56%); n=4 (**30 d**), 123-125 ^{o}C @ 0.5 mm Hg, (65%); n=5 (**30 e**), 142-144 ^{o}C @ 0.5 mm Hg, (70%); n=6 (**30 f**), 160-162 ^{o}C @ 0.5 mm Hg, (46%); n=7 (**30 g**), 200-202 ^{o}C @ 0.6 mm Hg, (50%); n=8 (**30 h**), 208-210 ^{o}C @ 0.45 mm Hg, (62%); n=9 (**30 i**), 218-220 ^{o}C @ 1 mm Hg, (70%); n=10 (**30 j**), 234-236 ^{o}C @ 1 mm Hg, (69%).

The following spectroscopic data for the heptyloxy analogue (**30 g**) is representative for the remaining series.

ν_{max} (thin film)/ cm^{-1} 3086w (ArH$_{str}$), 2931, 2858w (aliph C-H$_{str}$), 1607, 1513s (C=C$_{str}$), 1468s, 1341s (C-H$_{def}$) 1259-1115s (C-O$_{str}$), 845s (C-H$_{def}$ 2 adjacent H); δ_H (270 MHz; CDCl$_3$; Me$_4$Si) 0.9 (3H, t, CH$_3$, J=6.94 Hz), 1.36 (8H, m, CH$_2$), 1.81 (2H, quint, CH$_2$-<u>CH2</u>-CH$_2$-O), 4.03 (2H, t, -CH$_2$<u>CH$_2$</u>OAr), 6.92 (2H, d, ArH, J=9.16 Hz), 8.16 (2H, d, ArH, J=9.16 Hz); δ_C (67.9 MHz: CDCl$_3$; Me$_4$Si) 13.86 (CH$_3$) 22.43, 25.44, 28.79, 29.94, 31.35 (CH$_2$), 68.76 (CH$_2$-O), 114.23 (ArC), 125.7 (ArC) 141.07 (ArC$_Q$-NO$_2$), 163.57 (ArC$_Q$-O).

2.2.2   4-n-ALKOXYANILINES (**31a-j**) - GENERAL METHOD [80,81]

Commercial palladium on charcoal (10 % Pd/C) (0.35 g) was carefully added to a solution of the appropriate 4-n-alkoxynitrobenzene (**30 a-j**) (26 mmol) dissolved in absolute ethanol (100 ml). The mixture was fitted to an atmospheric hydrogenator and stirred continuously until the theoretical volume of hydrogen had been consumed. Thereafter, the reaction mixture was filtered through 'Celite', washed well with ethanol, and the filtrate was evaporated to dryness *in vacuo*. The crude residue was purified by vacuum distillation: n=1 (**31 a**) and n=2 (**31 b**) were supplied commercially; n=3 (**31 c**), 205-208 ^{o}C @ 4 mm Hg, (69 %); n=4 (**31 d**), 118-120 ^{o}C @ 1 mm Hg, (72 %); n=5 (**31 e**), 120-122 ^{o}C @ 0.5 mm Hg, (73 %); n=6 (**31 f**), 138-139 ^{o}C @ 0.5 mm Hg, (70 %); n=7 (**31 g**), 167-169 ^{o}C @ 0.6 mm Hg, (68 %); n=8 (**31 h**), 9 (**31 i**) and 10 (**31 j**), were isolated as the hydrochloride salt, with yields (77 %), (75 %) and (72 %), respectively.

The following spectroscopic data for the heptyloxy- analogue (**31 g**) is representative for the remaining series.

ν_{max} (thin film)/ cm^{-1} 3086w (ArH$_{str}$), 2931, 2858w (aliph C-H$_{str}$), 1607, 1513s (C=C$_{str}$) 1468, 1341s (C-H$_{def}$), 1259-1115s (C-O$_{str}$), 845s (C-H$_{def}$ p.p.d); δ_{H} (270 MHz; CDCl$_3$; Me$_4$Si) 0.8 (3H, t, CH$_3$), 1.36 (8H, m, CH$_2$), 1.66 (2H, quint, <u>CH$_2$</u>-CH$_2$-O), 3.85 (2H, t, -CH$_2$<u>CH$_2$</u>OAr), 6.56 (2H, d, ArH), 6.67 (2H, d, ArH); δ_{C} (67.9 MHz: CDCl$_3$; Me$_4$Si) 14.08 (CH$_3$), 22.64 26.02, 29.23, 29.94, 31.84 (CH$_2$), 68.64 (CH$_2$-O), 115.59 (ArC), 116.44 (ArC), 141.07 (ArC$_Q$-NH$_2$), 152.56 (ArC$_Q$-O).

2.2.3 4-(4-n-ALKOXYPHENYLAZO)PHENOLS (32 a-j) and 4-(4-n-ALKOXYPHENYLAZO)-FLUOROPHENOLS (33-37 a-j) – GENERAL METHOD FOR DIAZOTISATION AND COUPLING

A cooled (0 $^{\circ}$C) solution of sodium nitrite (1.0 g, 15 mmol) in water (50 ml) was added to a cooled solution/suspension of the appropriate 4-n-alkoxyaniline (**31 a-j**) (15 mmol) in HCl/water (5.4 ml: 27 ml). The reaction mixture was maintained at 0 $^{\circ}$C for 2 h to ensure successful diazotisation. Thereafter, a mixture of (fluoro) phenol (1.4 g, 15 mmol), sodium hydroxide (1.8 g, 45 mmol) and water (40 ml) was added, dropwise, with stirring to the above diazonium solution ensuring that the reaction temperature did not exceed 5 $^{\circ}$C. After stirring for 2 h, the ensuing orange precipitate was filtered (Büchner) and transferred into a separating funnel containing DCM (100 ml). The organic layer was extracted, washed with water (50 ml) and dried (MgSO$_4$). The crude residue was purified by flash column chromatography on silica gel (DCM), followed by repeated recrystallisation (hexane) of the desired fraction to afford a series 4-(4-n-alkoxyphenylazo)phenols (**32 a-j**) and 4-(4-n-alkoxyphenylazo)fluorophenols (**33-37 a-j**) as orange solids (38 – 44%)

4-(4-n-Alkoxyphenylazo)phenols (**32 a-j**)

m.p.s: n=1 (**32 a**), 140-141 $^{\circ}$C; n=2 (**32 b**), 130-130.7 $^{\circ}$C; n=3 (**32 c**); n=4 (**32 d**), 110-111.5 $^{\circ}$C: n=5 (**32 e**), 96.7-97.7 $^{\circ}$C; n=6 (**32 f**), 105.3-105.8 $^{\circ}$C; n=7 (**32 g**), 103.9-104.3 $^{\circ}$C; n=8 (**32 h**), 105.3-105.8 $^{\circ}$C; n=9 (**32 i**), 105-105.4 $^{\circ}$C; n=10 (**32 j**), 100.7-101.3 $^{\circ}$C.

The following spectroscopic data for 4-(4-n-heptyloxyphenylazo)phenol (**32 g**) is representative for the remaining members of the non-fluorinated 4-(4-n-alkoxyphenylazo)phenols.

ν_{max} (KBr)/ cm^{-1} 3320sb (O-H$_{st}$), 3039w (Ar-H$_{st}$), 2953, 2934, 2857w (C-H$_{st}$), 1597, 1498s (C=C$_{st}$), 1472s (C-H$_{st}$), 1244, 1105m (C-O$_{st}$), 842s (C-H$_{def}$, 2 adjacent H); δ_H (270 MHz; CDCl$_3$; Me$_4$Si) 0.89 (3H, t, CH$_3$), 1.32 (8H, m, CH$_2$), 1.81 (2H, quint, $\underline{CH_2}$-CH$_2$-O), 4.02 (2H, t, -CH$_2\underline{CH_2}$OAr), 5.4 (1H, s, -OH), 6.95 (2H, d, ArH), 7.0 (2H, d, ArH), 7.8 (2H,d, ArH, 7.83 (2H, d, ArH); δ_C (67.9 MHz: CDCl$_3$; Me$_4$Si) 14.08, 22.61, 25.98, 29.06, 29.2 ($\underline{CH_2}$-CH$_2$-O), 31.8 (CH$_2$), 68.35 (CH$_2$-O), 114.7 (ArC), 115.76 (ArC), 124.35 (ArC), 124.53 (ArC), 146.75 (ArC$_Q$),

158.86 (Ar$_Q$-OH), 161.27 (Ar$_Q$-OR); CHN Found: C, 72.93; H, 7.66; N, 8.94 %. Expected: C, 73.05; H, 7.74; N, 8.97 %; TLC (DCM), one spot, Rf; 0.15.

3-Fluoro-4-(4-n-alkoxyphenylazo)phenols **(33 a-j)**

m.p.s: n=1 (**33 a**), 141.5-143.4 ^{o}C; n=2 (**33 b**), 144.7-145.2 ^{o}C; n=3 (**33 c**) 124.3-125.1 ^{o}C; n=4 (**33 d**), 105-105.7 ^{o}C: n=5 (**33 e**), 107-107.4 ^{o}C; n=6 (**33 f**), 108.0-108.4 ^{o}C; n=7 (**33 g**), 97.7-98.0 ^{o}C; n=8 (**33 h**), 104.2-104.8 ^{o}C; n=9 (**33 i**), 115.2-115.5 ^{o}C; n=10 (**33 j**), 102.9-103.8 ^{o}C.

The following spectroscopic data for 3-fluoro-4-(4-n-heptyloxyphenylazo)phenol (**33 g**) is representative for the remaining members of this fluorinated series.

ν_{max} (KBr)/ cm^{-1} 3404 s.b (O-H$_{str}$), 3074w (Ar-H$_{str}$), 2998, 2949, 2848w (C-H$_{str}$), 1601, 1497s (C=C$_{str}$), 1266, 1113m (C-O$_{str}$), 837s (C-H$_{def}$, 2 adjacent H); δ_H (270 MHz; CDCl$_3$; Me$_4$Si) 0.92 (3H, t, CH$_3$), 1.41 (8H, m, CH$_3$<u>CH$_2$</u>CH$_2$-), 1.81 (2H, quint, <u>CH$_2$</u>-CH$_2$-O), 4.01 (2H, t, -CH$_2$<u>CH$_2$</u>OAr), 5.7 (1H, s, OH), 6.4 (1H, d, ArH), 6.66 (1H, d, ArH), 6.98 (2H,d, ArH), 7.68 (1H, t, ArH), 7.88 (2H, d, ArH); δ_C (67.9 MHz: CDCl$_3$; Me$_4$Si) 14.07 (CH$_3$), 22.65, 26.0, 29.18, 29.2, 31.8 (CH$_2$), 68.41 (CH$_2$-O), 103.9 (ArC, $^2J_{CF}$=22.8 Hz), 111.7 (ArC, $^4J_{CF}$=3 Hz), 114.72 (ArC), 119 (ArC), 124.79 (ArC), 135.3 (ArC$_Q$, $^2J_{CF}$=6.7 Hz), 147.12 (ArC$_Q$), 158.86 (ArC$_Q$-OH, $^3J_{CF}$=11.4 Hz), 158.99 & 162.78 (Ar-F, $^1J_{CF}$=257 Hz), 161.62 (ArC$_Q$-OR); CHN: Expected: C, 69.07; H, 7.02; N, 8.48 %. Found: C, 69.14; H, 7.08; N, 8.48 %; m.p. 98 ^{o}C. TLC (DCM), one spot, Rf; 0.16.

2-Fluoro-4-(4-n-alkoxyphenylazo)phenols **(34 a-j)**

m.p.s: n=1 (**34 a**), 132.6-133.6 ^{o}C; n=2 (**34 b**), 128.8-129.3 ^{o}C; n=3 (**34 c**) 119.1-119.6 ^{o}C; n=4 (**34 d**), 90.8-91.5 ^{o}C: n=5 (**34 e**), 88-88.2 ^{o}C; n=6 (**34 f**), 96.4-97.4 ^{o}C; n=7 (**34 g**), 92.1-92.6 ^{o}C; n=8 (**34 h**), 98.7-98.9 ^{o}C; n=9 (**34 i**), 99.9-101.5 ^{o}C; n=10 (**34 j**), 98.1-98.6 ^{o}C.

The following spectroscopic data for 2-fluoro-4-(4-n-heptyloxyphenylazo)phenol (**34 g**) is representative for the remaining members of this fluorinated series.

ν_{max} (KBr)/ cm^{-1}: 3404s,b (O-H$_{str}$), 3074w (Ar-H$_{str}$), 2998, 2949, 2848w (C-H$_{str}$), 1601, 1497s (C=C$_{str}$) 1266, 1113m (C-O$_{str}$), 837s (C-H$_{def}$, 2 adjacent H); δ_H (270 MHz; CDCl$_3$; Me$_4$Si) 0.92

(3H, t, CH$_3$), 1.41 (2H, sext, CH$_3$<u>CH$_2$</u>CH$_2$-), 1.81 (2H, quint, <u>CH$_2$</u>-CH$_2$-O), 4.01 (2H, t, -CH$_2$<u>CH$_2$</u>OAr), 5.53 (1H, s, OH), 6.96 (2H, d, ArH), 7.08 (1H, t, ArH), 7.63 (1H, d, ArH), 7.67 (1H, d, ArH), 7.85 (2H, d, ArH); δ_C (67.9 MHz: CDCl$_3$; Me$_4$Si) 14.07 (CH$_3$), 22.65, 26.0, 29.18, 29.2, 31.8 (CH$_2$), 68.41 (CH$_2$-O), 107.7 (ArC $^2J_{CF}$=18.68Hz), 114.72 (ArC), 117.03 (ArC, $^3J_{CF}$=2.1 Hz), 122.1 (ArC $^4J_{CF}$=3.1 Hz), 124.6 (ArC), 145.7 (ArC$_Q$-OH, $^2J_{CF}$=14.5 Hz), 146.5 (ArC$_Q$), 146.8 (ArC$_Q$, $^3J_{CF}$=5.19 Hz), 149.61+153.14 (Ar-F, $^1J_{CF}$=240 Hz), 161.55 (ArC$_Q$-OH);); CHN: Expected: C, 65.5; H, 6.36; N, 8.04 %; Found: C, 65.7; H, 6.42 ; N, 7.9 %; TLC (DCM), one spot, Rf; 0.22.

2,3-Difluoro-4-(4-n-alkoxyphenylazo)phenols (**35a-j**)

m.p.s: n=1 (**35 a**)[§]; n=2 (**35 b**), 146.2-147 ^{o}C; n=3 (**35 c**) 121.6-122.4 ^{o}C; n=4 (**35 d**), 118-119 ^{o}C: n=5 (**35 e**), 129.4-130.4 ^{o}C; n=6 (**35 f**), 117.3-117.6 ^{o}C; n=7 (**35 g**), 101-102 ^{o}C; n=8 (**35 h**), 99.9-101 ^{o}C; n=9 (**35 i**), 103.6-104.5 ^{o}C; n=10 (**35 j**), 106.7-107.2 ^{o}C.

The following spectroscopic data for 2,3-difluoro-4-(4-n-heptyloxyphenylazo)phenol (**35 g**) is representative for the remaining members of this fluorinated series.

ν_{max} (KBr)/ cm^{-1}: 3392s,b (O-H$_{str}$), 3070w (Ar-H$_{str}$), 2992, 2949, 2846w (C-H$_{str}$), 1600, 1491s (C=C$_{str}$), 1244, 1105m (C-O$_{str}$), 830s (C-H$_{def}$, 2 adjacent H); δ_H (270 MHz; CDCl$_3$; Me$_4$Si) 0.87 (3H, t, CH$_3$), 1.29 (8H, m, CH$_2$), 1.79 (2H, quint, <u>CH$_2$</u>-CH$_2$-O), 4.01 (2H, t, CH$_2$<u>CH$_2$</u>OAr), 6.0 (1H, s, OH), 6.79 (1H, t, ArH), 6.96 (2H, d, ArH), 7.49 (1H, t, ArH), 7.87 (2H, d, ArH); δ_C (67.9 MHz: CDCl$_3$; Me$_4$Si) 14.06 (CH$_3$), 22.63, 26, 29.16, 29.2, 31.74 (CH$_2$), 68.44 (CH$_2$-O), 111.8 (ArC$_Q$ $^4J_{CF}$=3.1 Hz), 112.15 (ArC$_Q$ $^4J_{CF}$=3.1 Hz), 114.75 (ArC), 124.8 (ArC), 135.67 (ArC$_Q$, $^2J_{CF}$=5.2 Hz), 138.56-142.3 (ArC$_Q$, $^1J_{CF}$=240 Hz, $^2J_{CF}$=13.5 Hz), 146.74 (ArC$_Q$), 146.9 (ArC$_Q$-OH), 147-150.89 (Ar-F, $^1J_{CF}$=261 Hz, $^2J_{CF}$=11.4 Hz), 162.5 (ArC$_Q$-OR); CHN: Expected: C, 65.5; H, 6.36; N, 8.04 %; Found: C, 65.7; H, 6.42 ; N, 7.9 %; TLC (DCM), one spot, Rf; 0.25.

[§] not determined

2,6-Difluoro-4-(4-n-alkoxyphenylazo)phenols (**36 a-j**)

m.p.s: n=1 (**36 a**)[§]; n=2 (**36 b**), 142.9-143.8 °C; n=3 (**36 c**)[§]; n=4 (**36 d**), 111.4-112 °C: n=5 (**36 e**), 124.7-125.4 °C; n=6 (**36 f**), 112.1-112.6 °C; n=7 (**36 g**), 95.8-96.0 °C; n=8 (**36 h**), 105.9-106.4 °C; n=9 (**36 i**), 104.2-104.8 °C; n=10 (**36 j**), 96-97 °C.

The following spectroscopic data for 2,6-difluoro-4-(4-n-heptyloxyphenylazo)phenol (**36 g**) is representative for the remaining members of this fluorinated series.

ν_{max} (KBr)/ cm^{-1}: 3320s,b (O-H$_{st}$), 3039w (Ar-H$_{st}$), 2953, 2934, 2857w (C-H$_{st}$), 1597, 1498s (C=C$_{st}$), 1472s (C-H$_{st}$), 1244, 1105m (C-O$_{st}$), 842s (C-H$_{def}$, 2 adjacent H); δ_H (270 MHz; CDCl$_3$; Me$_4$Si) 0.88 (3H, t, CH$_3$), 1.29 (8H, m, CH$_2$), 1.82 (2H, quint, <u>CH$_2$</u>-CH$_2$-O), 4.03 (2H, t, -CH$_2$<u>CH$_2$</u>OAr), 5.47 (1H, s, -OH), 6.96 (2H, d, ArH, J=8.8 Hz) 7.52 (2H, d, ArH), 7.84 (2H, d, ArH, J=8.8 Hz); δ_C (67.9 MHz: CDCl$_3$; Me$_4$Si) 14.07, 22.65, 31.8 (<u>CH$_2$</u>-CH$_2$-O), 68.41 (CH$_2$-O), 106.4 (ArC $^2J_{CF}$=23.9 Hz), 114.88 (ArC) 124.96 (ArC), 134.62 (ArC$_Q$, $^2J_{CF}$=21.5 Hz) 145.22 (ArC$_Q$, $^3J_{CF}$=7.3 Hz), 146.37 (ArC$_Q$), 149.97 & 153.6 (Ar-F, $^1J_{CF}$=240 Hz, $^3J_{CF}$=5.7 Hz), 162.51 (ArC$_Q$-OR); CHN: Expected: C, 65.5; H, 6.36; N, 8.04 %; Found: C, 65.61; H, 6.4; N, 7.94 %; TLC (DCM), one spot, Rf; 0.12.

3,5-Difluoro-4-(4-n-alkoxyphenylazo)phenols (**37 a-j**)

m.p.s: n=1 (**37 a**)[§]; n=2 (**37 b**), 149-149.5 °C; n=3 (**37 c**) 116.8-117.8 °C; n=4 (**37 d**), 120-121 °C: n=5 (**37 e**), 107.2-108.1 °C; n=6 (**37 f**), 116.6-114.4 °C; n=7 (**37 g**), 98.4-99.0 °C; n=8 (**37 h**), 98.3-99.2 °C; n=9 (**37 i**), 103.6-104.6 °C; n=10 (**37 j**), 105.0-105.4 °C.

The following spectroscopic data for 3,5-difluoro-4-(4-n-heptyloxyphenylazo)phenol (**37 g**) is representative for the remaining members of this fluorinated series.

ν_{max} (KBr)/cm^{-1}: 3534s,b (O-H$_{str}$), 3074w (Ar-H$_{str}$), 2953, 2934, 2857s (C-H$_{st}$), 1597, 1498s (C=C$_{st}$), 1472s (C-H$_{st}$), 1244, 1105s/m (C-O$_{str}$), 842s (C-H$_{def}$, 2 adjacent H) cm^{-1}; δ_H (270 MHz; CDCl$_3$; Me$_4$Si) 0.88 (3H, t, CH$_3$), 1.33 (8H, m, CH$_2$), 1.82 (2H, quint, <u>CH$_2$</u>-CH$_2$-O), 4.02 (2H, t, -CH$_2$<u>CH$_2$</u>OAr), 6.29 (1H, s, -OH), 6.48 (2H, d, ArH), 6.97 (2H, d, ArH), 7.89 (2H, d, ArH); δ_C (67.9 MHz: CDCl$_3$; Me$_4$Si) 14.09 (1, CH$_3$), 22.64, 25.98, 29.14, 29.21, 31.8 (CH$_2$), 68.41 (CH$_2$-

---

[§] not determined

O), 100.25 (ArC $^2J_{CF}$=24.9 Hz), 114.7 (ArC & ArC$_Q$), 124.57 (ArC), 147.6 (ArC$_Q$), 155.84-158.35 (Ar-F, $^1J_{CF}$=253 Hz, $^3J_{CF}$=8.6 Hz), 157.26 (ArC$_Q$-OH, $^3J_{CF}$=14.4 Hz), 161.99 (8, ArC$_Q$-OH); CHN: Expected: C, 66.28; H, 6.67; N, 7.73 %; Found: C, 66.18; H 6.77; N, 7.68 %; TLC (DCM), one spot, Rf; 0.14.

2.2.4 GENERAL METHOD FOR ESTERIFICATION (**SERIES I – XIII**)[82]

A mixture of the appropriate acid [either 3-(2-thienyl)acrylic acid or 3-(3-thienyl)acrylic acid or *trans*-cinnamic acid] (2.22 mmol), the appropriate 'azophenol' (**32-37**) (2.02 mmol), dicyclohexylcarbodiimide (2.22 mmol), dimethylaminopyridine (0.2 mmol) and dry CH$_2$Cl$_2$ (20 ml) was stirred at room temperature overnight. The ensuing white precipitate was isolated by Büchner filtration and discarded, whilst the filtrate was evaporated to dryness *in vacuo*. The resultant crude residue was purified by column chromatography on silica gel eluting with dichloromethane, followed by repeated recrystallisation from toluene until constant transition temperatures were achieved to give the desired esters are orange crystals. Yields of the thrice recrystallised esters were very consistent, being in the range of (55-60 %). The transition temperatures for members of **Series I**-**XIII** are listed in **Tables 2-14**, respectively of the results and discussion section.

3-(Thiophen-2-yl)-acrylic acid 4-(4-n-alkoxyphenylazo)phenyl esters (**Series I**), (**38 a-j**)

The following spectroscopic data for 3-thiophen-2-yl-acrylic acid 4-(4-n-heptyloxyphenylazo)phenyl ester (**38 g**) is representative for the remaining members of **Series I**
ν_{max} (KBr)/ cm^{-1}: 3092.5w (Ar-H$_{str}$), 2937, 2855w (C-H$_{str}$), 1730s (C=O$_{str}$), 1630s (alkene C=C$_{str}$), 1602, 1498s (C=C$_{str}$), 1256, 1112s (C-O$_{str}$), 843s (C-H$_{def}$, 2 adjacent H); δ_H (270 MHz; CDCl$_3$; Me$_4$Si) 0.9 (3H, t, CH$_3$), 1.32 (8H, m, -(CH$_2$)$_4$-), 1.84 (2H, quint, <u>CH$_2$</u>-CH$_2$-O), 4.03 (2H, t, <u>CH$_2$</u>-O), 6.43 (1H, d, <u>CH</u>=CH-O, J=16 Hz), 7.0 (2H,d, ArH), 7.1 (1H, m, ArH$_{[Thio]}$, J=4.1Hz), 7.31 (2H, d ArH), 7.32 (1H, d, ArH$_{[Thio]}$, J=3.2 Hz), 7.43 (1H, d, ArH$_{[Thio]}$, J=5.1 Hz), 7.9 (2H, d, ArH), 7.91(2H, d, ArH), 7.92 (1H, d, CH=<u>CH</u>-O, J=16 Hz); δ_C (67.9 MHz: CDCl$_3$;

Me$_4$Si) 14.08, 22.61, 25.99, 29.06, 29.21 (C$\underline{H_2}$-CH$_2$-O), 31.78 (CH$_2$), 68.39 (CH$_2$-O), 114.67 (Ar-C), 115.62 (C$\underline{H}$=CH-O), 122.14 (ArC), 123.69 (ArC), 124.76 (ArC), 128.29 (ArC$_{[Thio]}$), 129.31 (ArC$_{[Thio]}$), 131. (ArC$_{[Thio]}$), 139.23 (CH=C$\underline{H}$-O), 139.29 (ArC$_{Q[Thio]}$), 146.8 (ArC$_Q$), 150.38 (ArC$_Q$), 152.29 (ArC$_Q$), 161.75 (ArC$_Q$-O), 164.96 (CO$_2$); CHN Expected: C, 69.62; H, 6.29; N, 6.24 %; Found: C, 69.64; H, 6.24; N, 6.24 %; HRMS (ESCI) 449.1893 (M+H); TLC (DCM), one spot, Rf; 0.9.

3-(Thiophen-2-yl)-acrylic acid 4-(4-n-alkoxyphenylazo)-2-fluorophenyl esters (**Series VI**), (**42a-j**).

The following spectroscopic data for 3-thiophen-2-yl-acrylic acid 4-(4-n-butyloxyphenylazo)-2-fluorophenyl ester (**42 d**) is representative for the remaining members of **Series VI**.

ν_{max} (KBr)/cm^{-1}: 3092w (Ar-H$_{str}$), 2920, 2851w (C-H$_{str}$), 1735s (C=O$_{str}$), 1620s (alkene C=C$_{str}$), 1601, 1498s (C=C$_{str}$), 1255, 1121s (C-O$_{str}$), 838s (C-H$_{def}$, 2 adjacent H); δ_H (270 MHz; CDCl$_3$; Me$_4$Si) 0.92 (3H, t, CH$_3$), 1.41 (2H, sext, CH$_3$C$\underline{H_2}$CH$_2$-), 1.81 (2H, quint, C$\underline{H_2}$-CH$_2$-O), 4.01 (2H, t, -CH$_2$C$\underline{H_2}$OAr), 6.4 (1H, d, C$\underline{H}$=CH-O, J=15 Hz), 7.0 (2H, d, ArH), 7.09 (3H, m, ArH & ArH$_{[Thio]}$), 7.34 (1H, d, ArH$_{[Thio]}$ J=4.0 Hz), 7.45 (1H, d, ArH$_{[Thio]}$ J=6.0 Hz), 7.8 (1H, t, ArH), 7.93 (2H, d, ArH), 8.0 (1H, d, CH=C$\underline{H}$-O, J=15 Hz); δ_C (67.9 MHz: CDCl$_3$; Me$_4$Si) 14.07, 22.65, 31.8 (C$\underline{H_2}$-CH$_2$-O), 68.41 (CH$_2$-O), 110.7 (ArC, $^2J_{CF}$=22.8 Hz), 114.76 (ArC), 115.2 (C$\underline{H_2}$=CH$_2$-O), 117.65 (ArC, $^4J_{CF}$=3.1 Hz), 118.22 (ArC), 125.13 (ArC), 128.34 (ArC$_{[Thio]}$), 129.53 (ArC$_{[Thio]}$), 131.9 (ArC$_{[Thio]}$), 138.5 (ArC$_Q$, $^2J_{CF}$=7.27Hz), 139.14 (ArC$_{Q[Thio]}$), 139.68 (CH=C$\underline{H}$-O), 147.1 (ArC$_Q$), 152.9 (ArC$_Q$, $^3J_{CF}$=11.4 Hz), 157.87+161.68 (Ar-F, $^1J_{CF}$=258 Hz), 162.14 (ArC$_Q$-O), 164.49 (CO$_2$). C$_{23}$H$_{21}$FN$_2$O$_3$S expected: C, 65.08; H, 4.99; F, 4.48; N, 6.60 %; found: C, 64.99; H, 4.95; N, 6.61 %; HRMS (ESCI) 425.1335 (M+H); Heptyloxy homologue (**42 g**), C$_{26}$H$_{27}$FN$_2$O$_3$S expected C, 66.93; H, 5.83; N, 6.0 %; found: C, 66.93; H, 5.78; N, 5.91 %; TLC (DCM), one spot, Rf; 0.85.

3-(Thiophen-2-yl)-acrylic acid 4-(4-n-alkoxyphenylazo)-3-fluorophenyl esters **(Series IV)**, **(41 a-j)**.

The following spectroscopic data for 3-thiophen-2-yl-acrylic acid 3-fluoro-4-(4-n-butyloxyphenylazo)-3-fluorophenyl ester (**41 d**) is representative for the remaining members of **Series IV**.

ν_{max} (KBr)/ cm^{-1} 3061w (Ar-H$_{str}$), 2927, 2858w (C-H$_{str}$), 1735s (C=O$_{str}$), 1623s (alkene C=C$_{str}$), 1596, 1493s (C=C$_{str}$), 1268-1122s (C-O$_{str}$), 878s (C-H$_{def}$, 2 adjacent H); δ_H (270 MHz; CDCl$_3$; Me$_4$Si) 0.92 (3H, t, CH$_3$), 1.41 (2H, sext, CH$_3$CH$_2$CH$_2$-), 1.81 (2H, quint, CH$_2$-CH$_2$-O), 4.01 (2H, t, -CH$_2$CH$_2$OAr), 6.46(1H, d, CH$_2$=CH$_2$-O, J=16.0 Hz), 7.0 (2H, d, ArH), 7.08 (1H, t, ArH$_{[Thio]}$, J=3.7 Hz), 7.36 (2H, m, ArH$_{[Thio]}$ & Ar-H), 7.45 (1H, d, Ar-H), 7.72 (2H, m, ArH & Ar-H), 7.89 (2H, d, ArH), 7.9 (1H, d, CH=CH-O, J=16.0 Hz); δ_C (67.9 MHz: CDCl$_3$; Me$_4$Si) 14.07, 22.65, 31.8 (CH$_2$-CH$_2$-O), 68.41 (CH$_2$-O), 108.9 (ArC $^2J_{CF}$=19.7 Hz), 114.64 (ArC), 114.77 (CH$_2$=CH$_2$-O), 120.64 (ArC $^4J_{CF}$=3.1 Hz), 123.86 (ArC), 125.01 (Ar-C), 125.18 (ArC$_{[Thio]}$), 127.28 (ArC$_{[Thio]}$), 129.38 (ArC$_{[Thio]}$) ,139.15 (ArC$_{Q[Thio]}$), 139.6 (ArC$_Q$, $^2J_{CF}$=13.5 Hz), 139.89 (CH=CH-O, J=15.6 Hz), 146.51 (ArC$_Q$), 151.3 (ArC$_Q$, $^3J_{CF}$= 5.2 Hz), 152.74+156.44 (Ar-F, $^1J_{CF}$=250 Hz), 162.14 (ArC$_Q$-O), 164.37 (CO$_2$); C$_{23}$H$_{21}$FN$_2$O$_3$S expected C, 65.08; H, 4.99; F, 4.48; N, 6.60 %; Found: C, 65.08; H, 4.94; N, 6.66 %; HRMS (ESCI) 425.1326 (M+H); Heptyloxy homologue (**41 g**), C$_{26}$H$_{27}$FN$_2$O$_3$S expected C, 66.93; H, 5.83; N, 6.0 %; found: C, 67.0; H, 5.9; N, 5.85 %; TLC (DCM), one spot, Rf; 0.88.

3-(Thiophen-2-yl)-acrylic acid 4-(4-n-alkoxyphenylazo)-2,3-difluorophenyl esters **(Series VIII)**, **(43 a-j)**.

The following spectroscopic data for 3-thiophen-2-yl-acrylic acid 4-(4-n-butyloxyphenylazo)-2,3-difluorophenyl ester (**43 d**) is representative for the remaining members of **Series VIII**.

ν_{max} (KBr)/ cm^{-1} 3071w (Ar-H$_{str}$), 2928, 2859w (C-H$_{str}$), 1739s (C=O$_{str}$), 1621s (alkene C=C$_{str}$), 1598, 1496s (C=C$_{str}$), 1259, 1115s (C-O$_{str}$), 853s (C-H$_{def}$, 2 adjacent H); δ_H (270 MHz; CDCl$_3$; Me$_4$Si) 0.92 (3H, t, CH$_3$), 1.41 (2H, sext, CH$_3$CH$_2$CH$_2$-), 1.81 (2H, quint, CH$_2$-CH$_2$-O), 4.01

(2H, t, -CH$_2$$\underline{CH_2}$OAr), 6.42 (1H, d, $\underline{CH_2}$=CH$_2$-O J= 16.0 Hz), 7.0 (2H, d, ArH), 7.09 (2H, m, ArH & ArH$_{[Thio]}$), 7.35 (1H, d, ArH$_{[Thio]}$ J=3.5 Hz), 7.45 (1H, d, ArH$_{[Thio]}$ J=5.0 Hz), 7.55 (1H, t, ArH), 7.93 (2H, d, ArH), 8.1 (1H, d, CH=$\underline{CH}$=O, J= 16.0 Hz); δ_C (67.9 MHz: CDCl$_3$; Me$_4$Si) 14.07, 22.65, 31.8 ($\underline{CH_2}$-CH$_2$-O), 68.41 (CH$_2$-O), 111.7 (ArC $^3J_{CF}$=4.16Hz), 114 ($\underline{CH}$=CH-O), 114.8 (ArC), 118.03 (ArC $^3J_{CF}$=4.16Hz), 125.4 (ArC), 128.34 (ArC$_{[Thio]}$), 129.76 (ArC$_{[Thio]}$), 132.17 (ArC$_{[Thio]}$), 139 (ArC$_{Q[Thio]}$), 139.7 (ArC$_Q$, $^2J_{CF}$=5.2Hz), 140.3 (CH=$\underline{CH}$-O), 140.5 (ArC$_Q$, $^2J_{CF}$=14.5 Hz), 140.67-145.97 (Ar-F, $^1J_{CF}$=252.0 Hz, $^3J_{CF}$=12.5 Hz), 146.92 (ArC$_Q$), 147 & 150.87 (Ar-F, $^1J_{CF}$=257.0 Hz, $^3J_{CF}$=11.4 Hz), 162.47 (ArC$_Q$-O), 163.57 (CO$_2$); C$_{23}$H$_{20}$F$_2$N$_2$O$_3$S expected C, 62.43; H, 4.56; F, 8.59; N, 6.33 %; Found: C, 62.39; H, 4.49; N, 6.35 %; HRMS (ESCI) 443.1232 (M+H); Heptyloxy homologue (**43 g**), C$_{26}$H$_{26}$F$_2$N$_2$O$_3$S expected C, 64.45; H, 5.41; N, 5.78 %; found: C, 64.52; H, 5.35; N, 5.76 %; TLC (DCM), one spot, Rf; 0.85.

3-(Thiophen-2-yl)-acrylic acid 4-(4-n-alkoxyphenylazo)-3,5-difluorophenyl esters (**Series XII**), (**45 a-j**).

The following spectroscopic data for 3-thiophen-2-yl-acrylic acid 4-(4-n-butyloxyphenylazo)-3,5-difluorophenyl ester (**45 d**) is representative for the remaining members of **Series XII**.

ν_{max} (KBr)/cm^{-1} 3123w (Ar-H$_{str}$), 2950, 2853w (C-H$_{str}$), 1734s (C=O$_{str}$), 1616s (alkene C=C$_{str}$), 1597, 1502s (C=C$_{str}$), 1255, 1122s (C-O$_{str}$), 834s (C-H$_{def}$, 2 adjacent H); δ_H (270 MHz; CDCl$_3$; Me$_4$Si) 0.92 (3H, t, CH$_3$), 1.41 (2H, sext, CH$_3$$\underline{CH_2}CH_2$-), 1.81 (2H, quint, $\underline{CH_2}$-CH$_2$-O), 4.01 (2H, t, -CH$_2$$\underline{CH_2}$OAr), 6.52 (1H, d, $\underline{CH}$=CH-O J= 16.0 Hz), 7.0 (2H, d, ArH), 7.05 (2H, d, ArH), 7.1 (1H, t, ArH$_{[Thio]}$, J=5.64Hz), 7.34 (2H, d, ArH$_{[Thio]}$ J=3.5Hz), 7.47 (1H, d, ArH$_{[Thio]}$, J=5.0 Hz), 7.49 (1H, d, ArH$_{[Thio]}$) 7.88 (2H, d, ArH), 7.89 (1H, d, CH=$\underline{CH}$-O, J= 16.0 Hz); δ_C (67.9 MHz: CDCl$_3$; Me$_4$Si) 14.07, 22.65, 31.8 ($\underline{CH_2}$-CH$_2$-O), 68.41 (CH$_2$-O), 106.47 (ArC $^2J_{CF}$=23.9 Hz), 113.75 ($\underline{CH_2}$=CH$_2$-O), 114.83 (ArC), 124.06 (ArC$_Q$), 125.3 (ArC), 128.34 (ArC$_{[Thio]}$), 129.8 (ArC$_{[Thio]}$), 132.2 (ArC$_{[Thio]}$), 139.04 (ArC$_{Q[Thio]}$), 140.53 (CH=$\underline{CH}$-O), 146.26 (ArC$_Q$), 150.36 (ArC$_Q$, $^3J_{CF}$=7.3 Hz), 153.65 & 157.42 (Ar-F, $^1J_{CF}$=251.2 Hz, $^3J_{CF}$=5.2 Hz), 162.52 (ArC$_Q$-O), 163.07 (CO$_2$). C$_{23}$H$_{20}$F$_2$N$_2$O$_3$S expected C, 62.43; H, 4.56; F, 8.59; N, 6.33 %; Found: C, 61; H, 4.34; N, 6.18 %; HRMS (ESCI) 443.1238 (M+H); Heptyloxy homologue (**45**

54

g), $C_{26}H_{26}F_2N_2O_3S$ expected C, 64.45; H, 5.41; N, 5.78 %; found: C, 64.53; H, 5.4; N, 5.75 %; TLC (DCM), one spot, Rf; 0.85.

3-(Thiophen-2-yl)-acrylic acid 4-(4-n-alkoxyphenylazo)-2,6-difluorophenyl esters (**Series X**), (**44 a-j**).

The following spectroscopic data for 3-thiophen-2-yl-acrylic acid 4-(4-n-butyloxyphenylazo)-2,6-difluorophenyl ester (**44 d**) is representative for the remaining members of **Series X**.

ν_{max} (KBr)/ cm^{-1}: 3092w (Ar-H$_{str}$), 2937, 2865w (C-H$_{str}$), 1730s (C=O$_{str}$), 1630s (alkene C=C$_{str}$), 1602, 1498s (C=C$_{str}$), 1256, 1125s (C-O$_{str}$), 842s (C-H$_{def}$, 2 adjacent H); δ_H (270 MHz; CDCl$_3$; Me$_4$Si) 0.92 (3H, t, CH$_3$), 1.41 (2H, sext, CH$_3$$\underline{CH_2}CH_2$-), 1.81 (2H, quint, $\underline{CH_2}$-CH$_2$-O), 4.01 (2H, t, -CH$_2$$\underline{CH_2}$OAr), 6.38 (1H, d, $\underline{CH}$=CH-O, J= 16.0 Hz), 6.94 (2H, d, ArH), 6.97 (2H,d, ArH), 7.09 (1H, t, ArH$_{[Thio]}$ J=5.6 Hz), 7.35 (1H, d, ArH$_{[Thio]}$ J=4.7 Hz), 7.45 (1H, d, ArH$_{[Thio]}$, J=4.7 Hz), 7.89 (2H, d, ArH, J=8.9 Hz), 7.97 (1H, d, CH=$\underline{CH}$-O, J= 16.0 Hz); δ_C (67.9 MHz: CDCl$_3$; Me$_4$Si) 14.07, 22.65, 31.8 ($\underline{CH_2}$-CH$_2$-O), 68.41 (CH$_2$-O), 106.7 (ArC $^2J_{CF}$=28.0 Hz & $^3J_{CF}$=3.1 Hz), 114.7 (9, ArC & 17, $\underline{CH}$=CH-O), 125.04 (ArC & ArC$_Q$), 128.38 (ArC$_{[Thio]}$), 129.77 (ArC$_{[Thio]}$), 132.19 (ArC$_{[Thio]}$), 139 (ArC$_{Q[Thio]}$), 140.1 (CH=$\underline{CH}$-O), 147.6 (ArC$_Q$), 150.8 (ArC$_Q$, $^3J_{CF}$=13.5Hz), 154.0 & 157.74 (13, Ar-F, $^1J_{CF}$=258Hz, $^3J_{CF}$=7.26Hz), 162.52 (ArC$_Q$-O), 164.1 (CO$_2$). $C_{23}H_{20}F_2N_2O_3S$ expected C, 62.43; H, 4.56; F, 8.59; N, 6.33 %; Found: C, 62.35; H, 4.47; N, 6.28 %; HRMS (ESCI) 443.1235 (M+H); Heptyloxy homologue (**44 g**), $C_{26}H_{26}F_2N_2O_3S$ expected C, 64.45; H, 5.41; N, 5.78 %; found: C, 64.41; H, 5.4; N, 5.74 %; TLC (DCM), one spot, Rf; 0.89.

3-(Thiophen-3-yl)-acrylic acid 4-(4-n-alkoxyphenylazo)phenyl esters (**Series II**), (**39 a-j**).

The following spectroscopic data for 3-thiophen-3-yl-acrylic acid 4-(4-n-heptyloxyphenylazo)phenyl ester (**39 g**) is representative for the remaining members of **Series II**.

ν_{max} (KBr)/ cm^{-1} 3092.5w (Ar-H$_{str}$), 2937, 2855w (C-H$_{str}$), 1730s (C=O$_{str}$), 1630s (alkene C=C$_{str}$), 1602, 1498s (C=C$_{str}$), 1256, 1125s (C-O$_{str}$), 843s (C-H$_{def}$, 2 adjacent H); δ_H (270 MHz;

CDCl$_3$; Me$_4$Si) 0.92 (3H, t, CH$_3$), 1.35 (8H, m, -(CH$_2$)$_4$-), 1.82 (2H, quint, C̲H̲$_2$-CH$_2$-O), 4.04 (2H, t, CH$_2$-O), 6.46 (1H, d, C̲H̲=CH-O, J=16.0 Hz), 7.0 (2H, d, ArH) 7.33 (2H, d ArH), 7.38 (2H, m, ArH$_{[Thio]}$), 7.59 (1H, t, ArH$_{[Thio]}$, J=2.1 Hz), 7.87 (1H, d, CH=C̲H̲-O, J=15.8 Hz), 7.91 (2H, d, ArH), 7.3 (2H, d, ArH); δ$_C$ (67.9 MHz: CDCl$_3$; Me$_4$Si) 14.06, 22.61, 25.7, 29.06, 29.15 (C̲H̲$_2$-CH$_2$-O), 31.58 (CH$_2$), 68.33 (CH$_2$-O), 114.7 (ArC), 116.62 (C̲H̲$_2$=CH$_2$-O), 122.17 (ArC), 123.69 (ArC), 124.77 (ArC), 125.15 (ArC$_{[Thio]}$), 127.26(20, ArC$_{[Thio]}$), 129.14 (22, Ar-C$_{[Thio]}$), 137.31 (ArC$_{Q[Thio]}$), 140.29 (CH=C̲H̲-O), 146.76 (ArC$_Q$), 150.35 (ArC$_Q$), 152.27 (ArC$_Q$), 161.75 (ArC$_Q$-O), 164.36 (CO$_2$). C$_{26}$H$_{28}$N$_2$O$_3$S expected: C, 69.62; H, 6.29; N, 6.24 %; Found C, 69.62; H, 6.29; N, 6.24 %; HRMS (ESCI) 449.1901 (M+H); TLC (DCM), one spot, Rf; 0.88.

3-(Thiophen-3-yl)-acrylic acid 4-(4-n-alkoxyphenylazo)-2-fluorophenyl esters **(Series VII)**, **(47 a-j)**.

The following spectroscopic data for 3-thiophen-3-yl-acrylic acid 2-fluoro-4-(4-n-butyloxyphenylazo)-phenyl ester (**47 d**) is representative for the remaining members of **Series VII**.

ν$_{max}$ (KBr)/cm^{-1}: 3092w (Ar-H$_{str}$), 2937, 2855w (C-H$_{str}$), 1730s (C=O$_{str}$), 1630s (alkene C=C$_{str}$), 1602, 1498s (C=C$_{str}$), 1256, 1125s (C-O$_{str}$), 843s (C-H$_{def}$, 2 adjacent H); δ$_H$ (270 MHz; CDCl$_3$; Me$_4$Si) 0.92 (3H, t, CH$_3$), 1.41 (2H, sext, CH$_3$C̲H̲$_2$CH$_2$-), 1.81 (2H, quint, C̲H̲$_2$-CH$_2$-O), 4.01 (2H, t, -CH$_2$C̲H̲$_2$OAr), 6.4 (1H, d, C̲H̲=CH-O, J=16.0 Hz), 7.0 (2H, d, ArH), 7.04 (1H, m, ArH), 7.15 (1H, d, ArH), 7.36 (2H, m, ArH$_{[Thio]}$), 7.59 (1H, m, ArH$_{[Thio]}$), 7.8 (1H, d, ArH), 7.86 (1H, d, CH=C̲H̲-O, J=16.0 Hz), 7.93 (2H, d, ArH); δ$_C$ (67.9 MHz: CDCl$_3$; Me$_4$Si) 14.07, 22.65, 31.8 (C̲H̲$_2$-CH$_2$-O), 68.41 (CH$_2$-O), 110.7 (ArC, ^{2}J$_{CF}$=23.9 Hz), 114.72 (9, ArC), 116.17 (19, C̲H̲=CH-O), 117.65 (Ar-H, ^{4}J$_{CF}$=3.1 Hz), 118.16 (ArC), 125.12 (ArC & ArC$_{[Thio]}$), 127.34 (ArC$_{[Thio]}$), 129.34 ArC$_{[Thio]}$), 137.2 (ArC$_{Q[Thio]}$), 138.5 (ArC$_Q$, ^{2}J$_{CF}$=7.3 Hz), 140.7 (CH=C̲H̲-O), 147.06 (ArC$_Q$), 152.9 (ArC$_Q$, ^{2}J$_{CF}$=11.4 Hz), 157.86+161.67 (Ar-F, ^{1}J$_{CF}$=258.0 Hz), 162.11 (ArC$_Q$-O), 164.84 (CO$_2$); C$_{23}$H$_{21}$FN$_2$O$_3$S expected C, 65.08; H, 4.99; F, 4.48; N, 6.60 %;. Found: C, 65.12; H, 4.96; N, 6.64%; HRMS (ESCI) 425.1323 (M+H); Heptyloxy homologue

(**47 g**), $C_{26}H_{27}FN_2O_3S$ expected C, 66.93; H, 5.83; N, 6.0 %; found: C, 66.8; H, 5.79; N, 5.9 %; TLC (DCM), one spot, Rf; 0.84.

3-(Thiophen-3-yl)-acrylic acid 4-(4-n-alkoxyphenylazo)-3-fluorophenyl esters (**Series V**), (**46 a-j**).

The following spectroscopic data for 3-thiophen-3-yl-acrylic acid 4-(4-n-butyloxyphenylazo)-3-fluorophenyl ester (**46 d**) is representative for the remaining members of **Series V**.

ν_{max} (KBr)/ cm^{-1}: 3093w (C-H$_{str}$), 2919, 2857w (aliph C-H$_{str}$) 1736s (C=O$_{str}$), 1630s (alkene C=C$_{str}$), 1595, 1493s (C=C$_{str}$), 1298, 1121s (C-O$_{str}$), 838s (C-H$_{def}$, 2 adjacent H); δ_H (270 MHz; CDCl$_3$; Me$_4$Si) 0.92 (3H, t, CH$_3$), 1.41 (2H, sext, CH$_3$CH$_2$CH$_2$-), 1.81 (2H, quint, CH$_2$-CH$_2$-O), 4.01 (2H, t, -CH$_2$CH$_2$OAr), 6.46 (1H, d, CH=CH-O J=15.8 Hz), 7.0 (2H,d, ArH), 7.04 (3H, m, ArH & ArH$_{[Thio]}$), 7.36 (1H, t, ArH$_{[Thio]}$J=1.9 Hz), 7.72 (2H, m, ArH), 7.87 (1H, d, CH=CH-O, J=15.8Hz), 7.9 (2H, d, ArH); δ_C (67.9 MHz: CDCl$_3$; Me$_4$Si) 14.07, 22.65, 31.8 (CH$_2$-CH$_2$-O), 68.41 (CH$_2$-O), 108.9 (ArC $^2J_{CF}$=19.72Hz), 114.77 (ArC), 115.62 (CH=CH-O, J=16.0 Hz), 120.68 (ArC, $^4J_{CF}$=3.1 Hz), 123.87 (ArC), 125.01 (ArC), 125.18 (ArC$_{[Thio]}$), 127.28 (ArC$_{[Thio]}$), 129.38 (ArC$_{[Thio]}$), 137.25 (ArC$_{Q[Thio]}$), 139.6 (ArC$_Q$, $^2J_{CF}$=14.5 Hz), 140.94 (CH=CH-O, J=16.2 Hz), 146.51 (ArC$_Q$), 151.3 (ArC$_Q$, $^3J_{CF}$= 5.2 Hz), 152.74+156.44 (Ar-F, $^1J_{CF}$=251.0 Hz), 162.14 (ArC$_Q$-O), 164.37 (CO$_2$). $C_{23}H_{21}FN_2O_3S$ expected C, 65.08; H, 4.99; F, 4.48; N, 6.60 %;. Found: C, 65.11; H, 4.9; N, 6.59 %; HRMS (ESCI) 425.1332 (M+H); Heptyloxy homologue (**46 g**), $C_{26}H_{27}FN_2O_3S$ expected C, 66.93; H, 5.83; N, 5.78 %; found: C, 66.97; H, 5.82; N, 5.93 %; TLC (DCM), one spot, Rf; 0.91.

3-(Thiophen-3-yl)-acrylic acid 4-(4-n-alkoxyphenylazo)-2,3-difluorophenyl esters (**Series IX**), (**48 a-j**).

The following spectroscopic data for 3-thiophen-3-yl-acrylic acid 4-(4-n-butyloxyphenylazo)-2,3-difluorophenyl ester (**48 d**) is representative for the remaining members of **Series IX**.

ν_{max} (KBr)/ cm^{-1}: 3091w (Ar-H$_{str}$), 2953, 2857w (C-H$_{str}$), 1733s (C=O$_{str}$), 1629s (alkene C=C$_{str}$), 1601, 1498s (C=C$_{str}$), 1257,1118s (C-O$_{str}$), 841s (C-H$_{def}$, 2 adjacent H); δ_H (270 MHz; CDCl$_3$;

Me$_4$Si) 0.92 (3H, t, CH$_3$), 1.41 (2H, sext, CH$_3$$\underline{CH_2}CH_2$-), 1.81 (2H, quint, $\underline{CH_2}$-CH$_2$-O), 4.01 (2H, t, -CH$_2$$\underline{CH_2}$OAr), 6.46 (1H, d, $\underline{CH}$=CH-O J=15.8 Hz), 7.0 (2H,d, ArH), 7.06 (1H, m, ArH), 7.36 (2H, m, ArH$_{[Thio]}$), 7.59 (2H, m, ArH$_{[Thio]}$ & ArH), 7.89 (1H, d, CH=$\underline{CH}$-O, J=15.8 Hz), 7.93 (2H, d, ArH); δ_C (67.9 MHz: CDCl$_3$; Me$_4$Si) 14.07, 22.65, 31.8 ($\underline{CH_2}$-CH$_2$-O), 68.41 (CH$_2$-O), 111.7 (ArC$_Q$, $^4J_{CF}$=4.15 Hz), 114.7 (ArC), 116.62 ($\underline{CH}$=CH-O), 118 (ArC$_Q$, $^4J_{CF}$=4.15 Hz), 125.15 (ArC$_{[Thio]}$), 125.4 (ArC), 127.34 (ArC$_{[Thio]}$), 129.64 (ArC$_{[Thio]}$), 137.12 (ArC$_{Q[Thio]}$), 139.75 (ArC$_Q$, $^2J_{CF}$=5.2 Hz),　140.6 (ArC$_Q$, $^2J_{CF}$=10.4 Hz), 140.7 (CH=$\underline{CH}$-O), 141.36-146 (Ar-F, $^1J_{CF}$=238.8 Hz, $^2J_{CF}$=12.5 Hz), 146.9 (ArC$_Q$), 147.1-150.89 (Ar-F, $^1J_{CF}$=249.0 Hz, $^2J_{CF}$=11.4 Hz), 162.5 (ArC$_Q$-O), 163.97 (CO$_2$); C$_{23}$H$_{20}$F$_2$N$_2$O$_3$S expected C, 62.43; H, 4.56; F, 8.59; N, 6.33 %; Found: C, 62.36; H, 4.58; N, 6.35 %; HRMS (ESCI) 443.1231 (M+H); Heptyloxy homologue (**48 g**), C$_{26}$H$_{26}$F$_2$N$_2$O$_3$S expected C, 64.45; H, 5.41; N, 5.78 %; found: C, 64.47; H, 5.41; N, 5.75 %; TLC (DCM), one spot, Rf; 0.85.

3-(Thiophen-3-yl)-acrylic acid 4-(4-n-alkoxyphenylazo)-3,5-difluorophenyl esters (**Series XIII**), (**50 a-j**).

The **following** spectroscopic data for 3-thiophen-3-yl-acrylic acid 4-(4-n-butyloxyphenylazo)-3,5-difluorophenyl ester (**50 d**) is representative for the remaining members of **Series XIII**.

ν_{max} (KBr)/ cm^{-1}: 3102w (Ar-H$_{str}$), 2927, 2856w (C-H$_{str}$) 1742s (C=O$_{str}$), 1629s (alkene C=C$_{str}$) 1599, 1498s (C=C$_{str}$), 1251, 1115s (C-O$_{str}$), 872 (C-H$_{def}$, 2 adjacent H); δ_H (270 MHz; CDCl$_3$; Me$_4$Si) 0.92 (3H, t, CH$_3$), 1.41 (2H, sext, CH$_3$$\underline{CH_2}CH_2$-), 1.81 (2H, quint, $\underline{CH_2}$-CH$_2$-O), 4.01 (2H, t, -CH$_2$$\underline{CH_2}$OAr), 6.52 (1H, d, $\underline{CH}$=CH-O J=15.8 Hz), 7.0 (2H, d, ArH), 7.37 (2H, m, ArH$_{[Thio]}$), 7.57 (2H, ArH), 7.59 (1H, m, ArH$_{[Thio]}$), 7.88 (2H, d, ArH), 7.89 (1H, d, CH=$\underline{CH}$-O, J=15.8 Hz); δ_C (67.9 MHz: CDCl$_3$; Me$_4$Si) 14.07, 22.65, 31.8 ($\underline{CH_2}$-CH$_2$-O), 68.41 (CH$_2$-O), 106.6 (ArC $^2J_{CF}$=23.9 Hz), 114.8 (ArC & $\underline{CH}$=CH-O), 124.05 (ArC$_Q$), 125.16 (ArC$_{[Thio]}$), 125.2 (ArC), 127.31 (ArC$_{[Thio]}$), 129.67 (ArC$_{[Thio]}$), 137.14 (ArC$_{Q[Thio]}$), 141.59 (CH=$\underline{CH}$-O), 150.33 (ArC$_Q$), 150.33 (ArC$_Q$, $^3J_{CF}$=5.19 Hz), 153.64+157.42 (Ar-F, $^1J_{CF}$=246 Hz, $^3J_{CF}$=5.2 Hz), 162.51 (ArC$_Q$-O), 163.44 (CO$_2$). C$_{23}$H$_{20}$F$_2$N$_2$O$_3$S expected C, 62.43; H, 4.56; F, 8.59; N, 6.33 %;

Found: C, 62.41; H, 4.52; N, 6.27 %; HRMS (ESCI) 443.1240 (M+H); Heptyloxy homologue (**50 g**), $C_{26}H_{26}F_2N_2O_3S$ expected C, 64.45; H, 5.41; N, 5.78 %; found: C, 64.51; H, 5.41; N, 5.8 %; TLC (DCM), one spot, Rf; 0.87.

3-(Thiophen-3-yl)-acrylic acid 4-(4-n-alkoxyphenylazo)-2,6-difluorophenyl esters (**Series XI**), (**49 a-j**).

The following spectroscopic data for 3-thiophen-3-yl-acrylic acid 4-(4-n-butyloxyphenylazo)-2,6-difluorophenyl ester (**49 d**) is representative for the remaining members of Series **XI**.

ν_{max} (KBr)/ cm^{-1} 3093w (Ar-H$_{str}$), 2937, 2865w (C-H$_{str}$), 1730s (C=O$_{str}$), 1630s (alkene C=C$_{str}$), 1602, 1498s (C=C$_{str}$), 1256, 1125s (C-O$_{str}$), 843s (C-H$_{def}$, 2 adjacent H); δ_H (270 MHz; CDCl$_3$; Me$_4$Si) 0.92 (3H, t, CH$_3$), 1.41 (2H, sext, CH$_3$CH$_2$CH$_2$-), 1.81 (2H, quint, CH$_2$-CH$_2$-O), 4.01 (2H, t, -CH$_2$CH$_2$OAr), 6.4 (1H, d, CH=CH-O, J=16.0 Hz), 6.94 (2H, d, ArH), 7.0 (2H, d, ArH), 7.09 (1H, d, ArH$_{[Thio]}$, J=5.6 Hz), 7.35 (1H, d, ArH$_{[Thio]}$, J=3.7 Hz), 7.62 (1H, m, ArH$_{[Thio]}$), 7.88 (1H, d, CH=CH-O, J=16.0 Hz), 7.93 (2H, d, ArH); δ_C (67.9 MHz: CDCl$_3$; Me$_4$Si) 14.07, 22.65, 31.8 (CH$_2$-CH$_2$-O), 68.41 (CH$_2$-O), 106.7 (ArC $^2J_{CF}$=27.8 Hz), 114.8 (ArC), 115.85 (CH=CH-O), 125.13 (ArC), 125.21 (ArC$_{[Thio]}$), 127.5 (ArC$_{[Thio]}$), 129.38 (ArC$_Q$), 129.8 (ArC$_{[Thio]}$), 137.2 (ArC$_{Q[Thio]}$), 140.25 (CH=CH-O), 147.69 (ArC$_Q$), 150.9 (ArC$_Q$, $^3J_{CF}$=13.4 Hz), 154.68+157.32, (Ar-F, $^1J_{CF}$=252.7 Hz, & $^3J_{CF}$=7.7 Hz), 162.63 (ArC$_Q$-O), 1634.14 (CO$_2$). $C_{23}H_{20}F_2N_2O_3S$ expected C, 62.43; H, 4.56; F, 8.59; N, 6.33 %; Found: C, 62.39; H, 4.46; N, 6.3 %; HRMS (ESCI) 443.1232 (M+H); Heptyloxy homologue (**49 g**), $C_{26}H_{26}F_2N_2O_3S$ expected C, 64.45; H, 5.41; N, 5.78 %; found: C, 64.41; H, 5.4; N, 5.74 %; TLC (DCM), one spot, Rf; 0.90.

4-(4-n-Alkoxyphenylazo)phenyl cinnamates (**Series III**), (**40 a-j**).

The following spectroscopic data for 4-(4-n-heptyloxyphenylazo)phenyl cinnamate (**40 g**) is representative for the remaining members of **Series III**.

ν_{max} (KBr)/cm^{-1} 3094 w (Ar-H$_{str}$), 2937, 2855w (C-H$_{str}$), 1730s (C=O$_{str}$), 1630s (alkene C=C$_{str}$), 1602, 1498s (C=C$_{str}$), 1256, 1125s (C-O$_{str}$), 843s (C-H$_{def}$, 2 adjacent H); δ_H (270 MHz; CDCl$_3$;

Me$_4$Si) 0.92 (3H, t, CH$_3$), 1.35 (8H, m, -(CH$_2$)$_4$-, 1.82 (2H, quint, C<u>H</u>$_2$-CH$_2$-O), 4.04 (2H, t, C<u>H</u>$_2$-O), 6.46 (1H, d, C<u>H</u>=CH-O, J=15.8 Hz), 7.0 (2H, d, ArH), 7.33 (2H, d, ArH), 7.44 (3H, m, 2H, ArH), 7.61 (2H, t, ArH), 7.87 (1H, d, CH=C<u>H</u>-O, J=15.8 Hz), 7.91 (2H, d, ArH), 7.3 (2H, d, ArH); δ$_C$ (67.9 MHz: CDCl$_3$; Me$_4$Si) 14.06, 22.61, 25.7, 29.06, 29.15 (C<u>H</u>$_2$-CH$_2$-O), 31.58 (CH$_2$), 68.33 (CH$_2$-O), 114.7 (ArC), 117.02 (C<u>H</u>=CH-O), 122.16 (ArC), 123.69 (ArC), 124.75 (ArC), 128.34 (ArC), 129.01 (ArC), 130.8 (ArC), 134.07 (ArC$_Q$), 146.73 (ArC$_Q$), 146.95 (CH=C<u>H</u>-O), 150.37 (ArC$_Q$), 152.23 (ArC$_Q$), 161.74 (ArC$_Q$-O), 165.11 (CO$_2$). C$_{28}$H$_{30}$N$_2$O$_3$ expected C, 75.99; H, 6.83; N, 6.33 %; Found C, 75.96; H, 6.76; N, 6.25 %; HRMS (ESCI) 423.2327 (M+H); TLC (DCM), one spot, Rf; 0.85.

HO—⟨benzene⟩—NO$_2$

i. C$_n$H$_{2n+1}$Br, K$_2$CO$_3$
acteone, reflux

C$_n$H$_{2n+1}$O—⟨benzene⟩—NO$_2$ (**30 a-j**, where n = 1-10)

ii. 10% Pd/C, H$_2$,
EtOH, rt

C$_n$H$_{2n+1}$O—⟨benzene⟩—NH$_2$ (**31 a-j**, where n = 1 -10)

iii. a. NaNO$_2$, HCl, 0-5°C
b. C$_6$H$_{5-x}$F$_x$OH, NaOH
0-5°C, where x = 0,1,2

C$_n$H$_{2n+1}$O—⟨benzene⟩—N=N—⟨benzene (a,b,c,d,F)⟩—OH

where: a,b,c,d = H and n = 1-10 (**32 a-j**);
a- =F   and n = 1-10 (**33 a-j**);
b- =F   and n = 1-10 (**34 a-j**);
a,b- =F   and n = 1-10 (**35 a-j**);
b,c- =F   and n = 1-10 (**36 a-j**);
a,d- =F   and n = 1-10 (**37 a-j**)

iv. ArCH=CHCO$_2$H, DCC,
DMAP, CH$_2$Cl$_2$, rt

C$_n$H$_{2n+1}$O—⟨benzene⟩—N=N—⟨benzene (a,b,c,d,F)⟩—O—C(=O)—CH=CH—Ar

Where: Ar = 2-thienyl and a,b,c,d = H (n = 1-10) [Series **I**, (**38 a-j**)];
a- =F   (n = 1-10) [Series **IV**, (**41 a-j**)];
b- =F   (n = 1-10) [Series **VI**, (**42 a-j**)];
a,b- =F   (n = 1-10) [Series **VIII**, (**43 a-j**)];
b,c- =F   (n = 1-10) [Series **X**, (**44 a-j**)];
a,d- =F   (n = 1-10) [Series **XII**, (**45 a-j**)].
Where: Ar = 3-thienyl and a,b,c,d = H (n = 1-10) [Series **II**, (**39 a-j**)];
a- =F   (n = 1-10) [Series **V**, (**46 a-j**)];
b- =F   (n = 1-10) [Series **VII**, (**47 a-j**)];
a,b- =F   (n = 1-10) [Series **IX**, (**48 a-j**)];
b,c- =F   (n = 1-10) [Series **XI**, (**49 a-j**)];
a,d- =F   (n = 1-10) [Series **XIII**, (**50 a-j**)];
Where: Ar = phenyl and a,b,c,d = H   (n = 1-10) [Series **III**, (**40 a-j**)].

Scheme 1.   Generalised pathway for the synthesis of a variety of fluoro- and non-fluoro-substituted azobenzene-containing esters (**Series I-XIII**).

2.2.5   THIOPHEN-2-YL-ACETIC, -PROPANOIC, -BUTYRIC and -PENTANOIC ACID 4-(4-n-HEPTYLOXPHENYLAZO)PHENYL ESTERS (**Series XIV**), (**51-54**)

The desired esters were prepared using a similar procedure as described earlier in section 2.2.4 (p. 21), 2-(2-Thienyl)acetic acid, 3-(2-thienyl)propanoic acid, 4-(2-thienyl)butyric acid and 5-(2-thienyl)pentanoic acid were used instead of 3-(2-thienyl)acrylic acid.   The transition temperatures are listed in **Table 20** of the results and discussion section.

3-(2-Thienyl)acetic acid 4-(4-n-heptyloxyphenylazo)-phenyl ester (**51**)

Quantities: 2-(2-thienyl)acetic acid (0.11 g, 0.8 mmol), 4-(4-n-heptyloxyphenylazo)phenol (**32 g**) (0.25 g, 0.8 mmol), DCC (0.2 g, 0.97 mmol), DMAP (0.03 g, 0.25 mmol). Yield, 0.11 g, 31 %).

ν_{max} (KBr)/ cm^{-1}: 3072.5w (Ar-H$_{str}$), 2921, 2858w (C-H$_{str}$), 1759s (C=O$_{str}$), 1602, 1583, 1492s (C=C$_{str}$), 1246-1133s (C-O$_{str}$), 841s (2 adjacent H); δ_H (400 MHz; CDCl$_3$); 0.88 (3H, t, CH$_3$), 1.32 (8H, m, CH$_2$), 1.81 (6H, m, CH$_2$-CH$_2$), 4.02 (2H, t, CH$_2$-O), 4.11 (2H, s, CH$_2$-CO$_2$), 7.0 (2H, d, ArH), 7.06 (1H, d, ArH$_{[Thio]}$, J=5.0 Hz), 7.25 (2H, d, ArH), 7.26 (1H, d, ArH$_{[Thio]}$, J=5.0 Hz), 7.28 (1H, d, ArH$_{[Thio]}$, J=5.0 Hz), 7.89 (2H, d, ArH), 7.91 (2H, d, ArH); δ_C (100 MHz CDCl$_3$) 14.1, 22.6, 26, 29.03, 31.7 (CH$_2$), 35.6 (CH$_2$-CO$_2$), 68.35 (CH$_2$-O), 114.7 (ArC), 121.9 (ArC), 123.65 (ArC), 124.8 (ArC), 125.42 (ArC$_{[Thio]}$), 127 (ArC$_{[Thio]}$), 127.24 (ArC$_{[Thio]}$), 134.1 (ArC$_{Q[Thio]}$), 146.68 (ArC$_Q$), 146.69 (ArC$_Q$), 150.48 (ArC$_Q$), 151.97 (ArC$_Q$-O), 161.79 (ArC$_Q$-O), 168.64 (CO$_2$-); C$_{25}$H$_{28}$N$_2$O$_3$S Expected: C, 68.78; H, 6.46; N 6.42 %; Found: C, 68.93; H, 6.71; N, 6.46 %; TLC (DCM), one spot, Rf; 0.75.

3-(2-Thienyl)propanoic acid 4-(4-n-heptyloxyphenylazo)-phenyl ester (**52**)

Quantities: 3-(2-thienyl)propanoic acid (0.13 g, 0.8 mmol), 4-(4-n-heptyloxyphenylazo)phenol (**31g**) (0.25 g, 0.8 mmol), DCC (0.2 g, 0.97 mmol), DMAP (0.03 g, 0.25 mmol). Yield, 0.21 g, (58 %).

ν_{max} (KBr)/ cm^{-1}: 3073.5w (Ar-H$_{str}$), 2939, 2934, 2858w (C-H$_{str}$), 1759s (C=O$_{str}$), 1603, 1582, 1493s (C=C$_{str}$), 1259-1335s (C-O$_{str}$), 845s (2 adjacent H); δ_H (400 MHz; CDCl$_3$) 0.9 (3H, t, CH$_3$), 1.4 (10H, m, CH$_2$), 1.81 (2H, quin, (CH$_2$)$_x$-CH$_2$), 2.98 (2H, t, CH$_2$-$\underline{CH_2}$-CO$_2$), 3.33 (2H, t, $\underline{CH_2}$-CH$_2$-CO$_2$), 4.02 (2H, t, CH$_2$-O), 6.92 (1H, d, ArH$_{[Thio]}$ J=5.0 Hz), 6.97 (1H, m, ArH$_{[Thio]}$, J=3.4 Hz), 7.0 (2H, d, ArH), 7.18 (2H, d, ArH), 7.19 (1H, d, ArH$_{[Thio]}$, J=5.2 Hz), 7.89 (2H, d, ArH), 7.91 (2H, d, ArH); δ_C (100 MHz; CDCl$_3$) 14.1 (CH$_3$), 22.6, 24.25, 26, 25.1, 29.03 (CH$_2$), 31.7 (CH$_2$), 35.5 (CH$_2$-CH$_2$-CO$_2$), 68.35 (CH$_2$-O), 114.7 (ArC), 122 (ArC), 123.66 (ArC), 123.77 (ArC$_{[Thio]}$), 124.7 (ArC), 124.7 (ArC$_{[Thio]}$), 127.1 (ArC$_{[Thio]}$), 142.46 (ArC$_{Q[Thio]}$), 146.7 (ArC$_Q$), 150.41 (ArC$_Q$), 151.96 (ArC$_Q$), 161.76 (ArC$_Q$-O), 170.65 (CO$_2$-); C$_{26}$H$_{30}$N$_2$O$_3$S Expected: C, 69.3; H, 6.71; N, 6.22 %; Found: C, 70.1; H, 6.4; N, 6.0 %; TLC (DCM), one spot, Rf; 0.77.

4-(2-Thienyl)butyric acid 4-(4-n-heptyloxyphenylazo)-phenyl ester (**53**)

Quantities: 4-(2-thienyl)butyric acid (0.14 g, 0.8 mmol), 4-(4-n-heptyloxyphenylazo)phenol (**32 g**) (0.25 g, 0.8 mmol), DCC (0.2 g, 0.97 mmol), DMAP (0.03 g, 0.25 mmol). Yield, 0.18 g, (49 %).

ν_{max} (KBr)/ cm^{-1}: 3072.5w (Ar-H$_{str}$), 2955, 2921, 2858w (C-H$_{str}$), 1759s (C=O$_{str}$), 1602, 1583, 1492s (C=C$_{str}$), 1246-1332s (C-O$_{str}$), 841s (2 adjacent H); δ_H (400 MHz; CDCl$_3$) 0.89 (3H, t, CH$_3$), 1.32 (6H, m, (CH$_2$)$_x$-CH$_2$) 1.51 (2H, quin, CH$_2$) 1.81 (2H, quin, CH$_2$) 2.15 (2H, CH$_2$), 2.65 (2H, t, CH$_2$-O), 2.98 (2H, t, CH$_2$), 4.04 (2H, t, CH$_2$-CO$_2$), 6.84 (1H, d, ArH$_{[Thio]}$, J=3.68Hz), 6.95 (1H, t, ArH$_{[Thio]}$, J=5.0 Hz), 6.99 (2H, d, ArH), 7.14 (1H, d, ArH$_{[Thio]}$, J=5.04Hz), 7.2 (2H, d, ArH), 7.87 (2H, d, ArH), 7.9 (2H, d, ArH); δ_C (100 MHz: CDCl$_3$); 14.1 (CH$_3$), 22.6, 24.25, 26, 29.0-29.15, 31.1 (CH$_2$), 31.75 (CH$_2$ & CH$_2$-CO$_2$), 68.35 (CH$_2$-O), 114.8 (ArC), 122.07 (ArC), 123.4 (ArC$_{[Thio]}$), 123.64 (ArC), 124.26 (ArC$_{[Thio]}$ & ArC), 126.7 (ArC$_{[Thio]}$), 143.7 (ArC$_Q$), 146.7 (ArC$_{Q[Thio]}$), 150.36 (ArC$_Q$), 152.04 (ArC$_Q$), 161.75 (ArC$_Q$-O), 171.47 (CO$_2$-); C$_{27}$H$_{32}$N$_2$O$_3$S Expected: C, 69.8; H, 6.94; N, 6.03 %; Found: C, 69.97; H, 6.97; N, 5.89 %; TLC (DCM), one spot, Rf; 0.96.

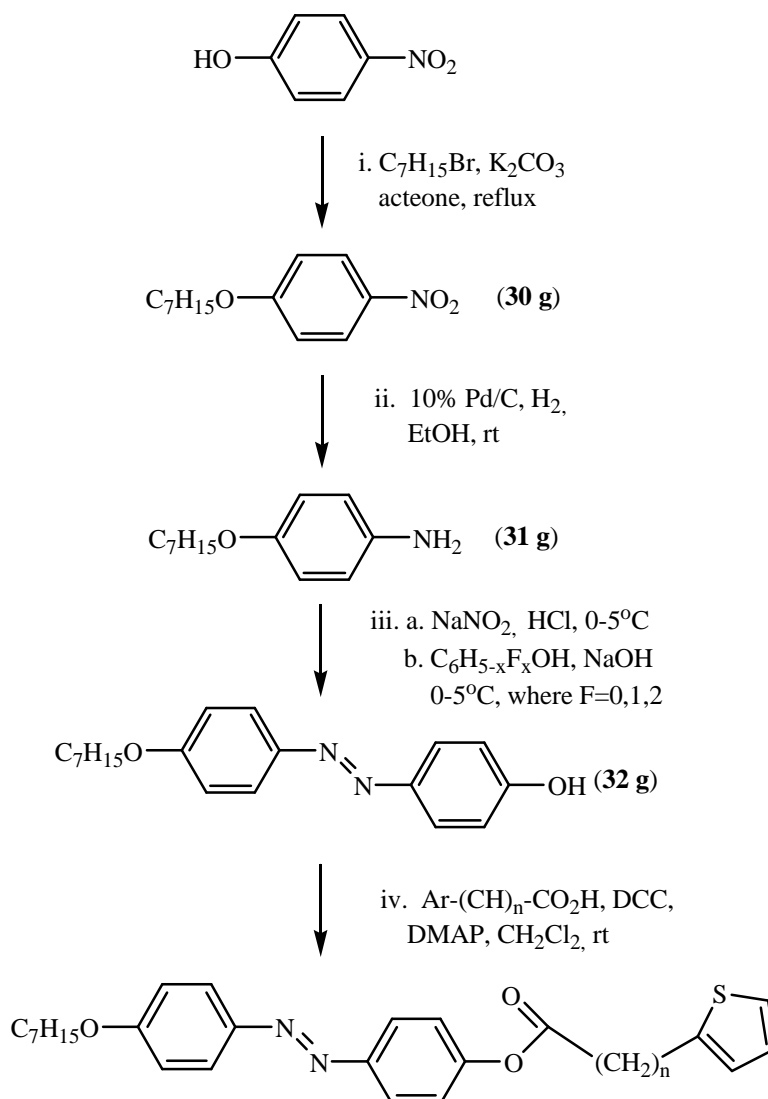*5-(2-Thienyl)pentanoic acid 4-(4-n-heptyloxyphenylazo)-phenyl ester* (**54**)

Quantities: 5-(2-thienyl)pentanoic acid (0.15 g, 0.8 mmol), 4-(4-n-heptyloxyphenylazo)phenol (**32 g**) (0.25 g, 0.8 mmol), DCC (0.2 g, 0.8 mmol), DMAP (0.03 g, 0.25 mmol). Yield, 0.18 g, (47 %).

ν_{max} (KBr)/ cm^{-1}: 3072.7w (Ar-H$_{str}$), 2955, 2940, 2862w (C-H$_{str}$), 1759s (C=O$_{str}$), 1607, 1583, 1492s (C=C$_{str}$), 1260-1125s (C-O$_{str}$), 842s (2 adjacent H); δ_H (400 MHz; CDCl$_3$) 0.88 (3H, t, CH$_3$), 1.32 (8H, m, CH$_2$) 1.81 (6H, m, CH$_2$-CH$_2$) 2.61 (2H, t, CH$_2$) 2.9 (2H, t, CH$_2$-O$_2$) 4.02 (2H, t, CH$_2$-O) 6.8 (1H, d, ArH$_{[Thio]}$, J=4.2 Hz) 6.91 (1H, d, ArH$_{[Thio]}$, J=5.3 Hz) 7.0 (2H, d, ArH) 7.09 (1H, d, ArH$_{[Thio]}$, J=5.0 Hz) 7.35 (2H, d, ArH) 7.87 (2H, d, ArH) 7.879 (2H, d, ArH); δ_C (100 MHz; CDCl$_3$); 14.1 (CH$_3$) 22.6, 24.25, 26, 29.0-29.5, 31.1, 31.7 (CH$_2$) 34.2 (CH$_2$-CO$_2$) 68.35 (CH$_2$-O) 114.8 (ArC) 122.08 (ArC) 123.1 (ArC$_{[Thio]}$) 123.64 (ArC) 124.26 (ArC$_{[Thio]}$) 124.7 (ArC) 126.7 (ArC$_{[Thio]}$) 144.7 (ArC$_Q$) 146.7 (ArC$_{Q[Thio]}$) 150.34 (ArC$_Q$) 150.08 (ArC$_Q$) 161.74 (ArC$_Q$-O) 171.69 (-CO$_2$-); C$_{28}$H$_{34}$N$_2$O$_3$S Expected: C, 70.26; H, 7.16; N 5.85 %; Found: C, 70.14; H, 7.24; N, 5.8 %; TLC (DCM), one spot, Rf; 0.81.

HO⎯⟨benzene⟩⎯NO_2

i. $C_7H_{15}Br$, K_2CO_3
acteone, reflux

$C_7H_{15}O$⎯⟨benzene⟩⎯NO_2 (**30 g**)

ii. 10% Pd/C, H_2,
EtOH, rt

$C_7H_{15}O$⎯⟨benzene⟩⎯NH_2 (**31 g**)

iii. a. $NaNO_2$, HCl, 0-5°C
b. $C_6H_{5-x}F_xOH$, NaOH
0-5°C, where F=0,1,2

$C_7H_{15}O$⎯⟨benzene⟩⎯N=N⎯⟨benzene⟩⎯OH (**32 g**)

iv. Ar-$(CH)_n$-CO_2H, DCC,
DMAP, CH_2Cl_2, rt

$C_7H_{15}O$⎯⟨benzene⟩⎯N=N⎯⟨benzene⟩⎯O⎯C(=O)⎯$(CH_2)_n$⎯⟨thiophene⟩

Series XIV
where n= 1 (**51**)
2 (**52**)
3 (**53**)
4 (**54**)

Scheme 2.   Generalised pathway for the synthesis of non-fluoro-substituted, azobenzene-containing esters with varying n-alkyl spacer (**Series XIV**).

2.2.6   4-CYCLOHEXYLACETOPHENONE OXIME (**55**) [83]

A mixture of 4-cyclohexylacetophenone (8.8 g, 43 mmol), hydroxylamine hydrochloride (8.3 g, 0.12 mol), ethanol (20 ml) and pyridine (60 ml) was heated under reflux for 3 h. The reaction was cooled and most of the solvent mixture was removed *in vacuo*. The residue was poured into water and the resultant white/yellow precipitate filtered off, washed with water and dried in a vacuum desiccator before purification by recrystallisation with ethanol to afford the desired oxime (**55**), 7.86 g (83 %), pale yellow crystals, m.p. 116.5-117.4 $^{\circ}$C (Lit. 117 $^{\circ}$C[83])

2.2.7   CYCLOHEXYANILINE (**56**) [83]

Phosphorous pentoxide (9.46 g, 47 mmol) was carefully added to a suspension of 4-cyclohexylacetophenone oxime (**55**) (7.3 g, 33 mmol) in dry toluene (190 ml). The mixture was heated under reflux for 15 minutes before being cooled and then added to a mixture of conc. hydrochloric acid (12.3 ml) and ethanol (67 ml) and heated under reflux for a further 4 hours. The reaction mixture was cooled, the solvent removed *in vacuo* and the resulting residue basified with 2M-aqueous sodium hydroxide. The compound was extracted with diethyl ether (3 x 100 ml), washed with water, dried (MgSO$_4$) and the solvent removed *in vacuo*. The crude residue was vacuum distilled to yield the desired aniline (**56**), 3.1 g (54 %), as a pale yellow liquid which solidified on standing, m.p. 53-55 $^{\circ}$C (Lit. 53-56 $^{\circ}$C[83])

2.2.8   4-(4-CYCLOHEXYLPHENYLAZO)PHENOL (**57**)

4-(4-Cyclohexylphenylazo)phenol (**57**) was prepared using a similar procedure as described earlier in section 2.2.3 (p. 47), but instead using cyclohexylaniline (**56**) (1.3 g, 7.5 mmol), phenol (0.7 g, 7.5 mmol). Yield, 1.25 g (60 %), m.p. 186.3-186.6 $^{\circ}$C.

ν_{max} (KBr)/ cm^{-1}: 3412m (OH$_{st}$), 3031w (Ar-H$_{str}$), 2920, 2848w (aliph C-H$_{str}$), 1591, 1498s (C=C$_{str}$) 1237-1098s (C-O$_{str}$), 843s (2 adjacent H); δ_H (400 MHz; CDCl$_3$) 1.38 (5H, m, cyclo-H) 1.86 (5H, m, cyclo-H) 2.56 (1H, t, cyclo-H) 6.9 (2H, d, ArH) 7.32 (2H, d, ArH) 7.8 (2H, d,

ArH) 7.84 (2H, d, ArH); δ_C(100 MHz: CDCl$_3$); 26.1 (cyc-C) 26.8 (cyc-C) 34.3 (cyc-C) 44.52 (cyc-C) 115.8 (ArC) 122.56 (ArC) 124.76 (ArC) 127.46 (ArC) 147.17 (ArC$_Q$) 150.96 (ArC$_Q$) 158.06 (ArC-OH); TLC (DCM), one spot, Rf; 0.21.

2.2.9   3-THIOPHEN-2-YL-ACRYLIC AND 3-THIOPHEN-3-YL-ACRYLIC ACID 4-(4-CYCLOHEXYLPHENYLAZO)PHENYL ESTERS (**58** and **59**) [**Series XV**]

The desired esters were prepared using a similar procedure as described earlier in section 2.2.4 (p.51). The transition temperatures are listed in **Tables 21** and **22** of the results and discussion section. A mixture of 3-(2- or 3-thienyl)acrylic acid, (0.23 g, 1.36 mmol), 4-(4-cyclohexylphenylazo)phenol (**57**) (0.38 g, 1.36 mmol), DCC (0.31 g, 1.5 mmol), DMAP (0.03 g, 0.2 mmol) and dry DCM (20 ml) was stirred at room temperature overnight. The ensuing white precipitate was isolated by Büchner filtration and discarded, whilst the filtrate was evaporated to dryness *in vacuo*. The resultant crude residue was purified by column chromatography on silica gel eluting with DCM, followed by repeated recrystallisation from toluene.

The following spectroscopic data is for 3-(2-thienyl)acrylic acid 4-(4-cyclohexylphenylazo)-phenyl ester (**58**), (**Series XV**).

ν_{max} (KBr)/ cm^{-1}: 3057w (C-H$_{str}$), 2923, 2848w (aliph C-H$_{str}$), 1724s (C=O$_{str}$), 1618s (alkene C=C$_{str}$), 1590, 1492s (C=C$_{str}$), 1281-1127s (C-O$_{str}$), 835s (2 adjacent H); δ_H (400 MHz; CDCl$_3$) 1.18 (10H, m, cyc-CH$_2$), 2.56 (1H, t, cyc. CH, J=6.84Hz), 6.4 (1H, d, <u>CH</u>=CH, J=15.6 Hz), 7.08 (1H, t, ArH$_{[Thio]}$, J=3.7 Hz), 7.31 (2H, d, ArH), 7.33 (2H, d, ArH), 7.34 (1H, d, ArH$_{[Thio]}$), 7.43 (1H, d, ArH$_{[Thio]}$, J=5.0 Hz), 7.83 (2H, d, ArH), 7.94 (2H, d, ArH), 7.96 (1H, d, CH=<u>CH</u>, J=16.04Hz); δ_C (100 MHz: CDCl$_3$); 26.07 (CH), 26.78, 34.28, 44.58 (CH$_2$), 115.68 (<u>CH</u>=CH), 122.29 (ArC), 123.02 (ArC), 124.02 (ArC), 127.62 (ArC), 128.4 (ArC$_{[Thio]}$), 129.45 (ArC$_{[Thio]}$), 131.9 (ArC$_{[Thio]}$), 139.35 (ArC$_{Q[Thio]}$), 139.35 (CH=<u>CH</u>), 150.44 (ArC$_Q$), 151 (ArC$_Q$), 151.74

(ArC$_Q$), 152.65 (ArC$_Q$-O), 165.06 (-CO$_2$); C$_{25}$H$_{24}$N$_2$O$_2$S Expected: C, 72.1; H, 5.81; N 6.73 %; Found: C, 72.2; H, 5.91; N, 6.81 %; TLC (DCM), one spot, Rf; 0.84.
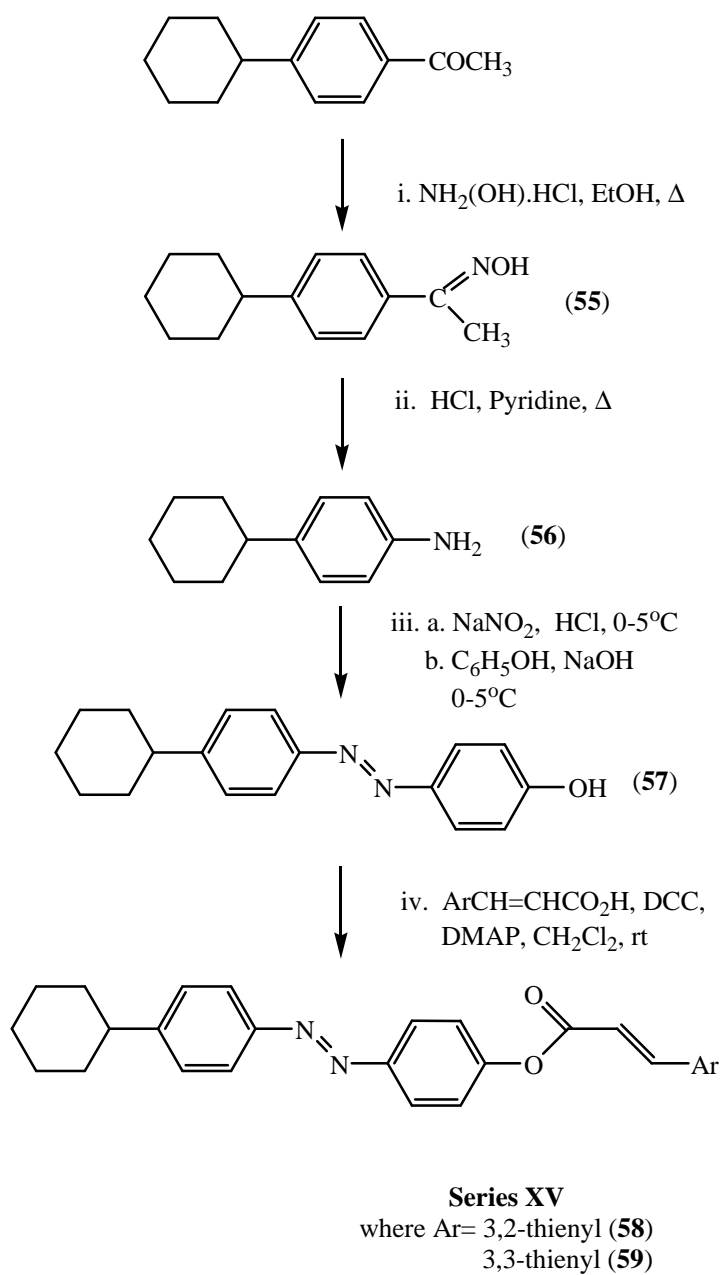
The following spectroscopic data is for 3-(3-thienyl)acrylic acid 4-(4-cyclohexylphenylazo)-phenyl ester (**59**), (**Series XV**).

ν_{max} (KBr)/ cm^{-1}: 3098w (Ar-H$_{str}$), 2922, 2849w (aliph C-H$_{str}$), 1732s (C=O$_{str}$), 1627s (alkene C=C$_{str}$), 1590, 1492s (C=C$_{str}$), 1277-1129s (C-O$_{str}$), 859s (2 adjacent H); δ_H (400 MHz; CDCl$_3$), 1.18 (10H, m, cyclo-CH$_2$), 2.56 (1H, t, cyclo-CH, J=6.84 Hz), 6.45 (1H, d, <u>CH</u>=CH, J=15.6 Hz), 7.31 (2H, d, ArH), 7.33 (2H, d, ArH), 7.34 (1H, d, ArH$_{[Thio]}$), 7.39 (1H, d, ArH$_{[Thio]}$, J=5.0 Hz), 7.61 (1H, s, ArH$_{[Thio]}$), 7.83 (2H, d, ArH), 7.94 (2H, d, ArH), 7.96 (1H, d, CH=<u>CH</u>, J=16.0 Hz); δ_C (100 MHz: CDCl$_3$); 26.07 (CH), 26.78, 34.28, 44.58, 116.68 (<u>CH</u>=CH), 122.3 (ArC), 123 (ArC), 124.02 (ArC), 125.26 (ArC$_{[Thio]}$), 127.4 (ArC $_{[Thio]}$), 127.62 (ArC), 129.28 (ArC$_{[Thio]}$), 137.41 (ArC$_{Q[Thio]}$), 140.45 (CH=<u>CH</u>), 150.43 (ArC$_Q$), 151.05 (ArC$_Q$), 151.76 (ArC$_Q$), 152.7 (ArC$_Q$-O), 165.5 (-CO$_2$); C$_{25}$H$_{24}$N$_2$O$_2$S Expected: C, 72.1; H, 5.81; N 6.73 %; Found: C, 72; H, 5.73; N, 6.61 %; TLC (DCM), one spot, Rf; 0.8.

i. NH$_2$(OH).HCl, EtOH, Δ

(55)

ii. HCl, Pyridine, Δ

(56)

iii. a. NaNO$_2$, HCl, 0-5°C
b. C$_6$H$_5$OH, NaOH
0-5°C

(57)

iv. ArCH=CHCO$_2$H, DCC,
DMAP, CH$_2$Cl$_2$, rt

Series XV
where Ar= 3,2-thienyl (**58**)
3,3-thienyl (**59**)

Scheme 3.   Generalised pathway for the synthesis of cyclohexylphenyl azobenzene-containing thienyl esters (**Series XV**).

2.2.10 2-(4-NITROPHENYL)THIOPHENE (60): Gomberg Reaction[84-86]

iso-Amyl nitrite (70 ml, 0.53 mol) was added to a stirred suspension of 4-nitroaniline (78 g, 0.54 mol) in thiophene (400 ml, 5.1 mol). After 20 minutes, the reaction initiated with vigorous effervescence and exotherm, which was controlled by cooling the reaction mixture with an ice bath. The mixture was then allowed to reflux for 3 h. The dark red mixture was cooled and concentrated *in vacuo*. The resulting precipitate was filtered off, washed well with light petroleum ether (b.p. 60-80 °C) and allowed to air-dry. The crude material was purified by column chromatography, eluting with dichloromethane followed by a second column chromatography, eluting with 1:1 dichloromethane: light petroleum ether (b.p. 60-80 oC) to furnish the desired 2-(4-nitrophenyl)thiophene (60), 28.5 g, (26 %), m.p. 138 °C (Lit. 137-138 °C[86]), as pale yellow crystals.

ν_{max} (KBr)/ cm^{-1}: 3103w (C=C$_{st}$), 2855w (C-H$_{st}$), 1592, 1501s (C=C$_{st}$), 1507, 1338, 1106s (N=O$_{st}$), 1420s (C-H$_{def}$), 842s (2 adjacent H); δ_H (400 MHz; CDCl$_3$) 7.7 (1H, t, ArH$_{[Thio]}$, J=3.7 Hz), 7.36 (1H, d, ArH$_{[Thio]}$, J=4.9 Hz), 7.39 (1H, d, ArH$_{[Thio]}$, J=3.7 Hz), 7.67 (2H, d, ArH), 8.15 (2H, d, ArH); δ_C (100 MHz: CDCl$_3$); 124.36 (ArC), 125.67 (ArC$_{[Thio]}$), 125.98 (ArC), 127.64 (ArC$_{[Thio]}$), 128.64 (ArC$_{[Thio]}$) 140.53 (ArC$_{Q[Thio]}$), 141.55 (ArC$_Q$), 146.59 (ArC$_Q$-NO$_2$); C$_{10}$H$_7$NO$_2$S : Expected: C, 58.52; H, 3.44; N, 6.82 %; Found: C, 58.49; H, 3.35; N, 6.67 %; TLC (DCM), one spot, Rf; 0.95.
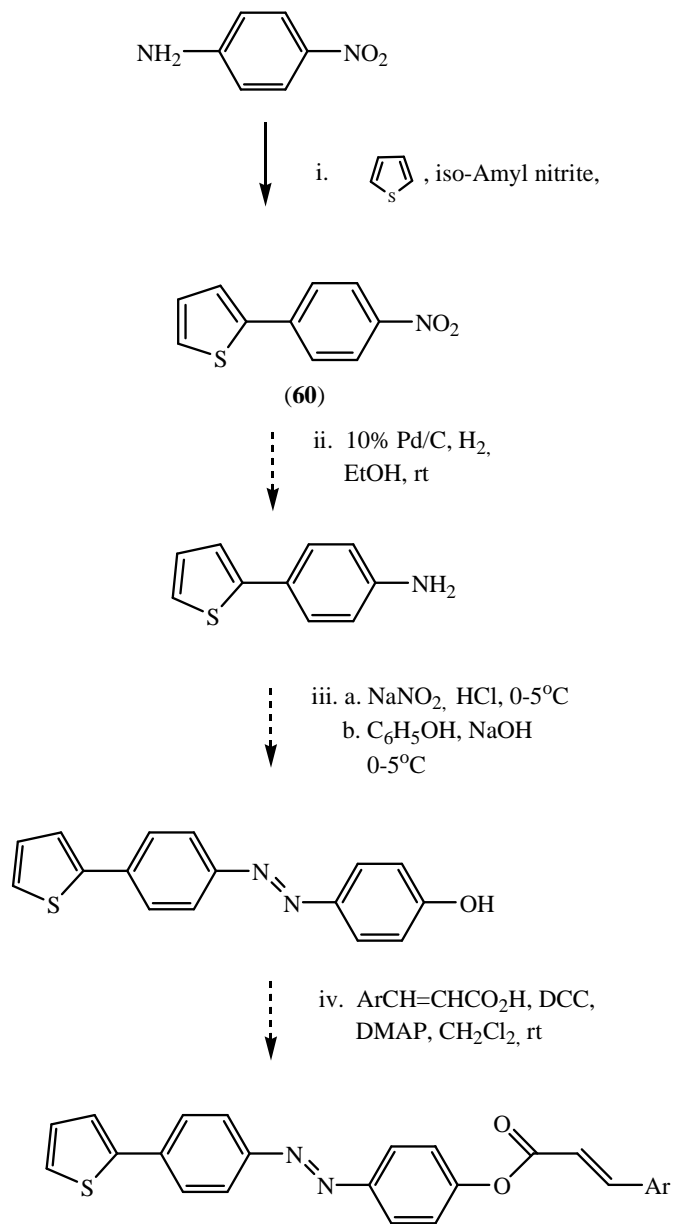
Scheme 4   Attempted synthetic pathway leading to **Series XVI**. (n.b. only compound (**60**) was prepared).

2.2.11 2-(4-NITROPHENYL)THIOPHENE (60): Suzuki coupling, Method 1

A mixture of 1-bromo-4-nitrobenzene (15.2 g, 75 mmol), Pd(PPh$_3$)$_4$ (0.76 g, 0.66 mmol, 1.3 mol%), 2M-aqueous sodium carbonate (30 ml) and toluene (75 ml) under a nitrogen atmosphere was heated under reflux for 30 minutes. The mixture was removed from the heat, a solution of thiophene-2-boronic acid (10.2 g, 80 mmol) in ethanol (30 ml) was added and reaction mixture was heated under continuous reflux for 5 days. Thereafter, the reaction was cooled, filtered through a glass wool plug and extracted into diethyl ether (150 ml). The two layers were passed through 'Celite' and the ethereal layer washed with water (150 ml), dried (MgSO$_4$) and the diethyl ether removed *in vacuo*. The resultant residue by purified by sublimation (70 $^{\circ}$C, 10mm/Hg) and recrystallisation with ethanol to furnish the desired 2-(4-nitrophenyl)thiophene (60), 6.15 g (41 %), m.p. (138-139 $^{\circ}$C (Lit. 137-138 $^{\circ}$C[86])as pale yellow crystals.

ν_{max} (KBr)/ cm^{-1}: 3103w (C=C$_{st}$), 2855w (C-H$_{st}$), 1592 & 1501s (C=C$_{st}$), 1507, 1338 & 1106s (N=O$_{st}$), 1420s (C-H$_{def}$), 842s (2 adjacent H); δ_H (400 MHz; CDCl$_3$), 7.7 (1H, t, ArH$_{[Thio]}$, J=3.7 Hz), 7.36 (1H, d, ArH$_{[Thio]}$, J=4.9 Hz), 7.39 (1H, d, ArH$_{[Thio]}$, J=3.7 Hz), 7.67 (2H, d, ArH), 8.15 (2H, d, ArH); δ_C (100 MHz: CDCl$_3$); 124.36 (ArC) 125.67 (ArC$_{[Thio]}$), 125.98 (ArC), 127.64 (ArC$_{[Thio]}$), 128.64 (ArC$_{[Thio]}$), 140.53 (ArC$_{Q[Thio]}$), 141.55 (ArC$_Q$), 146.59 (ArC$_Q$-NO$_2$); C$_{10}$H$_7$NO$_2$: Expected: C, 58.52; H, 3.44; N, 6.82 %; Found: C, 58.5; H, 3.37; N, 6.67 %; MS: [M+H]$^+$ M/Z=206; Exact Mass: 205; TLC (DCM), one spot, Rf; 0.95.

2.2.12 2-(4-NITROPHENYL)THIOPHENE (**60**): Suzuki Coupling, Method 2

Sodium hydride [50% dispersion in oil] (3.2 g, 68.6 mmol) was added, portionwise, to dry methanol (30ml) and the resultant mixture stirred at room temperature for 30 minutes. 4-Bromonitrobenzene (4.6 g, 22.8 mmol) was added to the resultant grey sodium methoxide/methanol mixture and heated under reflux with stirring for 30 minutes.

A mixture of thiophene-2-boronic acid (3.22 g. 25.2 mmol) dissolved in dry methanol (5ml) and Pd(PPh$_3$)$_4$ (0.76 g, 0.66 mmol, 1.3 mol%) was added in one portion to the mixture whilst under reflux and the reaction was monitored by TLC. After 36 hours the reaction was 'hot-filtered' to remove a yellow suspension and the resultant brown filtrate cooled to room temperature, from which yellow crystals emerged. The crystals were isolated and sublimed to yield starting material (first 2 crops) and then the pure product (following 2 crops), 2.1 g (46 %), m.p. 138-139 ^{o}C, (Lit. 137-138 ^{o}C[86]) as pale yellow crystals.

ν_{max} (KBr)/ cm^{-1}: 3103w (C=C$_{st}$) 2855w (C-H$_{st}$) 1592, 1501s (C=C$_{st}$), 1507, 1338, 1106s (N=O$_{st}$), 1420s (C-H$_{def}$), 842s (2 adjacent H); δ_H (400 MHz; CDCl$_3$); 7.7 (1H, t, ArH$_{[Thio]}$, J=3.7 Hz), 7.36 (1H, d, ArH$_{[Thio]}$, J=4.9 Hz), 7.39 (1H, d, ArH$_{[Thio]}$, J=3.7 Hz), 7.67 (2H, d, ArH), 8.15 (2H, d, ArH); δ_C (100 MHz: CDCl$_3$); 124.36 (ArC), 125.67 (ArC$_{[Thio]}$), 125.98 (ArC), 127.64 (ArC$_{[Thio]}$), 128.64 (ArC$_{[Thio]}$), 140.53 (ArC$_{Q[Thio]}$), 141.55 (ArC$_Q$), 146.59 (Ar$_Q$C-NO$_2$); C$_{16}$H$_{12}$N$_2$OS: Expected: C, 58.5; H, 3.4; N, 6.82 %; Found: C, 58.49; H, 3.36; N, 6.7%; MS: [M+H]$^+$ M/Z=206; Exact Mass: 205; TLC (DCM), one spot, Rf; 0.95.

2.2.13 4-(2-THIENYL) ANILINE (**61**)

Commercial palladium on charcoal (10 % Pd/C) (0.35 g) was carefully added to a solution of 2-(4-nitrophenyl)thiophene (**60**) (5 g, 24.4 mmol) dissolved in absolute ethanol (150 ml). The mixture was fitted to an atmospheric hydrogenator and stirred continuously until the theoretical volume of hydrogen had been consumed. Thereafter, the reaction mixture was filtered through 'Celite', washed well with ethanol, and the filtrate was evaporated to dryness *in vacuo*. The resulting beige solid was recrystallised twice with ethanol to afford the desired 4-(2-thienyl)aniline (**61**),4 g (94 %), m.p. 75-76 ^{o}C, as white crystals.

ν_{max} (KBr)/ cm^{-1}: 3441, 3358m (N-H$_{st}$), 3097w (Ar-H$_{st}$), 2864w (C-H$_{st}$), 1793, 1757w (N-H$_{def}$), 1616, 1501s (C=C$_{st}$), 1429s (C-H$_{def}$), 1291s (N-H$_{def}$), 816s (2 adjacent H); δ_H (400 MHz; CDCl$_3$); 6.68 (2H, d, ArH), 7.03 (1H, t, ArH$_{[Thio]}$, J=3.7 Hz), 7.16 (2H, m, ArH$_{[Thio]}$), 7.43 (2H, d, ArH); δ_C (100 MHz: CDCl$_3$); 115.4 (ArC), 121.36 (ArC$_{[Thio]}$), 123.18 (ArC$_{[Thio]}$), 125.25 (ArC$_Q$), 127.25 (ArC), 127.92 (ArC$_{[Thio]}$), 145.11 (ArC$_{Q[Thio]}$), 146.1 (ArC$_Q$-NH$_2$); C$_{10}$H$_9$NS Expected: C, 68.53; H, 5.18; N, 7.99 %; Found: C, 68.11; H, 5.29; N, 7.64 %; MS: [M+H]$^+$ M/Z= 176; Exact Mass: 175; TLC (DCM), one spot, Rf; 0.5.

2.2.14 4-(4-THIOPHEN-2-YL-PHENYLAZO)PHENOL – GENERAL METHOD FOR DIAZOTISATION AND COUPLING (**62**)

To a cooled (0°C) solution of sodium nitrite (3.33 g, 0.05 mol) in water (50 ml) was added to a cooled solution/suspension of 4-(2-thienyl)aniline (**61**) (8.8 g, 0.05 mol) in HCl / water (18 ml: 90 ml). The reaction mixture was maintained at 0 ^{o}C for 2 h to ensure successful diazotisation. Thereafter, a mixture of phenol (4.67 g, 0.05 mol), sodium hydroxide (6 g, 0.15 mol) and water (50 ml) was added, dropwise, with stirring to the above diazonium solution ensuring that the reaction temperature did not exceed 5 ^{o}C. After stirring for 2 h, the ensuing yellow/beige precipitate was filtered (Bűchner) and allowed to air-dry, whereupon the solid changed to a *forest green* colour. The crude product was mixed with DCM and silica gel (40 g) and the

slurry poured onto a pre-packed column. The crude residue was purified by flash column chromatography on silica gel (100 % DCM, slowly ramped up to 2 % ethanol/DCM), followed by repeated recrystallisation (hexane) of the desired fraction to yield the desired 4-(4-thiophen-2-yl-phenylazo)phenol (**62**), 5.6 g (40 %), m.p. 205 $^{\circ}$C, as bronze crystals.

ν_{max} (KBr)/ cm^{-1}: 3066wb (OH$_{st}$), 3055w (Ar-H$_{st}$), 2092, 2864w (C-H$_{st}$), 1244-1101s (C-O$_{str}$), 845s (2 adjacent H); δ_H (400 MHz; CDCl$_3$); 2.99 (1H, s, -OH), 6.88 (2H, d, ArH), 7.04 (1H, t, ArH$_{\{Thio\}}$, J=3.46Hz), 7.27 (1H, d, ArH$_{\{Thio\}}$, J=5.2 Hz), 7.34 (1H, d, ArH$_{\{Thio\}}$, J=3.4 Hz), 7.66 (2H, d, ArH), 7.8 (2H, d, ArH), 7.83 (2H, d, ArH); δ_C (100 MHz: CDCl$_3$); 115.69 (ArC), 123.04 (ArC), 123.76 (ArC$_{[Thio]}$), 124.87 (ArC), 125.55 (ArC$_{[Thio]}$), 126.2 (ArC), 128.16 (ArC$_{[Thio]}$), 136.06 & 146.75 (ArC$_Q$), 143.44 (ArC$_{Q[Thio]}$), 146.37 (ArC$_Q$), 151.67 (ArC$_Q$), 160 (ArC$_Q$-OH); C$_{16}$H$_{12}$N$_2$O: Expected: C, 68.55; H, 4.31; N, 9.99 %; Found: C, 66.43; H, 4.41; N, 9.75 %; MS: [M+H]$^+$ M/Z=281.2, Exact Mass: 280; TLC (DCM), one spot, Rf; 0.19.

2.2.15 3-THIOPHEN-2-YL-ACRYLIC ACID and 3-THIOPHEN-3-YL-ACRYLIC ACID 4-(4-THIOPHEN-2-YL-PHENYLAZO)-PHENYL ESTERS – GENERAL METHOD FOR ESTERIFICATION (**63** and **64**), (**SERIES XVI**)

A mixture of 3-(2 or 3-thienyl)acrylic acid, (0.23 g, 1.36 mmol), 4-(4-thiophen-2-yl-phenylazo)-phenol (**62**) (0.38g, 1.36 mmol), DCC (0.31 g, 1.5 mmol), DMAP (0.03 g, 0.2 mmol) and dry DCM (20 ml) was stirred at room temperature overnight. The ensuing white precipitate was isolated by Büchner filtration and discarded, whilst the filtrate was evaporated to dryness *in vacuo*. The resultant crude residue was purified by column chromatography on silica gel eluting with DCM, followed by repeated recrystallisation from toluene to afford (**63**) and (**64**), (**Series XVI**).

3-Thiophen-2-yl-acrylic acid 4-(4-thiophen-2-yl-phenylazo)-phenyl ester (**63**)

Yield, 0.25 g (44 %); m.p. 290-291 $^{\circ}$C, as orange crystals.

ν_{max} (KBr)/cm^{-1}: 3067w (Ar-H$_{str}$), 2937, 2865w (aliph C-H$_{str}$), 1732s (C=O$_{str}$), 1628s (alkene C=C$_{str}$), 1588, 1488s (C=C$_{str}$), 1300-1129s (C-O$_{str}$), 820s (2 adjacent H); δ_H (400 MHz; CDCl$_3$);

6.4 (1H, d, CH=$\underline{\text{CH}}$-O J=15.6 Hz), 7.11 (2H, m, ArH$_{[Thio]}$), 7.35 (3H, m, ArH, ArH$_{[Thio]}$, and ArH$_{[Thio]}$), 7.44 (2H, m, ArH$_{[Thio]}$ and ArH), 7.76 (2H, d, ArH), 7.94 (2H, d, ArH), 7.98 (2H, d, ArH), 7.99 (1H, d, $\underline{\text{CH}}$=CH-O, J=16.0 Hz); δ_C (100 MHz: CDCl$_3$); 115.68 (CH=$\underline{\text{CH}}$-CO), 122.36 (ArC), 123.7 (ArC), 124.19 (ArC & ArC$_{[Thio]}$), 126 (ArC $_{[Thio]}$), 126.45 (ArC), 129.48 (ArC$_{[Thio]}$ & ArC$_{[Thio]}$), 129.48 (ArC$_{[Thio]}$), 131.92 (ArC$_{[Thio]}$), 137.04 (ArC$_Q$), 139.34 (ArC$_{Q[Thio]}$), 139.46 (O-CH=$\underline{\text{CH}}$), 143.54 (ArC$_{Q[Thio]}$), 150.4 (ArC$_Q$), 151.687 (ArC$_Q$), 152.92 (ArC$_Q$-O), 165.01 (-CO$_2$); C$_{23}$H$_{16}$N$_2$O$_2$S$_2$ Expected: C, 66.32; H, 3.87; N, 6.73 %; Found: C, 66.13; H, 4.01; N, 6.7 %; TLC (DCM), one spot, Rf; 0.77.

3-Thiophen-3-yl-acrylic acid 4-(4-thiophen-2-yl-phenylazo)-phenyl ester (**64**)

Yield, 0.28 g (49 %); m.p. 217-218 ^{o}C, as orange crystals.

ν_{max} (KBr)/cm^{-1}: 3067w (Ar-H$_{str}$), 2937, 2865w (aliph C-H$_{str}$), 1732s (C=O$_{str}$), 1628s (alkene C=C$_{str}$), 1588, 1488s (C=C$_{str}$), 1300-1129s (C-O$_{str}$), 820s (2 adjacent H); δ_H (400 MHz; CDCl$_3$); 6.46 (1H, d, CH=$\underline{\text{CH}}$-CO J=16.1 Hz), 7.12 (1H, t, ArH$_{[Thio]}$, J=4.1 Hz), 7.32 (2H, m, ArH), 7.38 (3H, m, 2 ArH$_{[Thio]}$ & ArH), 7.43 (1H, d, ArH$_{[Thio]}$), 7.6 (1H, s, ArH$_{[Thio]}$), 7.76 (2H, d, ArH), 7.89(1H, d, $\underline{\text{CH}}$=CH-CO, J=16.0 Hz), 7.94 (2H, d, ArH) 7.98 (2H, d, ArH); δ_C (100 MHz: CDCl$_3$); 116.65 (CH$_2$=$\underline{\text{CH}}_2$-CO$_2$), 122.37 (ArC), 123.72 (ArC), 124.17 (ArC & ArC$_{[Thio]}$), 125.26 (ArC$_{[Thio]}$), 126 (ArC[$_{Thio]}$), 126.44 (ArC), 127.4 (ArC$_{[Thio]}$), 128.42 (ArC$_{[Thio]}$), 129.29 (ArC$_{[Thio]}$), 137.03 (ArC$_{Q[Thio]}$), 137.4 (ArC$_Q$), 140.49 ($\underline{\text{CH}}$=CH-O), 143.54 (ArC$_{Q[Thio]}$), 150.4 (ArC$_Q$) 151.68 (ArC$_Q$), 152.93 (ArC$_Q$-O), 165.04 (-CO$_2$); C$_{23}$H$_{16}$N$_2$O$_2$S$_2$ Expected: C, 66.32; H, 3.87; N, 6.73 %; Found: C, 66.47; H, 3.79; N, 6.67 %; TLC (DCM), one spot, Rf; 0.75.
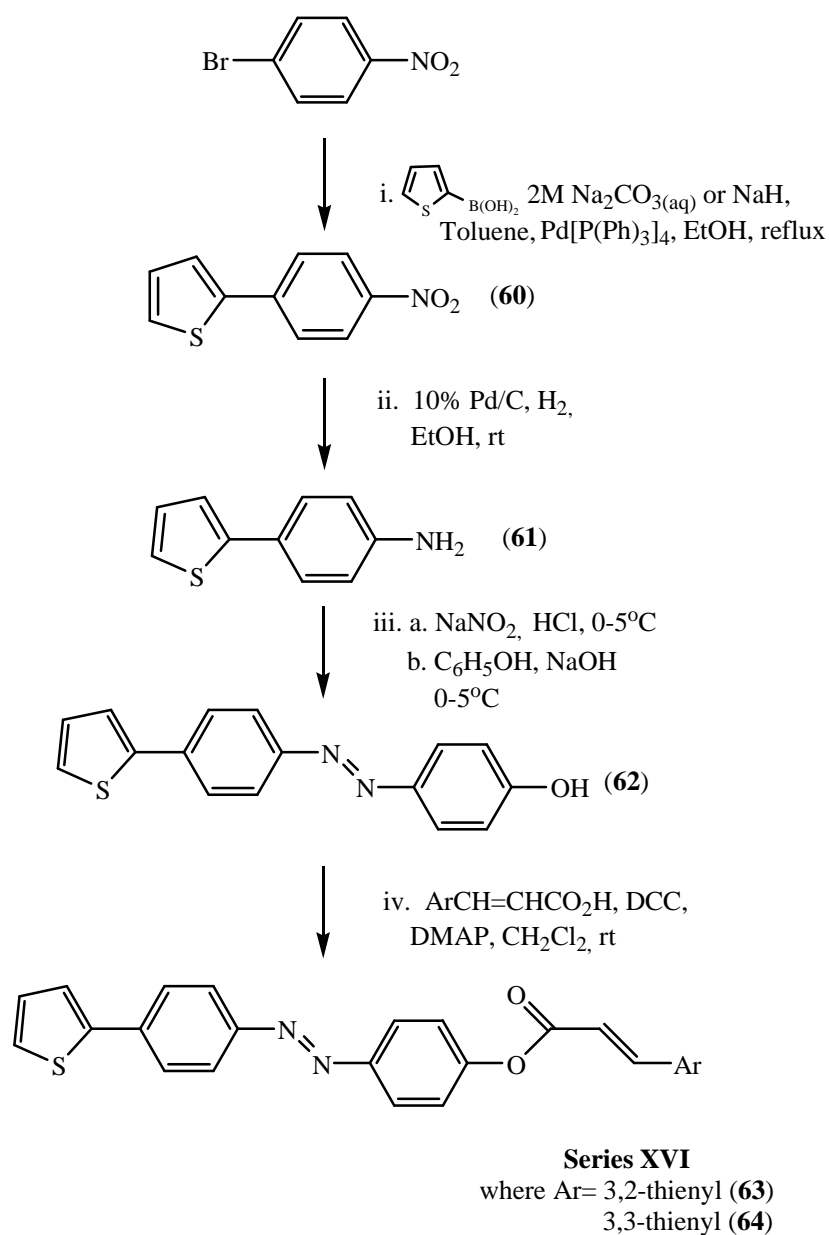
Scheme 5   Generalised pathway for the synthesis of 3-(2- & 3-thienyl)acrylic acid 4-(4-thiophen-2-yl-phenylazo)-phenyl esters (**Series XVI**).

RESULTS AND DISCUSSION

3   RESULTS AND DISCUSSION

This chapter reports and discusses the mesomorphic data of a variety of thiophene-containing azobenzene liquid crystals [**Series I-II**], their non-heterocyclic counterparts, *i.e.*, cinnamates [**Series III**] and their fluorinated counterparts [**Series IV-XIII**], with respect to the molecular structure. The photoresponsive behaviour of 3,2- thienyl compounds (**38 g,** and **41-45 g**) along with X-ray crystallographic data of representative compounds from **Series I, II** and **III** is also reported and discussed accordingly. Herein, this chapter shows:

i)   thiophene-containing azobenzenes are viable liquid crystals;

ii)   the disposition of the thiophene ring is important for mesophase stability ;

iii)   the number and disposition of lateral fluoro-substituents effects mesophase thermal stability;

iv)   thiophene-containing azobenzenes are photoresponsive;

v)   replacing the acrylic linkage with its saturated counterparts affects the photoresponsivity of the molecule.
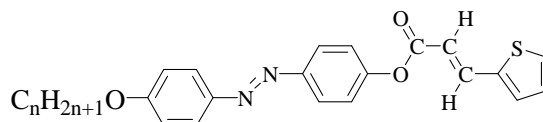
3.1 RESULTS

Ten members, n=1-10, of [**Series I-XIII**] were prepared and their mesomorphic data is represented both in tabular (**Table 1** [**Series I**]; **Table 2** [**Series II**]; **Table 3** [**Series III**]; **Table 4** [**Series IV**]; **Table 5** [**Series VI**]; **Table 6** [**Series VIII**]; **Table 7** [**Series X**]; **Table 8** [**Series XII**]; **Table 9** [**Series VII**]; **Table 10** [**Series VII**]; **Table 11** [**Series IX**]; **Table 12** [**Series XI**] and; **Table 13** [**Series XIII**]) and graphical format (**Plot 1** [**Series I**]; **Plot 2** [**Series II**]; **Plot 3** [**Series III**]; **Plot 4** [**Series IV**]; **Plot 5** [**Series VI**]; **Plot 6** [**Series VIII**]; **Plot 7** [**Series X**]; **Plot 8** [**Series XII**]; **Plot 9** [**Series VII**]; **Plot 10** [**Series VII**]; **Plot 11** [**Series IX**]; **Plot 12** [**Series XI**] and; **Plot 13** [**Series XIII**].

The mesomorphic data of the derivatives (**Series XIV**, **51-54**; **Series XV**, **58**, **59**; **Series XVI**, **63**, **64**) of the parent is represented in tabular format in **Tables 20** to **22**.

X-ray crystallographic data for **Series I**, **38 c**; **Series II**, **39 c**; **Series IV**, **41 c**; **Series VII**, **47 c**; **Series X**, **44 c**; **Series XII**, **45 c** and **Series XIII**, **50 c** is discussed in section 3.3, p. 114 and represented in tabular format in **Table 17**

UV-Vis steady-state photoresponsive studies and photo-induced liquid crystal transitions for **Series I**, **38 g**; **Series IV**, **41 g**; **Series VI**, **42g**; **Series VIII**, **43g**; **Series X**, **44g** and **Series XII**, **45 g** are described in section 3.4, p. 123.

n-alkyl	C-C	C-N	N-I	I-N	N-C	T_{N-I} - T_{C-N}*
CH_3	**147.8** *1.1*	**161.7** *20.1*	**235.7** *1.3*	**233.4** *1.3*	**105.6** *28.2*	74.0
C_2H_5		**178.2** *38.1*	**235.1** *1.7*	**233** *1.9*	**124** *26.6*	56.9
C_3H_7		**150.3** *57.8*	**216.3** *1.6*	**215.2** *1.4*	**111** *31*	66.0
C_4H_9		**159.2** *41.4*	**215.7** *2.0*	**214.3** *2.0*	**130.1** *36.3*	56.5
C_5H_{11}		**133.5** *34.5*	**201.4** *1.6*	**200.5** *1.7*	**108.2** *30.2*	67.9
C_6H_{13}		**136** *36.5*	**197.8** *1.8*	**195.8** *1.8*	**109.9** *32.9*	61.8
C_7H_{15}	**115.75** *5.0*	**124.3** *44.6*	**187.1** *1.6*	**186.2** *1.7*	**96.8** *30.3*	62.8
C_8H_{17}		**118.7** *34*	**183.7** *1.7*	**182.4** *1.6*	**98.9** *30.1*	65.0
C_9H_{19}		**130.3** *56.2*	**176.1** *1.5*	**175.2** *1.5*	**113.5** *45.5*	45.8
$C_{10}H_{21}$		**112.3** *41.0*	**172.4** *1.7*	**171.3** *1.6*	**89.6** *34.0*	60.1
Average			202.1			61.7

*Phase range = clearing point (T_{N-I}) – m.p. (T_{C-N})
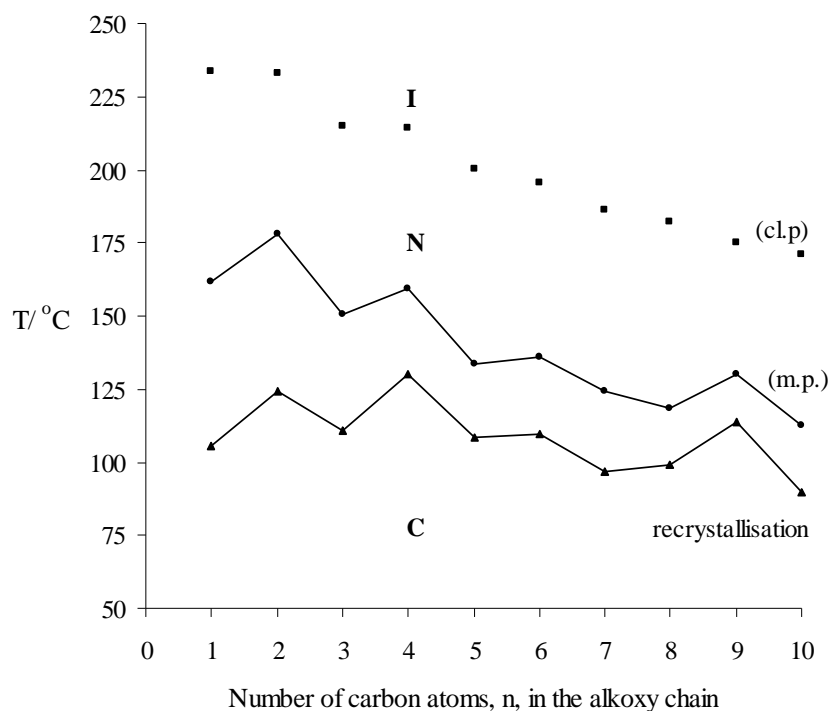
Plot 1: Transition temperature plot for the members of a homologous series of 3-thiophen-2-yl-acrylic acid 4-(4-n-alkoxyphenylazo)phenyl esters **(38 a-j) [Series I]**

Table 2: Transition temperatures (^{o}C) for an homologous series 3-thiophen-3-yl-acrylic acid 4-(4-n-alkoxyphenylazo)phenyl esters **(39 a-j) [Series II]**
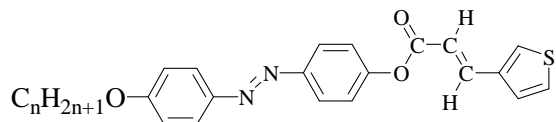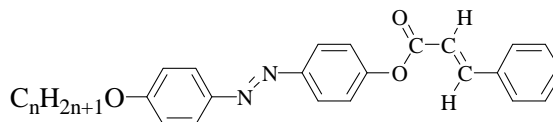
$$C_nH_{2n+1}O-\!\!\bigcirc\!\!-N\!\!=\!\!N-\!\!\bigcirc\!\!-O-C(=O)-CH=CH-\text{(thiophene)}$$

n-alkyl	C-C	C-N	N-I	I-N	N-C	$T_{N-I} - T_{C-N}$*
CH$_3$	-	**164.5**	**234.9**	**233.8**	**119.3**	70.4
		51.9	*1.8*	*1.8*	*48.2*	
C$_2$H$_5$	-	**161.1**	**243.2**	**240.6**	**125**	82.1
		37.1	*2.8*	*3.1*	*†*	
C$_3$H$_7$	-	**156.2**	**226**	**224.7**	**120.1**	69.8
		39.1	*1.9*	*1.9*	*27.7*	
C$_4$H$_9$	**105.8**	**154.4**	**224.6**	**222.9**	**122.5**	70.2
	9.7	*42.3*	*2.6*	*3.0*	*33.3*	
C$_5$H$_{11}$	-	**136.4**	**210**	**208.7**	**109.3**	73.6
		36.2	*2.3*	*2.4*	*21.6*	
C$_6$H$_{13}$	**93.5**	**134**	**204**	**201.5**	**105.3**	70.0
	10.1	*35.3*	*2.5*	*2.5*	*†*	
C$_7$H$_{15}$	**121.6**	**133.5**	**195.9**	**194.5**	**106.6**	62.4
	24.7	*35.2*	*1.8*	*2.1*	*28.6*	
C$_8$H$_{17}$	-	**126.6**	**191**	**190**	**96.3**	64.4
		38.1	*2.0*	*2.1*	*22.5*	
C$_9$H$_{19}$	-	**137.7**	**183.4**	**182.1**	**115.7**	45.7
		62.9	*1.6*	*1.8*	*31.4*	
C$_{10}$H$_{21}$	**110.1**	**123.3**	**180.7**	**179.2**	**97.6**	57.4
	48.6	*20.2*	*1.8*	*1.8*	*33.8*	
Average			209.4			66.6

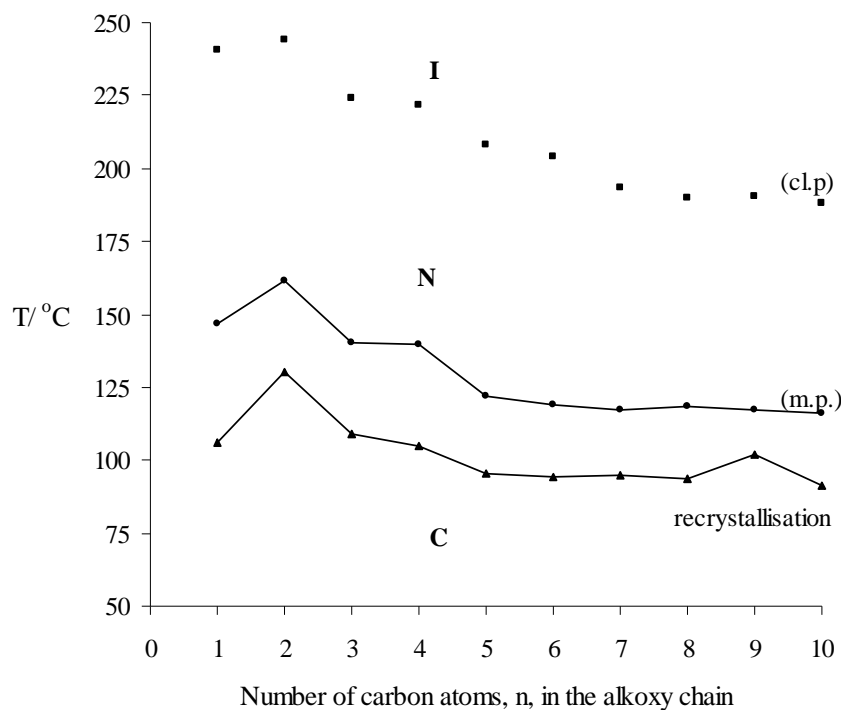*Phase range = clearing point (T_{N-I}) – m.p. (T_{C-N}), † Overlap of 2 phases
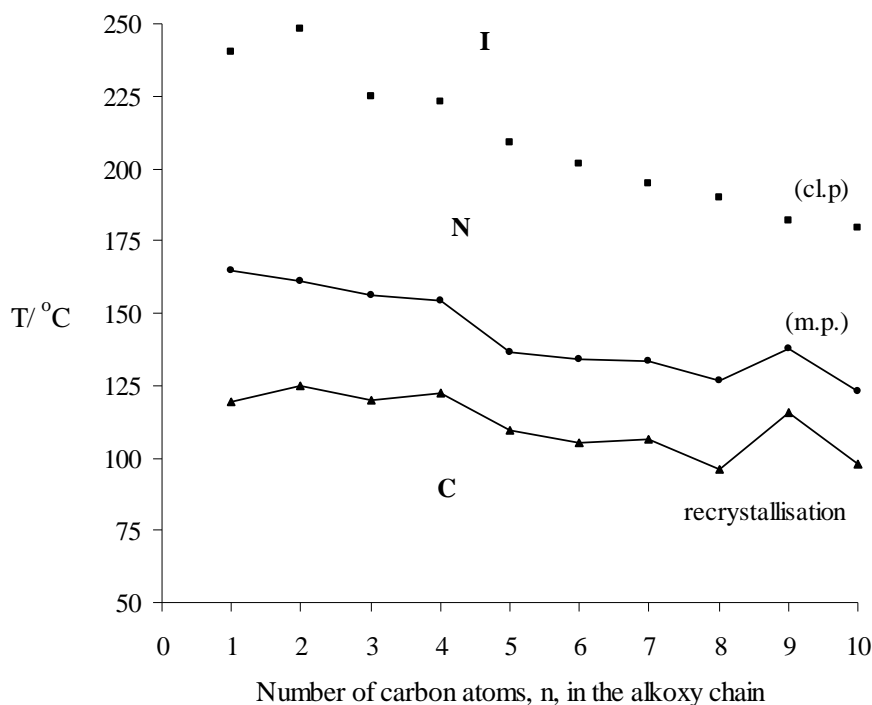
Plot 2: Transition temperature plot for the members of the homologous series of 3-thiophen-3-yl-acrylic acid 4-(4-n-alkoxyphenylazo)phenyl esters **(39 a-j) [Series II]**

Table 3: Transition temperatures (^{o}C) for a homologous series of 3-phenylacrylic acid 4-(4-alkoxyphenylazo)phenyl esters **(40 a-j) [Series III]**

$$C_nH_{2n+1}O-\text{⟨phenyl⟩}-N{=}N-\text{⟨phenyl⟩}-O-\overset{\displaystyle O}{\underset{}{C}}-\overset{\displaystyle H}{\underset{H}{C}}{=}\overset{H}{C}-\text{⟨phenyl⟩}$$

n-alkyl	C-C	C-N	N-I	I-N	N-C	$T_{N-I} - T_{C-N}$*
CH$_3$	**120.1** *4.4*	**146.5** *28.7*	**242.4** *1.3*	**240.6** *1.3*	**105.8** *23*	95.9
C$_2$H$_5$		**161.7** *34.4*	**246.5** *1.8*	**244.2** *1.9*	**130.2** *31.1*	84.8
C$_3$H$_7$	**93** *9.2*	**140.5** *33.4*	**225.7** *1.6*	**223.8** *1.6*	**109.2** *29.1*	85.2
C$_4$H$_9$		**139.5** *34.6*	**223.5** *1.7*	**221.7** *1.7*	**105.1** *30.2*	84
C$_5$H$_{11}$	**98.3** *3.9*	**121.8** *30*	**209** *1.5*	**208** *1.5*	**95.2** *27*	87.2
C$_6$H$_{13}$	**113.2** *5.7*	**118.9** *35.7*	**204.9** *1.6*	**204** *1.6*	**94.5** *31.5*	85.7
C$_7$H$_{15}$		**117.3** *36.9*	**195** *1.5*	**193.6** *1.5*	**94.7** *32.5*	77.7
C$_8$H$_{17}$		**118.3** *41.9*	**190.8** *1.5*	**189.7** *1.6*	**93.4** *34*	72.5
C$_9$H$_{19}$		**117.2** *32.4*	**194** *1.4*	**192.6** *1.4*	**92.1** *37.8*	76.8
C$_{10}$H$_{21}$		**116.3** *36.6*	**189** *1.7*	**188** *1.6*	**91.4** *33.3*	72.7
Average			212.1			82.3

*Phase range = clearing point (T_{N-I}) – m.p. (T_{C-N})
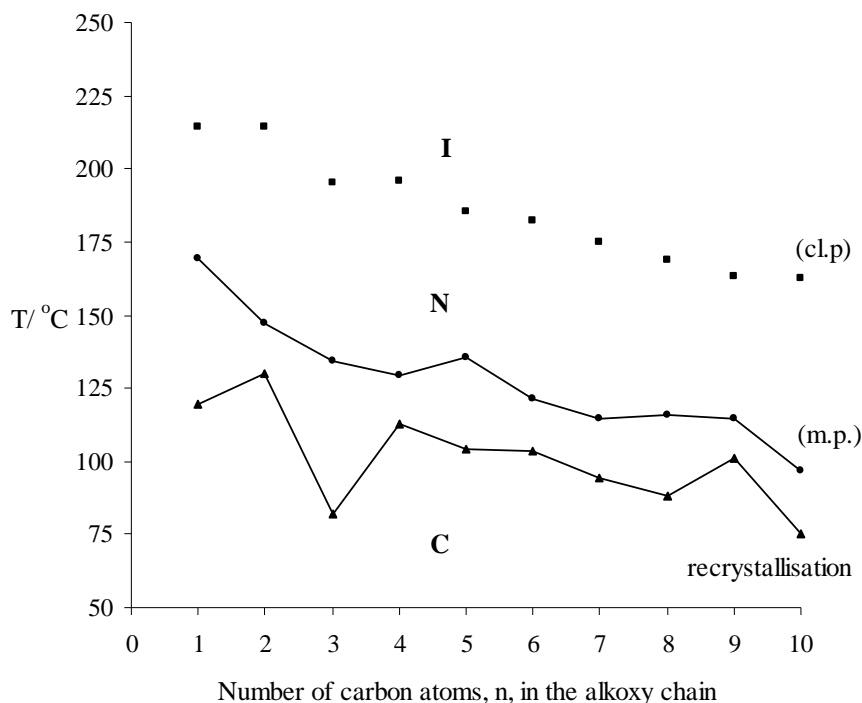

Plot 3: Transition temperature plot for the members of the homologous series of 3-phenylacrylic acid 4-(4-n-alkoxyphenylazo)phenyl esters **(40 a-j) [Series III]**

Table 4: Transition temperatures (^{o}C) for a homologous series of 3-thiophen-2-yl-acrylic acid 4-(4-n-alkoxyphenylazo)-3'-fluorophenyl esters **(41 a-j) [Series IV]**
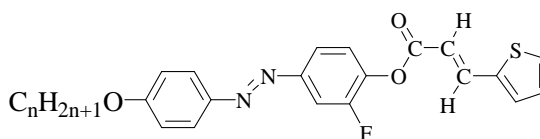
$$C_nH_{2n+1}O - \text{(structure)}$$
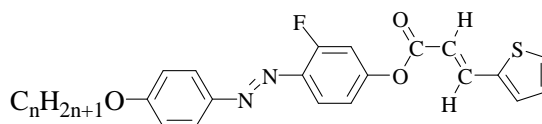
n-alkyl	C-C	C-N	N-I	I-N	N-C	$T_{N-I} - T_{C-N}$*
CH$_3$	**140.3** *15.3*	**169.4** *30.3*	**215.4** *1.6*	**214.5** *1.5*	**119.8** *41.3*	46.0
C$_2$H$_5$		**147** *31.6*	**216** *1.7*	**214.4** *1.6*	**130.3** *43.0*	69.0
C$_3$H$_7$		**134.6** *33.5*	**197.9** *1.5*	**195.5** *1.6*	**82.3** *33.9*	63.3
C$_4$H$_9$		**129.4** *72.2*	**196.5** *3.5*	**195.9** *3.9*	**113** *78.4*	67.1
C$_5$H$_{11}$		**135.4** *57.9*	**186** *2.2*	**185.3** *2.5*	**104** *53.2*	50.6
C$_6$H$_{13}$		**121.6** *25.6*	**183.3** *1.8*	**182.6** *2.0*	**103.7** *33.3*	61.7
C$_7$H$_{15}$		**114.9** *12.7*	**175.6** *0.7*	**174.8** *0.6*	**94.6** *11.9*	60.7
C$_8$H$_{17}$		**115.6** *28.4*	**167** *1.3*	**168.5** *1.1*	**88.4** *27.9*	51.4
C$_9$H$_{19}$		**114.5** *55.6*	164.1 *1.5*	163.5 *1.4*	**100.8** *40.4*	49.6
C$_{10}$H$_{21}$		**96.7** *31.4*	**163.3** *1.6*	**162.6** *1.6*	**75.0** *28.0*	66.6
Average			190.7			58.6

*Phase range = clearing point (T_{N-I}) – m.p. (T_{C-N})
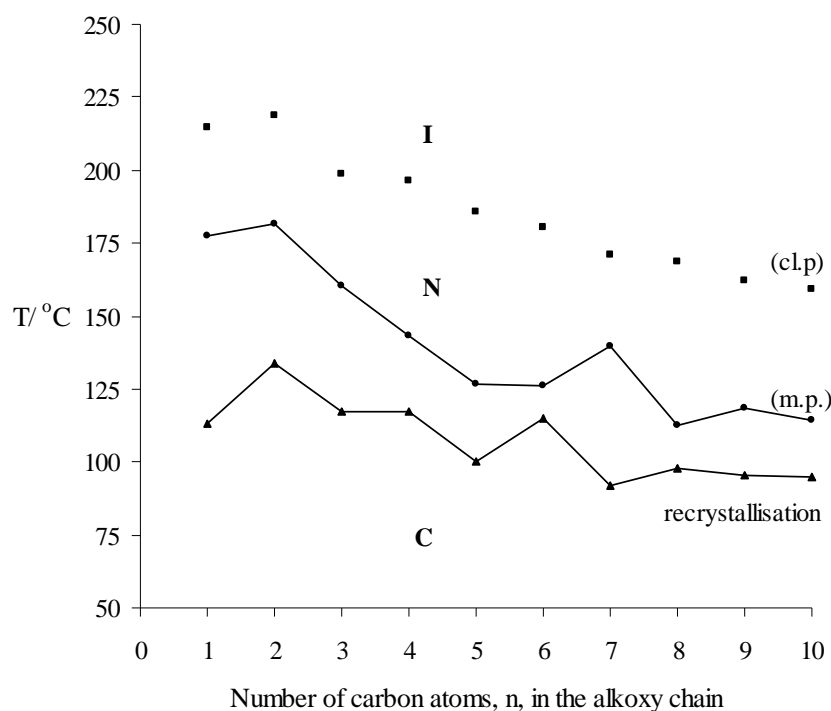

Plot 4: Transition temperature plot for the members of a homologous series of 3-thiophen-2-yl-acrylic acid 4-(4-n-alkoxyphenylazo)-3'-fluorophenyl esters **(41 a-j) [Series IV]**.

Table 5: Transition temperatures (^{o}C) for a homologous series of 3-thiophen-2-yl-acrylic acid 4-(4-n-alkoxyphenylazo)-2'-fluorophenyl esters **(42 a-j) [Series VI]**
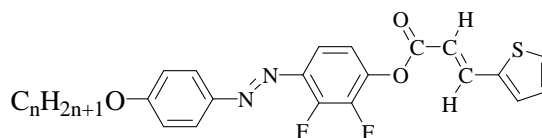

n-alkyl	C-C	C-N	N-I	I-N	N-C	T_{N-I} - T_{C-N}*
CH$_3$		**177.4**	**215.9**	**214.5**	**112.9**	
		36.7	*1.5*	*1.5*	*31.8*	38.5
C$_2$H$_5$		**181.5**	**220**	**218.6**	**133.6**	
		44.0	*2.1*	*2.1*	*41.7*	38.5
C$_3$H$_7$		**160.3**	**200**	**198.4**	**117.4**	
		39.3	*1.8*	*1.8*	*35.6*	39.7
C$_4$H$_9$		**143.1**	**199**	**196.5**	**117.4**	
		38.5	*2.1*	*2.0*	*31.3*	55.9
C$_5$H$_{11}$		**126.7**	**187.1**	**185.8**	**100**	
		51.3	*2.9*	*3.3*	*45.1*	60.4
C$_6$H$_{13}$		**125.9**	**181.1**	**180.4**	**114.8**	
		42.0	*1.6*	*1.8*	*33.3*	55.2
C$_7$H$_{15}$		**139.8**	**172.2**	**171.2**	**91.7**	
		12.6	*1.0*	*0.6*	*11.9*	32.4
C$_8$H$_{17}$		**112.8**	**169.3**	**168.6**	**97.5**	
		57.2	*1.9*	*1.8*	*50.3*	56.5
C$_9$H$_{19}$		**118.2**	**162.5**	**162**	**95.4**	
		65.8	*2.3*	*2.3*	*63.5*	44.3
C$_{10}$H$_{21}$		**114.4**	**159.6**	**158.9**	**94.7**	
		40.2	*2.1*	*2.0*	*37.8*	45.2
Average			186.7			46.6

*Phase range = clearing point (T_{N-I}) – m.p. (T_{C-N})

Plot 5: Transition temperature plot for the members of a homologous series of 3-thiophen-2-yl-acrylic acid 4-(4-n-alkoxyphenylazo)-2'-fluorophenyl esters **(42 a-j) [Series VI]**

Table 6: Transition temperatures (^{o}C) for a homologous series of 3-thiophen-2-yl-acrylic acid 4-(4-n-alkoxyphenylazo)-2',3'-difluorophenyl esters **(43 a-j) [Series VIII]**
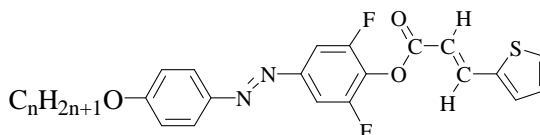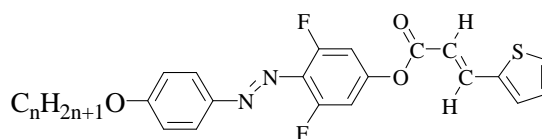
n-alkyl	C-C	C-N	N-I	I-N	N-C	T_{N-I} - T_{C-N}*
CH$_3$		**147.1**	**215.8**	**213.5**	**97.2**	
		30.6	*1.2*	*1.4*	*27.2*	68.7
C$_2$H$_5$		**158**	**221.7**	**219.6**	**114.5**	
		29.9	*1.2*	*1.3*	*26.1*	63.7
C$_3$H$_7$		**144.9**	**201.1**	**200.5**	**133**	
		35.6	*1.7*	*1.6*	*31.1*	56.2
C$_4$H$_9$		**140.1**	**199.7**	**198.1**	**86.5**	
		34.6	*2.0*	*1.8*	*38.5*	59.6
C$_5$H$_{11}$		**143.3**	**186.8**	**186.1**	**70**	
		44.6	*1.9*	*2.0*	*28.1*	43.5
C$_6$H$_{13}$		**117.3**	**182.7**	**182.1**	**96.2**	
		36.7	*1.7*	*1.7*	*29.0*	65.4
C$_7$H$_{15}$		**116.4**	**173**	**172.5**	**70.6**	
		35.3	*1.8*	*1.8*	*33.2*	56.6
C$_8$H$_{17}$		**125.6**	**171.1**	**170**	**77.1**	
		48.5	*2.3*	*1.9*	*44*	45.5
C$_9$H$_{19}$		**115.5**	**161.6**	**160.8**	**89.7**	
		55.1	*1.4*	*1.5*	*44.0*	46.1
C$_{10}$H$_{21}$		**113**	**160.9**	**160.1**	**86.7**	
		53.0	*1.6*	*1.7*	*35.1*	47.9
Average			185.5			55.3

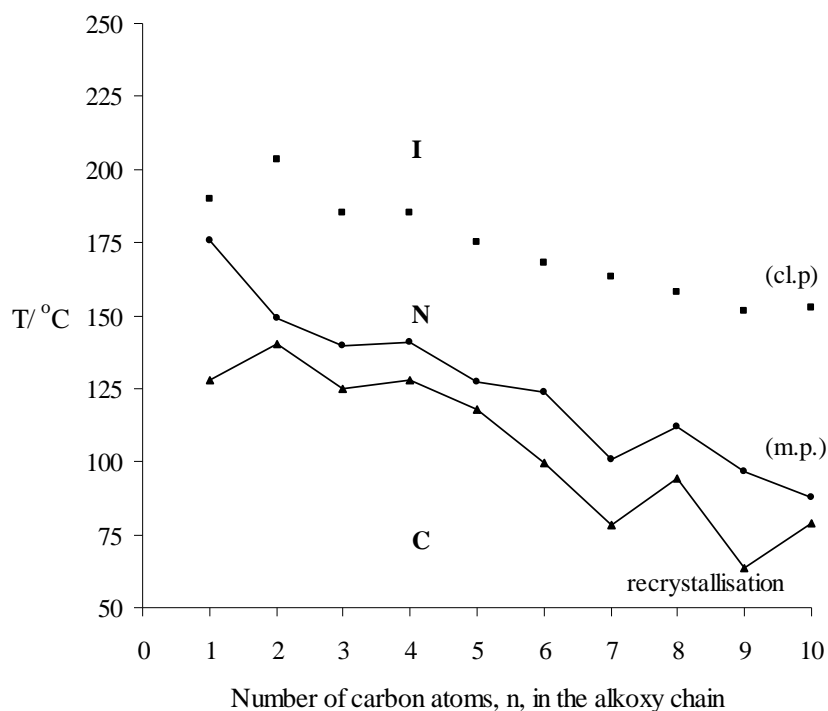*Phase range = clearing point (T_{N-I}) – m.p. (T_{C-N})
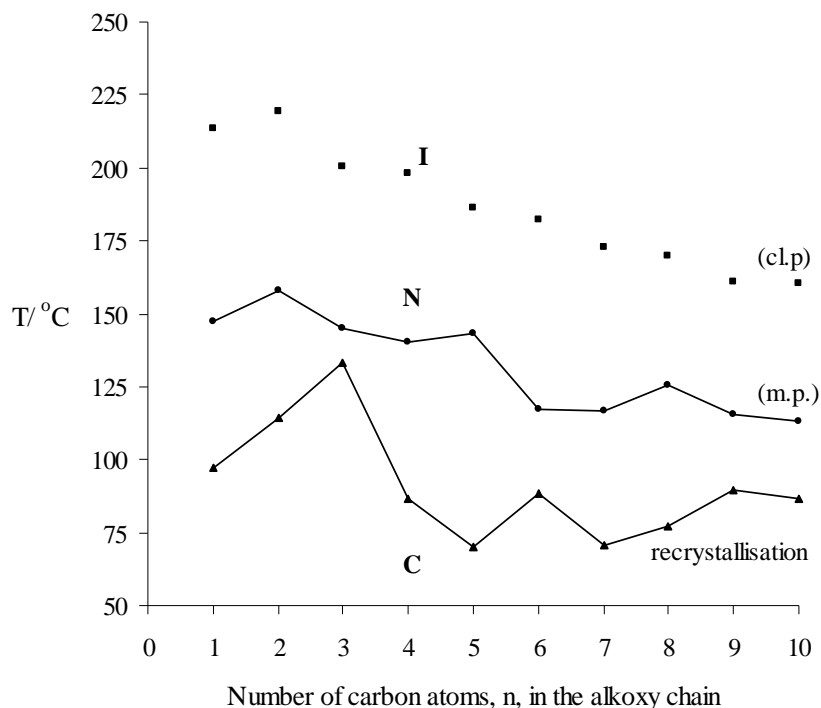
Plot 6: Transition temperature plot for the members of a homologous series of 3-thiophen-2-yl-acrylic acid 4-(4-n-alkoxyphenylazo)-2',3'-difluorophenyl esters **(43 a-j) [Series VIII]**.

Table 7: Transition temperatures (^{o}C) for a homologous series of 3-thiophen-2-yl-acrylic acid 4-(4-n-alkoxyphenylazo)-2',6'-difluorophenyl esters **(44 a-j) [Series X]**

$C_nH_{2n+1}O$ —(structure)—

n-alkyl	C-C	C-N	N-I	I-N	N-C	T_{N-I} -T_{C-N}*
CH$_3$		**157.5** *29.7*	**193.5** *1.9*	**191.0** *1.9*	**115.0** *28.9*	36.0
C$_2$H$_5$		**181.3** *36.4*	**204.4** *2.5*	**202.6** *2.5*	**155.1** *35.3*	23.1
C$_3$H$_7$		**159.6** *34.2*	**183.7** *2.3*	**182.9** *2.2*	**143.9** *33.5*	24.1
C$_4$H$_9$	**146.8** *8.2*	**150.1** *28.1*	**181.9** *2.9*	**181** *2.5*	**123** *29.27*	31.8
C$_5$H$_{11}$		**137** *35.2*	**171** *2.8*	**170.3** *2.8*	**101.8** *30.0*	34.0
C$_6$H$_{13}$		**106** *28.4*	**172** *2.1*	**171.3** *2.1*	**90.3** *29.4*	50.0
C$_7$H$_{15}$		**140.3** *50.0*	**157.1** *2.1*	**156** *2.3*	**88.5** *41.3*	16.8
C$_8$H$_{17}$		**115.3** *44.2*	**152.5** *2.2*	**151.2** *2.2*	**88.4** *41.8*	37.2
C$_9$H$_{19}$		**123** *47.3*	**147.3** *2.0*	**146.1** *2.0*	**93.6** *43.3*	24.3
C$_{10}$H$_{21}$		**133.6** *52.2*	**138.5** *1.9*	**137.5** *2.3*	**106.9** *40.6*	4.9
Average			170.6			28.2

*Phase range = clearing point (T_{N-I}) – m.p. (T_{C-N})
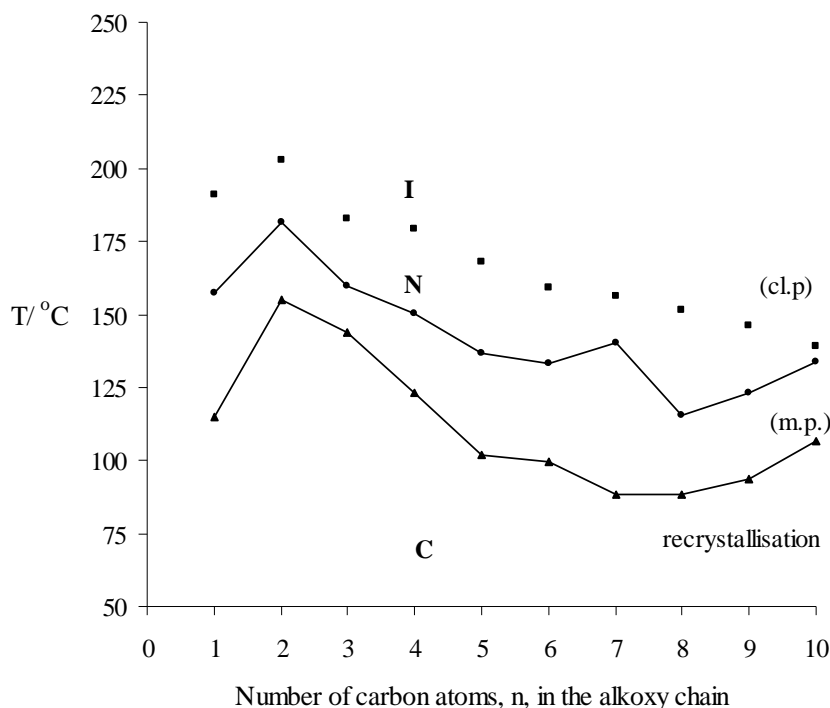
Plot 7: Transition temperature plot for the members of a homologous series of 3-thiophen-2-yl-acrylic acid 4-(4-n-alkoxyphenylazo)-2',6'-difluorophenyl esters **(44 a-j) [Series X]**.

Table 8: Transition temperatures (^{o}C) for a homologous series of 3-thiophen-2-yl-acrylic acid 4-(4-n-alkoxyphenylazo)-3',5'-difluorophenyl esters **(45 a-j) [Series XII]**
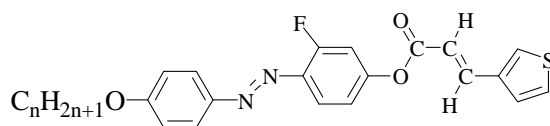

$C_nH_{2n+1}O$—〈 〉—N=N—...—O—C(=O)—CH=CH—thiophene

n-alkyl	C-C	C-N	N-I	I-N	N-C	$T_{N-I} - T_{C-N}$*
CH$_3$		**175.4** *38.2*	**190** *0.8*	**187** *0.9*	**128** *35.2*	14.6
C$_2$H$_5$		**149.4** *35.9*	**205.1** *1.3*	**203.5** *1.2*	**140.2** *30.7*	55.7
C$_3$H$_7$		**139.7** *41.3*	**186.4** *1.8*	**185.2** *1.8*	**125** *40*	46.7
C$_4$H$_9$		**140.6** *49.5*	**186.9** *2*	**185.2** *2*	**127.8** *47.7*	46.2
C$_5$H$_{11}$		**127** *56.8*	**175.5** *2.2*	**175** *2.2*	**117.8** *55.8*	48.5
C$_6$H$_{13}$		**123.9** *36*	**165.8** *3.2*	**165.3** *3.2*	**99.6** *46.2*	41.9
C$_7$H$_{15}$		**100.8** *27.2*	**163.9** *1.6*	**163.1** *1.6*	**78.2** *28.6*	63.1
C$_8$H$_{17}$		**111.7** *46.7*	**161** *1.8*	**160.2** *2*	**94.3** *41.1*	49.3
C$_9$H$_{19}$		**96.7** *36.9*	**152.9** *1.7*	**151.5** *1.7*	**63.6** *35.7*	56.2
C$_{10}$H$_{21}$		**87.5** *31.6*	**154** *1.8*	**152.9** *1.8*	**79** *29.2*	66.5
Average			174.2			48.9

*Phase range = clearing point (T_{N-I}) – m.p. (T_{C-N})

Plot 8: Transition temperature plot for the members of a homologous series of 3-thiophen-2-yl-acrylic acid 4-(4-n-alkoxyphenylazo)-3',5'-difluorophenyl esters **(45 a-j) [Series XII]**.

Table 9: Transition temperatures (^{o}C) for a homologous series of 3-thiophen-3-yl-acrylic acid 4-(4-n-alkoxyphenylazo)-3'-fluorophenyl esters **(46 a-j) [Series V]**
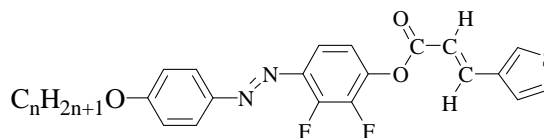
$C_nH_{2n+1}O$ —⟨phenyl⟩—N=N—⟨F-phenyl⟩—O—C(=O)—CH=CH—⟨thiophene-S⟩

n-alkyl	C-C	C-N	N-I	I-N	N-C	$T_{N-I} - T_{C-N}$*
CH₃		**169.4**	**215.4**	**214.5**	**119.8**	
		43.6	*1.4*	*1.3*	*38.9*	46.0
C₂H₅	**134.3**	**150.6**	**223.6**	**220.9**	**128**	
	5.5	*34.7*	*2.0*	*2.0*	*33.0*	73.0
C₃H₇		**134.7**	**203.5**	**202.2**	**97.8**	
		33.3	*1.9*	*1.9*	*26.7*	68.8
C₄H₉	**110.4**	**119.1**	**201.2**	**200.1**	**96.2**	
	6.7	*30.2*	*2.1*	*2.2*	*31.7*	82.1
C₅H₁₁		**114**	**192.6**	**192.1**	**85.3**	
		34.8	*1.8*	*1.8*	*27.3*	78.6
C₆H₁₃		**115.1**	**187.5**	**187.3**	**99.3**	
		37.6	*1.9*	*1.9*	*30.3*	72.4
C₇H₁₅		**99.8**	**177.9**	**170**	**76.9**	
		34.3	*1.7*	*1.7*	*23.7*	78.1
C₈H₁₇		**105.8**	**174.5**	**173.5**	**77.8**	
		30.3	*1.2*	*1.4*	*19.3*	68.7
C₉H₁₉		**99**	**167.7**	**167**	**69.7**	
		34.6	*1.5*	*1.5*	*31.7*	68.7
C₁₀H₂₁		**101.5**	**163.7**	**163.1**	**76.7**	
		30.3	*1.6*	*1.6*	*27.1*	62.2
Average			190.8			69.9

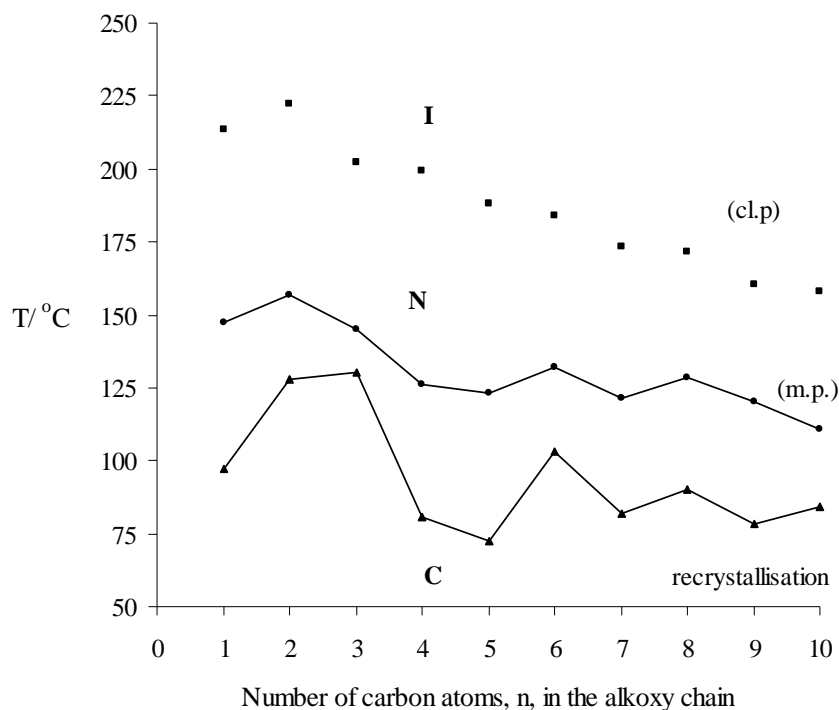*Phase range = clearing point (T_{N-I}) – m.p. (T_{C-N})
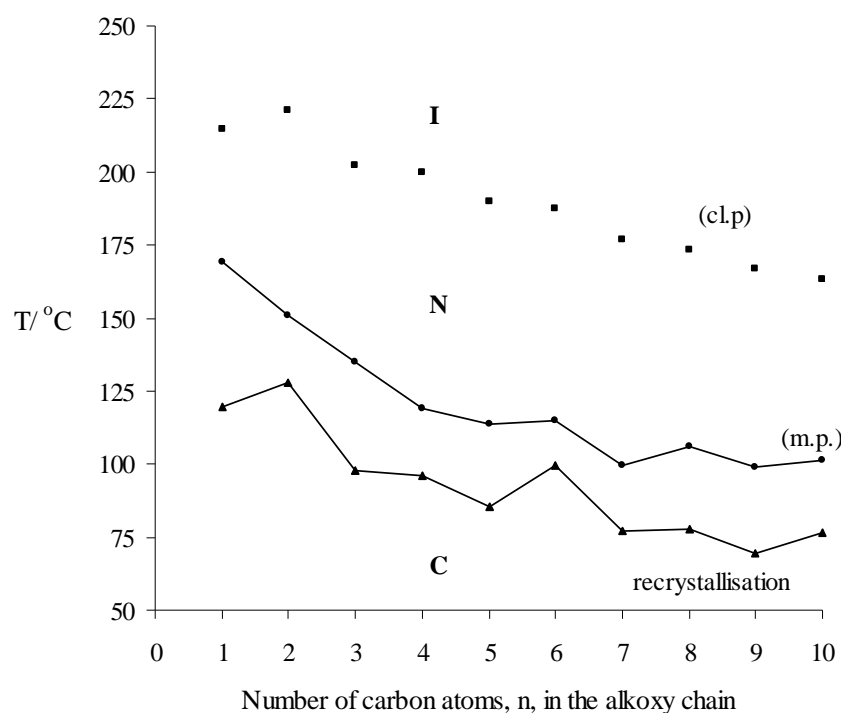
Plot 9: Transition temperature plot for the members of a homologous series of 3-thiophen-3-yl-acrylic acid 4-(4-n-alkoxyphenylazo)-3'-fluorophenyl esters **(46 a-j) [Series V]**.

Table 10: Transition temperatures (^{o}C) for a homologous series of 3-thiophen-3-yl-acrylic acid 4-(4-n-alkoxyphenylazo)-2'-fluorophenyl esters **(47 a-j) [Series VII]**

$$C_nH_{2n+1}O-\text{(aryl)}-N=N-\text{(aryl)}-O-C(=O)-CH=CH-\text{(thiophene)}$$
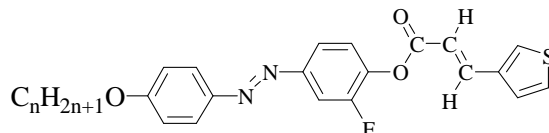
n-alkyl	C-C	C-N	N-I	I-N	N-C	T_{N-I} - T_{C-N}*
CH$_3$		**183** *38.5*	**213.7** *1.5*	**212.9** *1.5*	**133.7** *33.3*	30.7
C$_2$H$_5$		**195.4** *40.7*	**221.8** *2.3*	**219.8** *2.1*	**152.4** *37.5*	26.4
C$_3$H$_7$		**175.3** *40.7*	**201.5** *2.1*	**200** *2.0*	**150.7** *39.1*	26.2
C$_4$H$_9$		**152.8** *29.4*	**200** *1.1*	**199** 1.9	**120.5** *28.6*	47.2
C$_5$H$_{11}$		**135.2** *42.9*	**187** *2.4*	**186.6** *2.3*	**107.7** *38.3*	51.8
C$_6$H$_{13}$		**129.7** *30.4*	**183.5** *2.2*	**183.1** 2.1	**121.6** *28.0*	53.8
C$_7$H$_{15}$		**134.7** *52.1*	**167.5** *2.1*	**168** *1.9*	**94.9** *29.7*	32.8
C$_8$H$_{17}$		**126.6** *50.5*	**170** *2.1*	**169.3** *2*	**87.5** *37.3*	43.4
C$_9$H$_{19}$		**129** *48.0*	**162.5** *2.1*	**161.8** *2.1*	**97.1** *56.0*	33.5
C$_{10}$H$_{21}$		**114.8** *37.4*	**159.3** *1.9*	**159** *1.9*	**94** *35.7*	44.5
Average			186.7			39.0

*Phase range = clearing point (T_{N-I}) – m.p. (T_{C-N})
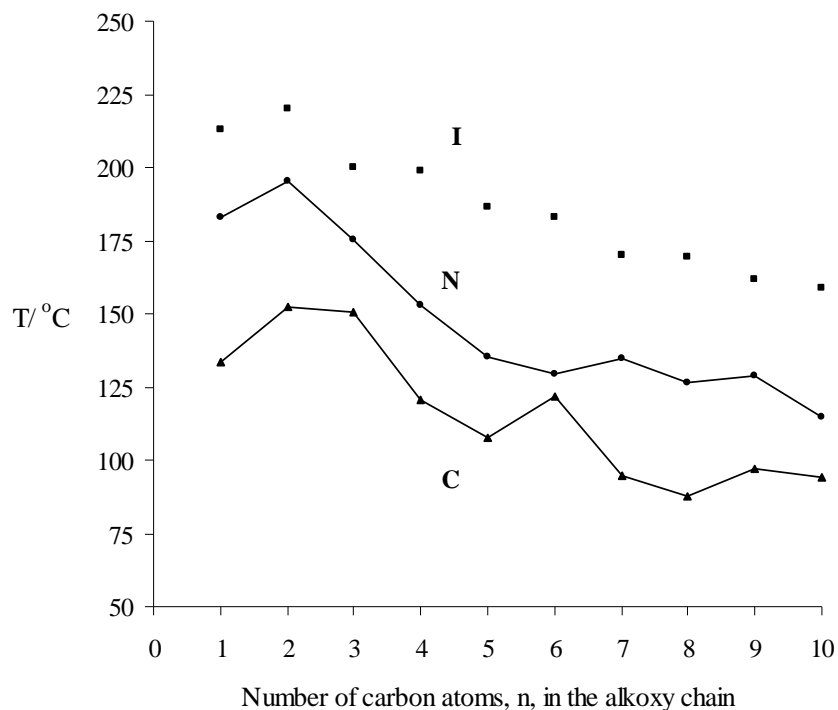
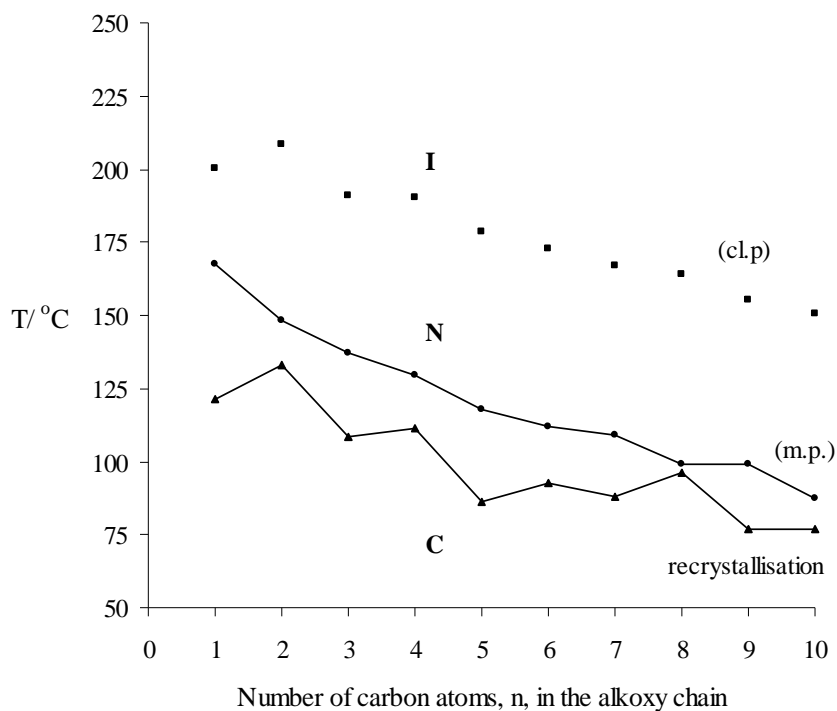**Plot 10:** Transition temperature plot for the members of a homologous series of 3-thiophen-3-yl-acrylic acid 4-(4-n-alkoxyphenylazo)-2'-fluorophenyl esters **(47 a-j) [Series VII]**.

89

Table 11: Transition temperatures (°C) for a homologous series of 3-thiophen-3-yl-acrylic acid 4-(4-n-alkoxyphenylazo)-2',3'-difluorophenyl esters **(48 a-j) [Series IX]**

n-alkyl	C-C	C-N	N-I	I-N	N-C	T_{N-I} - T_{C-N}*
CH₃		**147.1**	**215.8**	**213.5**	**97.2**	
		34.5	*1.5*	*1.4*	*29.1*	68.7
C₂H₅	**139.6**	**157**	**224.5**	**222.2**	**127.7**	
	4.7	*34.3*	*2.3*	*2.3*	*32.8*	67.5
C₃H₇		**145**	**203.1**	**202**	**130.2**	
		29.7	*1.9*	*1.9*	*28.7*	58.1
C₄H₉		**126.1**	**200.2**	**199.2**	**80.5**	
		40.2	*2.3*	*2.3*	*30.0*	74.1
C₅H₁₁		**123**	**188.9**	**188**	**72.2**	
		37.4	*2.0*	*2.0*	*23.5*	65.9
C₆H₁₃		**132**	**185.5**	**184.2**	**103.2**	
		44.9	*2.1*	*2.1*	*41.6*	53.5
C₇H₁₅		**121.3**	**174.3**	**173.3**	**82.1**	
		37.8	*1.6*	*1.8*	*38.9*	53
C₈H₁₇		**128.4**	**172.2**	**171.4**	**90**	
		39.5	*1.6*	*1.6*	*53.5*	43.8
C₉H₁₉		**120.1**	**161.3**	**160.2**	**78.2**	
		49.2	*2.2*	*2.0*	*44.8*	41.2
C₁₀H₂₁		**111**	**158.6**	**158**	**84.5**	
		59.2	*1.8*	*1.8*	*39.7*	47.6
Average			188.4			57.3

*Phase range = clearing point (T_{N-I}) – m.p. (T_{C-N})

Plot 11: Transition temperature plot for the members of a homologous series of 3-thiophen-3-yl-acrylic acid 4-(4-n-alkoxyphenylazo)-2',3'-difluorophenyl esters **(48 a-j) [Series IX]**.

Table 12:   Transition temperatures (°C) for a homologous series of 3-thiophen-3-yl-acrylic acid 4-(4-n-alkoxyphenylazo)-2',6'-difluorophenyl esters **(49 a-j) [Series XI]**
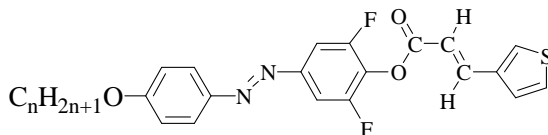
n-alkyl	C-C	C-N	N-I	I-N	N-C	T_{N-I} - T_{C-N}*
CH_3		**177.2** *32.1*	**189.5** *2.0*	**188.4** *2.0*	**128.2** *31.6*	12.3
C_2H_5	**175.5** *6.8*	**198.2** *45.0*	**199.8** *†*	**199.4** *2.8*	**189.4** *42*	1.6
C_3H_7		**171.3** *32.4*	**175.7** *†*	**174.5** *2.2*	**159.1** *35.6*	4.4
C_4H_9		**156.1** *37.3*	**175.0** *2.6*	**174.0** *2.7*	**130.9** *34.5*	18.9
C_5H_{11}	**137.5** *5.2*	**143.0** *42.6*	**162.0** *2.2*	**161.0** *2.3*	**113.0** *42.1*	19
C_6H_{13}		**133.4** *32.5*	**160.2** *2.8*	**159.0** *3.0*	**99.4** *49.2*	70.8
C_7H_{15}		**134.9** *35.1*	**149.0** *1.7*	**148.0** *1.7*	**82.0** *30.3*	14.1
C_8H_{17}		**126.0** *37.7*	**146.2** *2.4*	**145.3** *2.5*	**95.1** *35.4*	20.2
C_9H_{19}		**135.6** *36.6*	**138.6** *2.0*	**138.0** *2.0*	**107.2** *33.4*	3.0
$C_{10}H_{21}$		**131.6** *52.1*	**136.1** *1.6*	**135.2** *2.3*	**106.2** *39.6*	4.5
Average			164.9			16.9

*Phase range = clearing point (T_{N-I}) – m.p. (T_{C-N}),   † Overlap of 2 phases
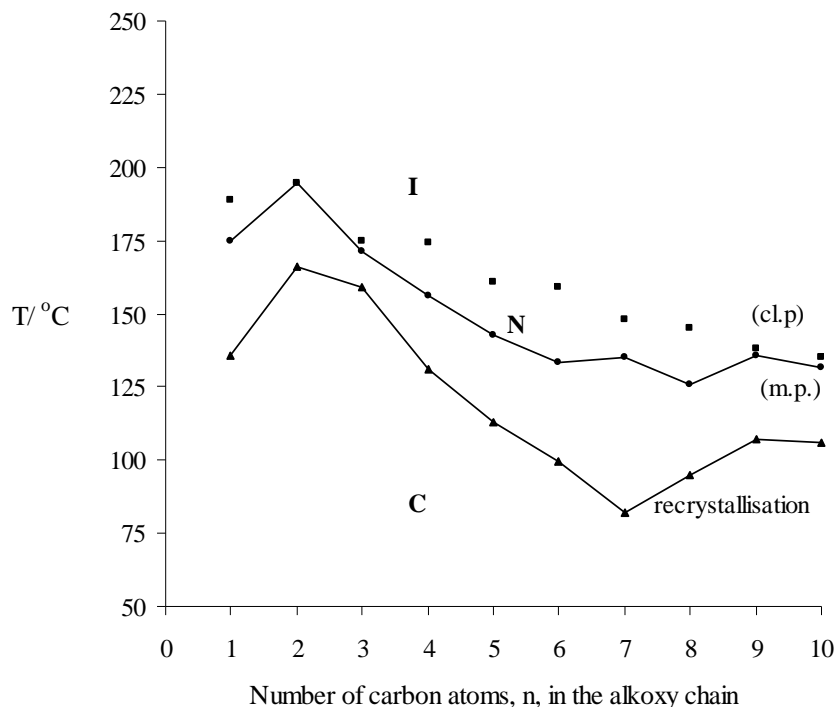
Plot 12:   Transition temperature plot for the members of a homologous series of 3-thiophen-3-yl-acrylic acid 4-(4-n-alkoxyphenylazo)-2',6'-difluorophenyl esters **(49 a-j) [Series XI]**.

Table 13: Transition temperatures (^{o}C) for a homologous series of 3-thiophen-3-yl-acrylic acid 4-(4-n-alkoxyphenylazo)-3',5'-difluorophenyl esters **(50 a-j) [Series XIII]**

$$C_nH_{2n+1}O{-}\text{(aryl)}{-}N{=}N{-}\text{(difluorophenyl)}{-}O{-}C({=}O){-}CH{=}CH{-}\text{(thiophene)}$$
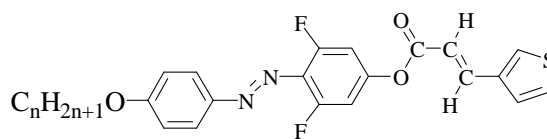
n-alkyl	C-C	C-N	N-I	I-N	N-C	$T_{N-I} - T_{C-N}$*
CH₃		**167.7** *41.3*	**201.7** *1.3*	**200.5** *0.6*	**121.3** *35.0*	34.0
C₂H₅		**148.3** *34.9*	**210.1** *2.1*	**208.3** *1.9*	**133.3** *31.8*	61.8
C₃H₇		**136.9** *34.5*	**192.1** *2.0*	**190.8** *1.5*	**108.3** *31.4*	55.2
C₄H₉		**129.4** *43.5*	**191.8** *2.6*	**190.6** *2.6*	**111.5** *32.4*	62.4
C₅H₁₁		**118** *31.6*	**179.5** *2.2*	**178.8** *2.0*	**86.1** *27.4*	61.5
C₆H₁₃		**112** *36*	**173.5** *1.9*	**172.7** *1.9*	**92.4** *22.3*	61.5
C₇H₁₅		**108.8** *35.1*	**167.4** *1.9*	**166.7** *1.9*	**88.3** *41*	58.6
C₈H₁₇		**99.3** *39.7*	**164.7** *2.2*	**163.8** *2.3*	**96.3** *34.1*	65.4
C₉H₁₉		**99.1** *30.1*	**156.2** *1.9*	**155.5** *1.9*	**77** *31*	57.1
C₁₀H₂₁		**87.3** *29.4*	**151.7** *1.7*	**150.7** *1.9*	**78** *29.4*	64.4
Average			178.9			58.9

* Phase range = clearing point (T_{N-I}) – m.p. (T_{C-N})

Plot 13: Transition temperature plot for the members of a homologous series of 3-thiophen-3-yl-acrylic acid 4-(4-n-alkoxyphenylazo)-3',5'-difluorophenyl esters **(50 a-j) [Series XIII]**.

3.1.1 TRANSITION TEMPERATURE PLOTS – OVERVIEW

As evidenced by the graphical plots, the odd-even effect is clearly observed for all series (*i.e.,* **Series I-XIII**). Observation of the odd-even effect is a very good indication of the purity of the compounds because it is only observed in very pure compounds. The data points correlating the N-I transition temperatures lie on two smooth curves which show an alternating odd-n and even-n effect, with the even numbered homologues (n= 2, 4, 6, 8, 10) lying uppermost. As mentioned in section 1.6.1.1, p. 22, the odd-even effect can be explained in terms of difference in the magnitude of the anisotropy of the intermolecular polarisability, $\Delta\alpha$, between adjacent pairs of homologues. $\Delta\alpha$ is the difference in molecular polarisability along the long molecular axis with respect to the molecular polarisability along the short molecular axis. Thus, for even alkoxy homologues, more C-C bonds lie on the long axis than the short axis and the magnitude of the anisotropy of molecular polarisation, $\Delta\alpha$, increases. Consequently the mesophase thermal stability also increases.

3.2   STRUCTURE-PROPERTY RELATIONSHIPS

3.2.1   INFLUENCE OF ALTERING THE NATURE AND DISPOSITION OF THE RIGHT-HAND TERMINAL AROMATIC GROUP OF THE ESTER

The influence of altering the nature and position of the right-hand terminally disposed aromatic moiety on mesophase type, thermal stability and phase range is summarised by the data displayed in **Table 14**. Irrespective of the terminal aromatic moiety all the homologues exhibit the nematic phase. A nematic thermal stability order may be expressed (shown below) demonstrating that replacement of a terminal phenyl moiety (**Series III**) with either a 3-thienyl-(**Series II**) or 2-thienyl- moiety (**Series I**) reduces the average clearing point (T_{N-I}) by 2.7 ^{o}C or 10 ^{o}C, respectively.

Ar =	Average T_{N-I}, ^{o}C	Average $T_{N-I} - T_{C-N}$, ^{o}C	Phase type
2-Thienyl (**Series I**)	202.1	61.7	N
3-Thienyl (**Series II**)	209.4	66.6	N
Phenyl (**Series III**)	212.1	82.3	N

$C_nH_{2n+1}O$—[structure]—Ar n = 1 - 10

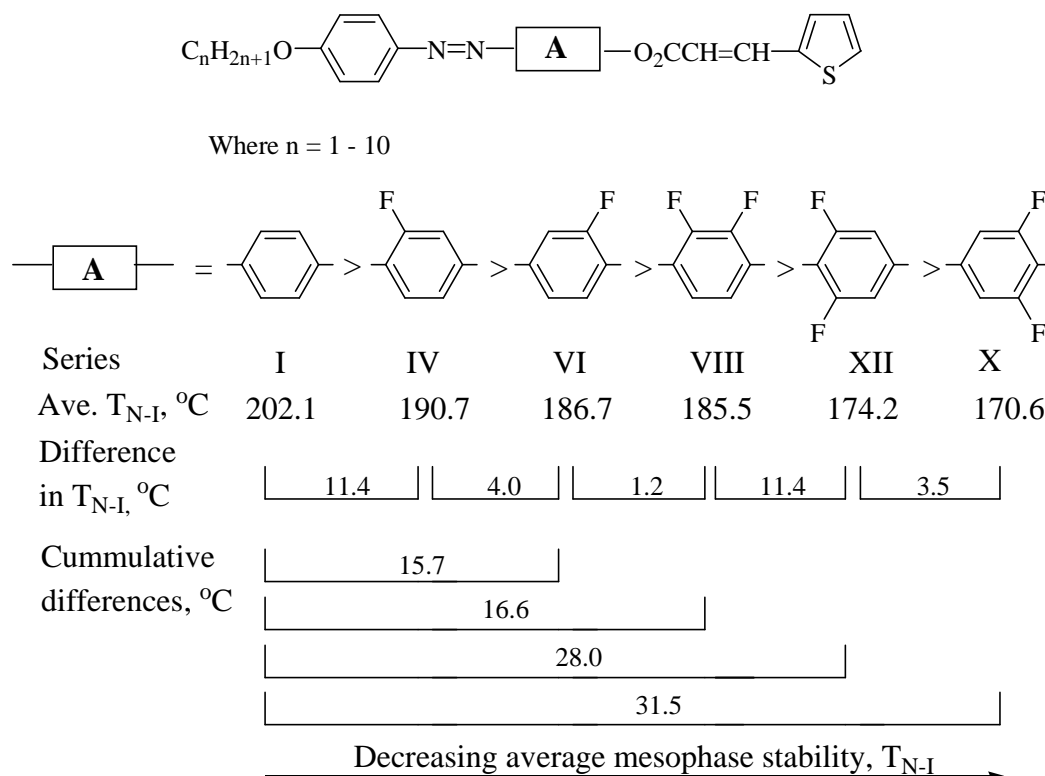**Table 14**.   Average T_{N-I} (clearing point), $T_{N-I} - T_{C-N}$ (phase range) and phase type for n = 1–10 homologues of **Series I-III**

[structure diagrams]   (Series **III**)   >   (Series **II**)   >   (Series **I**)
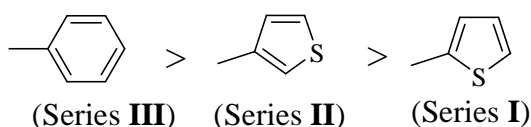
The above nematic mesophase stability order may be related to differences in linearity and subsequent packing of the molecules in the crystal lattice. As expected **Series III**, which serves as our control, gives best thermal stability due to its classical calamitic molecular architecture. The inherent molecular structure and chemistry of thiophene gives a non-linear structure which reduces the efficiency of packing and thus lowers mesophase thermal stability of members of

Series I and **II**. Interestingly, it appears that the packing efficiency and intermolecular attractions are stronger for 3-thienyl (**Series II**) than 2-thienyl (**Series I**), possibly implying a less strained system.

Likewise, the average phase range (T_{N-I}-T_{C-N}) shows a similar stability order: phenyl (**Series III**) > 3-thienyl (**Series II**) > 2-thienyl (**Series I**). In this instance, the change from phenyl to either 3-thienyl or 2-thienyl lowers the phase range by 15.7 ^{o}C or 20.6 ^{o}C, respectively.

Nabeshima *et al.*[79] have reported the n = 4–7 alkyl-substituted analogues of **Series I**. Comparison of the influence of alkyl- versus alkoxy-terminal chain on mesomorphic properties is summarised in **Table 15**. Replacement of a methylene unit, -CH_2-, with an oxygen atom increases mesophase thermal stability due to mesomeric relay of the lone pair of electrons on the oxygen atom with the azobenzene central core, increasing the molecular polarisability along the long axis of the molecule.

$C_nH_{2n+1}O$—⬡—N=N—⬡—O—C(=O)—CH=CH—Ar n = 1 - 10			
R =	**C-N, ^{o}C**	**N-I, ^{o}C**	**Phase range, ^{o}C**
C_4H_9O-	159.2	215.7	56.5
C_4H_9-	*112.0*	*171.0*	*59.0*
$C_5H_{11}O$-	133.0	201.4	67.9
C_5H_{11}-	*113.0*	*165.0*	*5.02*
$C_6H_{13}O$-	136.0	197.8	61.8
C_6H_{13}-	*114.0*	*157.0*	*43.0*
$C_7H_{15}O$-	124.7	187.1	62.4
C_7H_{15}-	*110.0*	*134.0*	*24.0*

* Phase range = clearing point (T_{N-I}) – m.p. (T_{C-N})

Table 15.   Mesomorphic properties of the n = 4-7 homologues of 3-thiophen-2-yl acrylic acid 4-(4-n-alkoxyphenylazo)phenyl esters (**Series I**) (top line) and 3-thiophen-2-yl acrylic acid 4-(4-n-alkylphenylazo)phenyl esters[79] (bottom line in italics).

3.2.2   INFLUENCE OF INTRODUCING LATERAL FLUORO-SUBSTITUENT(S)

The influence of introducing lateral fluoro-substituent(s) on mesophase type, thermal stability and phase range is summarised in **Table 16**.
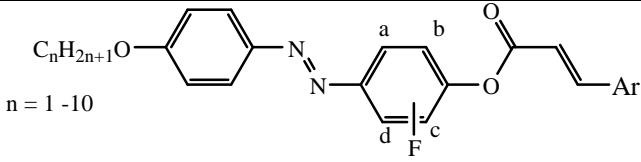
Ar =	Series	Position of fluorine(s)	Average T_{N-I}, ^{o}C	Average $T_{N-I}–T_{C-N}$, ^{o}C
2-Thienyl	I	-	202.1	61.7
2-Thienyl	IV	a-	190.7	58.6
2-Thienyl	VI	b-	186.7	46.6
2-Thienyl	VIII	a-, b-	185.5	55.3
2-Thienyl	X	b-, c-	170.6	28.2
2-Thienyl	XII	a-, d-	174.2	48.9
3-Thienyl	II	-	209.4	66.6
3-Thienyl	V	a-	190.8	69.9
3-Thienyl	VII	b-	186.7	39.0
3-Thienyl	IX	a-, b-	188.4	57.3
3-Thienyl	XI	b-, c-	164.9	16.9
3-Thienyl	XIII	a-, d-	178.9	58.9
Phenyl	III	-	212.1	82.3

Table 16.   Average T_{N-I} (clearing point), $T_{N-I} – T_{C-N}$ (phase range) and phase type for homologues n = 1-10 of **Series I**, **II**, **IV-XIII**

It is well now known that the influence of lateral fluorination on mesophase thermal stability[53], mesophase range and mesophase type is dependent upon subtle interplay of several factors, namely: number of lateral fluoro-substituents; disposition of lateral fluoro-substituents;

association and dissociation of polarity along and across the molecular long axis, and; steric crowding. Thus, a clear-cut rationale cannot always be deduced but instead tentative assumptions are inferred. To extract and rationalise the data listed in **Table 16** in to a meaningful structure-property relationship, it is best to initially review compounds derived from 3-(2-thienyl)acrylic acid (**Series I**, **IV**, **VI**, **VIII**, **X** and **XII**), followed by compounds derived from the isomeric 3-(3-thienyl)acrylic acid (**Series II**, **V**, **VII**, **IX**, **XI** and **XIII**) and finally, express an overall mesophase thermal stability order for the complete series of compounds, *i.e.*, **Series I**, **II**, **IV-XIII**.

3.2.2.1 INFLUENCE OF LATERAL FLUORINATION OF ACRYLATES DERIVED FROM 3-(2-THIENYL)ACRYLIC ACID (**Series I**, **IV**, **VI**, **VIII**, **X** AND **XII**)
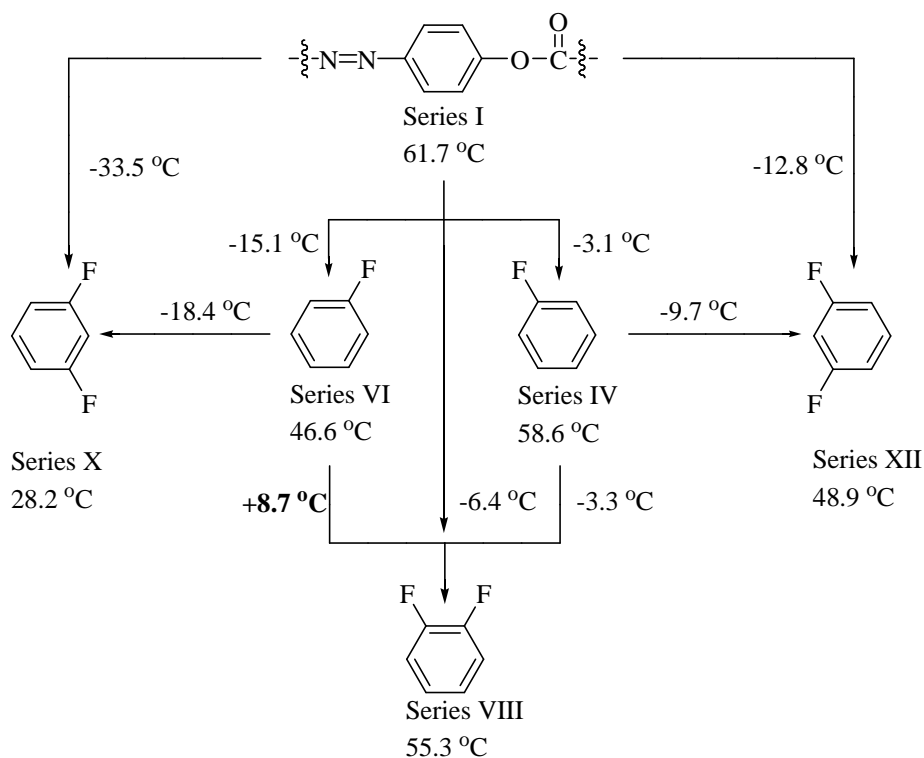
The influence of lateral fluorination on the average mesophase thermal stability (T_{N-I}) may be expressed by the stability order shown below.

$$C_nH_{2n+1}O \text{—} \bigcirc \text{—} N{=}N \text{—} \boxed{A} \text{—} O_2CCH{=}CH \text{—} \langle S \rangle$$

Where n = 1 - 10

$$\boxed{A} \; = \; \bigcirc \; > \; \bigcirc_F \; > \; \bigcirc_{F,F} \; > \; \bigcirc_{F,F} \; > \; \bigcirc_{F,F} \; > \; \bigcirc_{F,F}$$

Series	I	IV	VI	VIII	XII	X
Ave. T_{N-I}, °C	202.1	190.7	186.7	185.5	174.2	170.6

Difference in T_{N-I}, °C

| 11.4 | 4.0 | 1.2 | 11.4 | 3.5 |

Cummulative differences, °C

15.7

16.6

28.0

31.5

Decreasing average mesophase stability, T_{N-I} →

Comparison with parent non-fluorinated analogues (**Series I**: average T_{N-I}, 202.1 °C), reveals inclusion of either a mono- or di-fluoro-substituent(s) decreases the average mesophase thermal stability. Interestingly, 3-fluoro-substitution (**Series IV**: average T_{N-I}, 190.7 °C) provides most stable fluorinated compounds whereas 2,6-difluoro-substitution (**Series X**: average T_{N-I}, 170.6 °C) reveals the least thermally stable series. Across-axis substitution appears to be more detrimental to mesophase thermal stability than along the same molecular axis. This may be further exemplified by the flow chart overleaf which shows changes in magnitude of the average clearing point based on the number and disposition of fluoro-substituents.

$-\{-N=N-\langle\rangle-O-\overset{\overset{O}{\|}}{C}-\}-$

Series I
202.1 °C

-31.5 °C

-14.1 °C

-11.4 °C

-27.9 °C

F ... F

-16.1 °C

Series VI
186.7 °C

Series IV
190.7 °C

-16.6 °C

Series X
170.6 °C

Series XII
174.2 °C

-1.2 °C

-16.6 °C

-5.2 °C

F   F
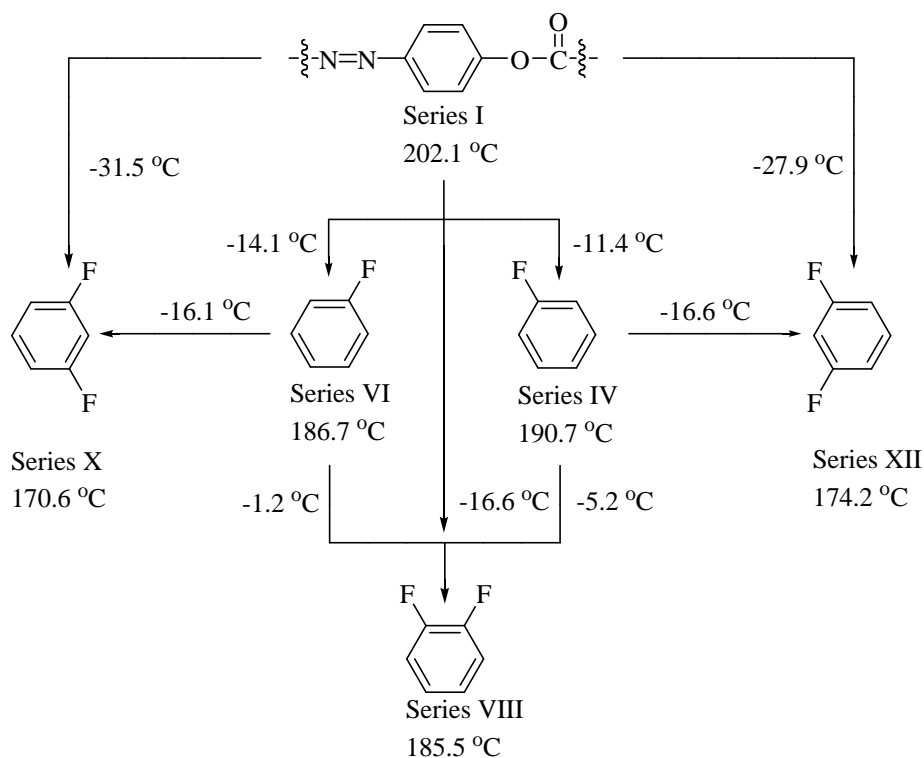
Series VIII
185.5 °C

Compared with the non-fluorinated parent compound (**Series I**: average T_{N-I}, 202.1 °C), introduction of a mono-fluoro-substituent either on an *outer edge* (**Series VI**: *ortho-* to the -O$_2$C-, linkage and *meta-* to the azo-linkage) or an *inner edge* (**Series IV**: *ortho-* to the –N=N-, linkage and *meta-* to the –O$_2$C-linkage) lowers the thermal stability by 15.4 °C and 11.4 °C, respectively. The lateral fluoro-substituent increases molecular breadth and its disposition does not seem to be too significant as only a minor difference in mesophase thermal stability between the two mono-fluoro-substituted isomers is detected, *i.e.,* **Series VI** (average T_{N-I}, 186.7 °C) and **Series IV** (average T_{N-I}, 190.8 °C).
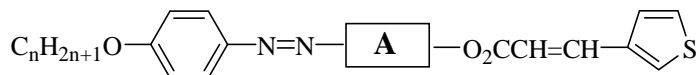
However, the influence of introducing a second lateral fluoro-substituent on mesophase thermal stability is dependent upon the initial disposition of the first fluoro-substituent and its inclusion thereafter, *i.e.*, either on the same side (**Series VIII**) or across the molecular long axis (**Series X** or **Series XII**). Introduction of a second fluoro-substituent across the molecular axis in **Series VI** (average T_{N-I}, 186.7 °C) to generate **Series X** (average T_{N-I}, 170.6 °C) lowers thermal stability by 16.1 °C. A similar trend is observed when a second across-axis fluoro-substituent is introduced in **Series IV** (average T_{N-I}, 190.7 °C) generating **Series XII** (average T_{N-I}, 174.2 °C)

99

revealing a decrease in thermal stability of 16.6 $^{\circ}$C. The drop in thermal stability by a magnitude of approximately 16 $^{\circ}$C (average of 16.1 and 16.6 $^{\circ}$C) merely reflects a further increase in lateral broadening and interannular twisting. The latter will be evident at either end of the phenyl ring since one end is attached to -N=N- and the other to –O_2C-.
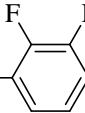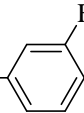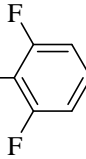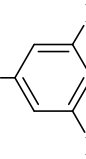
The introduction of a second fluoro-substituent on the same side of the molecular long axis (adjacent to initial fluoro-substituent), *i.e.*, **Series VIII**, slightly decreases mesophase thermal stability. A progressive increase in lateral fluorination does not lower mesophase thermal stability markedly, as demonstrated by going from either **Series IV** or **Series VI** to **Series VIII**. Introduction of a second lateral substituent to **Series VI** (average T_{N-I}, 186.7 $^{\circ}$C) to give **Series VIII** (average T_{N-I}, 185.5 $^{\circ}$C) nominally decreases thermal stability by 1.2 $^{\circ}$C. However, inclusion of a second lateral substituent to **Series IV** (average T_{N-I}, 190.8 $^{\circ}$C) to give Series **VIII** (average T_{N-I}, 185.5 $^{\circ}$C) decreases thermal stability by 5.3 $^{\circ}$C suggesting a reduction of polar electronic effects or detrimental conformational ordering of the molecule.

The influence of lateral fluorination on the average mesophase range (T_{N-I}-T_{C-N}) may be expressed by the stability order shown below.

$C_nH_{2n+1}O$—⟨benzene⟩—N=N—[A]—$O_2CCH=CH$—⟨thiophene, S⟩

Where n = 1 - 10

—[A]— = ⟨phenylene⟩ > ⟨3-F phenylene⟩ > ⟨3,4-diF phenylene⟩ > ⟨2,6-diF phenylene⟩ > ⟨2-F phenylene⟩ > ⟨3,5-diF phenylene⟩

Series	I	IV	VIII	XII	VI	X
Ave. T_{N-I}-T_{C-N}, °C	61.7	58.6	55.3	48.9	46.6	28.2
Difference in T_{N-I}-T_{C-N}, °C		3.1	3.3	6.4	2.3	18.3

Cumulative differences, °C:

6.4

12.8

15.1

33.5

Decreasing average mesophase range, T_{N-I}-T_{C-N} →
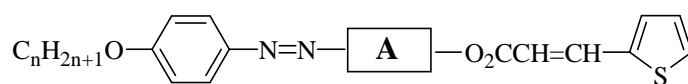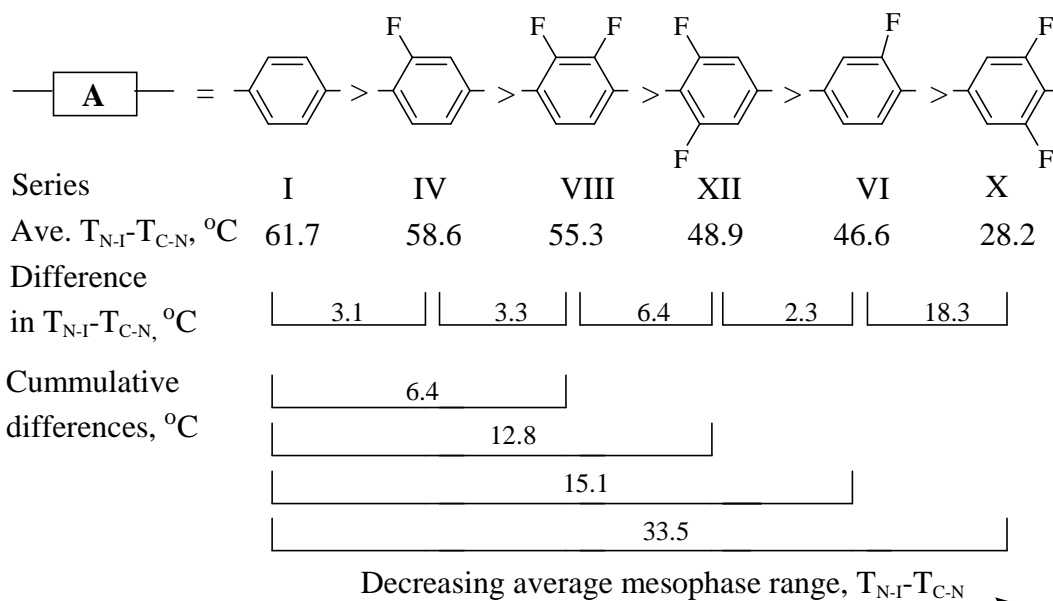
Comparison with parent non-fluorinated homologues (**Series I**: average T_{N-I}-T_{C-N}, 61.7 °C), reveals inclusion of either a mono- or di-fluoro-substituent(s) decreases the average mesophase range. Interestingly, 3-fluoro-substitution (**Series IV**: average T_{N-I}-T_{C-N}, 58.6 °C) provides most stable fluorinated compounds whereas 2,6-difluoro-substitution (**Series X**: average T_{N-I}-T_{C-N}, 28.2 °C) reveals the smallest mesophase range for the series. Outer edge substitution appears to be more detrimental to mesophase range than inner edge substitution. This may be further exemplified by the flow chart below which shows changes in magnitude of the average phase range based on the number and disposition of fluoro-substituents.

$-\\!\\!\\!\\!\\xi\\!\\!-N=N-$ ⟨ring⟩ $-O-\\overset{\\overset{\\displaystyle O}{\\|}}{C}\\!\\!-\\xi-$

Series I
61.7 °C

-33.5 °C

-15.1 °C

-3.1 °C

-12.8 °C

F ⟨ring⟩ F

-18.4 °C

F ⟨ring⟩

Series VI
46.6 °C

F ⟨ring⟩

Series IV
58.6 °C

-9.7 °C

F ⟨ring⟩ F

Series X
28.2 °C

+8.7 °C

-6.4 °C

-3.3 °C

Series XII
48.9 °C

F ⟨ring⟩ F

Series VIII
55.3 °C

Compared with the non-fluorinated parent compound (**Series I**: average T_{N-I}-T_{C-N}, 61.7 °C), introduction of a mono-fluoro-substituent either on an *outer edge* (**Series VI**: *ortho-* to the -O_2C-, linkage and *meta-* to the azo-linkage) or an *inner edge* (**Series IV**: *ortho-* to the –N=N-, linkage and *meta-* to the –O_2C-linkage) lowers the mesophase range by 15.1 °C and 3.1 °C, respectively. The lateral fluoro-substituent may increase molecular breadth, but the disposition with regards to the neighbouring groups seems to be the most significant factor for mesophase range in this series. Addition of a second fluoro-substituent to the most stable mono-fluorinated series (**Series IV**) on the same side of the molecular axis to give **Series VIII**, to give a difluorinated species (**Series VIII**) is far less detrimental to mesophase range than mono-fluorination on an *outer edge* (**Series VI**).

The influence of introducing a second lateral fluoro-substituent on mesophase range (T_{N-I}-T_{C-N}) is dependent upon the initial disposition of the first fluoro-substituent. As with mesophase thermal stability (T_{N-I}), introduction of a second fluoro-substituent across the molecular axis in **Series IV** (average T_{N-I}-T_{C-N}, 58.6 °C) to generate **Series XII** (average T_{N-I}-T_{C-N}, 48.9 °C) lowers thermal stability by 9.7 °C. However, with both fluoro-substituents on the *inner* edge, the

mesophase range is still higher by 2.3 ^{o}C than that of the mono-fluorinated **Series VI** (average T_{N-I}-T_{C-N}, 46.6 ^{o}C).

The introduction of a second fluoro-substituent on the same side of the molecular long axis (adjacent to initial fluoro-substituent), *i.e*., **Series IV**, only slightly decreases or even enhances mesophase range. A progressive increase in lateral fluorination does not always lower mesophase thermal stability significantly, as demonstrated by going from **Series VI** to **Series VIII**. Introduction of a second lateral substituent to **Series IV** (average T_{N-I}-T_{C-N}, 58.6 ^{o}C) to give **Series VIII** (average T_{N-I}-T_{C-N}, 55.3 ^{o}C) nominally lowers thermal stability by 3.3 ^{o}C. Inclusion of a second lateral substituent, however, to **Series VI** (average T_{N-I}-T_{C-N}, 46.6 ^{o}C) to give **Series VIII** (average T_{N-I}-T_{C-N}, 55.3 ^{o}C) enhances thermal stability by 8.7 ^{o}C.

3.2.3   INFLUENCE OF LATERAL FLUORINATION OF ACRYLATES DERIVED FROM 3-(3-THIENYL)ACRYLIC ACID (**SERIES II, V, VII, IX, XI AND XIII**)

The mesophase stability order, shown below, for esters derived from 3-(3-thienyl)acrylic acid (**Series II**, **V**, **VII**, **IX**, **XI** and **XIII**) is noticeably different from the order shown by

Where n = 1 - 10

Series	II	V	IX	VII	XIII	XI
Ave. T_{N-I}, °C	209.4	190.8	188.4	186.7	178.9	164.9

Difference in T_{N-I}, °C: 18.6   2.4   1.7   7.8   14.0

Cummulative differences, °C: 21.0   22.7   30.5   44.5

their isomeric counterparts derived from 3-(2-thienyl)acrylic acid, *i.e.*, (**Series I, IV, VI, VIII, X** and **XIII**), implying a strong dependency of both the disposition of the terminal thienyl moiety and fluoro-substituent.

As shown by the flowchart overleaf, which maps the influence of increasing the number of lateral fluoro-substituents on mesophase thermal stability, inclusion of a mono-fluoro-substituent on an inner edge (**Series V**, average T_{N-I}, 190.8 °C) decreases thermal stability by 18.6 °C, whereas on an outer edge (**Series VII**, average T_{N-I}, 186.7 °C) thermal stability decreases by 22.7 °C. The magnitude of decrease in thermal stability is more than for their isomeric counterparts derived from 3-(2-thienyl)acrylic acid, *i.e.*, **Series IV** and **VI**. There is a nominal difference of 4.1 °C in thermal stability between **Series V** and **VII**. Inclusion of a second fluoro-substituent on the same side of the molecular axis in **Series V or VII** to give

Series IX exemplifies a 'space-fill effect' where little change in thermal stability is observed between **Series V** and **IX** (2.4 °C). An enhancement of thermal stability by 1.7 °C is detected when a second fluoro-substituent adjacent to the first is introduced in **Series VII**. There appears to be a synergistic effect between the fluoro-substituent and the ester linkage.
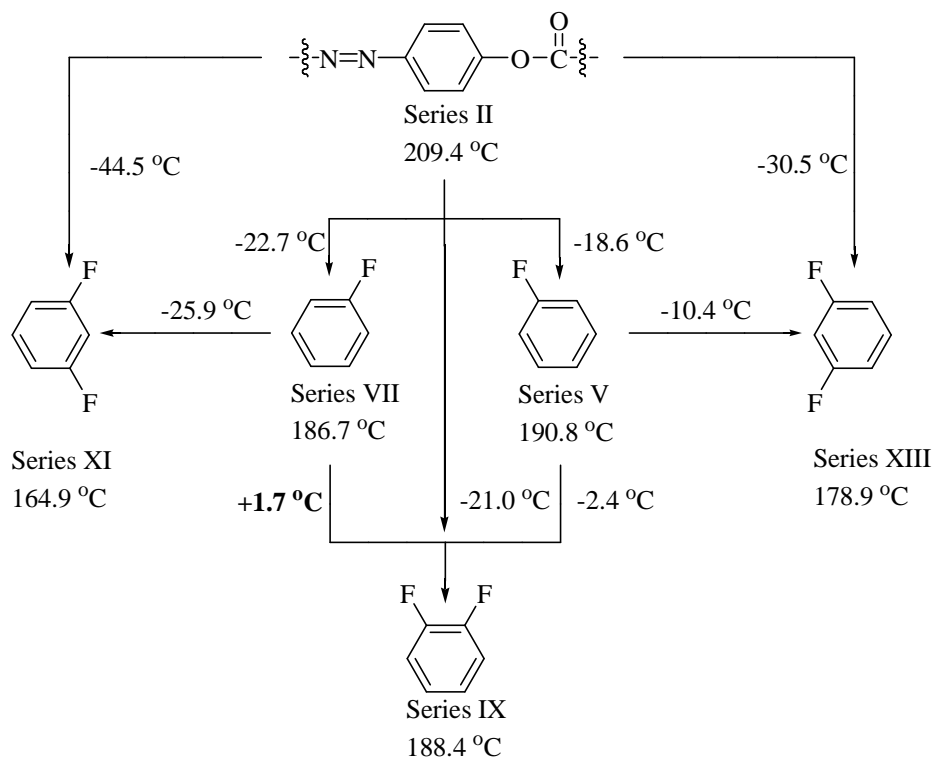
Once again, across-axis difluoro-substitution is more detrimental to mesophase thermal stability than along the long molecular axis. Again, 2,6-difluoro-substitution (**Series XI**, average T_{N-I}, 164.9 °C) affords the least thermally stable series and is 14 °C less stable than its 3,5-disubstituted isomeric counterpart (**Series XIII**, average T_{N-I}, 178.9 °C). This is a more severe decrease than observed for the isomeric across-axis compounds derived from the 3-(2-thienyl)acrylyl moiety as shown overleaf, where the 2.6-disubstituted series is 3.6 °C less stable than its 3,5-disubstituted isomeric counterpart (**Series XIII**, average T_{N-I}, 178.9 °C). A dependency on the disposition of the two lateral across-axis fluoro-substituents is evident.
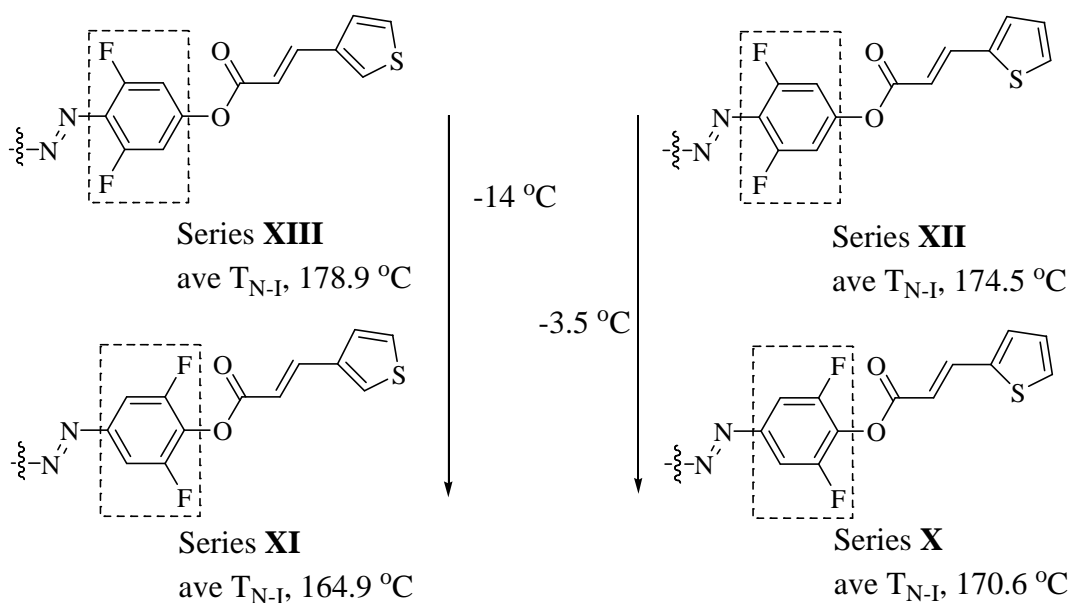
Alternatively, the influence of the disposition of the terminal thiophene in the isomeric across-axis difluoro-substituted compounds may be investigated as summarised below.
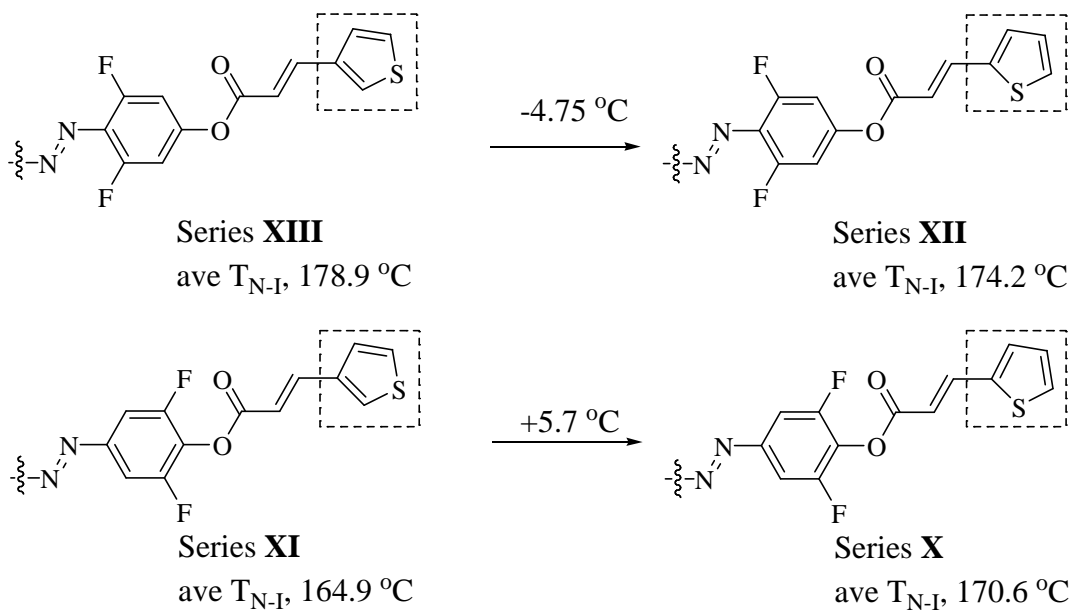
When the fluoro-substituents are located on an *inner edge*, the 3-(3-thienyl)acrylyl-derived compounds (**Series XIII**, average T_{N-I}, 178.9 °C) are 4.8 °C more stable than the 3-(2-thienyl)acrylyl counterparts (**Series XII**, average T_{N-I}, 174.2 °C). However, the opposite is observed for the outer fluoro-substituents and 3-(3-thienyl)acrylyl-derived compounds (**Series XI**, average T_{N-I}, 164.9 °C) are 5.7 °C less stable than the 3-(2-thienyl)acrylyl counterparts

(**Series X**, average T_{N-I}, 170.6 $^{\circ}$C). The disposition of the thiophene ring does play an important role in mesophase thermal stability, either showing enhancement or destabilisation.

The influence of lateral fluorination on the average mesophase range (T_{N-I}-T_{C-N}) for this set of homologues, may again be expressed by the stability order shown below.

where n=1-10

Series	V	II	XIII	IX	VII	XI
T_{N-I}-T_{C-N}, $^{\circ}$C	69.9	66.6	58.9	57.3	39.0	16.9
Difference in T_{N-I}-T_{C-N}, $^{\circ}$C	3.3		7.7	1.6	18.3	22.2

Cummulative differences, $^{\circ}$C

11

12.6

30.9

53.0
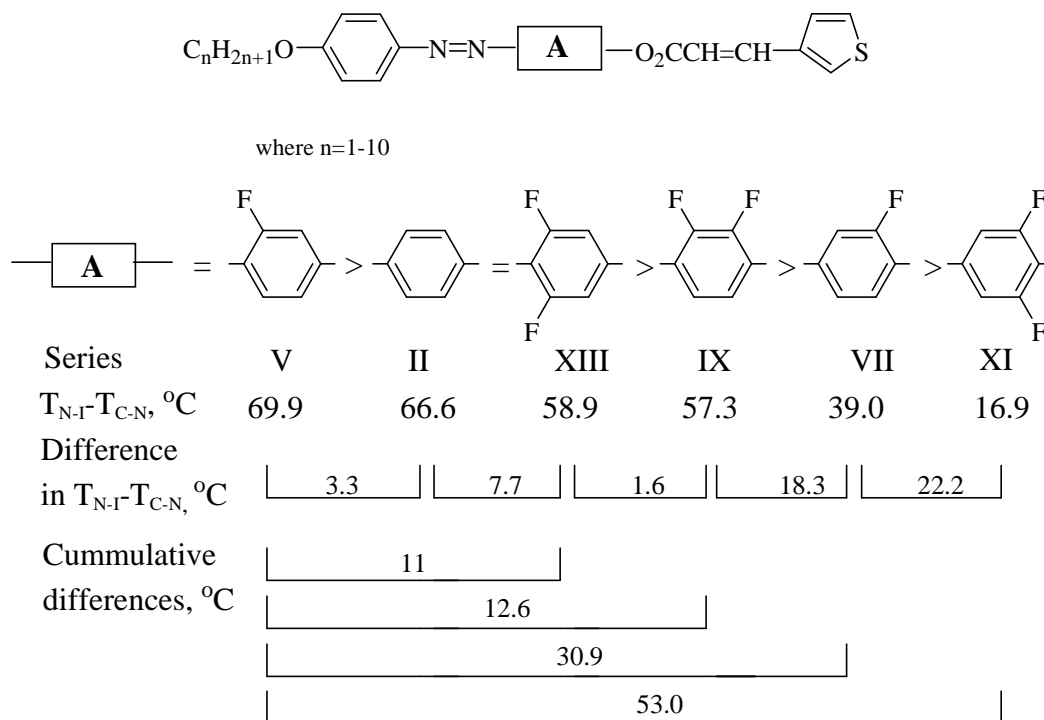
Comparison with parent non-fluorinated analogues (**Series II**: average T_{N-I}-T_{C-N}, 66.6°C), reveals inclusion of either a mono- or di-fluoro-substituent(s) in these series does not always decreases the average mesophase range (T_{N-I}-T_{C-N}). Interestingly, 3-fluoro-substitution (**Series V**: average T_{N-I}-T_{C-N}, 69.9 $^{\circ}$C) provides most stable compounds of all, whereas 2,6-difluoro-substitution (**Series XI**: average T_{N-I}-T_{C-N}, 16.9 $^{\circ}$C) reveals the smallest mesophase range (T_{N-I}-T_{C-N}) of all the series. *Outer edge* substitution appears to be more detrimental to mesophase range than *inner edge* substitution and may be further exemplified by the flow chart below which shows changes in magnitude of the mesophase range based on the number and disposition of fluoro-substituents.

$-N=N-$ ... $-O-C-$ (with O double bond, C=O)

Series II
66.6 °C

-49.7 °C

-27.6 °C

+3.3 °C

-7.7 °C

-22.1 °C

-9.7 °C

Series VII
39.0 °C

Series V
69.9 °C

Series XI
16.9 °C

Series XIII
58.9 °C

+18.3 °C

-9.3 °C

-12.6 °C
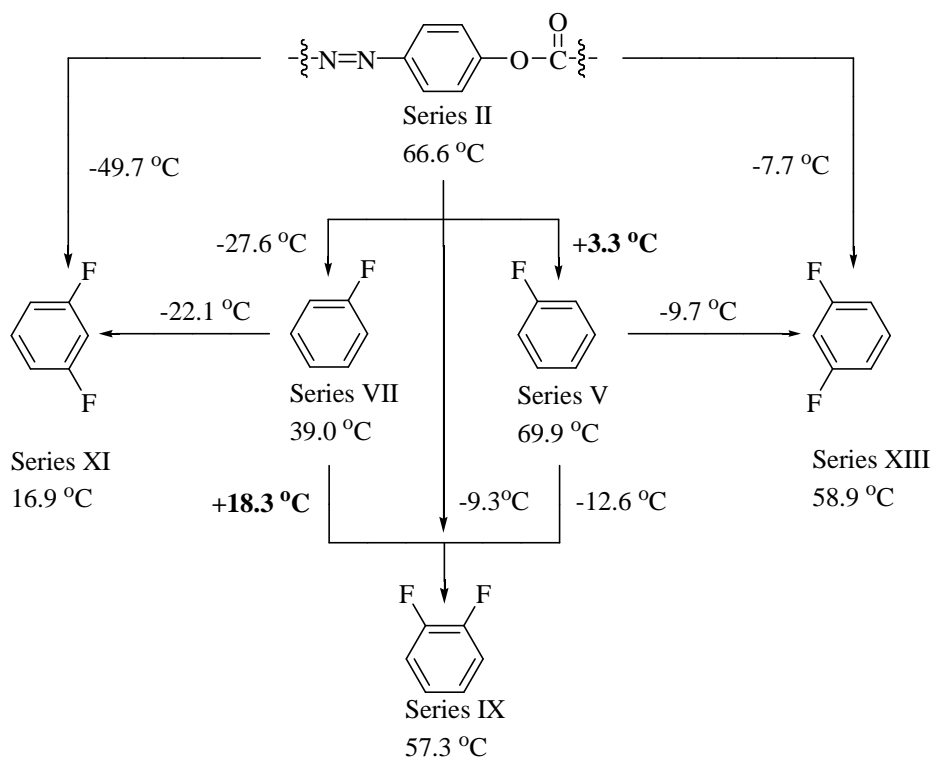
Series IX
57.3 °C

Compared with the non-fluorinated parent compound (**Series II**: average T_{N-I}-T_{C-N}, 66.6 °C), introduction of a mono-fluoro-substituent either on an *outer edge* (**Series VII**: *ortho-* to the -O_2C-, linkage and *meta-* to the azo-linkage) is extremely detrimental to the mesophase range, lowering the range by 27.6 °C. Substitution on an *inner edge* (**Series V**: *ortho-* to the –N=N-, linkage and *meta-* to the –O_2C-linkage) enhances the mesophase range by 3.3 °C. The lateral fluoro-substituent may increase molecular breadth, appearing in this case, reliant on the disposition with regards to the neighbouring groups and seems to be the most significant factor for mesophase range in this series. Addition of a second fluoro- to the most stable fluorinated series (**Series V**) along the molecular axis to give **Series IX**, is far less detrimental to mesophase range than a mono-fluoro-substituent either on an *outer edge* (**Series VII**).

The influence of introducing a second lateral fluoro-substituent on the mesophase range is dependent upon the initial disposition of the first fluoro-substituent. As with mesophase thermal stability (T_{N-I}), introduction of a second fluoro-substituent across the molecular axis in **Series V** (average T_{N-I}-T_{C-N}, 69.9 °C) to generate **Series XIII** (average T_{N-I}-T_{C-N}, 58.9 °C) lowers mesophase range by 9.7 °C. However, with both fluoro-substituents on the *inner* edge, the

108

mesophase range is still higher by 19.9 ^{o}C than that of the mono-fluorinated **Series VII** (average T_{N-I}-T_{C-N}, 39.0 ^{o}C).

As is the case for the 3,2-thienyl homologues, the introduction of a second fluoro-substituent on the same side of the molecular long axis *i.e.*, **Series IX**, decreases mesophase range of the parent homologue (**Series II**). A progressive increase in lateral fluorination again lowers mesophase range (demonstrated by going from **Series V** to **Series IX**). Introduction of a second lateral substituent to **Series V** (average T_{N-I}-T_{C-N}, 69.9 ^{o}C) to give **Series IX** (average T_{N-I}-T_{C-N}, 57.3 ^{o}C), however, lowers mesophase range by approximately 10 ^{o} more than the 3,2-thienyl homologue (12.6 ^{o}C compared to 3.3 ^{o}C). However, inclusion of a second lateral substituent to **Series VII** (average T_{N-I}-T_{C-N}, 39.0 ^{o}C) to give **Series IX** (average T_{N-I}-T_{C-N}, 57.3 ^{o}C) enhances the mesophase range by 10 ^{o} more than the 3,2- thienyl homologue (18.3 ^{o}C compared to 8.7 ^{o}C), suggesting a greater enhancement of polar electronic effects or that better conformational ordering of the molecule is attainable due to the disposition of the thiophene.

3.2.4   SUMMARY OF OVERALL THERMAL STABILITY
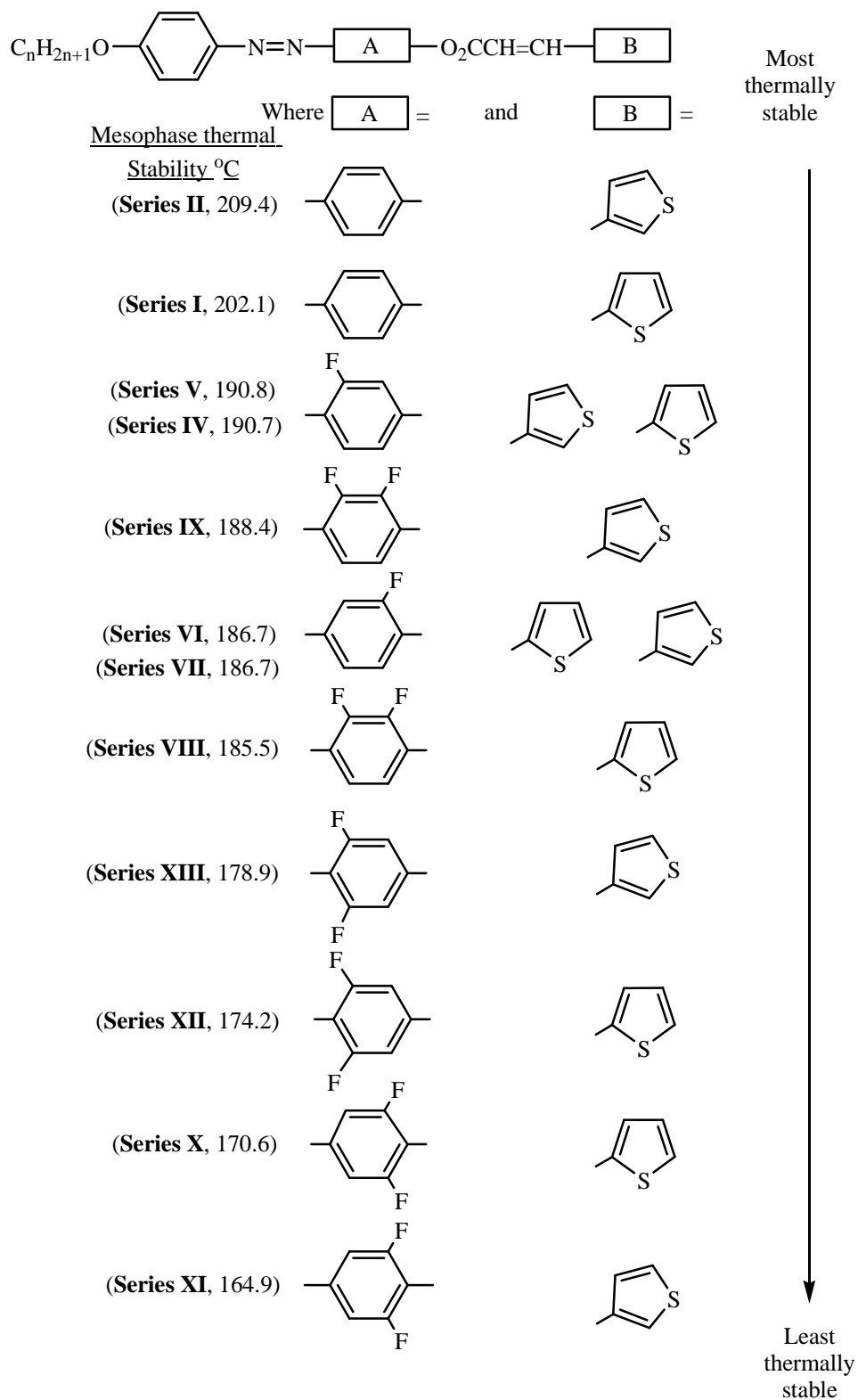
Figure 30:   Summary of average mesophase thermal stability for members (n=1–10) of **Series I, II** and **IV-XIII**.

The thermal stability order shown in **Figure 30**, based on the average T_{N-I} transition temperatures for members (n=1–10) of series derived from 2- and 3- terminally disposed thiophene reveals:

i.   In non-fluorinated systems, 3-thienyl substitution is more stable than 2-thienyl substitution.

ii.   For mono-fluoro substitution, an *outer* edge (*ortho-* to the ester linkage, –O$_2$C-, and *meta-* to the azo linkage, -N=N-) disposition of the fluoro substituent is more detrimental to the thermal stability than *inner edge* disposition (*ortho-* to the azo linkage, -N=N-, and *meta-* to the ester linkage, -O$_2$C-) regardless of 2- or 3-thienyl attachment, e.g., both **Series VI** (*outer* edge, 2-thienyl) and **Series VII** (*outer* edge, 3-thienyl) are less stable than their *inner* edge isomeric counterparts **Series IV** and **Series V**.

iii.   For a fixed position of the fluoro-substituent, either *inner* or *outer* edge, the disposition of thienyl ring has little or no influence on the average thermal stability, e.g., both **Series VI** and **VII** have the same thermal stability (186.7 $^{\circ}$C) and the thermal stability of **Series IV** and **V** differs by just 0.1 $^{\circ}$C.

iv.   Difluoro-substitution across the molecule (**Series X – XIII**) is more detrimental to the thermal stability than difluoro-substitution along the molecular axis (**Series VIII**). Similar to mono-fluoro substitution, inner and outer effects are noted, whereby an outer disposition is more detrimental to mesophase thermal stability than an inner disposition of the two across-axis fluoro substituents.

$C_nH_{2n+1}O$ —⬡— $N=N$ — [A] — $O_2CCH=CH$ — [B]

Where [A] = and [B] =
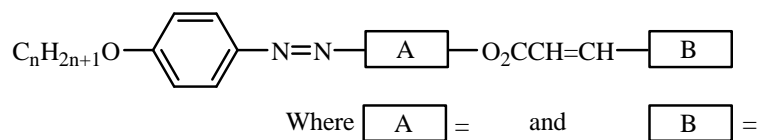
Mesophase Range, °C

(**Series V**, 69.9)

(**Series II**, 66.6)

(**Series I**, 61.7)

(**Series XIII**, 58.9)

(**Series IV**, 58.6)

(**Series IX**, 57.3)

(**Series VIII**, 55.3)

(**Series XII**, 48.9)

(**Series VI**, 46.6)

(**Series VII**, 39.0)

(**Series X**, 28.2)

(**Series XI**, 16.9)

Decreasing range

Figure 31: Summary of the average mesophase range (T_{C-N}–T_{N-I}) for members (n=1–10) of **Series I, II,** and **IV-XIII**.

The stability order for mesophase range shown in **Figure 31** reveals:

i. Interestingly, a mono lateral fluoro-substituent located on an *inner edge* gives the broadest mesophase range (**Series V**), better than its non-fluorinated counterpart (**Series II**).

ii. *Inner edge* di-lateral across-axis fluoro substituent (**Series XIII**) gives the broadest mesophase range compared with any other mono- or difluoro systems, except for **Series V**. Interestingly, the mesophase range of **Series XIII**, when compared with its isomeric counterpart, **Series XII**, is higher by a magnitude of 10 $^{\circ}$C inferring a strong dependency on the disposition of the thienyl ring.

iii. *Outer edge* mono- (**Series VI** and **VII**) or di-lateral across-axis fluoro substitution (**Series X** and **XI**) gives the lowest mesophase range.

3.3   X-RAY STUDIES

Single crystal X-ray diffraction analyses were kindly performed by Dr F. Krebs of the Risø National Laboratory, Denmark and Dr A. Whitwood of the University of York, on the propyloxy-homologues of **Series I, II, IV, VII, X, XII** and **XIII**.   **Figure 22** displays diagrammatic representations (in order of melting point, with the most stable first) of the molecules obtained from X-ray crystallographic data (interpreted by The Cambridge Crystallographic Data Centre, Mercury package).
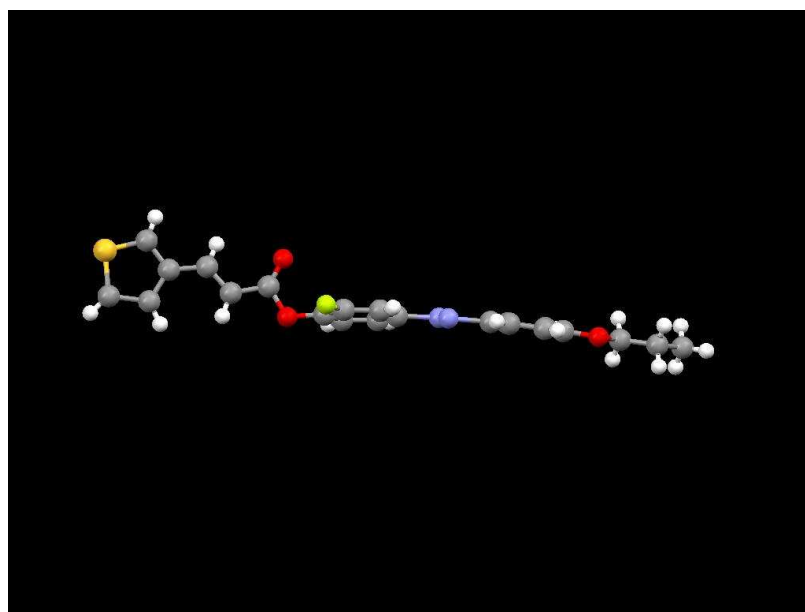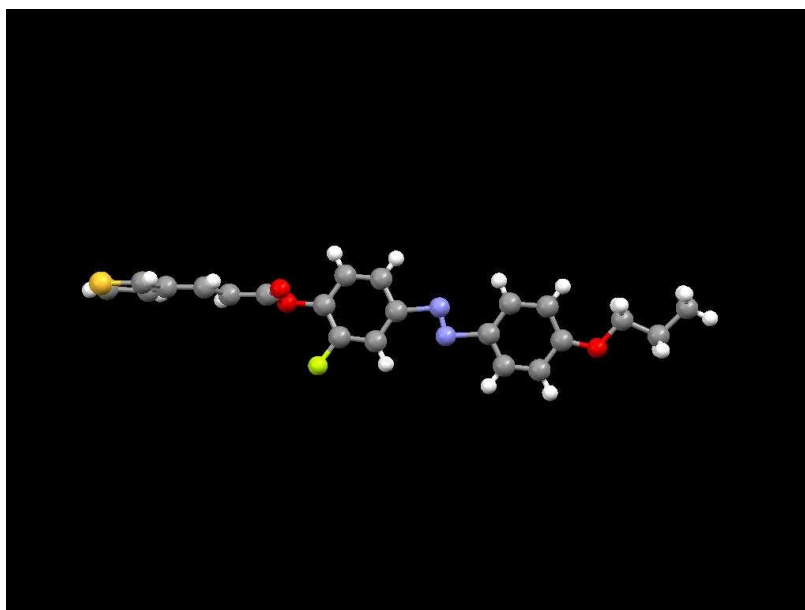
Series VII (m.p. 175.3 ^{o}C)
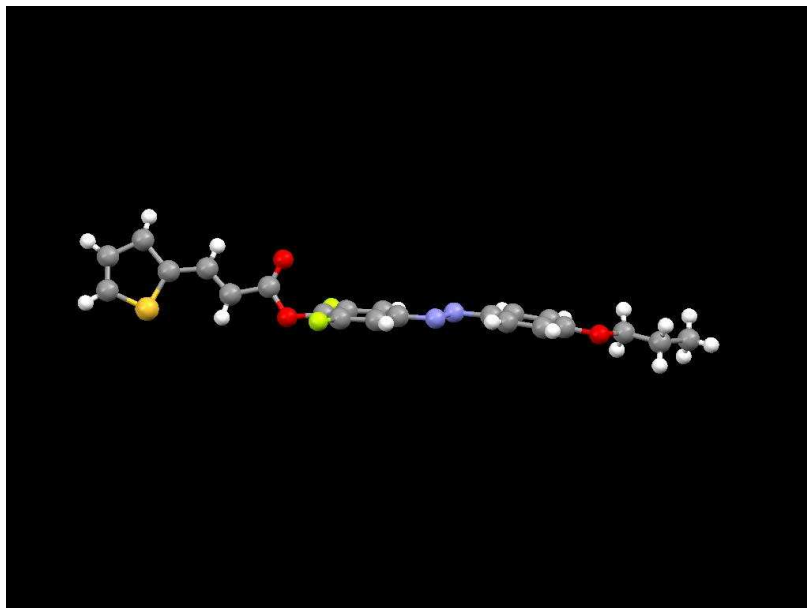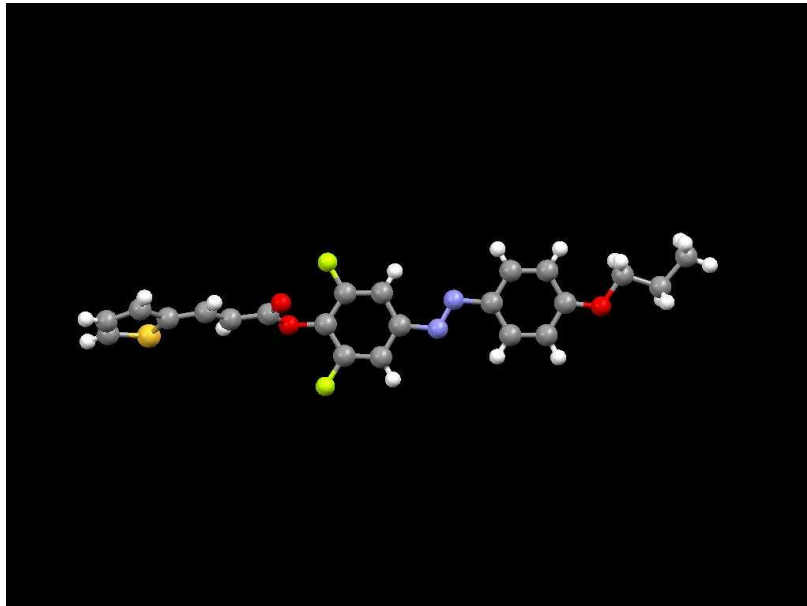
Series X (m.p. 159.6 °C)

Series II (m.p. 156.2 °C)

116
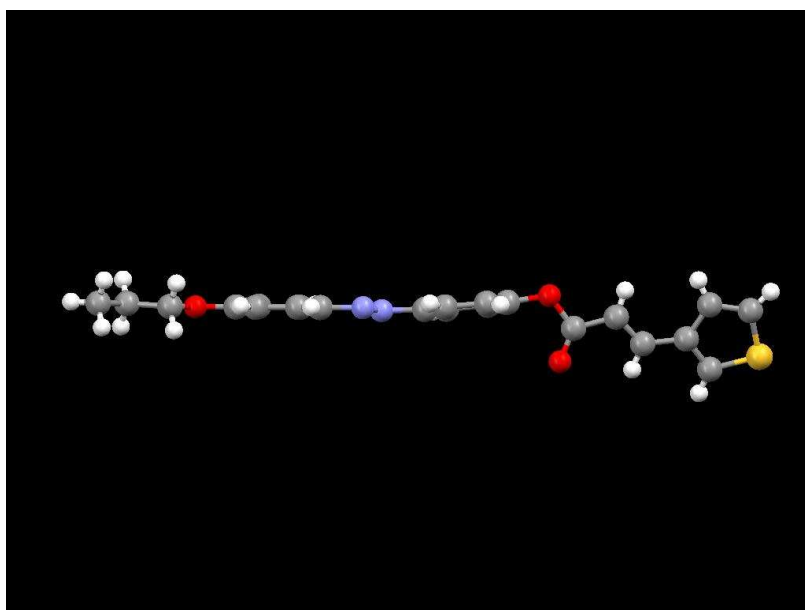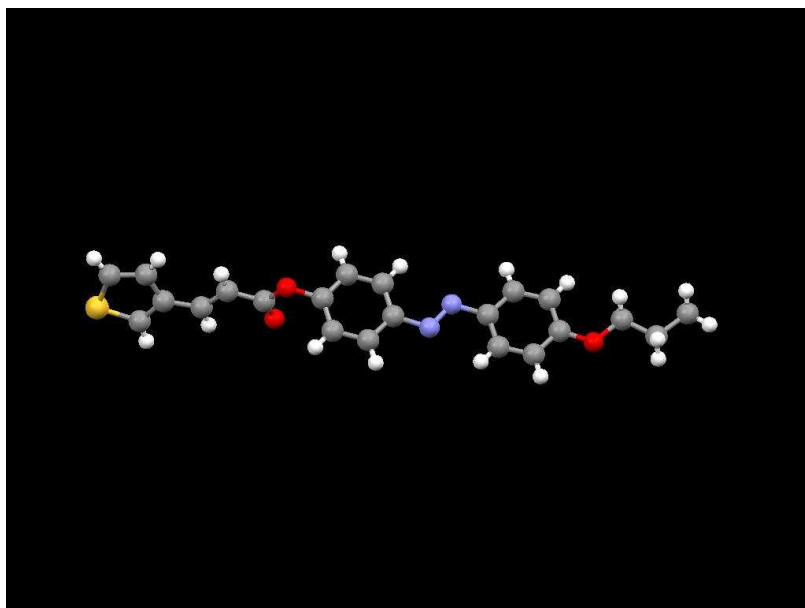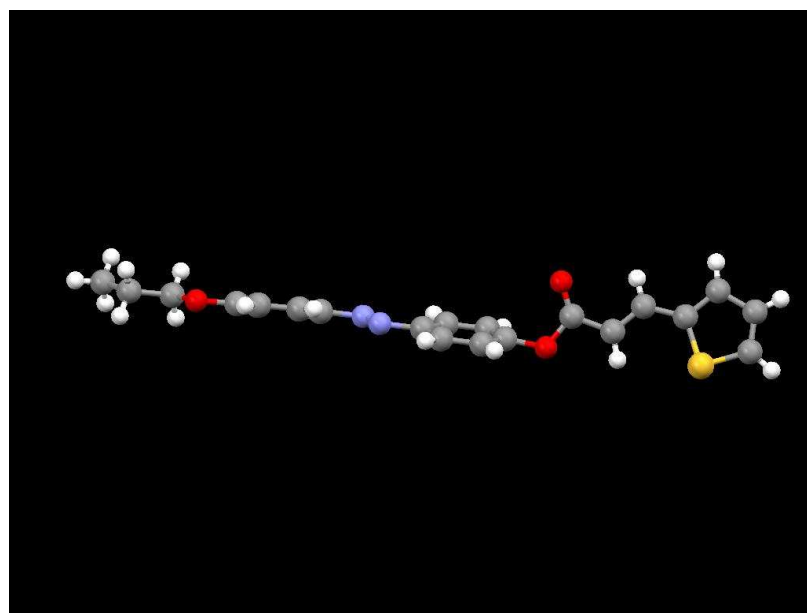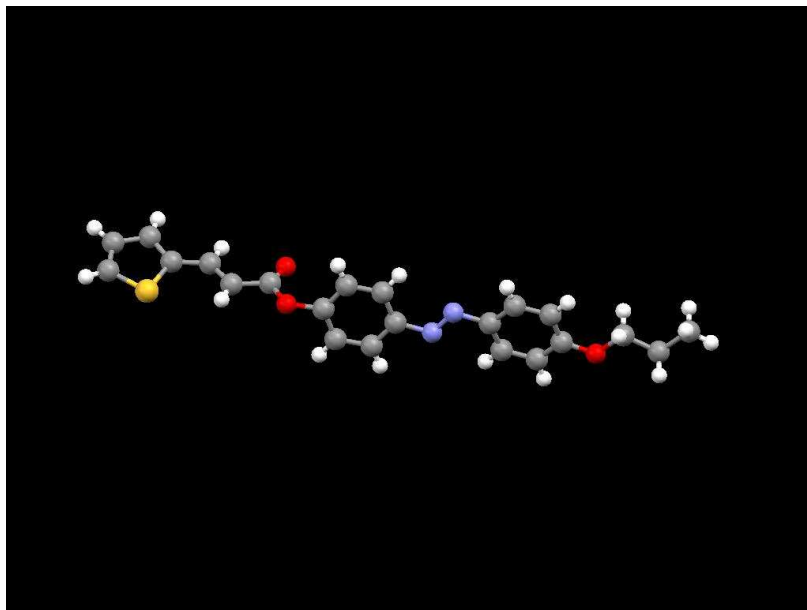
Series I (m.p. 150.3 $^{\circ}$C)
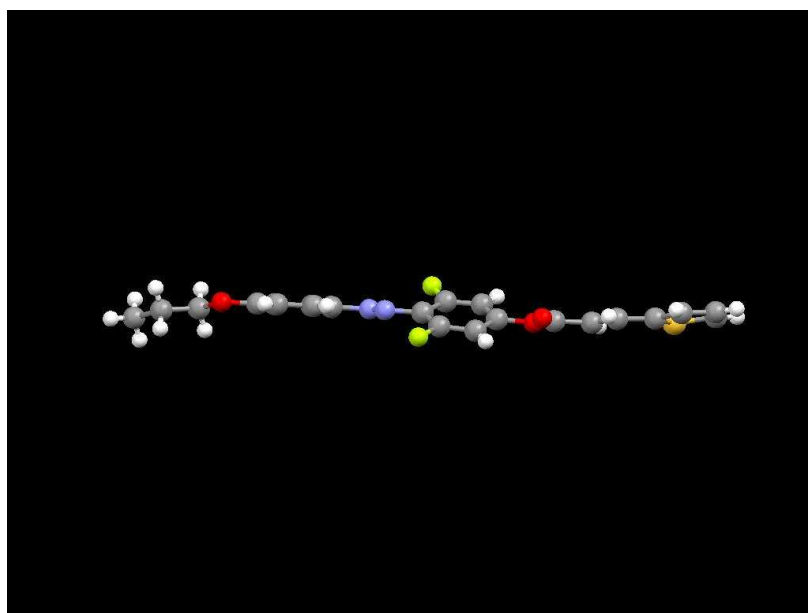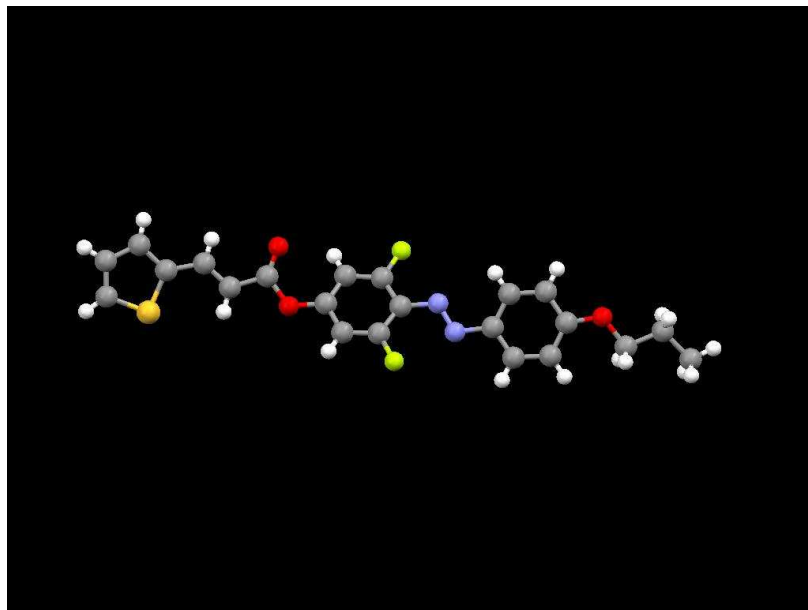
Series XII (m.p.139.7 °C)
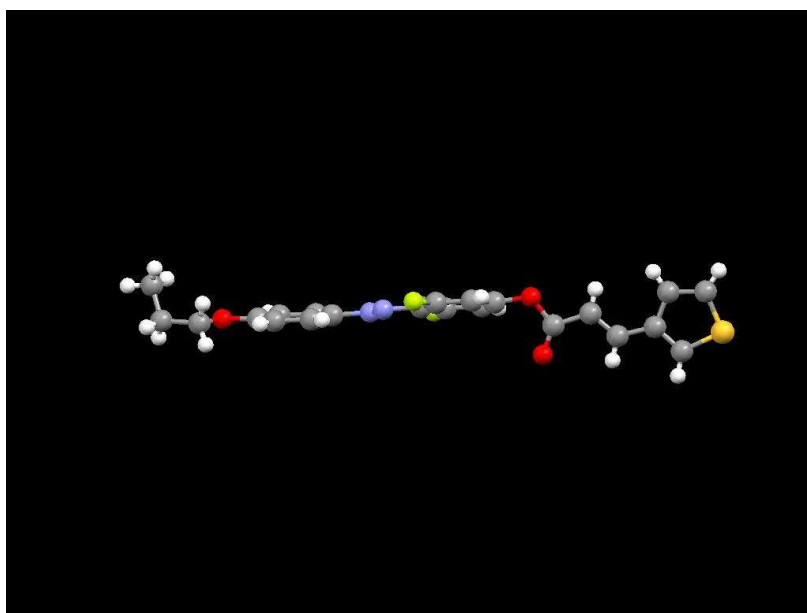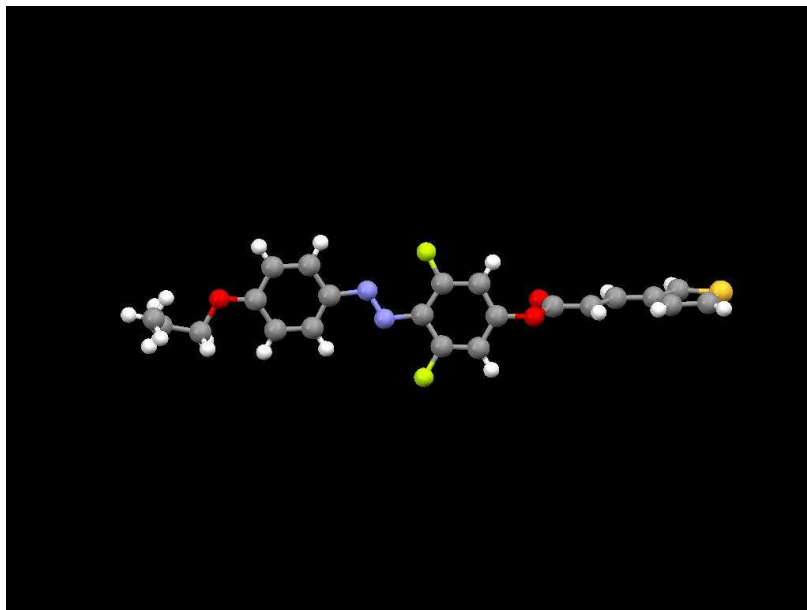
Series XIII (m.p. 136.9 ^{o}C)
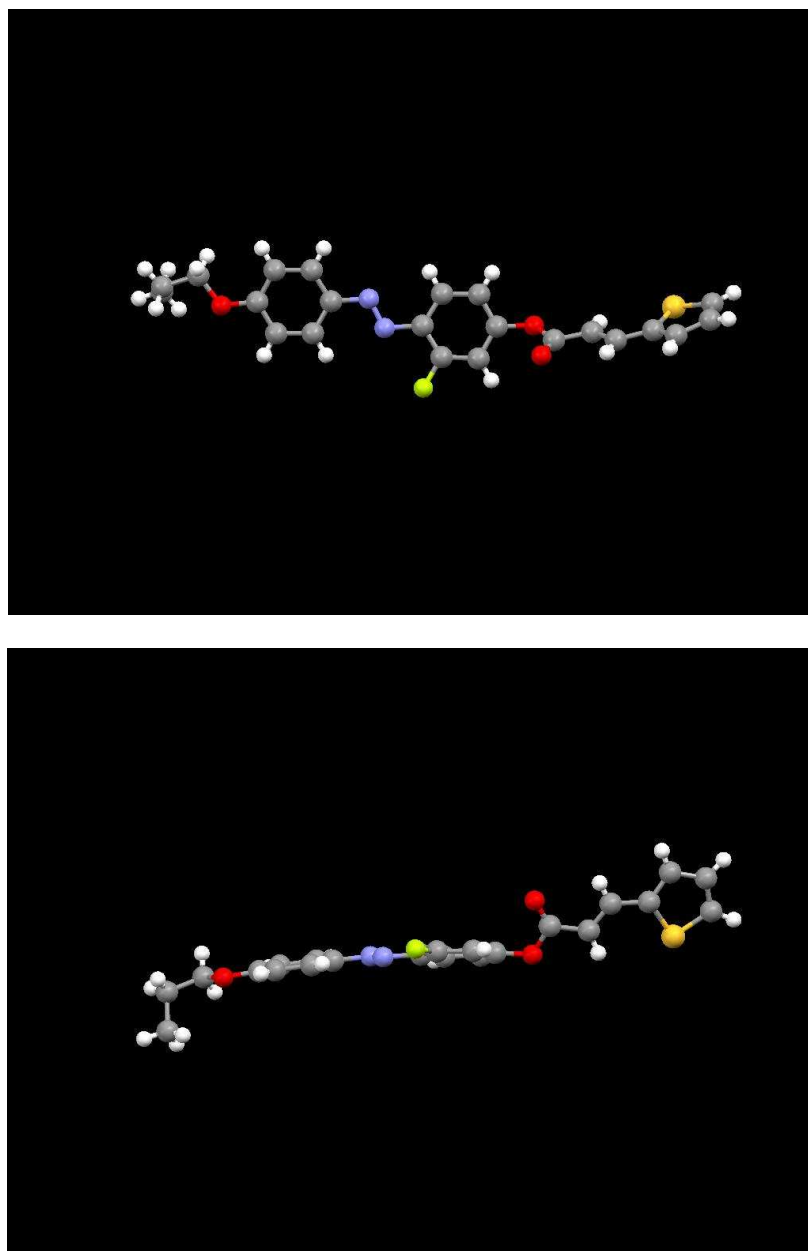
Series IV (m.p. 134.6 °C)

Figure 32: Structural representations of the propyloxy-homologues of Series **I**, **II**, **IV**, **VII**, **X**, **XII** and **XIII** listed in order of thermal stability (interpreted by The Cambridge Crystallographic Data Centre, Mercury package)

Propyloxy homologue of	M.p. (°C)	Packing of molecule within unit cell	N=N/N=N Distance between neighbouring molecules in unit cell (Å)	C-O/C=O Distance between neighbouring molecules in unit cell (Å)	N=N linking group alignment with respect to neighbouring molecule in unit cell	Torsion angle of Aromatics across azo linkage (°)
Series VII	175.3	Head to Tail	13.624	13.594	Over alkoxy- group	9.02
Series X	159.6	Head to Tail	9.976	10.275	Over Alkene	1.15
Series II	156.2	Head to Tail	7.976	8.525	Over N=N	1.72
Series I	150.3	Head to Tail	9.368	7.774	Over N=N	12.29
Series XII	139.9	Head to Tail	4.024	11.948	Over fluorinated aromatic ring	24.76
Series XIII	136.9	Head to Tail	6.237	5.653	Over fluorinated aromatic ring	9.91
Series IV	134.6	Head to Tail	13.115	11.421	Over N=N	8.94

Table 17: Preliminary data obtained from Mercury X-ray analysis software

From the structures shown in **Figure 32** and the data listed in **Table 17**, the following tentative relationships may be inferred.

    i.   X-Ray analysis confirms that proposed structures are correct and that all compounds exhibit a *trans*-configuration of the acrylic and azo groups.

    ii.   Linearity of the molecule could be a dominant factor. If the propyloxy- chain is aligned along the long molecular axis, then melting points appear to be higher than the homologues with the propyloxy chain arranged in a direction approximately parallel to the long molecular axis (**Series VII**, **X**, **II**, **I** and **XII** are higher melting than **XIII** and **IV**). Melting points are also enhanced by the 3-thienyl disposition in this situation.

    iii.   The direction of the propyloxy- terminal group with regards to the long molecular axis appears lead to a greater increase in melting point than the disposition of the terminal thiophene ring.

    iv.   Melting points appear to be enhanced when with a fluorine substituent on the *outer edge* (*meta* to the –N=N- linkage [**Series VII** and **X**]) much more than when the fluorine substituent is on the *inner edge* (**Series XII**, **XIII**, **IV**), with non-fluorination being intermediate of the two (**Series I** and **II**).

    v.   It appears that having difluoro-substitution on an *inner edge* (*ortho* to the –N=N- linkage [**Series XII** and **XIII**]) enhances the melting point as apposed to mono-substitution (**Series IV**). The opposite appears true for *outer edge* (*meta* to the –N=N- linkage, *ortho* to the ester group) fluoro substituted compounds (**Series VII** compared to **Series X**).

    vi.

It must stressed that other factors such as packing arrangements, direction of the dipole from the thiophene within a unit cell and torsion angles within a molecule may also play a role in the melting points compounds. However, without a more in depth study, it is not possible to draw direct correlation on these factors.

3.4 PHOTORESPONSIVE STUDIES

Photoresponsive investigations were undertaken on the fluoro- and non-fluoro- homologues of the 3-(thiophen-2-yl)acrylic acid 4-(4-n- heptyloxyphenylazo)phenyl esters (**Series I**, **IV**, **VII**, **VIII**, **X** and **XII** *i.e.*, compounds **38 g**, **41 g**, **42 g**, **43 g**, **44 g** and **45 g** respectively.

The UV-Vis absorption spectra (**Figure 33 a-f**) were measured in spectroscopic grade THF solutions using a diode array spectrophotometer (Agilent 8453e UV-Vis Spectrophotometer). Light sources of 367 nm and 434 nm causing *E-* to *Z-* and *Z-* to *E-* photoisomerisation were obtained by irradiation from a Hg-Xe lamp (Supercure-203S, San-ei Electric MFG Co.) passed through an interference filter of the required wavelength onto a quartz cuvette filled with the required sample. Sampling was taken at five second intervals (over a period of 40 seconds), followed by a final irradiation for five minutes.
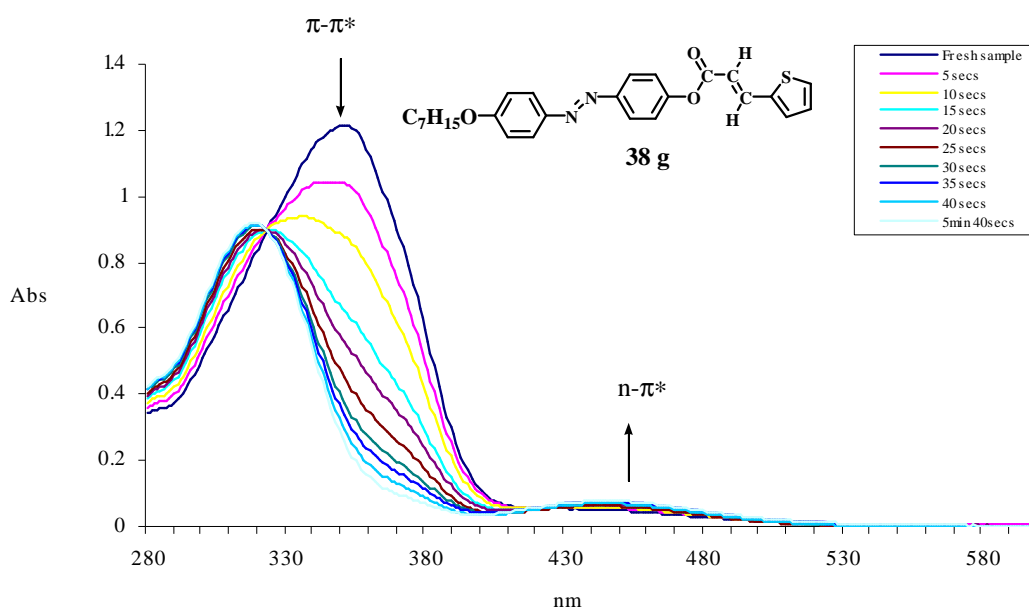
Figure 33 a
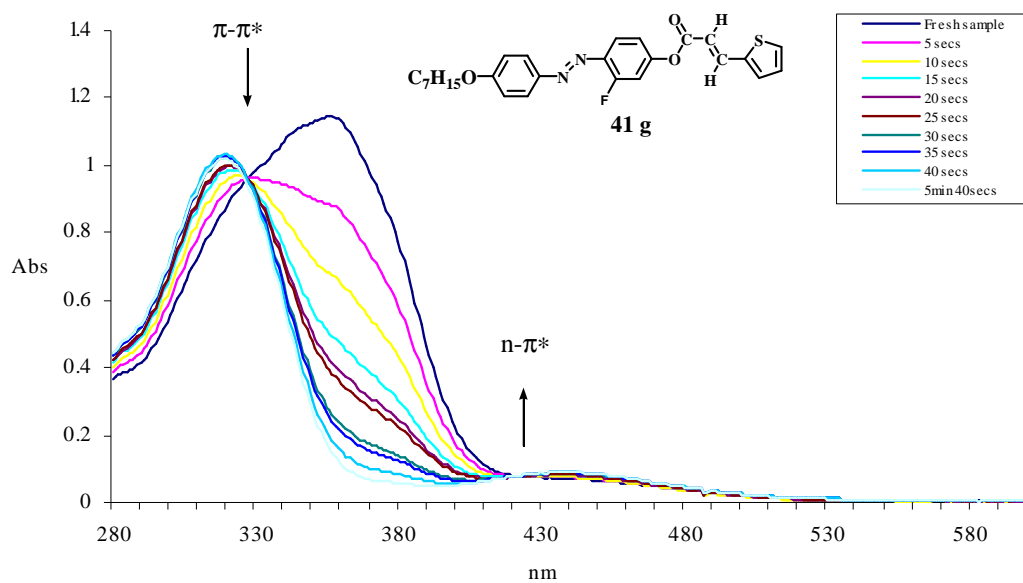
Figure 33 b
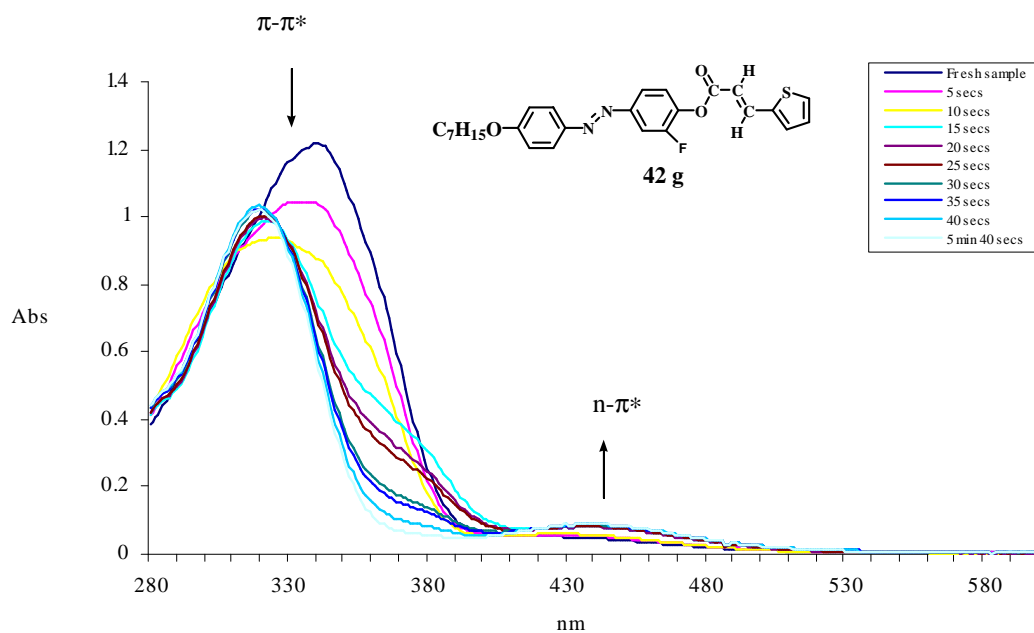
Figure 33 c
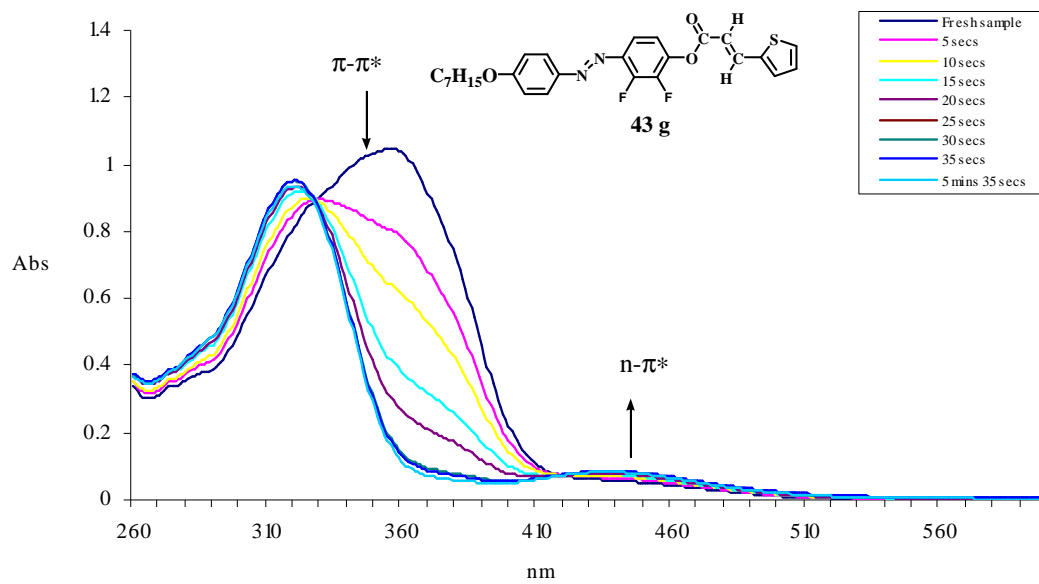
Figure 33 d
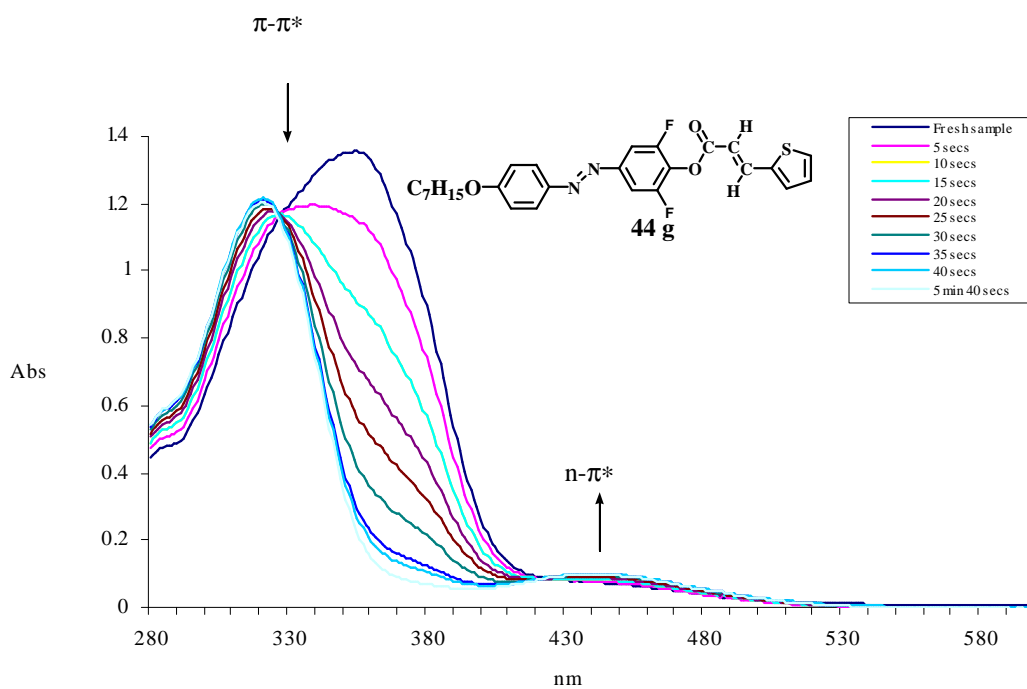
Figure 33 e
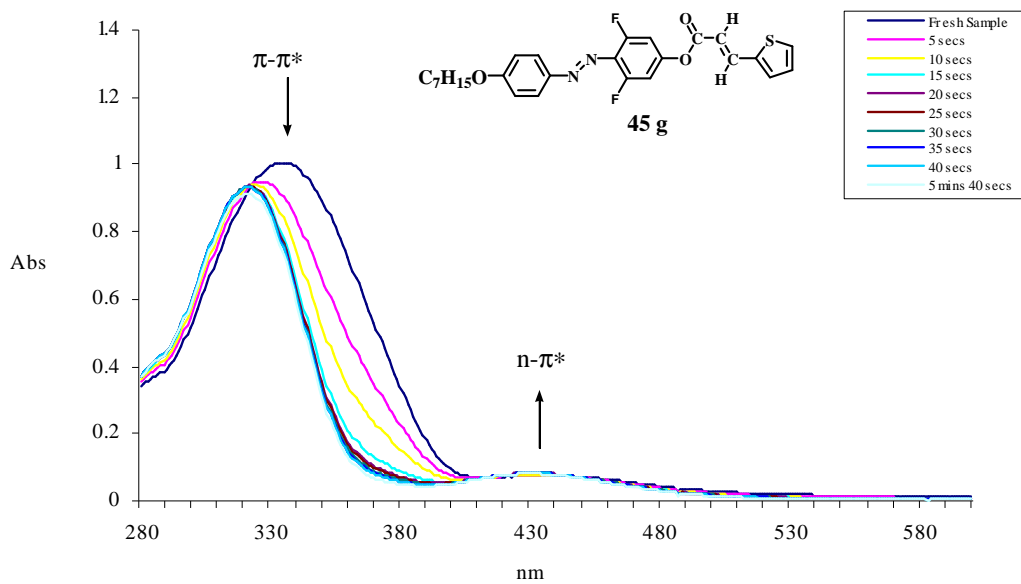
Figure 33 f

Figure 33 a-f: Absorption spectra of compounds (**38 g**, **41 g**, **42 g**, **43 g**, **44 g** and **45 g**) showing π-π* and n- π* absorptions when UV irradiated at 367 nm corresponding to the *trans to cis-(E-Z)* configuration of the azo moiety

Compound	Concentration in THF (mol dm^{-3})	λ_{max} (nm)	Logε_{max}	Isobestic Points (nm)		λ of Hypsochromic shift (nm)	λ and increase in (*Abs*) of Hyperchromic effect
				π-π*	n-π*		
Series I, 38 g	4.99 x 10^{-5}	352	4.386	323	420	318	427 to 446 nm, *(+0.0234)*
Series IV, 41 g	3.09 x 10^{-5}	357	4.570	327	421	319	436 to 441 nm, *(+0.0188)*
Series VI, 42 g	3.44 x 10^{-5}	342	4.546	320	416	320	434 to443 nm (+0.0288)
Series VIII, 43 g	2.89 x 10^{-5}	342	4.521	327	420	320	430 to 437 nm, *(+0.0067)*
Series X, 44 g	4.35 x 10^{-5}	354	4.495	326	424	321	434 to 441 nm, *(+0.0182)*
Series XII, 45 g	2.85 x 10^{-5}	335	4.552	323	419	322	No change, *(+0.005)*

Table 18:   Data from samples in THF irradiated at 367 nm showing shifts in the spectra that possibly correspond to *trans-cis* isomerisation of the N=N central linking group.

From the **Figure 33 a-f** and **Table 18**, it would appear that irradiation of the samples at 367nm, causes a hypsochromic shift and a hypochromic effect on the π-π* (335-352 nm) band. At the same time, a small bathochromic shift and hyperchromic effect of the *n*- π* (427-446 nm) absorption band is observed. Two clear isobestic points at approximately 327 nm and 420 nm were also observed and the photoreaction appeared to reach a photostationary state[54] (after 5 minutes).

The samples previously irradiated at 367 nm were then irradiated at 434 nm. The resulting spectra are shown in **Figure 34 a-f**. The data from the experiment is displayed in **Table 19**;
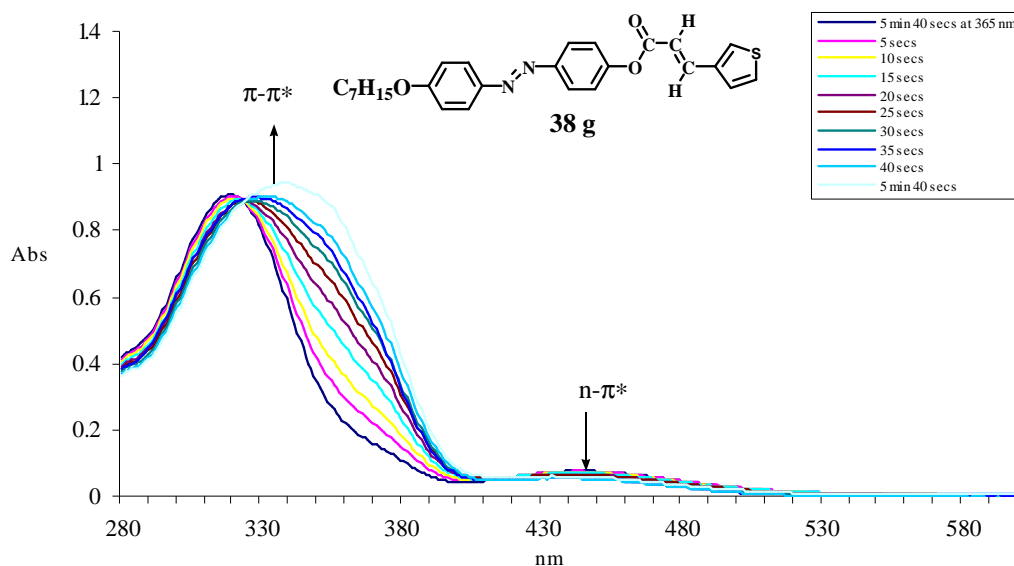
Figure 34 a
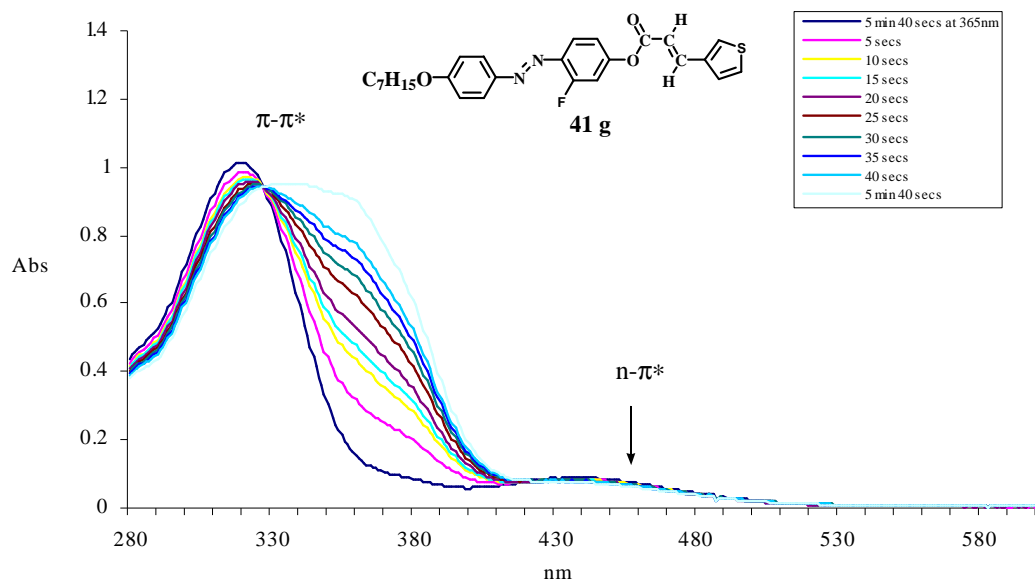
Figure 34 b
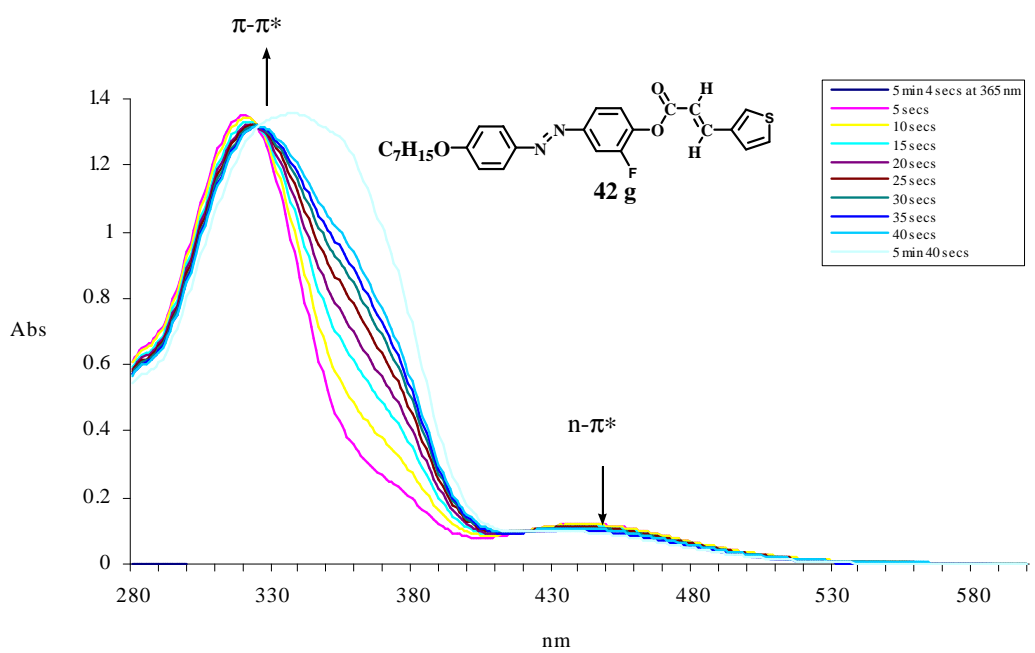
Figure 34 c
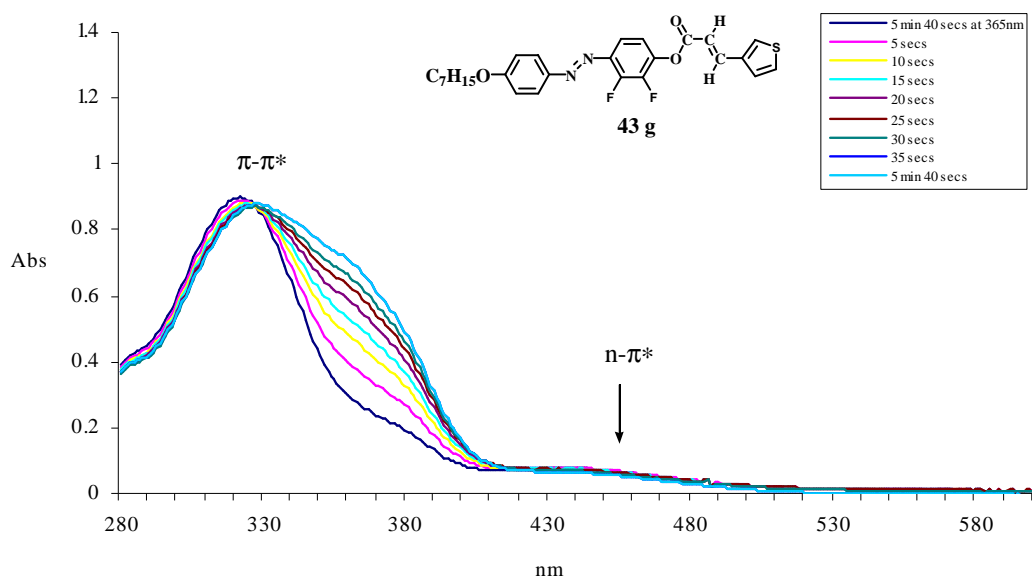
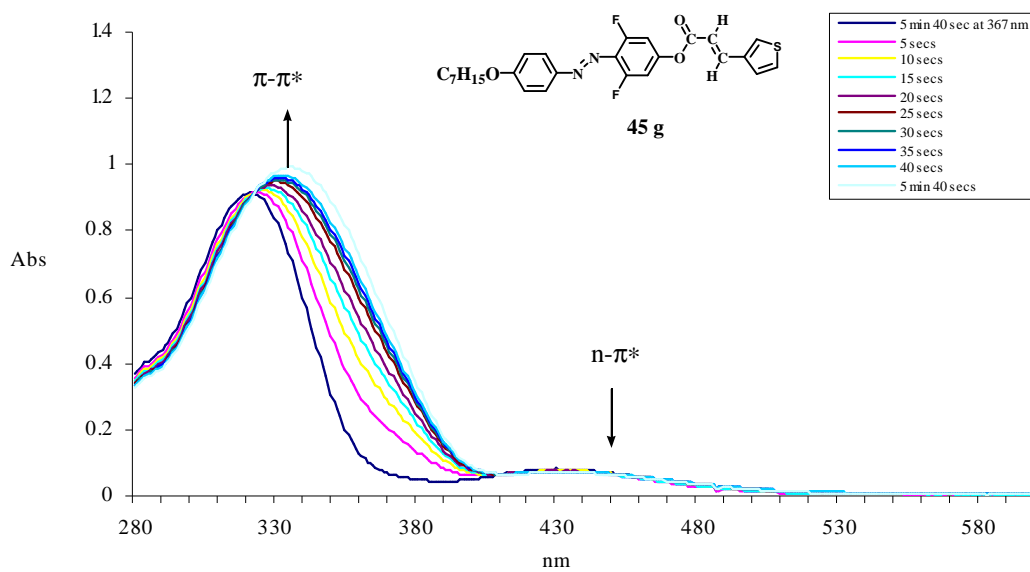**Figure 34 d**
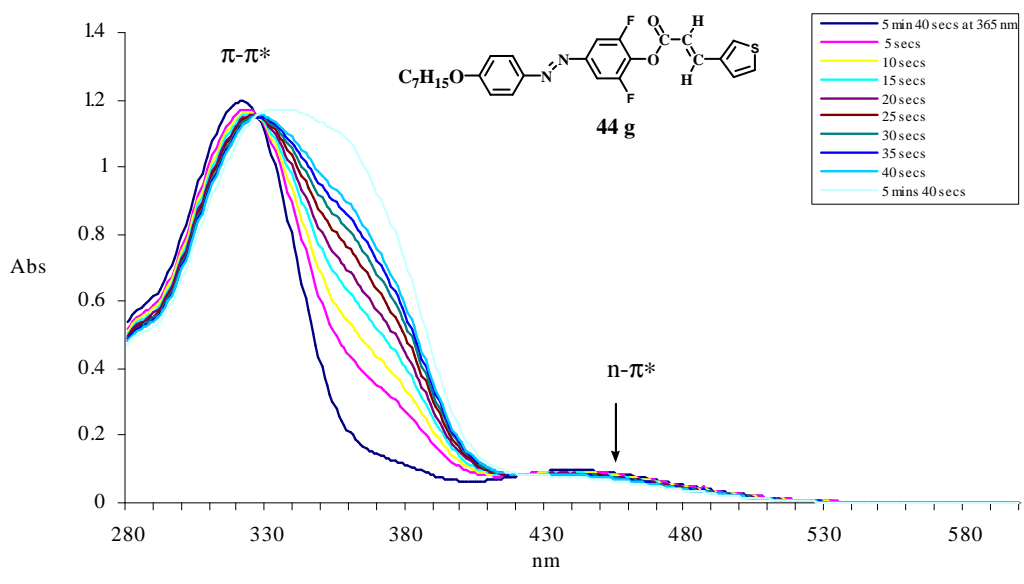
Figure 34 e

Figure 34 f

Figure 34 a-f: Absorption spectra of compounds (**38 g, 41 g, 42 g, 43 g, 44 g, 45 g**),
showing π-π* and n- π* absorptions when irradiated with visible light at 434
nm, possibly corresponding to the *cis-trans-*(*Z-E*) configuration of the azo
moiety.

Compound	Concentration in THF (mol dm^{-3})	λ_{max} (nm)	Logε_{max}	Isobestic Points (nm)		λ of Bathochromic shift (nm)	λ and Abs of Hypochromic shift
				π-π*	n-π*		
Series I, 38 g	4.995 x 10^{-5}	338	4.28	325	417	338	449 -0.0175
Series IV, 41 g	3.09 x 10^{-5}	319	4.51	329	422	343	441 -0.014
Series VI, 42g	3.44 x 10^{-5}	323	4.59	326	417	340	445 (-0.0122)
Series VIII, 43 g	2.89 x 10^{-5}	320	4.49	328	418	328	442 -0.0138
Series X, 44 g	4.35 x 10^{-5}	321	4.43	327	423	334	443 -0.022
Series XII, 45 g	2.85 x 10^{-5}	336	4.54	323	411	336	436 0.01

Table 19: Data from samples in THF irradiated at 434 nm showing shifts in the spectra that possibly correspond to *cis-trans* isomerisation of the N=N central linking group.

From **Figure 34 a-f**, a bathochromic shift and hypochromic effect is evident for all compounds. This suggests a possible reversible Z- to E- photoisomerisation and could infer that the materials analysed are '*photo-switchable*'.

The observed interchange between the (E)/(Z)- isomers of thiophene-based compounds initiated in the presence of UV light *i.e.*, photoisomerisation, emphasises the applicability of this type of thiophene-based compound for use in photo-assisted surface regulation.

3.5 THE INFLUENCE OF ALTERING THE LEFT AND RIGHT TERMINALLY DISPOSED GROUPS

3.5.1 INFLUENCE OF REPLACING THE RIGHT-HAND TERMINAL ACRYLIC ESTER WITH ALKYL ESTERS OF VARYING CHAIN LENGTH [**Series XIV**]

The influence of altering the nature of the right-hand terminal group by replacement of the acrylic bond with a range of alkyl spaced thienyl esters on mesophase type, thermal stability and phase range is summarised by the data displayed in **Table 20**. Even with the change of the terminal ester moiety, all the homologues still exhibit the nematic phase alone.

Series XIV

R =	C-N (^{o}C)	N-I (^{o}C)	Phase range (T_{N-I}-T_{C-N}) (^{o}C)
-CH=CH- (**38 g**)	124.3	187.1	62.8
-CH$_2$- (**51**)	-	-	-
-(CH$_2$)$_2$- (**52**)	113.6	(106.7)	6.9
-(CH$_2$)$_3$- (**53**)	94.4	(72.3)	22.1
-(CH$_2$)$_4$- (**54**)	99.0	(63.0)	36.0

Table 20. Average T_{N-I} (clearing point), $T_{N-I} - T_{C-N}$ (phase range) and phase type for a range of alkyl length terminally disposed groups (n.b. homologous compound **38 g** is included for comparative purposes)

From the table above, it is possible to note that with the replacement of the acrylic bond from the homologous **Series I**, mesophase thermal stability and mesophase range are lowered considerably. It is also of interest that the direct unsaturated homologue and its further extended counterpart both exhibit only a monotropic phase. It also worth noting that by shortening the

ester chain length by one carbon (compared with the **Series I** homologue), liquid crystallinity is lost. *Whilst studying the compounds above some profound photoresponsive behaviour was noted (See section 4, Optical textures).*

3.5.2 <u>INFLUENCE OF REPLACING THE LEFT-HAND TERMINAL ALKOXY-GROUP WITH EITHER A 2-THIENYL- OR CYCLOHEXYL-GROUP AND THE EFFECT UPON MESOPHASE RANGE AND MESOPHASE THERMAL STABILITY (**58** and **63**)</u>

The influence of altering the nature of the left-hand terminally disposed alkoxy- group on mesophase phase range, type and thermal stability is summarised by the data displayed in **Table 21**. Replacement of the left hand terminal alkoxy moiety of **Series I** with cyclohexyl- or 2-thienyl- moiety has varied effects on the thermal properties of the molecule.
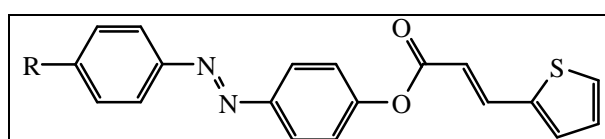
R =	C-N (^{o}C)	N-I (^{o}C)	Phase range (T_{N-I}-T_{C-N}) (^{o}C)
(**58**)	164.4	225.0	60.6
(**63**)	207.1	299.3	92.2

Table 21.   Average T_{N-I} (clearing point), T_{N-I} – T_{C-N} (phase range) and phase type for a range of varied left-hand terminally disposed groups

Table 21 shows that replacing the alkoxy group with a thiophene ring stabilises the mesophase thermal stability and mesophase range in comparison to **Series I** by 97.2 ^{o}C and 30.5 ^{o}C respectively. This is possibly due to the increased molecular polarisability from the dipole of a second thiophene entity whilst attaining a high degree of rigidity and linearity. This assumption is reinforced if the stability is compared with the two alkyl spaced relatives (see future work, chapter 6, p. 147), which one would expect to have a greater flexibility.

Replacement of the alkoxy- moiety by a cycloalkyl group also increases the mesophase thermal stability by 22.9 ^{o}C, again reinforcing the inference that increased rigidity, increases the thermal stability. However, there is a marginal decrease in mesophase range of -0.9 ^{o}C.

136

3.5.3   INFLUENCE OF REPLACING THE LEFT-HAND TERMINAL ALKOXY GROUP
         WITH EITHER A 2-THIENYL- OR CYCLOHEXYL- GROUP, AS WELL AS,
         ALTERING THE DISPOSITION OF THE RIGHT-HAND TERMINAL THIOPHENE
         RING (**59** and **64**)

The influence of altering the nature of the left-hand terminal alkoxy- group and the disposition

of the right hand terminal aromatic group of the ester on mesophase thermal stability and phase

range is summarised by the data displayed in **Table 22**. Replacement of the left hand terminal

alkoxy moiety with a cyclohexyl- or thiophene whilst altering the disposition of the right hand

terminated thiophene to 3-thienyl allows;

i   comparisons to the effect of altering the right hand alkoxy terminal group on **Series II**

         and;

ii   comparisons of altering the disposition of the right hand terminated thiophene group on

         the compound in **Table 21**.
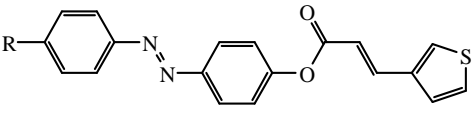
R =	C-N (^{o}C)	N-I (^{o}C)	Phase range (T_{N-I}-T_{C-N}) (^{o}C)
(**59**)	169.3	223.6	54.3
S (**64**)	215.8	303.7	87.9

Table 22.   Average T_{N-I} (clearing point), T_{N-I} – T_{C-N} (phase range) and phase type for a
                 range of varied left and right-hand terminally 2thienyl disposed groups

The data in **Table 22** interestingly shows that the disposition of the thiophene ring, in this

series, has a far lesser effect on mesophase thermal stability of the 3,2- counterparts, than for

their alkoxy homologues (**Series II**). For the cyclohexyl- derivative, the 2-thienyl ester is the

more stable isomer with a thermal stability of just 1.4 ^{o}C higher than that of the 3-thienyl ester.

The reverse is the case with the thiophene terminal group where the 3,3-isomer is just 3.8 ^{o}C

higher than that of the 3,2- isomer.

4   OPTICAL TEXTURES

All the homologues, n=1-10, of [**Series I-XIII**] are liquid crystalline. All exhibit the nematic phase alone on heating from the crystalline solid and on cooling from the isotropic liquid, *i.e.*, enantiotropic nematic liquid crystals. The nematic phase is detected easily on cooling from the isotropic liquid. The appearance of tiny, highly coloured (birefringent), spherical droplets emanating from the isotropic liquid (optically extinct, dark background, LHS of Plate 1) marks the onset of the nematic phase (RHS of **Plate 1**). The droplets tend to coalesce as the temperature decreases to form a classical threaded (Schlieren) texture of a nematic phase exhibiting 2- and 4-point brush defects (**Plate 2**).
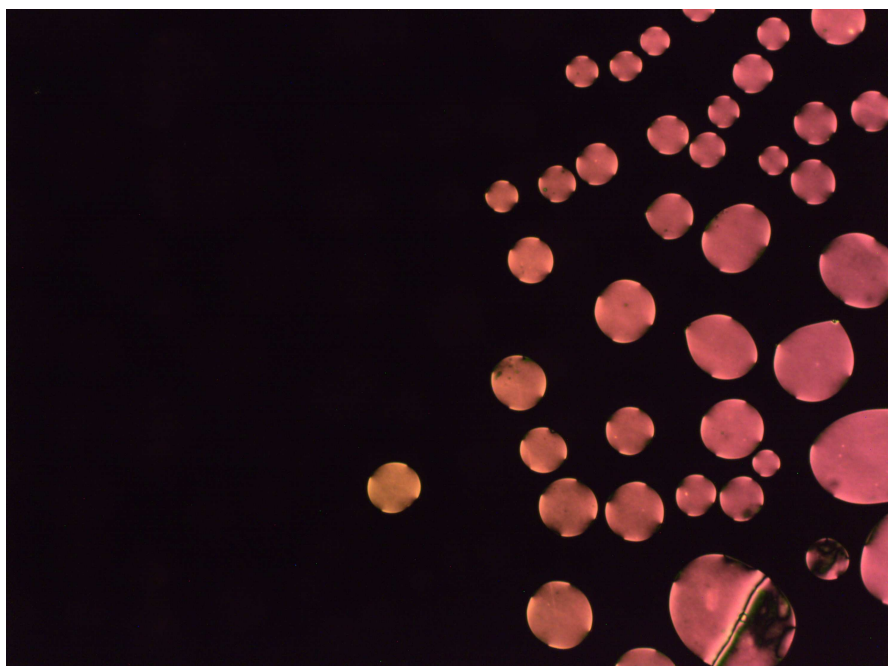
Plate 1   Appearance of nematic droplets from the isotropic liquid and the onset of the classical threaded texture of the nematic phase.
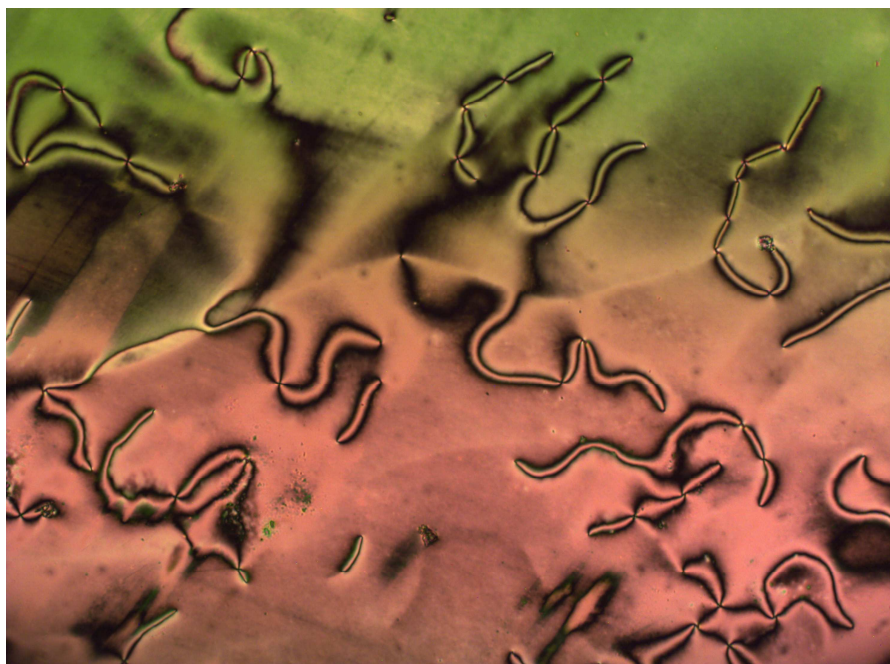
Plate 2   Classical threaded or Schlieren texture of the nematic phase.

Homologues of **Series XIV**, in which the acrylic moiety has been replaced by a saturated alkane [with the exception of n=1]), show the same textures as the parent compound. However, interestingly, at a fixed temperature just below the clearing point the N-I transition may be effect by light. Thus, as the light intensity is increased, the nematic phase appears to become brighter exhibiting increased Brownian motion (**Plates 3 a-c**) and then becomes optically extinct as it transforms in to the isotropic liquid (**Plates 3 d-e**). Photo-induced N-I transition occurs very quickly, within seconds, and the isotropic liquid remains until the light intensity is decreased or switched off.
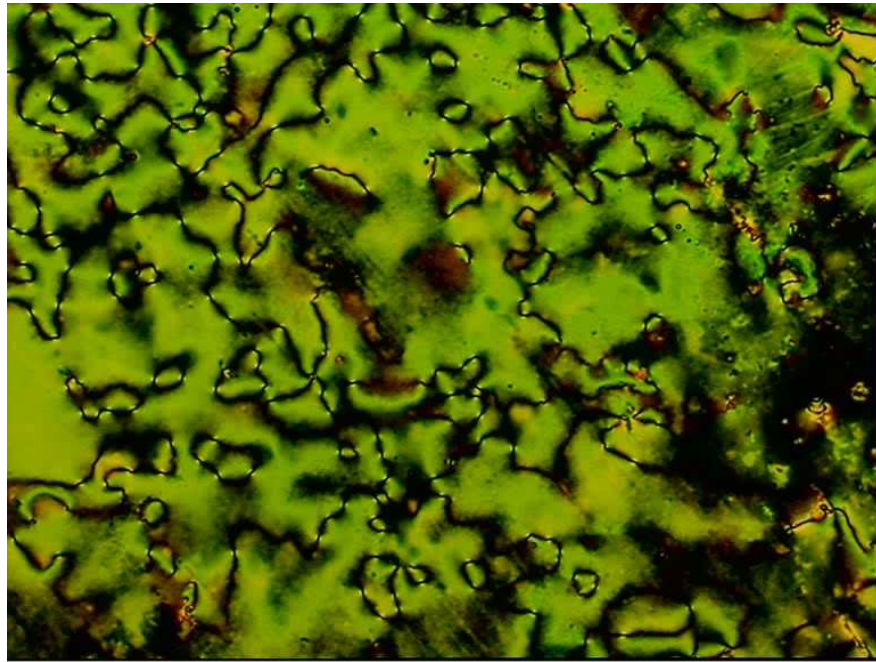
Plate 3 a　　　　Nematic texture, just below the clearing point at low light intensity
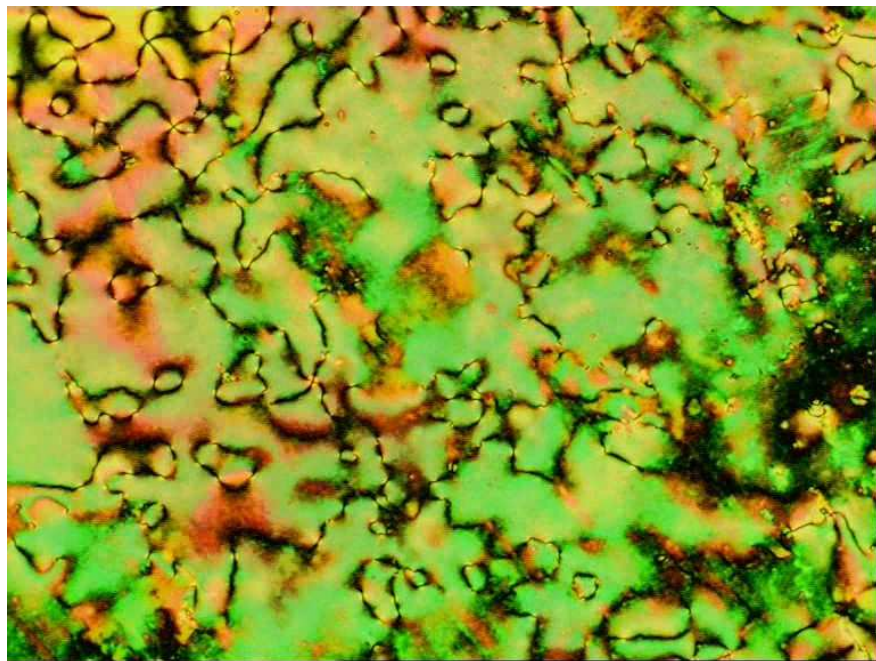

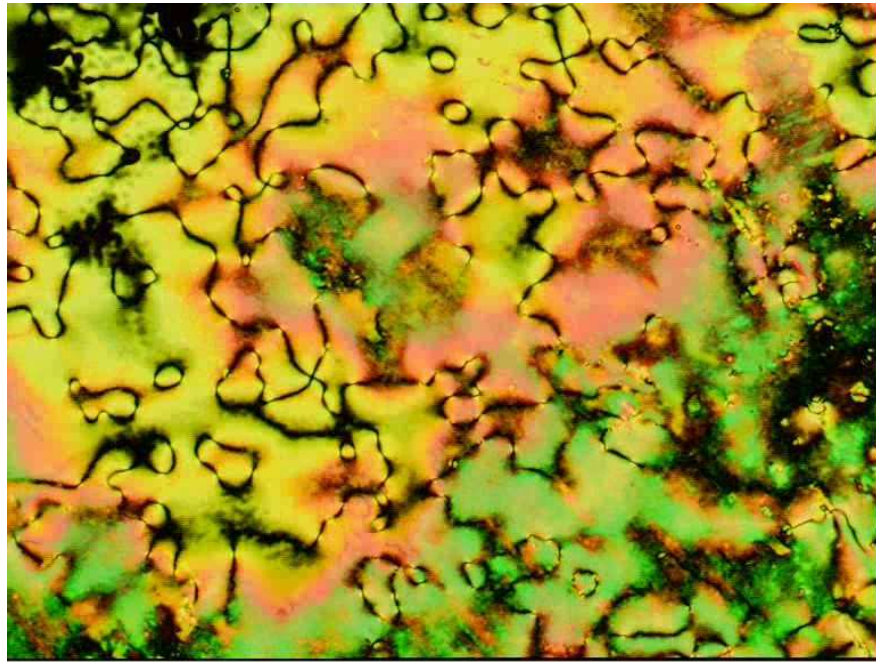**Plate 3 b**　　Increase in light intensity gives brilliant birefringence and the texture appears to shimmer.

Plate 3 c　　　　The nematic phase begins to extinguish into isotropic

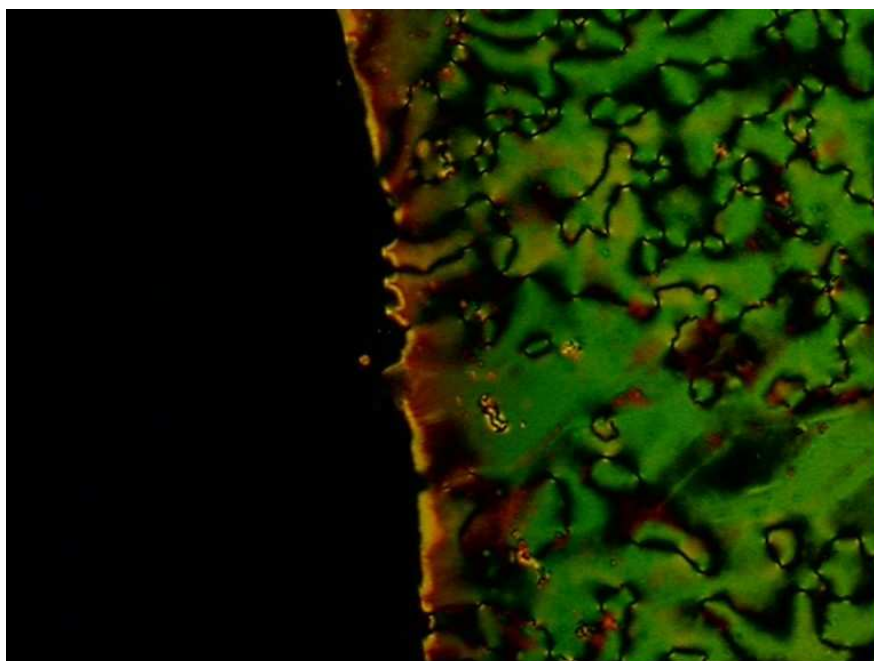**Plate 3 d**　　　　Nematic phase rapidly extinguishes into the isotropic liquid from top left.

Plate 3 e   The edge of the 'hole created by illumination.

Plates 3 a-e The nematic phase of **Series XIV** (**53**, where n=3) upon increasing illumination at constant temperature just below the clearing point.

Another interesting optical feature was shown by the 'pentyl' homologue of **Series XIV**. Similar photoresponsive behaviour at constant temperature was noted but this time a homogeneous (**Plates 4 a-b**) to homeotropic alignment (**Plate 4 c-d**) change occurred.

Plate 4 a   Nematic phase at low illumination (homogeneous)

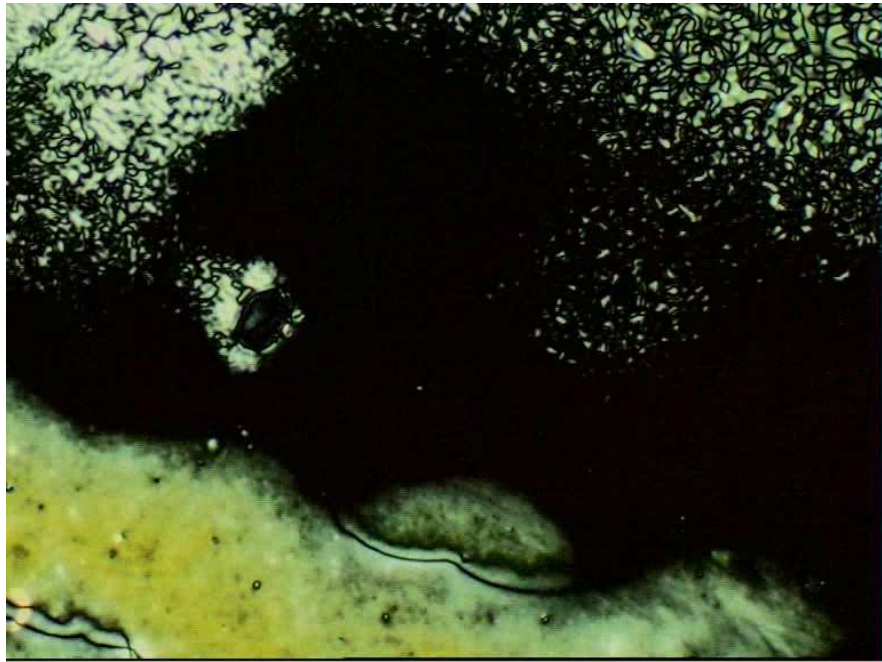**Plate 4 b**   Light intensity is increased and the phase start to extinguish

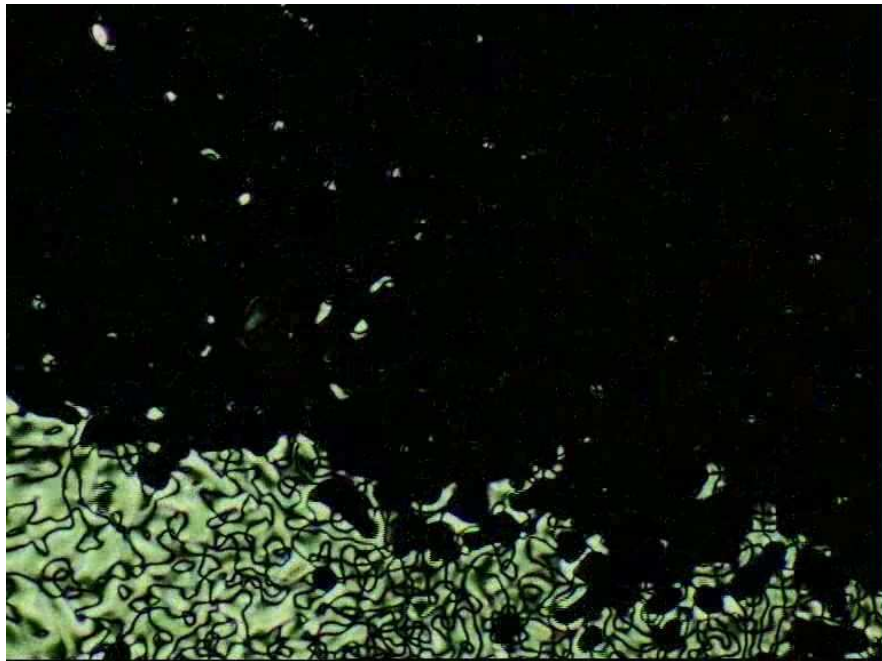**Plate 4 c**   The homogeneous alignment tending to homeotropic alignment

Plate 4 d   The alignment change is followed by the sample going to the isotropic liquid
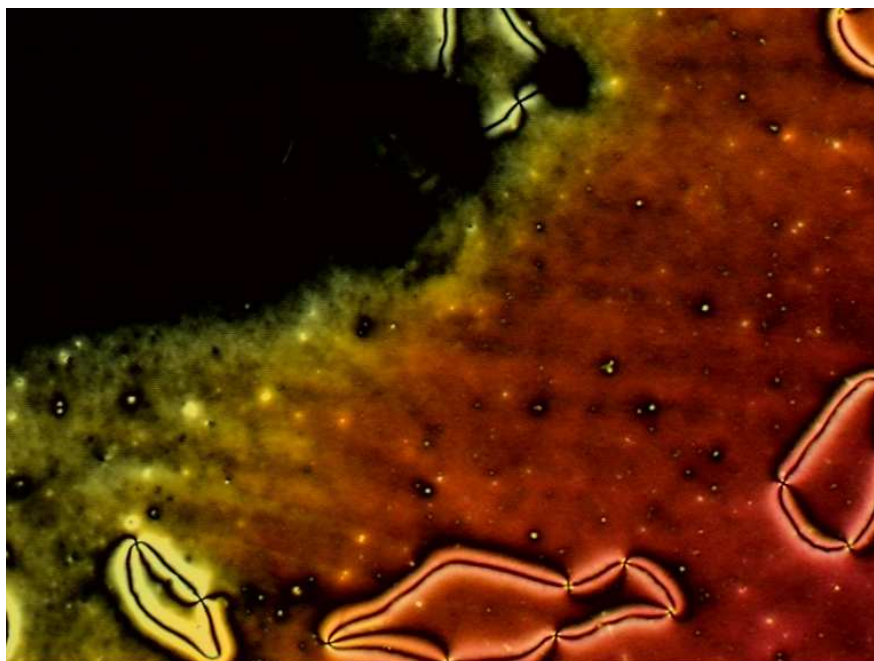
Plate 4 e   The edge of the 'hole' slowly starts to revert from the isotropic liquid back to the nematic phase.

Plates 4 a-e   The nematic phase of **Series XIV** (**54**, where n=4) exhibiting subtle homogeneous to homeotropic change of alignment during isothermal photo-induced N-I transition.

The plates above show the photoresponsitivity of compound (**31**) to intense multi-spectrum light. The sample displays a classical nematic phase coalescing from nematic droplets (**Plate 4 a**), just below the clearing point. As the light intensity is increased, the nematic phase rapidly starts to extinguish (**Plate 4 b**). However, before going to the isotropic liquid, a change of alignment in the nematic phase can be seen travelling through the field of view from the top right (**Plate 4 c**). This is quickly extinguished as the phase goes to the isotropic liquid (**Plate 4 d**). This time the 'hole' created slowly reverts back to the nematic phase as the illumination is decreased (**Plate 4 e**).

Plates 3 a-e and **4 a-e** demonstrate how manipulation of a core molecule can lead to a change in chemo-physical properties. The two compounds shown above display photoresponsitivity to a broad spectrum light source whereas, the parent compounds (**Series I-XIII**) appear to be wavelength specific (367 nm for *trans-cis* and 434 nm for *cis-trans* isomerisation).

5   CONCLUSIONS

From the results and elucidated structure property relationship study, several conclusions may be drawn.

i.   Thiophene azo-esters (**Series I, II, IV-XIII**) are nematogenic.

ii.   X-Ray crystallography of single crystals showed that the proposed structures were correct with both the azo and the acrylic groups in the *E*-conformation.

iii. Linearity plays a key role in the mesophase thermal stability of the compounds. This is demonstrated by the mesophase thermal stability order of the **Series I-III** compounds (phenyl > 3-thienyl > 2-thienyl) and also in the melting points when viewed in respect of X-ray analysis.

iv.   For mono-fluorination, the mesophase thermal stability was greatest when the fluoro-substituent was in an *ortho* position with respect to the –N=N- linkage (*inner edge*), independent of the disposition of the terminal thiophene.

v.   For difluoro-substitution, mesophase stability is greater when fluorination is along the molecular axis as opposed to across the axis, with across axis fluorination being more detrimental to the mesophase thermal stability when it is *meta* to the –N=N- linkage and *ortho* to the ester group (*outer edge*). This was also the case for mono fluorine-substitution.

vi.   UV photoresponsive studies showed that *E/Z*- isomerisation occurred in solution (THF) at 364 nm, with reverse *Z/E* isomerisation indicated at 434 nm, showing the applicability of thiophene based compounds for photoresponsive applications.

vii. Removal of the acrylic bond from the parent compound resulted in lowering of mesophase thermal stability, possibly as a result of reduction in rigidity and hence linearity (**Series XIV**).

viii. Replacement of the terminal alkoxy-group with a terminal thiophene greatly increases the mesophase thermal stability, possibly as a result of both increased rigidity and also an increase in $\Delta\alpha$ (**Series XV**).

FUTURE WORK

5   **FUTURE WORK**

The wealth of chemistry is enormous in the scope of any structure-property relationship study. For example, at the time of completing this research preliminary work was initiated on several structures (**Figure 35**) that could have potential for use as; i) photoresponsive chiral nematic liquid crystals [90-94], ii) materials that could increase the optical anisotropy [95][96], iii) materials with potential for use in nonlinear optical applications [97, 98] and photoresponsive polymers [99-101] for use in data storage, holography[102], photoalignment (recently in ferroelectric systems [103, 104]) and photo-switching [105, 106].
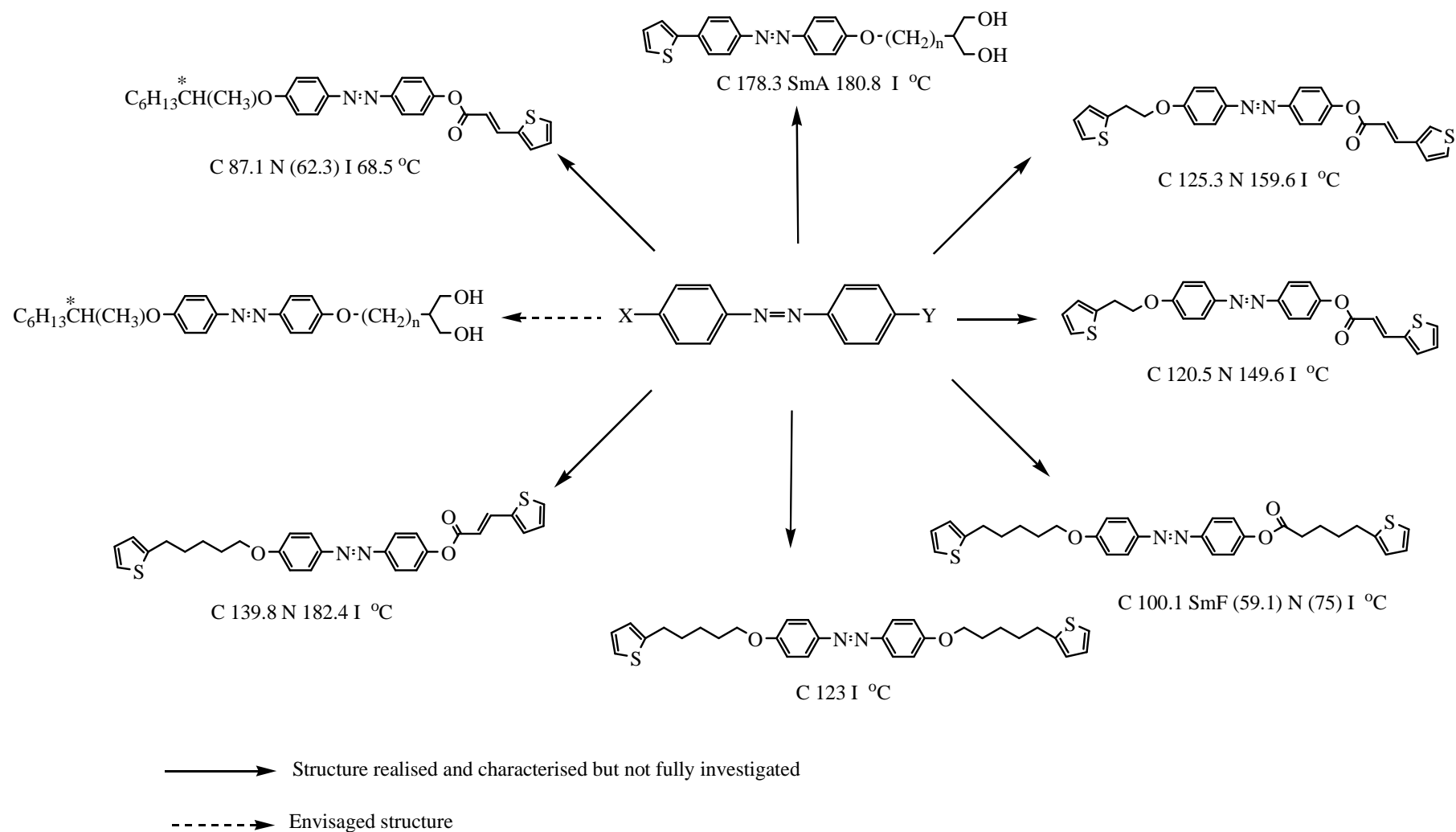
Figure 35   Diagrammatic representation of envisaged structures for further study arising from an azobenzene core, based on previously synthesised compounds whose structure-property relationship have been elucidated

148

REFERENCES

REFERENCES

1. F. Reinitzer, *Monash. Chem.*, 1888, **9**, 421; F. Reinitzer, *Liq. Cryst.*, 1989, **5(1)**, 7 (translation).

2. O. Lehmann, *Z.Physik. Chem.*, 1889, **18**,273.

3. L. Gattermann and A. Ritschke, *Ber. Dtsch. Chem. Ges.*, 1890, **320**, 122.

4. D. Vorländer, *'Kristallinisch-flüssige Substanzen'*, Enke Stuttgart, 1908.

5. D. Vorländer, *Ber. Dtsch. Chem. Ges*, 1908, **41**, 2033.

6. E. Bose, *Z. Phys.*, 1908, **9**, 708.

7. H. Zocher, *Z. Phys*, 1927, **28**, 790.

8. L. S. Ornstein and W. Kast, *Trans. Faraday Soc.*, 1933, **29**, 930.

9. C. W. Oseen, *Trans. Faraday Soc.,* 1933, **29**, 883.

10. G. Friedel, *Ann. Physik.*, 1922, **18**, 273.

11. F. Meyer and K. Dahlem, *Leibigs Ann.,* 1902, **122**, 320.

12. G. Tammann, *Ann. Physik*, 1901, **4**, 524; 1902, **8**,103; 1906, **19**, 421.

13. W. Nernst, *Z. Elektrochem.,* 1906, **12**, 431.

14. G. H. Brown and W.G. Shaw, *Chem. Rev.*, 1957, **57**, 1049.

15. W. Maier, and A. Saupe, *Nature*, 1954, **13a**, 564; 1954, **14a**, 882; 1960, **15a**, 287; W. Maier and A. Saupe, *Zeit. Naturforsch.*, 1958, **13a**, 564.

16. G. W. Gray, *'Molecular Structure and the Properties of Liquid Crystals'*, Academic Press, London and New York, (1962).

17. M. Schadt and W. Helfrich, *Appl. Phys. Lett.*, 1971, **18**, 127.

18. G. W. Gray, K. J. Harrison and J. A. Nash, *Electron. Lett.*, 1973, **9**, 130.

19. N.A Clark and S.T Lagerwall., *Appl. Phys. Lett.*, 1980, **36**, 899.

20. 'New Directions in Liquid Crystals', *Phil. Trans. R. Soc. A*, ed. J.M. Thompson, 2006, **364**, 2565.

21. D. Demus, *Liq. Cryst.*, 1989, **5**, 75.

22. S. Kumar, *Chem. Soc. Rev.*, 2006, **35**, 83

23. R. A. Reddy and C. Tschierske, *J. Mater. Chem.,* 2006, **16**, 907.

24. R. Achten, A. Koudjis, M. Giesbers, A.T.M. Marcelis and E.J.R. Sudholter, *Liq. Cryst.*, 2005, **3**, 277.

25. S. Chandrasekhar, B.K. Sadashiva and K.A. Suresh, *Pranama*, 1977, **9**, 471.

26. L.A. Madsen, T.J. Dingemans, M. Nakata and E.T. Samulski, *Phys. Rev. Lett*., 2006, 219804/1.

27. J. D. Bernal and D. Crowfoot, *Trans. Faraday Soc.,* 1933, **29**, 1032.

28. A.J. Slaney, I. Nishiyama, P. Styring and A.W. Goodby, *J. Mater. Chem.,* 1997, **2**, 805.

29. *Smectic Liquid Crystals, Textures and Structures*, eds. G.W. Gray and J.W. Goodby, Blackie Academic Press, (1984).

30. H. Sackman and D. Demus, *Mol. Cryst. Liq. Cryst. Lett.*, 1973, **21**, 239.

31. C.R. Safinya, M. Kaplan, J. Als-Nielsen, R.J. Birgeneau, D. Davidov, J.D. Lister, D.L. Johnson and M.E. Neubert, *Phys. Rev. B*, 1980, **21**, 4149.

32. A.J. Leadbetter, '*Thermotropic Liquid Crystals- (Critical Reports on Applied Chemistry)*', ed. G.W. Gray, John Wiley and Sons, Chichester, Vol. 22, Chap. 1, 1987.

33. *Ferroelectric Liquid Crystals, Principles, Properties and Applications*, Eds. J.W. Goodby, S.A. Pickin, R. Blinc, N. A. Clark, S.T. Lagerwall, M.A. Osipov, T. Sakurai, K. Yoshino and B. Zenks, Gordon and Breach Science Publishers Ltd., Philadelphia and Reading, 1991.

34. *Structure and Bonding*, J. W. Goodby, Spinger-Verlag (Berlin), 1999.

35. A.D.L. Chandani, E. Gorecka, Y. Ouchi, H. Takezoe and A. Fukuda, *Jap. J. Appl. Phys.*, 1989, **28**, L1265.

36. A. D. L. Chandani, E. Gorecka, Y. Ouchi, H. Takezoe and A. Fukuda, *Jap. J. App. Phys.*, 1988, **27**, L276.

37. R.B. Meyer, L. Liebert, L. Strzelecki and P.J. Keller, *J. Phys. Paris Lett.,* 1975, **36**, 669.

38. G. Gray, *Mol. Cryst. Liq. Cryst.*, 1969, **7**, 127.

39. P.J. Collings and M. Hird, '*Introduction to Liquid Crystals'*, Taylor and Francis, New York, 1997.

40. K.J. Toyne, '*Thermotropic Liquid Crystals- (Critical Reports on Applied Chemistry)'*, ed. G.W. Gray John Wiley and Sons, Chichester, Vol. 22, Chap. 2, 1987.

41. G.W. Gray, J.B. Hartley and B. Jones, *J. Chem. Soc.*, 1955, 1412.

42. G.W. Gray, '*Liquid Crystals and Plastic Crystals'*, eds. G.W. Gray and P.A. Windsor, Ellis Horwood Ltd., Chichester, 1974, Vol 1, Chap. 2.

43. G.W. Gray and D.G McDonnell, *Mol. Cryst. Liq. Cryst.*, 1979, **53**, 147.

44. G.W. Gray and B.M. Worrall, *J. Chem. Soc.*, 1959, 1545.

45. G.W. Gray and B. Jones, *J. Chem. Soc.*, 1954, 683.

46. M. Hird, K.J. Toyne, G.W. Gray, D.G. McDonnell and I.C. Sage, *Liq. Cryst.*, 1985, **18**, 1.

47. M. Hird and K.J. Toyne, *Mol. Cryst. Liq. Cryst.,* 1998, **323**, 1.

48. N. Carr, G.W. Gray and D.G. McDonnell, *Mol. Cryst. Liq. Cryst.,* 1983, **97**, 13.

49. S.M. Kelly, *Liq. Cryst.*, 1989, **5**, 7.

50. G.W. Gray, M. Hird, D. Lacey and K.J Toyne, *Mol. Cryst. Liq. Cryst.,* 1989, **172**, 165.

51. M.J. Goulding and S. Greenfield, *Liq. Cryst.*, 1993, **13**, 345.

52. G.W. Gray, M. Hird, D. Lacey and K.J Toyne, *J. Chem. Perkin Trans. 2.*, 1989, 2041.

53. M. Hird, *Chem. Soc. Rev.,* 2007, **36**, 2070.

54. J. Hoogboom, T. Rasing, A.T. Rowan and J.N. Roeland, *J. Mater. Chem.*, 2006, **16**, 1305.

55. K. Ichimura, *Chem. Rev.,* 2000, **100**, 1847.

56. T. Ikeda, *J. Mater. Chem.*, 2003, **13**, 2037.

57. W. M Gibbons, P.J. Shannon, S-T. Sun and B.J. Swetlin, *Nature*, 1991, **351**, 49.

58. K. Ichimura, Y. Suzuki, T. Seki, A. Hosoki and K. Aoki, *Langmuir*, 1988, **4**, 1214.

59. L. Komitov, K. Ichimura and A. Strigazzi, *Liq. Cryst.*, 2000, **27**, 51.

60. K. Ichimura, *Photochromism: Molecules and Systems*, ed. H. Durr and Bouas-Laurent, Elsevier, Amsterdam, 1990.

61. P. Greiss, *Liebigs Ann. Chem.*, 1858, **106**, 123.

62. G.S. Hartley, *Nature*, 1937, **140**, 278.

63. M. Irie, *Chem. Rev.*, 2000, **100**, 1683.

64. M. Eich and J.H. Wendorff, *Makromol. Chem.*, 1987, **8**, 59.

65. R. Berg, S. Hvilsted and P.S. Ramanujam, *J. Am. Chem. Soc.*, 1999, **20**, 121, 4738.

66. '*Photo-reactive materials for Ultrahigh Density Optical Memory*', ed. M. Irie, Elsevier Science, Amsterdam, 1994.

67. T. Ikeda, J-I Mamiya and Y. Yu, *Angew. Chem. Int. Ed.*, 2007, **46**, 506.

68. E. Sackmann, *J. Am. Chem Soc.*, 1971, **93**, 7088.

69. W.E. Haas, K.F. Nelson, J.E. Adams and G.A. Dir, *J. Electrochem. Soc.,* 1974, **351**, 49.

70. W.J. Gibbons, P.J. Shannon, S-T. Sun and B.J. Sweetlin, *Nature*, 1991, 351, 49.

71. D.J. Byron, A.S. Matharu, S.N.R. Shirazi, A.R. Tajbakhsh and R.C. Wilson, *Liq. Cryst.*, 1993, **3**, 645.

72. J.L. Butcher, D. J. Byron, S.N.R. Shirazi, A. R. Tajbakhsh, R.C. Wilson and J. Bunning, *Mol. Cryst. Liq. Cryst.*, 1991, 19, 327.

73. J.L. Butcher, D.J. Byron, A.S. Matharu and R.C. Wilson, *Liq. Cryst.*, 1995, **19**, 387.

74. A.S. Matharu, R.C. Wilson and C. Grover, *Mol. Cryst. Liq. Cryst*. 1999, 332, 2813.

75. A.S. Matharu, C. Grover, L. Komitov and G. Anderson, *J. Mater. Chem.*, 2000, **10**, 1303.

76.   A.S. Matharu, S.J. Cowling and G. Wright, *Liq. Cryst.*, 2007, **34**, 489.

77.   R. McDonald, D. Lacey, P. Watson, S. Cowling and P. Wilson, *Liq. Cryst.*, 2005, **32**, 319.

78.   A. Seed, *Chem. Soc. Rev.*, 2007, **36**, 2046.

79.   Y. Nabeshima, A. Shishido, A. Kanazawa, T. Shiono, T. Ikeda and T. Hiyama, *Chem. Mater.,* 1997, **9**, 1480.

80.   C. Weygand and R. Gabler, *J. Prakt. Chem.*, 1940, **155**, 322.

81.   R. Nodzu, H. Watanabe, S. Kuwata, C. Nagaishi and T. Terematsu, *J. Pharm. Soc. Jpn*, 1954, **74**, 872.

82.   A. Hassner and V. Alexandria, *Tet. Lett.*, 1978, **46**, 4475.

83.   D.J Byron, A.S. Matharu, M. Rees and R.C. Wilson, *Mol. Cryst. Liq. Cryst.*, 1995, **258**, 229.

84.   M. Gomberg and W.E. Bachmann, *J. Am. Chem. Soc*. 1924, **42**, 2339.

85.   M. Julliard, S. Chan, G. Vernin and J. Metzger, *Helv. Chim. Acta.*, 1978, **61**, 2941.

86.   J.R. Beadle, S.H. Korzeniowski, D.E. Rosenberg, B.J. Garcia-Slanga and G.W. Gokel, *J. Org. Chem*. 1984, **49**, 1594.

87.   N. Miyaura, T. Yanagi and A. Suzuki, *Synth Commun*., 1981, **11**, 513.

88.   W.J. Thompson and J. Gaudino, *J. Org. Chem.,* 1984, **59**, 5237.

89.   A.R. Martin and Y. Yang, *Acta. Chem. Scand.*, 1978 **47**, 4475.

90.   C.H. Legge and G.R. Mitchell, *J. Phys. D; Appl. Phys*, 1992, **25**, 492.

91.   Q. Li, L. Li, J. Kin, H-S Park and J. Williams, *Chem. Mater.*, 2005, **17**, 6018.

92.   J-H. Liu, P-C. Yang, Y-K. Wang and C-C. Wang, *Liq. Cryst.*, 2006, **33**, 237.

93.   A. Bobrovsky, V. Shibaev and J. Wendorff, *Liq. Cryst.*, 2007, **34**, 1.

94.   A. Bobrovsky and V. Shibaev, *Polymer*, 2006, **47**, 4310.

95.   A. Seed, K.J. Toyne and J.W. Goodby, *J. Mater. Chem.,* 1995, **5**, 653.

96.   A. Seed, K.J. Toyne, J.W. Goodby and M. Hird, *J. Mater. Chem.,* 2000, **10**, 2069.

97. A. Seed, G. Cross, K.J. Toyne and J.W. Goodby, *Liq. Cryst.*, 2003, **30**, 1089.

98. Y. Shirota, *J. Mater. Chem.*, 2000, **10**, 1.

99. G.S. Kumar and D.C. Neckers, *Chem. Rev.*, 1989, **89**, 1915.

100. T. Ikeda, S. Horuichi, D.B. Karanjit, S. Kurihara and S. Tazuke, *Makromolecules*, 1990, **23**, 42.

101. M-H. Li, P. Auroy and P. Keller, *Liq. Cryst.,* 1999, **26**, 351.

102. D. Li, J. Yang, R. DeMasi, X. Ke and M. Wang, *Optics Communications*, 2004, **235**, 275.

103. S. Sevigny, L. Bouchard, S. Motallebi and Y. Zhoa, *Liq. Cryst.*, 2005, **32**, 599.

104. G. Wang, S. Leclair, L-A. Roy and Y. Zhoa, *Liq. Cryst.*, 2005, **32**, 125.

105. J-H. Liu and H-Y. Wang, *J. Appl. Poly. Sci.*, 2004, **91**, 789.

106. A. Archut, F. Vogtle, L. De Cola, G.C. Azzellini, V. Balzani, P.S. Ramanujam and R. Berg, *J. Chem. Eur.*, 1998, **4**, 699.

APPENDICES

Structure-Property investigation of 2- and 3-thienylacrylates bearing laterally fluorinated azobenzene moieties

A. S. Matharu[*a] and D. Chambers-Asman[b]

[a]Department of Chemistry, University of York, Heslington, York. England YO10 5DD.

[b]Division of Chemistry, Nottingham Trent University, Nottingham, England NG11 8NS.

Abstract

*The synthesis, transition temperatures and structure-property relationships of a variety of thiophene-containing azobenzene esters derived from either 3-(2-thienyl)acrylic acid (Series **I, IV, VI, VIII, X** and **XII**) or 3-(3-thienyl)acrylic acid (Series **II, V, VII IX, XI** and **XIII**) and appropriate fluoro- and non-fluoro-substituted 'azophenols' are reported. For comparative purposes, the non-heterocyclic counterparts, i.e., cinnamates (Series **III**) were also prepared and are reported.*

All seventy final esters are mesomorphic, exhibiting the nematic phase alone. Their mesomorphic properties are dependent upon the disposition of the terminal thiophene moiety. In general 3-thienyl-sustitution gives thermally more stable compounds than 2-thienyl-substitution.

*Influence of mono- (Series **IV, V, VI** and **VII**) and di- (Series **VIII, IX, X, XI, XII** and **XIII**) lateral fluoro-substitution on mesomorphic properties is investigated in detail. Lateral fluorination lowers mesophase thermal stability and its extent is dependent upon the number and disposition of the lateral fluoro-substituents. Di-lateral fluorination across the long molecular axis is more detrimental to mesophase thermal stability than along the long molecular axis.*

---

[*] Author for correspondence